Electrorheological fluids as smart medicines with potential in controllable drug delivery

Davies, Jayne Louise

Award date:
1999

Awarding institution:
University of Bath

Electrorheological Fluids as Smart Medicines with Potential in Controllable Drug Delivery

Submitted by

Jayne Louise Davies, BPharm, MRPharmS.

for the degree of Doctor of Philosophy

of the University of Bath

1999

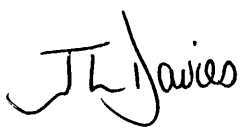

ProQuest LLC
789 East Eisenhower Parkway
P.O. Box 1346
Ann Arbor, MI 48106-1346

Acknowledgements

I wish to convey appreciation and sincere thanks to my supervisors Professor John Staniforth and Dr. Ian Blagbrough. My gratitude extends to my industrial supervisors Dr. David Jordan (HMR, Swindon, UK) for his interest and support throughout my research and Dr Ralph Heasley (HMR, Kansas City, USA).

There is an array of people who have, in their own way, helped me at various stages during the course of my research. Professor Harry Block and Dr. Paul Rattray (Cranfield University, UK) for putting me on the right track at the beginning of my work. Rod Murray, Leslie Steele and his colleagues in the Science Schools Workshop who skilfully machined many pieces of equipment for my research. Professor David Rodgers (Department of Electrical and Electronic Engineering, University of Bath) for his help and advice on Gauss' flux theorem. In addition, the staff at TA Instruments (Leatherhead, UK) have been helpful both in the context of a support team, and as a source of advice on rheology. I would also like to thank Ursula Potter (Electron Optics, University of Bath), Dr. Paul Christie, Richard Sadler and Dominic Carrington.

A big "Thank you" to my chums, both old and new, for all the memories.

Lastly, I would also like to thank my Gran and Grand-pa, who have provided endless support, encouragement and for always being there through good and bad times.

To Mum and Dad,

in loving memory.

Abstract

The feasibility of a novel controllable drug-delivery system incorporating electrorheological (ER) fluids has been investigated. The ER response of a model fluid, microcrystalline cellulose (MCC) in 100 cSt silicone oil under low applied electric fields (50 - 500 V/mm) has been studied; tacrine was examined as a model drug. Flow and creep-recovery experiments have been used synergistically to develop an understanding of the ER response in relation to various factors: particle concentration, particle size, moisture content and the magnitude of the applied electric field.

A traditional Franz cell was modified for use with low viscosity formulations by the addition of a glass lip, an insulating o-ring and an interchangeable mesh support that acted as the lower electrode. The modified diffusion cell was validated using suspensions of tacrine in 100 cSt silicone oil. The ability of ER fluids to hinder or halt the release of tacrine upon application of an electric field was assessed using the aforementioned factors.

The yield stress values ranged from 0.0928 Pa s (± 0.0035) to 7.9610 Pa s (± 0.2269) for MCC concentrations of 1.0 to 20.0 % w/w (sieve fraction below 45 μm) respectively. The yield stress value rose to 8.4081 Pa s (± 0.1456) for suspensions prepared with the sieve fraction 90 - 125 μm. In general, the addition of tacrine had little or no significant effect on the yield stress. The production of a yield stress was believed to be related to particle chain formation and we obtained microscopic evidence of such chain formation even at low applied electric fields. A biphasic release profile was proposed for the release of tacrine from silicone oil; after an initial period of rapid release, the curve approached a quasi-equilibrium followed by a slow approach to the final equilibrium. Basal drug delivery from ER fluids was found to follow a similar pattern. Anomalous behaviour was observed with suspensions prepared with the sieve fraction 90 - 125 μm, particularly with mesh apertures of 45 and 90 μm. Upon application of an electric field (250 V/mm), the release of tacrine through the 90 μm mesh aperture was halted.

Abbreviations

A: Area

ac: Alternating current

C: Concentration

C_o: Concentration of solute in the organic phase

C_w: Concentration of solute in the water phase

d: Distance

D: Diffusion coefficient

dc: Direct current

ε_o: Permittivity of free space

ε': Dielectric constant

ER: Electrorheological

EVAc: Ethylene vinyl acetate copolymer

F: Force

γ: Strain

$\dot{\gamma}$: Shear rate

η: Shear viscosity

η_B: Bingham viscosity

η_E: Viscosity under field

η_o: Residual shear viscosity

η_o: Viscosity under no field

m: Mass

m_l: Mass of liquid

m_p: Mass of powder

I: Current

J_c: Shear compliance

J_d: Rate of transfer per unit area of section

J_o: Elastic string compliance

J_t: Total creep compliance

k: Viscosity coefficient

K_{ER}: Dielectric constant (electrorheological fluid)

K_{liquid}: Dielectric constant (liquid phase)

K_{solid}: Dielectric constant (solid phase)

l: Length

LLS: Laser light scattering

n: Power law index (m: Herschel-Bulkley equation)

ν: Kinematic viscosity

M: Total amount of drug release at a given time

P: Power

r: Radius

R: Resistance

ρ: Density

σ: Shear stress

σ_{HB}: Herschel-Bulkley yield stress

σ_o: Constant shear stress

σ_y: Yield stress

τ: Tortuosity

TDD: Transdermal drug delivery

UV: Ultraviolet

v: velocity

V: Voltage (potential difference)

x: Space coordinate measured normal to the section

Throughout this thesis the units of dynamic viscosity have been written as Pa s.

Aims

The principal aim of this study is to investigate the feasibility of utilising electrorheological (ER) fluids as controllable drug-delivery systems.

In addition to discussing the composition and rheological behaviour of ER fluids, the introduction (Chapter One) briefly reviews recent advances in controlled drug delivery. The experimental work is divided into three sections, dealing with the characterisation of the model ER systems (Chapter Two), rheological properties (Chapters Three and Four) and the investigation of the delivery of tacrine from ER fluids (Chapters Five and Six).

Flow and creep-recovery experiments will be used synergistically to develop an understanding of the ER response of a model fluid, microcrystalline cellulose (MCC) in 100 cSt silicone oil, under the influence of low applied electric fields ($\leq$ 500 V/mm).

Furthermore, the objectives of this study include the development of methodology to investigate the drug diffusion from ER fluids. A related objective is to develop an understanding of the mechanisms involved in drug diffusion from ER fluids. It is envisaged that the presence of particle chains under the influence of an applied electric field will result in the slowing or halting of drug diffusion from ER fluids. Thus, we aim to assess the potential of ER fluids in medicines.

Chapter One

Introduction

1.1. Controlled Drug-Delivery Devices

Drug delivery may be broadly subdivided into three categories: conventional single-dose or bolus medicines, constant-rate release devices and controlled drug-delivery devices. When a conventional drug-delivery dosage form such as a tablet or oral liquid is administered, a single or bolus release of drug occurs. This burst of plasma drug-levels is followed by a decay to values below the therapeutic concentration. As a result, frequent and repeated dose administration is required. One consequence of this is oscillation of the plasma drug concentration profile between therapeutic and sub-therapeutic levels. The reality that the optimum therapeutic concentration may only be attained for a relatively short period of time is the primary driving force in the search for novel drug-delivery methods. Constant-rate delivery devices address some of the problems associated with conventional systems. These devices are designed to maintain the drug level within the desired therapeutic range (Langer, 1980; Kost and Langer, 1992). There are clinical situations where this approach yields unsatisfactory release profiles, e.g. in the delivery of insulin for patients with diabetes mellitus (Kost, 1993).

Controlled-release administration of therapeutic agents has become an important area of research and significant advances in theories and methodologies have been made. Controlled release implies a predictable and reproducible release profile relatively independent of the surrounding environment (e.g. Kydonieus, 1980). Controlled drug-delivery devices, for oral administration or by implant, capable of releasing a therapeutic agent by well defined kinetics, are a significant improvement over conventional dosage forms. These devices do not yet represent the desired therapy. Ultimately, release should be achieved only in response to the physiological requirements.

Recent studies in the area of chronopharmacology indicate that the onset of certain diseases exhibit strong circadian temporal dependencies (for example: Hrushesky, 1985; Reinberg, 1988 and 1992; Levy, 1991), thus paving the way for further optimisation of

drug-delivery profiles by pulsatile or self-regulated delivery. These periodic alterations in parameter values can result in a periodic modulation of plasma drug-levels and drug effects even if the drug is infused at a constant rate intravenously to steady state (Reinberg, 1992; Burnette, 1998). Based on this, it would seem reasonable that one might be able to achieve, by proper modulation of drug delivery, a maximum therapeutic effect.

Advantages associated with improved drug delivery include the maintenance of drug levels within the therapeutic range, the reduction of side-effects due to site-specific targeted delivery and increased patient compliance as a result of improved dosage regimens (Langer and Peppas, 1981; Langer, 1998). These benefits must be weighed against the potential disadvantages such as dose dumping, surgical implantation and the difficulties in halting release (Langer and Peppas, 1981).

Polymer-based systems for injection or implantation are typically uniform dispersions of drug particles in a biocompatible polymeric material (Langer et al., 1981), which may be either non-biodegradable e.g. silicone rubber (Golomb et al., 1987; Johnston et al., 1989) and ethylene-vinyl acetate copolymer (EVAc) (Langer and Folkman, 1976; Edelman et al., 1996) or biodegradable e.g. lactic/glycolic acid copolymers (Kitchell and Wise, 1985; Floy et al., 1993). An advantage of biodegradable controlled release systems is that they do not need to be removed surgically after drug depletion (Langer, 1980). There are three mechanisms by which drugs are delivered from polymeric drug-delivery based systems: (1) diffusion of the drug species from or through the system according to Fick's law; (2) a chemical or enzymatic reaction leading to degradation of the system (Heller, 1988) and (3) solvent activation, either through osmosis or swelling (Brannon-Peppas and Peppas 1989; Langer, 1998). Comprehensive reviews have been written on polymeric drug delivery by Langer and co-workers: Langer and Peppas (1981), Kost and Langer (1992) and Langer (1998).

A number of different techniques have been examined for producing controlled drug-delivery device systems which more closely resemble the normal physiological process. Thus, the amount of drug released accords with the physiological needs (Kost, 1990; Langer, 1998). Drug delivery may be controlled in one of two ways, either by application of an external intervention (externally regulated or pulsatile) or as a result of the detection of a control variable leading to feedback information and resulting in the output being adjusted accordingly (self-regulated).

1.2. Pulsed and Self-Regulated Delivery

There are a number of clinical situations where "on demand" drug delivery would be beneficial e.g. in diabetes mellitus or in the treatment of angina pectoris. Methods for achieving complex drug-release profiles from polymeric systems have focused on modifying the responses to specific external stimuli such as electric (Kwon et al., 1991) or magnetic (Edelman et al., 1985) fields; exposure to ultrasound (Kost et al., 1989); temperature (Hoffman et al., 1986; Okano et al., 1990) and light (Mathiowitz and Cohen, 1989). Self-regulated systems utilise several approaches as rate-controlled mechanisms such as pH-sensitive polymers (Heller, 1988; Siegel et al., 1988) and enzyme-substrate reactions (Fischel-Ghodsian et al., 1988; Heller, 1988).

1.2.1. Externally-Regulated Systems

1.2.1.1. Magnetically Enhanced Polymeric Drug Delivery

Magnetically triggered systems are comprised of drug molecules and magnetic beads uniformly dispersed within a polymeric matrix. Drug release is constant until an external oscillating magnetic field causes a higher rate (Hsieh et al., 1981; Edelman et al., 1985; Kost et al., 1985 and 1987). Early *in vitro* characterisation provided information on the critical parameters affecting the release rate, namely the magnetic field strength and

the mechanical properties of the polymer matrix (Hsieh et al., 1981; Edelman et al., 1985; Kost et al., 1985). *In vivo* implants comprising of EVAc impregnated with insulin and embedded magnets were placed subcutaneously in diabetic rats for two months (Kost et al., 1987). It was found that upon exposure to the magnetic field, the blood glucose levels were reproducibly lowered as a result of insulin release (Kost et al., 1987). It is believed that the embedded magnets move back and forth within the polymer matrix thereby exerting pressure on, and squeezing drug out of, the matrix pores (McCarthy et al., 1984; Edelman et al., 1985). These magnet-polymer systems have the added benefit over implantable pumps that there are no catheters, external lines and moving parts. Furthermore, no significant inflammatory response was detected in different *in vivo* assay sites using the polymer-based system with (Hsieh et al., 1981) and without (Langer et al., 1981; Brown et al., 1983) embedded magnets.

1.2.1.2. Ultrasonically Triggered Systems

The use of ultrasound as an external means of modulating delivery from polymeric devices has been reported (Kost et al., 1989; Levy et al., 1989; Kost, 1993). Increased release rates were observed within two minutes post-application of the ultrasonic trigger to biodegradable polymers implanted in rats (Kost et al., 1989). The system was capable of repeated modulation, with the release-rate returning to baseline levels between ultrasound applications (Miyazaki et al., 1988; Kost et al., 1989). Furthermore, non-erodible polymeric systems composed of EVAc have been developed by Miyazaki et al. (1983; 1985; 1988) that are capable of delivering the anticancer agent 5-fluorouracil or insulin. Release rates of zinc bovine insulin from EVAc matrices were 15-times higher when exposed to ultrasound compared with basal diffusion-controlled release rate. Typically, ultrasound values used for *in vivo* are 1 W/cm^2 applied over a period of 30 min (Kost et al., 1989; Miyazaki et al., 1988). Experimental evidence indicates that cavitation by the

ultrasound waves may be partially responsible for augmented drug release (Mitragotri et al., 1995b), in addition the increase in temperature observed by Miyazaki et al. (1988) might also be considered responsible.

1.2.1.3. Thermo-responsive Polymeric Drug Delivery

Stimuli-sensitive polymers which change their structure and physical properties in response to external signals have promising potential in the design of drug-delivery systems. The concept of self-regulating antihyperpyretic drug delivery is perceived attainable through the increase in body temperature observed in a disease state (Hoffman et al., 1986). Temperature-sensitive polymers can be classified into two groups based on the origin of thermosensitivity in aqueous swelling (Hoffman et al., 1986; Bae et al., 1987). The first is based on polymer-water interactions, whilst the second is based on additional polymer-polymer interactions. A pulsatile drug-release pattern regulated by temperature changes has been demonstrated (Hoffman et al., 1986).

1.2.1.4. Electrically Controlled Drug Delivery

Electrochemically controlled release is based on polymers which bind and release bioactive compounds in response to an electrical signal (Miller et al., 1987). The polymer has two redox states, only one of which is suitable for ion binding. Drug ions are bound in one redox state and released from the other. The attached electrodes serve to switch the redox states and the amount of current passed can control the amount of ions released. This area of controlled drug delivery has not attracted as much interest as other pulsatile drug-delivery systems.

1.2.2. Self-Regulated Systems

A self-regulated drug-delivery system can be defined as one capable of receiving feedback information and adjusting the drug release in response. Self-regulated drug delivery has been reviewed by Heller (1988) and Kost and Langer (1992). An example of an enzyme-substrate pH-sensitive reaction is detailed. When the pH inside the polymer system changes, the solubility of the drug shifts dramatically, which changes the diffusion or dissolution driving force, and hence the release rate changes correspondingly (Heller, 1988). Fischel-Ghodsian et al. (1988) investigated the feasibility of an enzymatically controlled insulin delivery system, utilising the knowledge that insulin solubility increases with decreasing pH. The controlled release system was prepared using EVAc, insulin and the enzyme glucose oxidase. The enzymatic reaction with external glucose was shown to decrease the pH in the microenvironment by the production of glycolic acid (Fischel-Ghodsian et al., 1988).

1.3. Transdermal Drug Delivery

Transdermal drug delivery (TDD) offers several advantages over traditional drug-delivery methods such as oral delivery. Specifically, TDD benefits from the ability to circumvent first-pass metabolism and the delivery can be interrupted simply by removing the drug-laden patch from the skin. Despite the potential advantages of TDD, few drugs can be administered across the skin at therapeutic levels, due to the remarkable barrier properties of the stratum corneum (e.g. Bronaugh and Maibach, 1989). TDD has found limited clinical applications however. This is largely because transport of most drugs across the skin is slow, exhibiting large lag times of hours to days and steady-state rates which are typically sub-therapeutic for a variety of disease states (Mitragotri, 1995a; Kost et al., 1996; Johnson et al., 1996; Singh and Bhatia, 1996). As a result, ultrasound and electric fields have been studied as approaches in the enhancement of transport rates.

These TDD approaches have been combined synergistically in an attempt to further enhance delivery.

1.3.1. Ultrasound Transdermal Drug Delivery

TDD has been shown to increase through ultrasound (Levy et al., 1989; Julian and Zentner, 1990; Mitragotri et al., 1995a and b), the frequency and intensity of which is dependent upon the thickness and permeability of the skin at the exposure site (e.g. Tyle and Agrawala, 1989). Therapeutic levels of ultrasound are applied at frequencies between 1 to 3 MHz, with corresponding intensities of 0 to 2 W/cm^2 (Mitragotri et al., 1995b; Mitragotri et al., 1996). Such levels have been used in an attempt to enhance the delivery of low molecular weight (< 500 Da) drugs across the human skin (Skaun and Zenter, 1984), as well as proteins such as insulin (e.g. Mitragotri et al., 1995a). Typically, delivery is enhanced 10-fold (Mitragotri et al., 1995b), although in many cases, no enhancement of TDD has been observed upon application of therapeutic ultrasound. Due to this uncertainty and inefficiency, therapeutic ultrasound TDD has found limited clinical application. Sub-therapeutic frequencies, in the region of 20 kHz and an intensity of 125 mW/cm^2 resulted in an increase in the transdermal transport of salicylic acid, for example by a factor of at least 300 (Mitragotri et al., 1996). Enhanced transdermal delivery is believed to arise through several mechanisms of which cavitation, the generation and oscillation of gas bubbles leading to disorder in the stratum corneum lipid bilayer (Edwards and Langer, 1994; Mitragotri et al., 1995b), attracts the most attention. Application of low frequency ultrasound does not appear to cause any long-term damage to the barrier properties of the epidermis (Skaun and Zenter, 1984; Mitragotri et al., 1996).

1.3.2. Electrically Modified Transdermal Drug Delivery

Electrically controlled membrane permeability has recently received increased attention as a means of systemic drug delivery (Banga and Chien, 1988; Singh and Bhatia, 1996). Iontophoresis has been performed at either constant voltage or constant current. The literature is consistent on the fact that the imposition of an electric field results in a decrease in skin resistance (Oh et al., 1993; Kalia and Guy, 1995). D'Emanuele and Staniforth (1991, 1992a and b, 1993) demonstrated the feasibility of using electrophoresis in the development of a controlled TDD system. Currents were typically in the range of 0 to 2.5 mA, with typical power requirements of approximately 3 mW. A linear relationship was found between the propranolol hydrochloride delivery rate and the current enabling a feedback controlled device to be proposed. Pulsed direct current has been found to be equally or more effective in facilitating the skin permeation of drugs (Liu et al., 1988; Bagniefski and Burnette, 1990) as well as reducing the incidence of skin irritation and subsequent damage (Okabe et al., 1986). *In vivo* experiments have been conducted on diabetic rats (Liu et al., 1988) using constant rate and pulsed dc electric fields. Liu and co-workers (1988) found that constant dc electric fields have little significant effect on the blood glucose levels, whereas blood glucose levels markedly decreased when pulsed dc electric fields, at the same current density (0.33 mA/cm^2), were applied for short time periods (typically ms).

Prausnitz et al. (1996b) investigated the TDD of calcein under low voltage constant electric fields and high voltage pulsed electric fields. The range of transdermal voltages used for high voltage pulsing was 40 to 450 V, with corresponding transient peak current densities of approximately 0.1 to 5 A/cm^2. A transition at approximately 100 to 150 V was observed, below which the flux increases were fully reversible (Prausnitz et al., 1993). Typically, pulses of duration less than 1 ms are favourable to minimise nerve stimulation (Ledger, 1992), the limits are approximately 0.5 A/cm^2 in terms of sensation. High voltage

pulsing has been shown to provide some advantages over conventional iontophoresis. Steady-state flux can be reached within minutes and maintained for many hours (Prausnitz et al., 1993 and 1996b); this reduction in lag time may lend itself to applications requiring rapid onset and/or complex drug delivery profiles.

Electroporation is believed to work, in part, by creating transient pores in the lipid bilayers of the stratum corneum (Prausnitz et al., 1993 and 1996a; Pliquett et al., 1995). Edwards et al. (1995) proposed that the voltage across the skin, which could be calculated from the sum total of the individual voltage drops across the stratum corneum's lipid bilayers, of which there are approximately 100 (Elias, 1991). Electroporation of a single bilayer occurs at a voltage of approximately 1 V (Freeman et al., 1994). Therefore iontophoresis would occur at voltages of less than or equal to 100 V, whilst electroporation would occur above this value (Edwards et al., 1995). The passage of electric current through the skin provokes sensations ranging from localised temperature changes, through tingling and itching to outright pain (Ledger, 1992). Tolerated iontophoretic applications are in the region of 0.5 mA/cm^2 (Banga and Chein, 1988; Burnette and Ongpipattanakul, 1988). As the total amount of current that can be passed through the skin is limited to the battery of the iontophoretic device and the tolerance of the patient, the efficacy becomes a key question in determining the practicality for a given drug therapy.

1.3.3. Synergistic Transdermal Drug Delivery

Johnson et al. (1996) proposed a synergistic combination of two chemical enhancers, linoleic acid and ethanol, with therapeutic ultrasound would result in a dramatic increase in the permeability of corticosterone for example. Chemical enhancers have been shown previously to increase transdermal drug transport via several mechanisms including increased solubility of the drug in the donor formulation (Knutson et al., 1993), increased partitioning into the stratum corneum, induced disorder of the lipid bilayer

(Barry, 1987; Mak et al., 1990; Ongpipattanakul et al., 1991) and disruption of the intracellular proteins. The ratio of permeability of corticosterone with ethanol and linoleic acid with ultrasound was increased by a factor of 14. On a similar basis, Kost et al. (1996) hypothesised that the combination of electric field and ultrasound would result in an enhancement of the transdermal delivery of calcein and sulphorodamine. Results indicated that in combination with ultrasound, the required voltage decreased from 95 V without ultrasound to 75 V with ultrasound.

1.4. Mechanical Pumps and Implantable Batteries

Mechanical diffusion pumps may be considered as either constant or controlled drug-delivery systems depending on their complexity. There are several types of infusion pump namely external pumps and implantable devices. Portable external pumps offer several advantages: ability to administer multiple drugs at a desired volume, with the ability to halt administration by the patient (Sefton, 1984). Disadvantages are associated with the need for a venous or arterial access device connected to tubing, together with the inconvenience of the device. Infusion pumps offer a number of advantages (Langer, 1980) in particular for drugs which are poorly absorbed or inactivated upon digestion. Advantages over other types of delivery device are the ease of replenishment and the administration of large volumes and multiple dose therapies. The advantages of a totally implanted pump are the convenience to the patient, coupled with the reduced risk of infection and the inability towards tampering. Cost and biocompatibility are disadvantages associated with the development of such devices, but mechanical failure resulting in either dose dumping or blockage of the pump are potential risks post-implantation.

Insulin delivery in pancreatectomised dogs was investigated using an implanted controlled release micropump (Sefton et al., 1990), based on diffusion, where the

concentration difference is the driving force. Augmentation of the delivery rate was achieved by means of an external dc power supply.

SynchroMed™ pumps are implantable, battery powered devices that release drug from the reservoir at pre-programmed intervals (Medtronic Technical Manual). Usually, these devices are implanted in the abdominal region, with the drug delivering catheter directed to the delivery site. Lithium-thionyl-chloride battery has a capacity of 2 ampere hours with an operating voltage of 3.6 V. The life of the battery is dependent on the rate and extent of drug delivery and typically for 0.5 ml of drug delivered per day, the battery will fail within 4 years.

Pacemakers are used for the long-term management of sino-atrial node disease and in treatment of advanced atrio-ventricular block. Pacemakers are implanted subcutaneously and connected to the heart by insulating wires terminating at one or more electrodes. The power source is driven by lithium batteries, with an expected life of between 7 and 10 years. Typically, the batteries are composed of lithium/iodine, lithium/silver vanadium oxide and lithium/carbon monofluoride, with varying nominal capacities ranging from approximately 0.5 to 2.5 ampere hours. A significant challenge in the development of implantable batteries, both as pacemakers and for other biomedical applications is the necessity to predict the performance of the cell. Pacemaker failure is usually caused by battery expiry, however this can usually be detected by regular monitoring of the patient. Infection around the power source may respond to antibiotics, but often requires re-implantation of the unit at an alternative site.

1.5. Rheology

Rheology can be defined as the science of the deformation and flow of matter. This definition was conceived by Bingham and adopted as the official definition by the American Society of Rheology in 1929.

1.5.1. Definitions of Rheological Flow Models

In its simplest form, flow describes the relationship between the stress (related to the force applied) and the shear rate (speed with which the fluid flows) of a sample (Figure 1.1). The ideal shear experiment would involve placing the test fluid between two parallel plates a distance (d) apart. One plate is now moved at a constant velocity (v) with respect to the other without altering the gap.

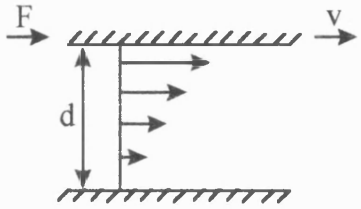

Shear stress $\sigma = \frac{F}{A}$ Shear rate $\gamma = \frac{v}{d}$ Viscosity $\eta = \frac{\sigma}{\gamma}$

Figure 1.1. Diagrammatic representation of the ideal shear experiment. Shear stress, shear rate and viscosity, where F is the applied force, A is the area (m^2), v is the velocity and d is the distance (m) are defined.

The rheological behaviour of most samples can be divided in to two categories, Newtonian and non-Newtonian. For a Newtonian fluid, the flow curve will take the form of a straight line passing through the origin, with the slope being equal to the reciprocal of the viscosity (Figure 1.2).

$$\sigma = \eta\dot{\gamma} \qquad \text{Equation 1.1}$$

where σ is the shear stress, $\dot{\gamma}$ is the shear rate and η is the shear viscosity with the SI units of Ns/m^2 (Pa s). The kinematic viscosity, ν, of a fluid is defined as:

$$\nu = \frac{\eta}{\rho}$$

where ρ is the density of the fluid. The unit of kinematic viscosity is m^2/s (Stoke).

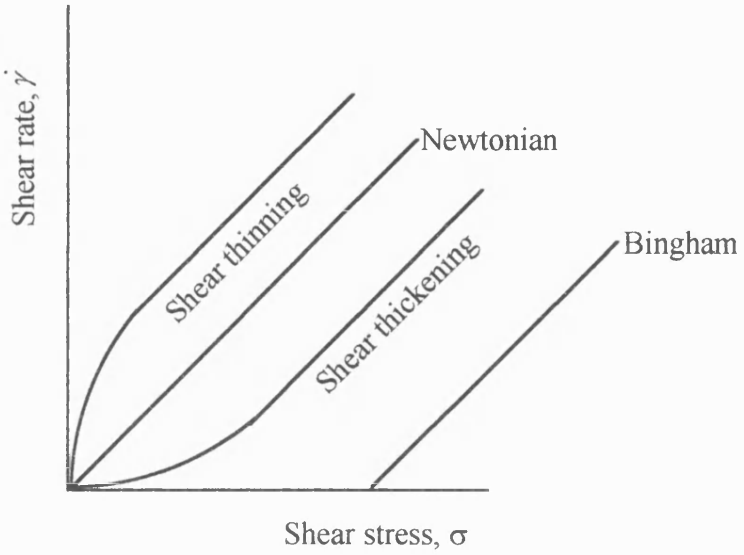

Figure 1.2. Idealistic rheograms of the shear stress - shear rate behaviour of various rheological flow models.

Non-Newtonian fluids can be subdivided into shear thinning (pseudoplastic) and shear thickening (dilatant) materials. Materials which exhibit shear thinning behaviour show a decrease in viscosity as the shear rate increases. Shear thinning can be described mathematically by the Power law model (e.g. Harris, 1977):

$$\sigma = k\dot{\gamma}^n \qquad \text{Equation 1.2}$$

where n, the Power law index ($n < 1$), is a measure of the degree of non-Newtonian behaviour and k is the viscosity coefficient; the higher the value of k the more viscous the fluid. Materials that exhibit shear thickening behaviour show an increase in viscosity as

the shear rate increases (Barnes, 1989). Shear thickening can also be described mathematically using the Power law equation, where the shear rate index is ($n > 1$).

The third time-independent response, where a shear stress independent viscosity is achieved once a finite yield stress has been surpassed, can be described using the Bingham model (discussed below).

1.5.2. The Yield Stress

The existence of the dynamic yield stress for any material is still controversial. Barnes and Walters (1985) contend that the dynamic yield stress is nothing more than an empirical constant that depends upon the experimental conditions and is thus not a real physical property. With the advent of rheometers capable of measuring shear rates in the region of 10^{-5} 1/s, the question of whether samples exhibit a yield stress is further questioned. Hartnett and Hu (1989), in an attempt to disprove Barnes and Walter's claim, performed an experiment where a ball placed in a fluid failed to travel any measurable distance over an extended time period. Furthermore, a logarithmic plot of the viscosity versus shear stress will tend to infinity for yield stress samples (Nguyen and Boger, 1992).

Yield stress fluids are structured materials, where the rheology is strongly dependent on the history and it has, therefore, been found that the yield stress can be sensitive to the duration and time of measurement (Cheng, 1986). Recognising the problem involved in experimental determination of the yield stress, Blair (1933) proposed a practical definition of the yield stress as "any critical stress below which no flow can be observed under the condition of experimentation". The British Standard (1975) definition of the yield stress is "the stress above which the substance is an elastic solid and below it is a liquid with a plastic viscosity, η" such that:

$$\sigma = \sigma_y + \eta\dot{\gamma}$$

where σ_y is the yield stress that must be exceeded to start flow. The minimum stress required to initiate flow in a yield stress fluid, however, is not necessarily the dynamic yield stress described above, but rather the static yield stress.

1.5.2.1. Rheological Models for Yield Stress Fluids

Several empirical and theoretical models have been proposed and used to describe the rheological behaviour of yield stress fluids. Typically, three yield stress values characterise the rheological behaviour of a material. The first is the elastic-limit yield stress and represents the transition between the elastic and plastic deformation. The static yield stress is defined as the minimum stress necessary to deform irreversibly the material. Whilst the value obtained by extrapolation of the flow curve is known as the "apparent" yield stress or the dynamic yield stress. On several occasions, a given fluid can be equally described by more than one model, resulting in different yield stress values (Keentok, 1982; Nguyen and Boger, 1983).

The Bingham model represents the ideal case where the structure responsible for the yield stress breaks down completely as soon as the applied shear stress overcomes the yield value. The Bingham model states that shear rate independent viscosity is maintained once a yield stress has been exceeded.

$$\sigma = \sigma_y + \eta_B\dot{\gamma} \qquad \text{Equation 1.3}$$

where σ_y is the yield stress and η_B is the Bingham viscosity.

In most cases, the linearity of the flow curve is only obtained at high shear stresses or shear rates. This is probably because the structure responsible for the yield behaviour

may breakdown gradually during shear and its complete disruption may occur only at high stresses (Nguyen and Boger, 1992). Non-linear behaviour may be described by the following empirical equation, originally proposed by Herschel and Bulkley (1926):

$$\sigma = \sigma_{HB} + k\dot{\gamma}^m$$

where τ_{HB} is the yield stress and k and m are constants, equivalent to the power law parameters commonly used for approximating the behaviour of many viscous fluids. When $m < 1$ the fluid is yield pseudoplastic, and $m > 1$ corresponds to yield dilatant behaviour. If $m = 1$ the equation reduces to the Bingham equation.

1.6. Electrorheological Fluids

Electrorheology describes the rapid and reversible change in viscosity exhibited by certain suspensions of solid particles in electrically non-conducting liquids upon application of an electric field (e.g. Winslow, 1949; Block and Kelly, 1988). Electrorheological (ER) fluids can run freely like water, ooze like honey or solidify like gelatine, depending on the electric field. The ER response is extremely rapid; although full structure formation after application of an electric field can take several seconds, the viscosity increases significantly over a millisecond time scale (Sprecher et al., 1987; Halsey, 1992; Weiss and Carlson, 1992; Klingenberg et al., 1993). The ER effect is completely reversible upon removal of the applied electric field.

In the absence of an electric field most ER fluids, to a first approximation, behave as Newtonian fluids in accordance with Equation 1.1. Upon application of an electric field, typically between 1-5 kV/mm, ER fluids undergo a pseudo-phase change from liquid to solid which may be described by the Bingham equation (Equation 1.2) (Uejima, 1972; Gast and Zukoski, 1989; Marshall et al., 1989; Klingenberg, 1990). The existence of a

static yield stress is demonstrated by the solidification of an ER fluid between two electrodes (Winslow, 1949; Bullough, 1992). In addition, falling ball experiments described previously were conducted by Zitter and co-workers (1994a and b) under the influence of an electric field. An electric current is observed to flow through the fluid when it is subjected to the electric field; the response is non-ohmic (Brooks, 1990).

1.6.1. Applications

ER fluids have been implicated in the design of ubiquitous devices such as clutches, first proposed by Winslow (1947) and subsequently modified and improved by Stevens et al. (1988), Monkman (1993) and Stanway and Sproston (1994). The potential uses of ER fluids, extends beyond the automotive industry into robotics, where their application in "pick and place" robots (Shulman et al., 1981) and shape-sensing finger pads (Monkman, 1992) have been proposed

The potential of ER fluids beyond the realms of engineering has only recently begun to be realised. The rapid and easily controlled response time of ER fluids together with the strength and elasticity of siloxane gel have been exploited to create an artificial striated skeletal muscle (Bohon and Krause, 1998). Composite gels of differing ratios were prepared and subjected to dc and ac electric fields ranging from 300 V/mm to 2.5 kV/mm. Electric field magnitude and ER fluid concentration were found to influence the displacement, or the ability of the gel to compress, between two flexible electrodes. The concentration of siloxane gel was critical in terms of the restoring properties of the composite gels upon removal of the electric field. Bohon and Krause (1998) concluded that the reality of an artificial muscle was achievable with the advent of active ER fluids at low applied electric fields.

In 1996, despite efforts to improve ER fluids and eliminate their shortcomings, Parthasarathy and Klingenberg (1996) pronounced that there were currently no

commercially available ER fluid based device; a statement which holds true today. The main limitation has been the lack of effective fluids in terms of properties, stemming largely from insufficient understanding of the underlying mechanisms (Hartsock et al., 1991; Weiss et al., 1993). The presence of water in fluids introduces problems associated with current and temperature limitations of the device (Gast and Zukoski, 1989; Weiss and Duclos, 1994). Applications require fluids with large field-induced rheological changes, low conductivities (small power requirements), and which are non-abrasive, environmentally benign, and stable against sedimentation, irreversible flocculation, and chemical degradation (Hartsock et al., 1991).

1.6.2. Composition of Electrorheological Fluids

The substrates used over the past fifty years to formulate ER fluids are so diverse that the conclusion might easily be drawn that, given the right additive, almost any particle could be used (Block and Kelly, 1988). However, it is recognised that there are a number of attributes common to all the materials used in the particulate phase, namely hydrophilicity, porosity and the ability to polarise under an electric field (Stangroom, 1983). A comprehensive list of candidates for the dispersed phase can be found in the reviews by Block and Kelly (1988) and Gast and Zukoski (1989). Table 1.1 highlights several pharmaceutically acceptable compositions.

Most formulations require the presence of water, in the range between 5 and 10 % by weight (Block and Kelly, 1988), to activate or enhance performance (Winslow, 1949; Klass and Martinek, 1967; Block and Kelly, 1988). Furthermore, complete drying of these formulations has been shown to result in the destruction of the ER effect (Uejima, 1972; Deinega and Vinogradov, 1984; Kordonsky et al., 1991; Kawai et al., 1994 and 1996). With systems where additives are necessary, water is not unique as alcohols (Takeo and Omura, 1976), ethylene glycol (Winslow, 1953), dimethylamine and formamide (Takeo

and Omura, 1976) have all been proposed as alternatives to water. In general, it is thought that the activated systems are all capable of ionic conductance.

Particulate phase	Dispersing medium	Additive	Reference
Gelatine	Olive oil Mineral oil	Water	Winslow (1947)
Microcrystalline cellulose	Silicone oil	Water	Yatsuzuka et al. (1995) Kawai et al. (1996)
Silica	Silicone oil	Water	Kawai et al. (1994) Kawai et al. (1996)
Starch	Mineral oil	Water	Winslow (1947)

Table 1.1. Examples of electrorheological fluid composition

1.6.2.1. Particle Size and Shape

In most cases, the diameter of the particles used in ER fluids range from 10 to 100 μm (Winslow, 1947 and 1949; Stangroom, 1983; Block and Kelly, 1988; Stanway and Sproston, 1994); the limits beyond which no ER activity is evident are not clearly defined. Large particles are undesirable in ER fluid formulations for a number of reasons, not least their increased propensity to more rapid sedimentation in the non-electrified state. The electrode gap places an upper limit on particle size, as a result it is generally recommended that the maximum particle size be less than one-tenth of the distance between the electrodes (Stangroom, 1983). A lower limit must exist, as at some stage Brownian motion may overcome the interactions that give rise to the ER effect (Block and Kelly, 1988). Several researchers have investigated the effect, both experimentally (Shih and Conrad, 1994) and theoretically (Ota and Miyamoto, 1993 and 1994), of particle size on the ER response. Shih and Conrad (1994) discovered an increase in yield stress values

with particle size. Whilst Ota and Miyamoto (1994) investigated the optimum particle-size distribution using a complex simulation involving the many-body effect (or cubic-particle chain model) and discovered that ER fluids consisting of the same size particles gave the largest yield stress.

Particle shape may play a part in the ER effect. In an electric field, elongated particles combine effectively forming complex structures (Asano et al., 1997), but form weaker connections at the electrode surface compared to spherical particles. Fibres and elongated particles are known to undergo much larger polarisations than spheres, so that on polarisation grounds such particles may be more advantageous in ER applications (Block, 1992).

1.6.2.2. Disperse Phase Concentration

The response of ER fluids to the application of a field is strongly dependent upon the concentration of the disperse phase. Increasing the concentration of the dispersed phase not only increases the yield stress (Jordan and Shaw, 1989; Stanway and Sproston, 1994) of the fluid in the presence of an electric field, but also enhances the zero-field viscosity due to particle crowding i.e. the higher the viscosity, the more energy is expended in forcing the base fluid around the closely packed particles. Of course, by this reasoning, it follows that the zero-field viscosity can be decreased by lowering the volume fraction. However, by doing this, a larger electric field is required to produce a similar yield stress enhancement. For best results, the particulate phase should make up between 10 to 40 % by weight of the mixture (Pool, 1990).

1.6.2.3. The Continuous Phase

Adriani and Gast (1988) predicted that ER activity will occur in any system where there is a substantial difference in dielectric permittivity between the dispersed phase and

the medium. Stangroom (1984) lists the desired properties of the liquid and includes hydrophobicity, low viscosity, high boiling point, low freezing point, high electrical resistance and high dielectric strength. In practice, it is difficult to obtain liquids of a high dielectric constant owing to the rigorous purification requirements when used in high field applications (Gallagher, 1975). Thus, in practice, the continuous medium is nearly always of low permittivity and is usually an insulating oil. A list of the more common carrier liquids has been compiled by Block and Kelly (1988). Such liquids can withstand both contamination without adverse effects and high electric fields without breakdown. Obviously, low conductivity is desirable for the reduction of power consumption.

1.6.2.4. Applied Electric Field

Generally, electric fields in excess of 1 kV/mm are applied with fluids operating practically at much larger fields. Dielectric breakdown places an upper limit on the electric field (Block and Kelly, 1988). Little research has been carried out in the field of electrorheology on the behaviour of ER fluids at low applied electric fields (below 1 kV/mm). Upon application of an electric field of the order 1 kV/mm, ER fluids exhibit yield stress values ranging from 10 to 15000 Pa (Chen et al., 1991).

The quest for high yield stress ER fluids dominates the literature, where the need for such fluids is driven by the nature of the applications (e.g. brake and clutch proposals). In response to Block (1988), several investigators have conducted experiments below 1 kV/mm and acknowledged the development of an ER response (Marshall et al., 1989; Chen et al., 1991; Gandhi and Thompson, 1992; Parthasarathy and Klingenberg, 1996; Wu et al., 1996; Hao, 1997; Lue and Mao, 1997). The formation of a yield stress was not observed until 240 V/mm by Lue and Mao (1997) using a corn starch in silicone oil dispersion; the yield stress at 240 V/mm, estimated from the published graphs, was 1 Pa rising to 8 Pa at 600 V/mm. Gandhi and Thompson (1992) investigated the rheological

properties of an ER fluid comprising of 45 % corn starch and 55 % silicone oil, at electric fields as low as 20 V/mm. The yield stress values were estimated, from published graphs, to be approximately 5, 8, 10 and 100 Pa for applied electric fields of 20 V/mm, 50 V/mm, 100 V/mm and 600 V/mm respectively. A volume fraction of 0.13 lithium poly(methacrylate) dispersed in a chlorinated hydrocarbon oil was investigated by Marshall et al. (1989) at applied electric fields of 50, 100, 200 and 400 V/mm. We have estimated the yield stress values, at a shear rate of 10^{-4} 1/s, are 0.001, 0.006, 0.02 and 0.1 Pa respectively. Sakai et al. (1997) predicted the formation of particle chains, albeit sparse, at applied electric fields as low as 50 V/mm. To the best of our knowledge, there is no published review of ER behaviour at low applied electric fields.

1.6.3. Mechanisms

The occurrence of a yield stress suggests the presence of structure. In Winslow's original publication (1949), he observed that upon application of an electric field, the particles within an ER fluid aligned in the direction of the field forming a chain-like or fibrous structure. Such fibrils are considered to be of paramount importance in the ER phenomenon, as they are presumed to provide the mechanical support which led to the development of a yield stress. Several mechanisms have been proposed (reviewed by Parthasarathy and Klingenberg, 1996) for the origin of the ER effect, of which electrostatic polarisation and water bridging have received most attention. Although the electrostatic polarisation mechanism appears to explain most experimental observations, other phenomena are likely to influence behaviour in some systems and under some conditions. Furthermore, given the chemical diversity of ER fluids, it seems unlikely that they all work in exactly the same manner.

The electrostatic polarisation mechanism, proposed originally by Winslow (1949), attributes the origin of the ER effect to the field induced polarisation of the disperse phase

relative to the continuous phase. In this model's most general form, polarisation can arise from a number of charge transport mechanisms, including electronic, atomic, dipolar, nomadic or migration (interfacial) polarisation. Ignoring any net particle charge, a particle's charge distribution can be described as a dipole aligned with the applied electric field. Neighbouring dipolar particles are attracted to each other when pairs are aligned with the external field, and repel when perpendicular to the field, thus producing the fibrous structures observed experimentally. In order for the suspension to flow, the fibrous columns must be deformed or broken; the large increase in shear stress, and thus the apparent viscosity, arises from the work required to overcome the attractive dipolar particle interactions. The most widely accepted polarisation mechanisms involve bulk or interfacial processes (Klass and Martinek, 1967; Gast and Zukoski, 1989; Block et al., 1990). Bulk polarisation involves creation or alignment of molecular dipoles within the confines of the particulate or continuous phase. Interfacial polarisation can involve migration of charge through the particles, along the surface of the particles, or within the double layer region of the dispersion (Havelka and Pialet, 1996). The electrostatic model assumes that the ER fluids are dispersions of dielectric, non-conducting particles in a low dielectric medium and that free charges and charge transfer can be neglected. This model is based on the fact that particles polarise and apply a force to neighbouring particles as a result of the permittivity mismatch between the particles and the continuous phase. In practice, ER fluids are more complex. A number of studies have been carried out to extend this model to include conductivity (Wu and Conrad, 1997a).

One theory proposed by Stangroom (1983) proposed the formation of water bridges between adjacent particles, the number of which depends on the electric field and moisture content. When the field is applied, ions move out of the pores, carrying water to the particle surface and thus permitting the formation of bridges between particles. When the field is removed, surface tension pulls the water back into the particle pores. See et al.

(1993) support the formation of water bridges as the underlying mechanism, whilst Tamura et al. (1993) modified the theory introducing interfacial polarisation. Furthermore, as water in bulk has a large dielectric constant (Gast and Zukoski, 1989) and can generate mobile ions (either by solvation or self-dissociation). However, its influence on particle polarisation and its ability to alter the response through electrostatic polarisation mechanism should not be ignored. Water adhering to the surface of particles could greatly increase their dielectric constant as water is easily polarised. However, the advent of anhydrous ER fluids (Block and Kelly, 1988; Filisko and Radzilowski, 1990; Gow and Zukoski, 1990) has provided counter evidence for the necessity of water. Thus, while water may play a role in some systems, it is unlikely that water alone produces an ER effect.

Pertinent to these pharmaceutical studies, is the possibility that certain suspensions exhibit an electrically induced decrease in apparent viscosity. The so-called "negative" ER effect, is believed to be as a direct result of electrophoresis (Boissy et al., 1995). Traditionally, the particulate phase in ER fluids is of a higher conductivity than the suspending fluid. The inability of these new fluids to form stable chains upon application of an electric field arises from the attraction of the low conductivity particles to one electrode (Boissy et al., 1995; Trlica et al., 1996; Wu and Conrad, 1997b). This novel ER response has been demonstrated by poly (methyl methacrylate) in mineral oil (Boissy et al., 1995) and magnesium hydroxide in silicone oil (Trlica et al., 1996).

Chapter Two

General Characterisation of Materials

2.1. Materials

Microcrystalline cellulose (MCC) was kindly donated by Penwest Pharmaceuticals Co. (Patterson, USA). Three grades of MCC were employed: Emcocel 50M (Lot No. E5D7C21), LM50 (Lot No. L5S6003X) and XLM90 (Lot No. X9F5003X). Laboratory grade poly(dimethyl-siloxane) 200® fluid (silicone oil) of dynamic viscosity 100 cSt (25 °C) was supplied by Aldrich (Gillingham, UK). In order to remove any traces of moisture, the silicone oil was kept over a molecular sieve (8-12 mesh, Aldrich, Gillingham, UK), which was replaced every six weeks. Super-refined oils were received from Croda Oleochemicals (Goole, UK). In order to prevent rancidity, these oils were stored in well-filled, air-tight, light-resistant containers under nitrogen. Linoleic acid (*Z,Z*-9,12-octadecadienoic acid) and oleic acid (*Z*-9-octadecenoic acid) were supplied by SAF (Poole, UK). Linoleic and oleic acids were stored in air-tight, light-resistant containers under nitrogen at 2 °C.

Oil	Batch number	Oil	Batch number
Linoleic acid	110H8452	Peanut	PP5/504
Oleic acid	105H8449	Safflower	PP5/517
Almond	PP4/408	Sesame seed	PP6/326
Apricot kernel	PP4/466	Soyabean	PP6/345

Table 2.1. Batch numbers for super-refined oils

Tacrine hydrochloride hydrate (BN: 86H3647) was obtained from SAF (Poole, UK) and stored desiccated below 4 °C. All other chemicals and solvents used were of HPLC grade (Fisons Scientific Equipment, Loughborough, UK). Throughout this thesis tacrine hydrochloride hydrate has been abbreviated to tacrine.

2.2. Characterisation of Materials

2.2.1. Preparation of Size Fractions and Particle-Size Analysis

A representative sample of MCC powder was separated according to size using a vibrational dry-sieving technique and particle-size distributions were separately determined. MCC powders were sieved in 25-30 g lots on a stack of test sieves (BS and ISO specifications; Endecotts Ltd., London, UK), of nominal aperture diameters 125, 90, 75, 63 and 45 μm. The sieve stack was mechanically vibrated (Fritsch Analysette, Christison Scientific, Gateshead, UK), at approximately 50 Hz, for two periods of 15 min. The sieves were cleaned with a brush, to unblock the mesh between sieving. Each sieve fraction was then air-jet sieved (Alpine, Augsburg, Germany) for 6 min in order to remove undersized particles (or fines). In addition, particles having a sieve fraction below 45 μm were collected.

Two methods, depending on the nature of the material, were employed to determine the particle-size distributions. Particle-size analysis of all the materials studied was by laser light scattering (LLS), with a Malvern Mastersizer X (Malvern Instruments Ltd., Malvern, UK). The scattered light from the cloud of powder traversing the laser beam is collected to a multi-element detector. Using a Fourier Transform lens, the scattered light is presented as a stationary diffraction pattern. The scattering of the particles is predicted by either Fraunhofer, or more generally the Mie theory (Malvern Instruments Technical Information). The particle diameter was calculated by comparison with a spherical particle of an equivalent volume and quoted as the median particle diameter. For each method, three readings were carried out on each sample.

a) Dry-Powder Feeder

The LLS was configured to be used in conjunction with a dry powder feeder, into which a representative powder sample was placed. The 300 mm lens was chosen, enabling

particles between 1.2 to 600 μm to be detected. The laser was switched on and a background reading performed. The feeder was switched on and the powder agitated, before traversing the laser beam. Size analysis on LM50 and XLM90 was conducted on the sieve fraction below 45 μm.

b) Stirred Sample Cell

The particle-size distribution of tacrine was measured using the stirred sample cell in conjunction with the 45 mm lens enabling particle sizes as low as 0.1 μm to be measured. When using a wet cell, a suitable dispersant is used to suspend a representative powder sample. In this case, 0.1 % lecithin in cyclohexane was found to form an adequate dispersion. The dispersion was sonicated (Decon FS300b, Decon®, UK) for 5 min prior to measurements. The stirred sample cell was filled with 0.1 % lecithin in cyclohexane and allowed to circulate, before a background reading was taken. Using a pipette, the drug dispersion was added to the cell until an obsuraction (or the laser obstruction) of 15-20 % was achieved.

2.2.2. Scanning Electron Microscope

The scanning electron microscope has provided much of the information required on the particle shape. It was found that all MCC needed to be dried at 60 °C for 24 h before observation. This was to minimise initial problems associated with charging of the particles, caused by the presence of residual moisture. Samples were mounted on aluminium discs using double-sided adhesive tape and sputter coated with gold (Sputter Coater, Model S15B, Edward's High Vacuum, Sussex, UK). To prevent charring of the samples, coating was carried out for two periods of 5 min using a chamber pressure of 7 mBar. Scanning electron microscope studies (JSM 6330, Japanese Electron Optics Ltd, Tokyo, Japan) were carried out using an incident beam of 10 kV, which was selected to

avoid sample damage. Samples of tacrine were visually examined under a scanning electron microscope (JSM 6310, Japanese Electron Optics Ltd, Tokyo, Japan). The samples were coated with gold for two periods of three min each. Photomicrographs were taken with the accelerating voltage set to 15 kV.

2.2.3. Moisture Content Measurements

Water content of the powders was determined using a Mettler LP16 Infrared Dryer (Mettler Toledo AG, Switzerland) linked to a Mettler PM 2500 Delta Range balance (Mettler Toledo AG, Switzerland). This method of moisture determination utilises infrared radiation to penetrate the material and heat it from the bottom. A sample of MCC (~ 1 g) was heated to 105 °C, until constant weight was achieved (British Pharmacopoeia, 1993). Three readings were taken and the mean value calculated.

2.2.4. True Density Determination of Microcrystalline Cellulose

Powder true density was determined using helium pycnometry (AccuPyc 3310, Micromeritics, USA). All powders analysed were dried in a forced convection oven (Gallenkamp Incubator, Model 1H-ISO, UK) at 60 °C for 24 h. The dried powder (~ 1.5 g) was accurately weighed into the sample cell. Helium gas was used to pressurise the sample chamber and the pressure recorded. An additional volume was connected to the sample cell and the subsequent pressure recorded. From the pressure readings, the volume of the sample cell and the additional volume, the true density of the sample was determined. The true density was calculated by dividing the mass of the sample by the sample volume. The pycnometer calculates the mean true density value from ten readings.

The true density of Emcocel 50M was found to be 1.581 g/cm^3 (± 0.002).

2.2.5. Determination of the Relative Density of Silicone Oil

The precise volume of a capillary stopper density bottle (Fisher Scientific, Loughborough, UK) was determined at 37 °C by weighing before and after the addition of Milli-Q water, free from air (degassed using helium). This determination was performed five times and a mean value calculated. The volume was calculated by dividing the weight by the known density of water at 37 °C (0.993360 g/ml) (Handbook of Chemistry and Physics, 1969). All oils were gently heated in a Gyratory water bath shaker (Model G76, New Brunswich Scientific Co. Inc., New Jersey, USA) to approximately 37 °C. After thermal equilibration, the oils were placed in the calibrated density bottle and weighed. The temperature of each oil was verified (Jenway 2060 thermometer, ± 0.5 °C, UK), after each weighing. The results were replicated (n = 5) and mean density values calculated.

2.2.6. Solubility Determination of Tacrine in Distilled Water

The solubility of tacrine was determined, by UV analysis, following the equilibration of a saturated solution (Pharmaceutical Codex, 1979). The saturated solution was equilibrated in a gyratory water bath at 25 °C and 37 °C over 24 h. After equilibration, the vial was centrifuged and the concentration of the supernatant determined at a wavelength of 240 nm. Five measurements were carried out at each temperature.

The solubility of tacrine hydrochloride hydrate in distilled water at 25 °C and 37 °C was 74 mg/ml (± 0.54) and 82 mg/ml (± 0.36) respectively.

2.2.7. Determination of the Silicone Oil/Water Partition Coefficient

The partition coefficient (P) of a solute is defined as the ratio of the concentration in the two phases at equilibrium, and is usually presented as: $P = C_o/C_w$, where C_o is the concentration of the solute in the organic phase and C_w is the concentration of the solute in the aqueous phase. The partition coefficient of tacrine in silicone oil/water was measured

using a shake-flask method (Pharmaceutical Codex, 1979). A solution of tacrine in distilled water was prepared and shaken with an equal volume of silicone oil. The aqueous drug phase was equilibrated with the silicone oil for 24 h at 37 °C. The two phases were separated and the aqueous phase analysed by UV spectrophotometry for drug concentration (n = 5).

2.2.8. Dielectric Constants Determination

The behaviour of ER fluids in response to an applied electric field is thought to be governed by a mismatch in the dielectric constants between the disperse and suspending phases (Gow and Zukoski, 1990). The dielectric constant is a measure of how easily a material polarises in an electric field and can provide a useful prediction of the effectiveness of the ER fluid. The dielectric constant can be calculated using a parallel plate capacitor to measure the capacitance (or the ability to store electric charge).

$$C = \frac{\varepsilon_0 \varepsilon' A}{d} \qquad \text{Equation 2.1}$$

where A is the area of the plates (m^2), d is the distance between the plates (m), ε_o is the permittivity of free space (8.85×10^{-12} F/m) and ε' is the dielectric constant of the material.

The measurement of the dielectric constant under quiescent conditions was carried out using a static permittivity micrometer Jig D321 (General Radio, UK) in conjunction with a GenRad 1689M Precision RLC Digibridge (universal bridge used to measure inductance, capacitance and resistance). A sinusoidal alternating voltage (ac) at approximately 1.275 V was generated in the form of a periodic waveform denoted by frequency. It is assumed that the applied electric field is low enough to ignore interactions between particles and hence chain formation. The parallel-plate capacitor employed in the

dielectric constant measurements is illustrated in Figure 2.1. The upper (UE) and central lower (CE) electrodes have diameters of 34.2 and 52.0 mm respectively, with the lower electrode having a outer PTFE guard.

The zero-gap point was measured by decreasing the plate separation whilst monitoring the resistance on the RLC Digibridge (set to 1 kHz or default). The air capacitance was measured 10 times and the mean value calculated. As $C_{air} = \varepsilon_o A/d$, where A is the surface area of the electrode, then it follows that $C_{air}d$ should be constant and take the value of $\varepsilon_o A$. Assuming no edge effects, this cell constant should be 8.13 pFmm. The cell is so designed that edge effects are considered negligible at the gaps used.

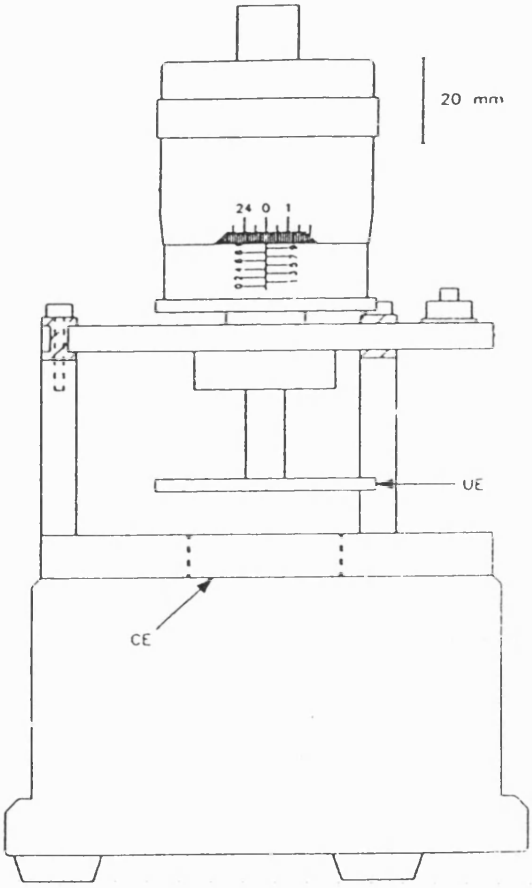

Figure 2.1. Diagrammatic representation of the parallel plate capacitor (Reproduced from Rattray, 1994).

A small volume of the fluid to be tested was poured on to the middle of the lower electrode, and the upper electrode slowly lowered to minimise the risk of trapping air bubbles. The gap between the plates was 250 μm (± 0.5 %). Measurements were made over the frequency range 12 Hz -1 x 10^5 Hz using the GenRad 1689M Precision RLC Digibridge (General Radio, UK). For each frequency, five measurements were taken and the mean value calculated. All dielectric measurements were made at ambient temperatures (typically 20 - 22 °C). The dielectric constant of 100 cSt silicone oil and the other oils have been calculated in the following experiments. The effect of the addition of the disperse phase (MCC sieve fraction below 45 μm) has also been investigated along with the relationship between concentration of the disperse phase and dielectric constant.

2.2.9. Assay of Tacrine by Ultraviolet Spectrophotometry

A 7.5 μg/ml solution of tacrine in distilled water was prepared and a scan performed on a double-beam spectrophotometer (Perkin Elmer, Beaconsfield, UK) using 1 cm path length quartz cuvettes. The solution was scanned, over the range 190 to 390 nm, to determine a suitable wavelength for UV assay. This procedure was repeated for tacrine in propan-2-ol.

A validation of the Beer-Lambert law was undertaken to ensure a linear relationship existed between the concentration of tacrine and the absorbance. Triplicate stock solutions (A, B and C) of approximately 50 μg/ml tacrine in distilled water were prepared. A series of standard solutions (5 dilutions) were prepared, in duplicate, from each stock solution to cover the concentration range 0.5 to 6.0 μg/ml. Triplicate readings were made for each standard solution. Similarly, a series of standard solutions were prepared covering the concentration range 1.0 to 25.0 μg/ml and the UV absorbance determined at 324 nm. A validation of tacrine in propan-2-ol, over the aforementioned concentration range, was also conducted at a wavelength of 324 nm.

2.3. Results and Discussion

2.3.1. Preparation of Size Fractions and Particle Size Analysis

Particle-size data for MCC powders are shown in Table 2.2. Particle-size distributions for Emcocel 50M, LM50 and XLM90 are presented in Appendix One (A 1.1 to A 1.7).

Material	d (0.1)		d (0.5)		d (0.9)	
	Mean	SD	Mean	SD	Mean	SD
Emcocel 50M						
90 – 125 μm	78.43	1.02	128.34	4.56	200.33	2.62
75 - 90 μm	59.47	1.58	106.64	1.25	179.39	0.38
63 - 75 μm	51.85	1.14	90.12	1.23	155.74	1.18
45 - 63 μm	36.56	0.99	68.32	2.08	125.81	0.70
< 45 μm	13.29	0.17	32.99	0.83	70.61	0.22
LM50 (< 45 μm)	4.93	0.21	26.36	1.79	70.94	4.81
XLM90 (< 45 μm)	12.30	0.99	35.82	1.12	72.01	3.29

Table 2.2. Particle-size analysis of Emcocel 50M, LM50 and XLM90 sieve fractions.

Laser light scattering methods assume that the particles are spherical and present data in terms of an equivalent volume diameter, that is the diameter of a sphere having the same volume as the particle under analysis. Scanning electron photomicrographs indicate the MCC particles are cylindrical and this may account for the higher than expected median diameters obtained.

Tacrine was found to have a wide size-distribution with 90 % of particles below 30.35 (± 1.02) and 10 % below 0.33 (± 0.00). The median equivalent volume particle diameter for tacrine was 5.47 (± 0.06). The particle-size distribution is shown in Appendix One (A 1.8). The particle size properties were considered acceptable for the present study and therefore the tacrine was used as supplied.

2.3.2. Scanning Electron Microscope

The scanning electron photomicrographs shows Emcocel 50M particles to be irregularly shaped, with some particles appearing almost dendritic and some roughly spherical. Figure 2.2 shows the scanning electron photomicrograph of Emcocel 50M of sieve fraction 90 - 125 μm. The remaining photomicrographs are displayed in Appendix Two (A 2.1 to A 2.4). Inherently low moisture grades of MCC (LM50 and XLM90) are shown in Appendix Two (A 2.5 and A 2.6 respectively). These particles, as for Emcocel 50M, are typically irregularly shaped. The tacrine particles are irregularly shaped with a wide particle distribution (Figure 2.3).

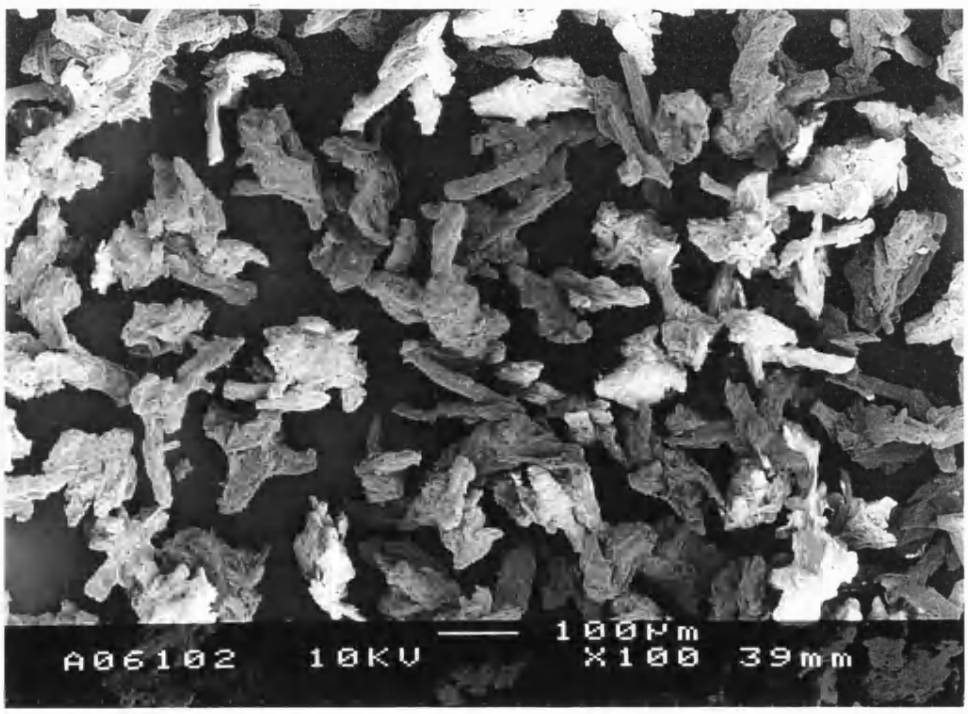

Figure 2.2. Scanning electron photomicrograph showing Emcocel 50M (sieve fraction 90 - 125 μm) at an accelerating voltage of 10 kV (x 100).

Figure 2.3. Scanning electron photomicrograph showing tacrine at an accelerating voltage of 15 kV (x 1000).

2.3.3. Moisture Content Measurements

The moisture contents of the three grades of Emcocel employed in these studies are shown in Table 2.3.

Material	Moisture content (%)	Nominal moisture content (%)*
Emcocel 50M	4.21 (0.06)	< 6.0
Emcocel LM50	2.87 (0.27)	< 3.0
Emcocel XLM90	1.69 (0.12)	< 1.5

Table 2.3. Moisture content of Emcocel samples. Standard deviation values are shown in brackets (n = 5). *Moisture content determined by Penwest Pharmaceutical Co. Patterson, New York, using a loss on drying method.

The moisture contents of different grades of Emcocel were determined and found to be comparable to the technical information provided (Penwest Pharmaceuticals Co.). The low moisture grades of MCC (LM50 and XLM90) were sieved in a temperature controlled environment (21.0 ± 0.2 °C) with variable humidity (~ 45 %). Under these experimental conditions, the hygroscopic nature of MCC is likely to result in moisture uptake during the sieving process. LM50 and XLM90 are dried to the required moisture content prior to packaging, thereby retaining similar physicochemical properties to Emcocel 50M.

2.3.4. Determination of the Relative Density of Silicone Oil

The relative density of each oil at 37 °C is given in Table 2.4. The density of 100 cSt silicone oil, at 20 °C, quoted by the manufacturer, was 0.960 g/ml, which is comparable to the value obtained (0.95511 g/ml).

Material	Density (g/ml)	Standard deviation
Silicone oil (100 cSt)	0.95511	2.15×10^{-3}
Almond oil	0.90247	1.71×10^{-4}
Apricot oil	0.90277	4.37×10^{-4}
Peanut oil	0.90174	2.97×10^{-4}
Safflower oil	0.90944	2.45×10^{-4}
Sesame seed oil	0.90389	2.37×10^{-4}
Soya bean oil	0.90903	1.66×10^{-4}

Table 2.4. Relative density measurements of silicone oil and other oils at 37 °C.

2.3.5. Determination of the Silicone Oil/Water Partition Coefficient

The silicone oil/water partition coefficient was calculated to be 0.104 (± 0.003). Sathyan et al. (1995) calculated the partition coefficient of tacrine in mineral oil/water to be 0.79. The value calculated is relatively low considering the lipophilic nature of tacrine (Madden et al., 1995). The criteria outlined for the choice of organic phase

(Pharmaceutical Codex, 1979), namely that the phases are immiscible and of high purity enabling good reproducibility, have been fulfilled. The partition coefficient provided a measure of the affinity of tacrine for the silicone oil. The value calculated does not represent the situation in the diffusion cell, as the drug is diffusing from silicone oil into the aqueous medium.

2.3.6. Dielectric Constant Determination

The distance between the electrodes was 250 μm (2.5×10^{-4} m) and the cell constant ($\varepsilon_o A$) as calculated from the air capacitance (32.1 pF ± 0.2) was found to be 7.78 pFmm (± 0.2) (7.78×10^{-15} Fm). Using Equation 2.1, the dielectric constant at each frequency was calculated from the measured capacitance. Figure 2.4 shows the dielectric constants for silicone and BP oils obtained over the frequency range 12 Hz to 10^5 Hz. The dielectric constant of 100 cSt silicone oil was 2.74, which is comparable to other values obtained (Conrad et al., 1991; Sprecher et al., 1992). In all the oils studied, the dielectric constant exhibited a gradual decrease over the frequency range 12 Hz to 10^5 Hz. The dielectric constants for the BP oils were higher than silicone oil, indicating an increased ability to store charge.

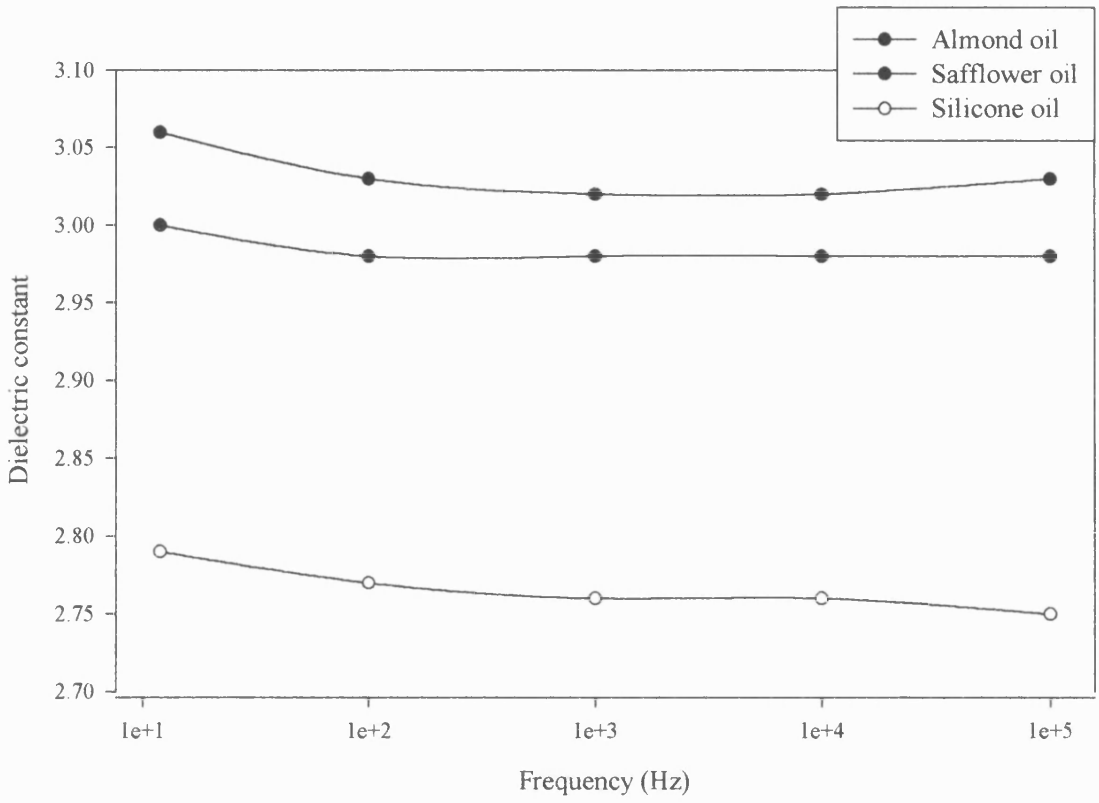

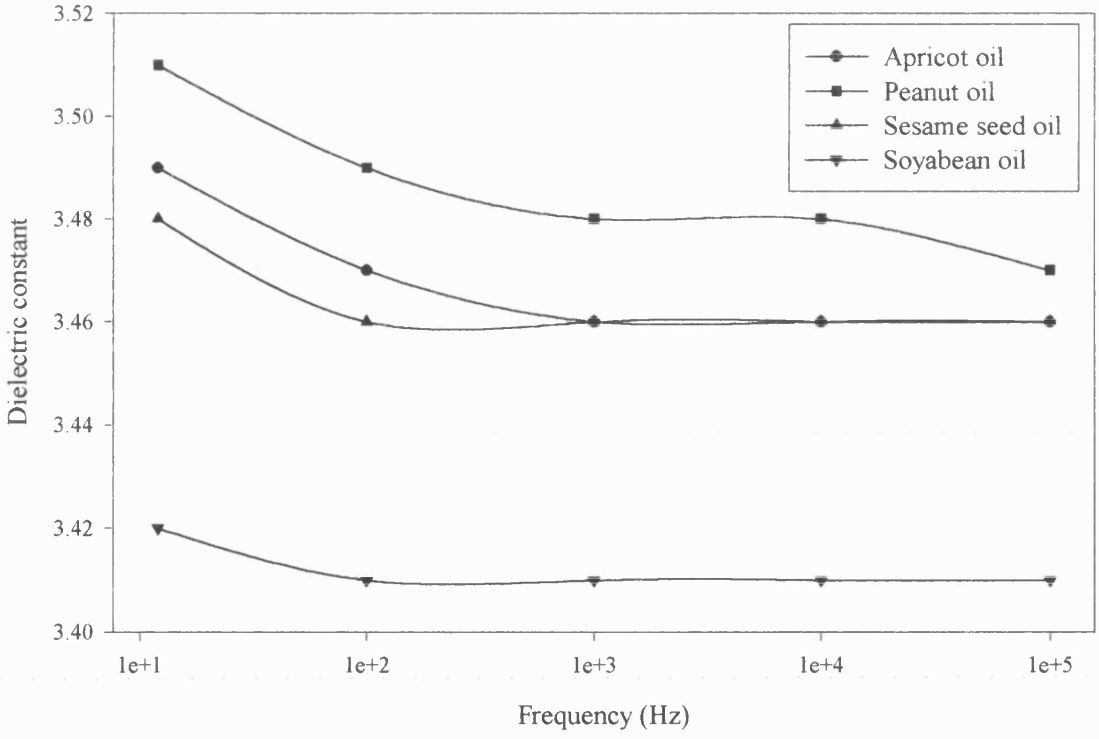

Figure 2.4. Dielectric constants over a range of frequencies of silicone oil and various BP oils. Error bars representing the standard deviation (n = 5), are smaller than the symbols used.

The effect of disperse phase concentration on the dielectric constant is shown in Figure 2.5. The dielectric constant was observed to slightly decrease with increasing frequency for the ER fluids studied in the quiescent state. This response is mirrored in studies of ER fluids in ac fields which have revealed a decrease in viscosity with frequency (Klass and Martinek, 1967; Uejima, 1972). When an ac electric field is applied to a dielectric material the polarisation requires time to reach equilibrium. The decrease in the ER effect at high frequencies is indicative of a migration polarisation mechanism (Block et al., 1988; Weiss et al., 1993; Hao et al., 1995). This effect can be understood by considering the time-dependence for particle polarisation and the resulting particle-particle interactions.

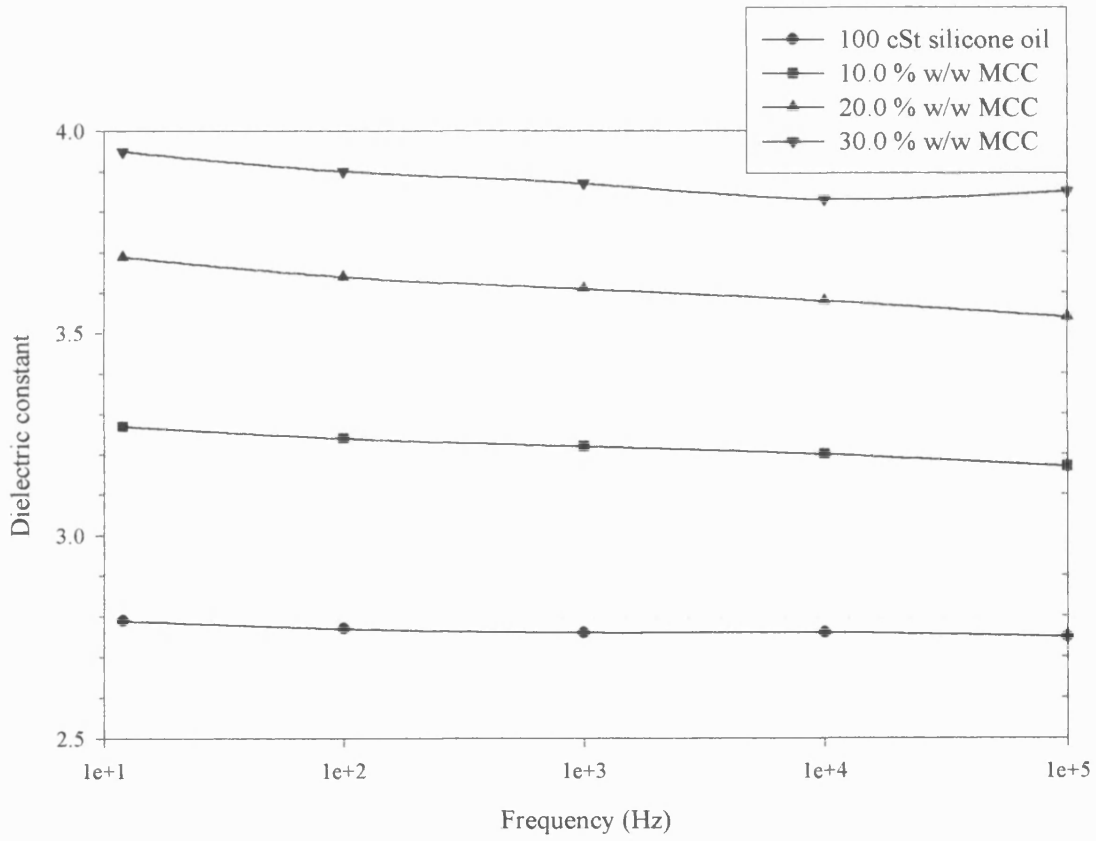

Figure 2.5. Dielectric constants of silicone oil alone and in combination with different concentrations of MCC (sieve fraction below 45 μm) over the frequency range 12 Hz to 10^5 Hz. Error bars representing the standard deviation (n = 5) are smaller than the symbols used.

Due to the difficulty in measuring the dielectric properties of powder, the dielectric constant of the solid phase (K_{Solid}) was estimated using the linear rule of mixtures:

$$K_{ER} = \phi K_{Solid} + (1-\phi)K_{Liquid} \qquad \text{Equation 2.2}$$

where K_{ER} and K_{Liquid} are the dielectric constants of the ER fluid and the liquid phase respectively. ϕ is the volume fraction of the solid phase. The dielectric constant of MCC (sieve fraction below 45 μm), as calculated from Equation 2.2, is 11.39 (± 0.73).

2.3.7. Assay of Tacrine by Ultraviolet Spectrophotometry

Figures 2.6 and 2.7 are the UV scans, between 190 and 390 nm, for tacrine in distilled water and propan-2-ol respectively. The maximum peak absorbance occurred at 240 nm, which coincided with published values (Ekman et al., 1989; Hartvig et al., 1990), in addition, twin peaks occurred at 324 nm and 342 nm. The calibration plots for tacrine in distilled water, at 240 nm, were linear (Figure 2.8). Least square regression analysis was performed on the data and presented in Table 2.5.

Preparation	Gradient		Intercept		r^2
	Estimated	S.D.	Estimated	S.D.	
Dilution A1	0.1477	0.0009	-0.0008	0.0033	0.99989
Dilution A2	0.1475	0.0007	0.0064	0.0026	0.99993
Dilution B1	0.1496	0.0006	-0.0040	0.0024	0.99994
Dilution B2	0.1471	0.0008	0.0038	0.0030	0.99991
Dilution C1	0.1485	0.0007	0.0024	0.0026	0.99993
Dilution C2	0.1498	0.0005	-0.0035	0.0020	0.99996

Table 2.5. Linear regression data for UV analysis of tacrine in distilled water at 240 nm.

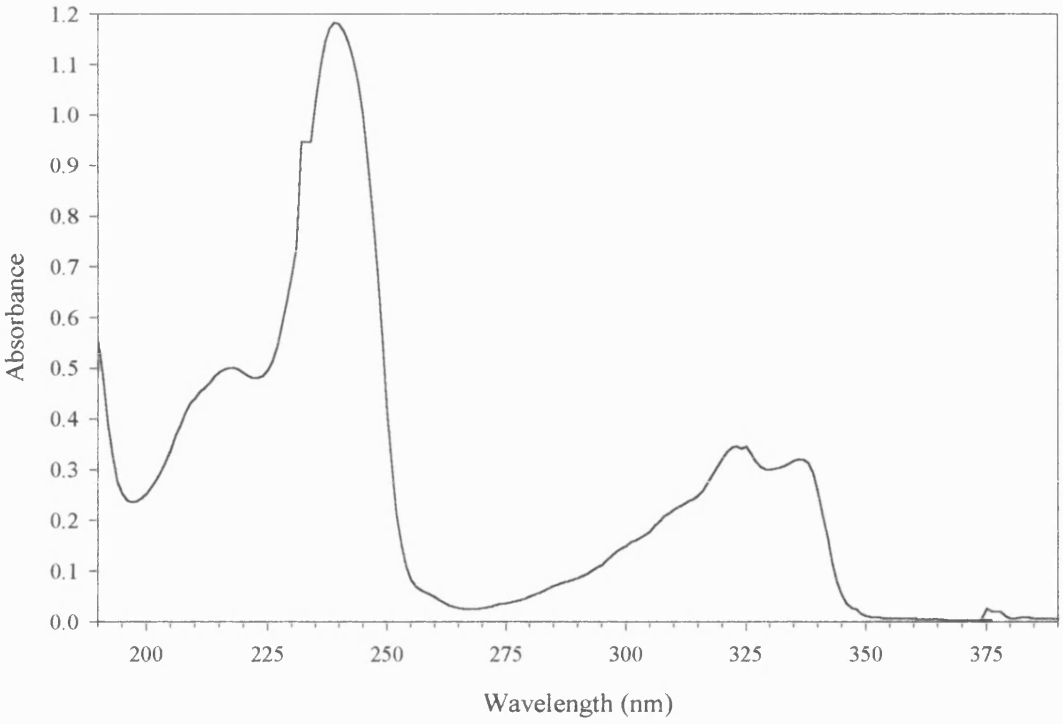

Figure 2.6. UV spectrum of tacrine at a concentration of 7.5 µg/ml in distilled water.

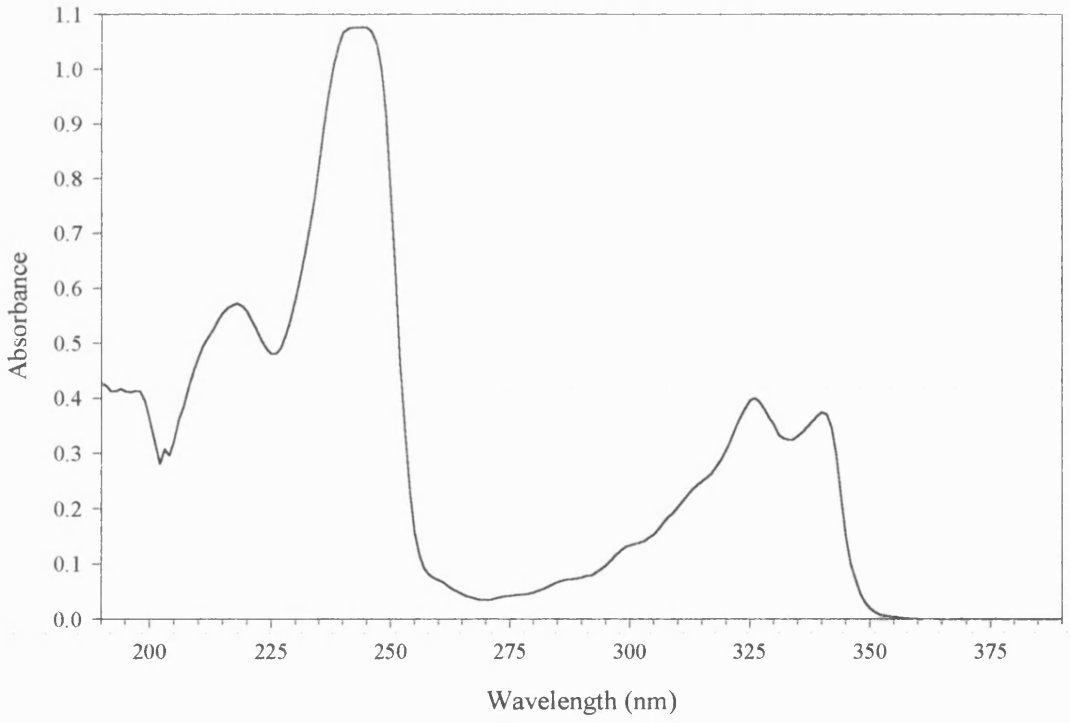

Figure 2.7. UV spectrum of tacrine at a concentration of 7.5 µg/ml in propan-2-ol.

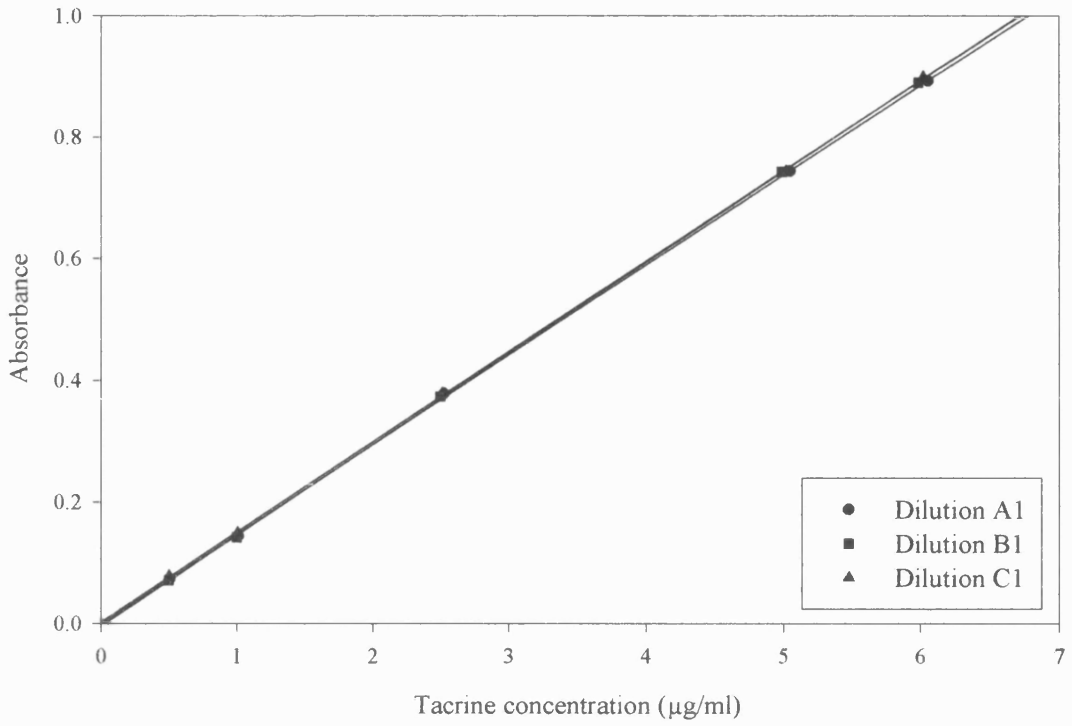

Figure 2.8. Calibration curve for tacrine in distilled water as determined by UV analysis at 240 nm.

Replicate samples of 2.5 µg/ml and 5 µg/ml gave 95 % confidence limits of ± 0.15 % and 0.91 % respectively. The *t-test* indicated no significance difference between the duplicate calibration data plots (for example stock solution A: $t_{critical} = 0.01$, $t_{tab} = 2.447$, p = 0.05). Furthermore, on combining the results obtained for all stock solutions, the least square regression (r^2)was determined to be 0.99984, with a linear equation of y = 0.1484x + 0.0007. The analysis of tacrine by UV detection was therefore considered appropriate over the concentration range examined.

In accordance with the Beer-Lambert law, the relationship between the concentration of tacrine in distilled water and the absorbance (at 324 nm) was linear (Figure 2.9). The combined equation for all stock dilutions, in distilled water, was:

$y = 3.1040x + 0.0035$, with a linear regression (r^2) of 0.99987. As we found with water, the relationship between the concentration of tacrine in propan-2-ol and the absorbance (at 324 nm) was linear. The combined equation for all stock dilutions, in propan-2-ol, was: $y = 3.6061x + 0.0038$, with a linear regression (r^2) of 0.99991.

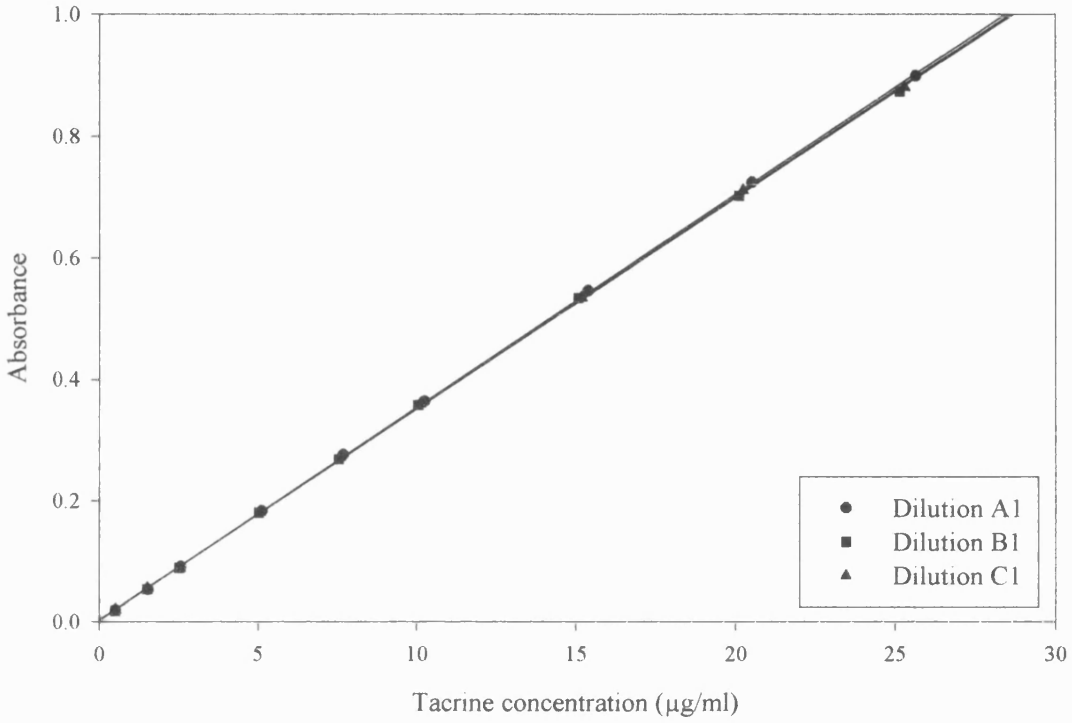

Figure 2.9. Calibration curve for tacrine in distilled water as determined by UV analysis at 324 nm.

Tacrine hydrochloride hydrate exists in aqueous solution in the form of the conjugate acid of the weak base, together with its Cl^- counterion. The pH of the aqueous solution, together with the pK_a value plays a vital role in the degree of ionisation. The existence of different ionic species may result in different UV spectra. The dependence of pH on the degree of ionisation of a weak base can be illustrated using the Henderson-Hasselbach equation:

$$pH = pK_a + \log \frac{[Base]}{[Acid]}$$

According to the Henderson-Hasselbach equation, when the pH is approximately equal to the pK_a value, 50 % of the species are present in the ionised form; as such small changes in the pH can have a dramatic effect on the proportion of ionised to unionised species present. For efficient ionisation, the pH of the medium should be outside the range, pK_a ± 2. The pK_a values of tacrine (g) and a range of similar compounds (Figure 2.10) were obtained from the literature (Table 2.6).

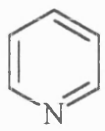

Pyridine
(a)

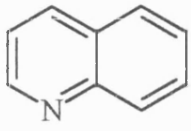

Quinoline
(b)

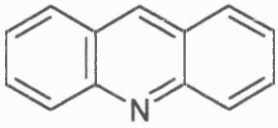

Acridine
(c)

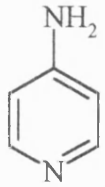

4-Aminopyridine
(d)

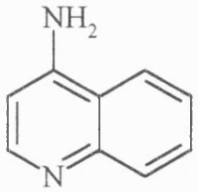

4-Aminoquinoline
(e)

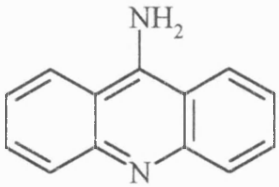

9-Aminoacridine
(f)

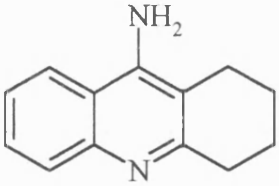

9-Amino-1,2,3,4-tetrahydroacridine
(g)

Figure 2.10. Chemical structures of pyridine (a), quinoline (b), and the 4-amino derivatives (d and e respectively), acridine (c) and its 9-amino derivative (f). The chemical structure of tacrine (g) is also illustrated.

Compound	pK_a	Conditions	Reference
Pyridine (a)	5.23	Water; 20-25 °C	Perrin et al., 1981
Quinoline (b)	4.92	Water; 20-25 °C	Perrin et al., 1981
Acridine (c)	5.60	Water; 20 °C (± 5)	Albert and Goldacre, 1946
4-aminopyridine (d)	9.25	Water; 20 °C	Albert and Serjeant, 1971
4-aminoquinoline (e)	9.17	Water; 20 °C	Albert et al., 1948
9-aminoacridine (f)	9.99	Water; 20 °C (± 5)	Albert and Goldacre, 1946
9-amino-1,2,3,4-tetrahydroacridine (g)	9.40	50 % ethanol 20 °C (± 5)	Albert and Goldacre, 1946

Table 2.6. The pK_a values of pyridine, quinoline, acridine and their amino-derivatives in water at 20 °C (± 5). The pK_a value of tacrine in 50 % ethanol is provided.

Not unexpectedly, the pK_a values show that the removal of one or two benzene rings from acridine (c) has no profound affect on the basicity of the pyridine ring (Albert and Goldacre, 1943; 1946). In all cases, the addition of an amine group in the position opposite the ring nitrogen atom results in an increase in the basicity of the compounds. The corresponding pK_a value for 9-aminoacridine (f) in 50 % ethanol at 20 °C is 9.45 (Albert and Goldacre, 1946). These values are all quoted at 20-25 °C, Albert and Sejeant (1971) have shown that, in water, bases become weaker as the temperature rises. The pH of distilled water was measured to be 6.6, which would suggest that the tacrine is almost completely ionised (99.96 %) throughout the UV determination experiments.

2.4. Preparation of Electrorheological Fluids

ER fluids were prepared on a % w/w basis. The viscosity of the silicone oil used was such that pouring was difficult, therefore we chose to use a weight measurement. Suspensions were prepared by first weighing the appropriate quantity of powder into a vial followed by the silicone oil. The sample was sonicated for two periods of 15 min each.

2.5. Conclusions

In this chapter, we have reported in detail the physicochemical properties of the ER fluid constituents employed. MCC powders have been separated according to size using a sieving technique and the particle-size distributions were separately determined. Scanning electron photomicrographs have been used in conjunction with the particle size distributions to obtain a complete overview of the physical properties of MCC powders. Moisture content has been shown in various studies to have a significant effect on the ER response (Klass and Martinek, 1967), therefore three grades of MCC of inherently different moisture contents were analysed using an infrared drying technique. The dielectric mismatch between the two phases is thought to contribute to the ER response and it was therefore considered important to investigate the dielectric properties of the components. The dielectric constant for the BP oils employed in the study were significantly higher than silicone oil. Furthermore, the addition of MCC in to silicone oil resulted in an increase in the dielectric constant indicating a strong dependence of the particulate phase on the ER response.

The solubility of tacrine in distilled water provided a measure of the affinity of tacrine for the solvent of choice used later in the diffusion cell (Chapter Five). Furthermore, the silicone oil/water partition coefficient of 0.104 (± 0.003) indicates an affinity of tacrine for water. The use of UV spectrophotometry has been investigated, at pH 6.6, in order to determine the tacrine concentration in the diffusion cell.

The application of an electric field has a dramatic effect on the rheological behaviour of ER fluids resulting in the ability of these fluids to run freely like water, ooze like honey or solidify like gelatine. The flow properties have been extensively investigated and are reported in Chapter Three. The conclusions we draw there often rely upon the information determined in this Chapter.

Chapter Three

Flow Properties of Electrorheological Fluids

3.1. Introduction

Rheology is the science of the deformation and flow of matter. In this Chapter, we focus on the flow behaviour of ER fluids in the absence and presence of an applied electric field. ER fluids exhibit Newtonian behaviour under no field conditions. Upon application of an electric field, ER fluids undergo a metamorphosis from fluid to solid, resulting in an increase in viscosity. In terms of flow behaviour, ER fluids under the influence of an applied electric field behave, to a first approximation, as Bingham fluids. The Bingham yield stress can be defined as the stress which must be exceeded before flow starts.

The model ER fluid chosen for this study is microcrystalline cellulose (MCC) in silicone oil. At the commencement of these studies, there was knowledge of the ER behaviour of our model ER fluid at electric fields between 1 and 3 kV/mm (Yatsuzuka et al., 1995; Kawai et al., 1996). Yatsuzuka et al. (1995) investigated the effect of particle shape, weight fraction, surface conductivity and applied electric field on various grades of MCC and silica in silicone oil. They found that the yield stress increased proportionally with weight fraction for all sample fluids. The ER effect was also enhanced by increasing the applied electric field, possibly resulting from enhanced electrostatic interactions between neighbouring particles. They found that particle shape plays an important role in the ER effect, with cylindrical particles having a higher yield stress.

The initial objective of this study is to investigate the flow properties of our model ER fluids under no applied electric field. Such behaviour will provide essential information on the viscosity of ER fluids during routine laboratory handling. The rheology of suspensions and the influences of particle concentration and particle size on the resultant fluid viscosity (Pa s) will be examined. The prediction of suspension viscosity using Einstein's equation (Equation 3.1) will be investigated.

Currently, few research groups have acknowledged the development of a yield stress below 1 kV/mm (Marshall et al., 1989; Chen et al., 1991; Gandhi and Thompson,

1992; Malins and Lacey, 1994; Parthasarathy and Klingenberg, 1996). With this in mind, a further aim of the present study is to characterise the flow behaviour, at electric fields of 500 V/mm and below, as a function of particle concentration, particle size, moisture content and applied electric field. Clearly, in the case of implants, it is critical to have a physiologically acceptable electric field. In order to provide correlation with future studies on the diffusion profile of tacrine from ER fluids, we have investigated the effect of the addition of tacrine to suspension rheology and Bingham yield stress. Tacrine, an acetylcholinesterase inhibitor, was chosen as a suitable candidate as an intraspinal implant for potential application in the treatment of neurodegeneration, particularly in Alzheimer's disease and senile dementia (Forsyth et al., 1989; Small, 1992).

Although a number of particulate phase components of typical ER fluids could be considered as pharmaceutically acceptable, there appear to be no pharmaceutically acceptable oils. In controlled drug delivery applications, particularly parenterals, it would be necessary to use approved constituents. For this reason, we have studied the ER behaviour of suspensions of MCC (sieve fraction below 45 μm) in different BP oils. Peanut and sesame seed oils are used in the formulation of sustained-release intramuscular injections (Pharmaceutical Codex, 1983). Almond oil is also cited as a vehicle for injections (Pharmaceutical Codex, 1983). Soyabean oil has replaced peanut oil, as a result of anaphylactic shock syndrome, in total parenteral nutrition regimens (Excipients Handbook, 1994). Glycerides of oleic acid are the major constituent of apricot kernel (68.0 %) (Femenia et al., 1995), safflower (63.0 %) (Croda Information), peanut (56.0 %) (Excipients Handbook, 1994) and sesame seed oil (45 %) (Excipients Handbook, 1994). Linoleic acid, in the form of glycerides, is the primary constituent of soyabean (50.0 to 57.0 %) (Excipients Handbook, 1994) and sweet almond oils (75 %) (British Pharmacopoeia, 1993). Suspensions prepared with the major long-chain fatty acid components were also assessed for ER behaviour.

3.2. Materials

MCC (Emcocel 50M, LM50 and XLM90), 100 cSt silicone oil and BP oils as previously described in Section 2.1. A 0.1 % w/v aqueous solution of potassium chloride (BN 38767 464, Fisons, Loughborough, UK) in freshly distilled water was prepared.

3.3. Modification of the CSL^2 Rheometer for Electrorheological Measurements

A controlled stress rheometer (CSL^2 100, TA Instruments, Leatherhead, UK) was specially modified to allow the application of an electric field across test fluids. A diagrammatic representation of the modifications carried out to enable ER measurements to be conducted is illustrated in Figure 3.1. Figure 3.2 depicts the rheometer set-up during ER measurements, whilst Figure 3.3 shows the modified parallel plate, insulated draw rod and protective casing.

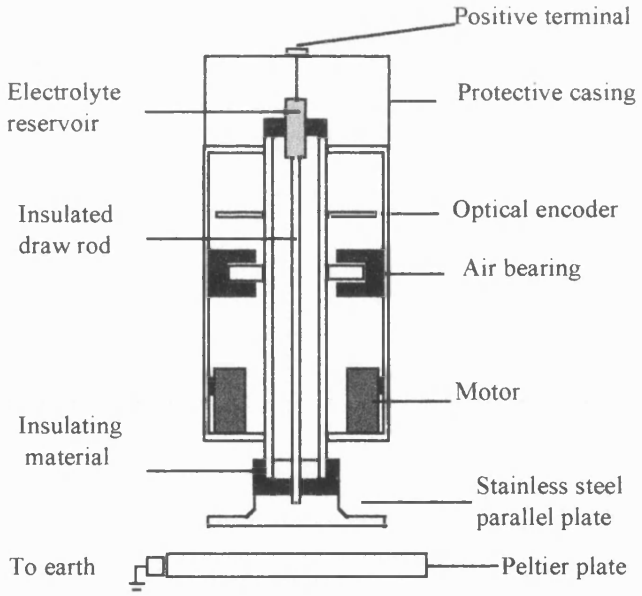

Figure 3.1. Diagrammatic representation of the ER conversion of the CSL^2 rheometer showing a parallel-plate geometry (reproduced from TA Instruments manual).

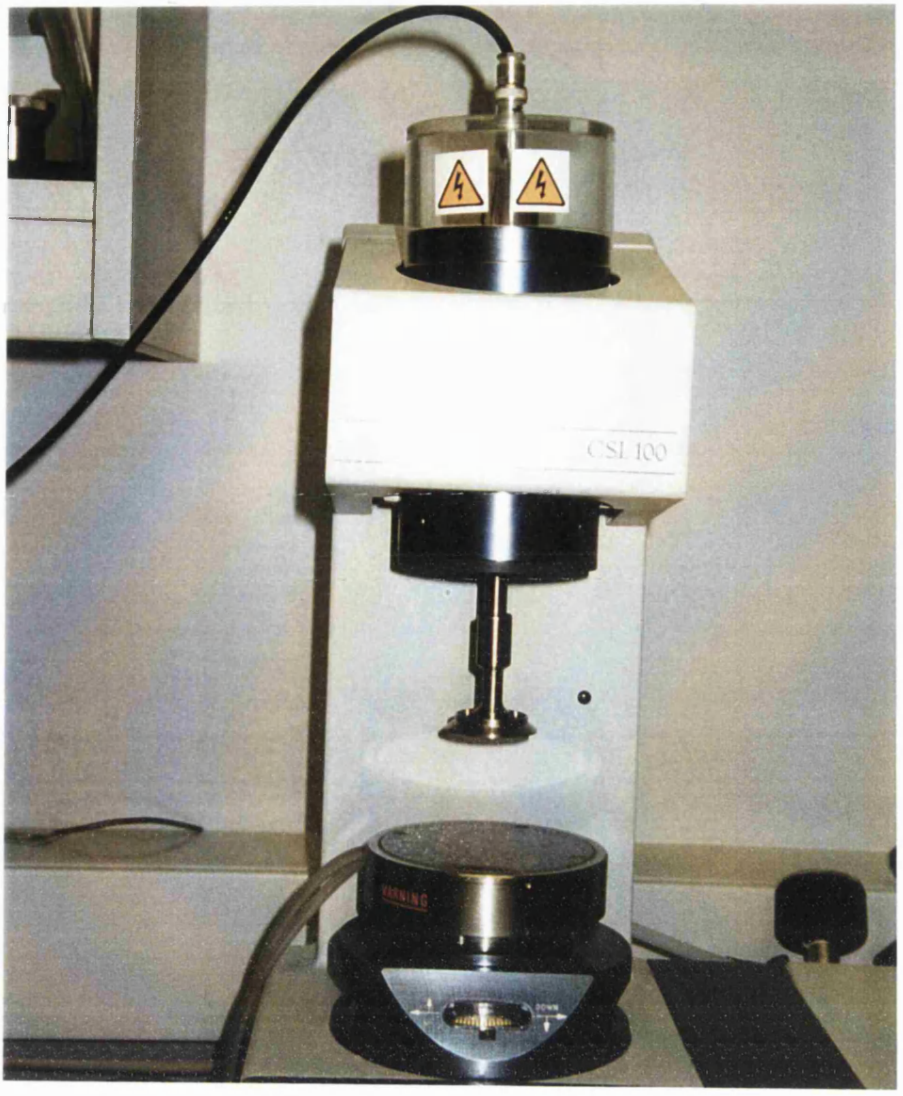

Figure 3.2. Photograph showing the rheometer conversion for the ER measurements.

Firstly, the draw rod is insulated with an insulating heat-shrinked sleeving (RS Components, UK) except for the threaded portion at the tip. At the opposite end, a small electrolyte filled reservoir containing aqueous potassium chloride forms the link between the positive terminal of the power supply and the rheometer. An insulated seat completes the isolation process, so that the potential difference is only apparent at the draw-rod tip. The draw-rod tip screws into the conductive geometry, enabling electrical connection to be made. By earthing the other components of the geometry, it is the sample alone which experiences the applied electric field. For reasons of safety, a protective perspex screen was used to shield the rheometer during all applied electric-field experiments.

Figure 3.3. Photograph showing the modified parallel plate, insulated draw rod and protective casing.

Careful consideration must be given to the choice of geometry, as the effect of the electric field must be taken into account. A uniform gap is required for ER applications, thus practical designs include either the concentric cylinder or parallel plate (Figure 3.4). Sharp edges should be avoided to reduce electric-field edge effects.

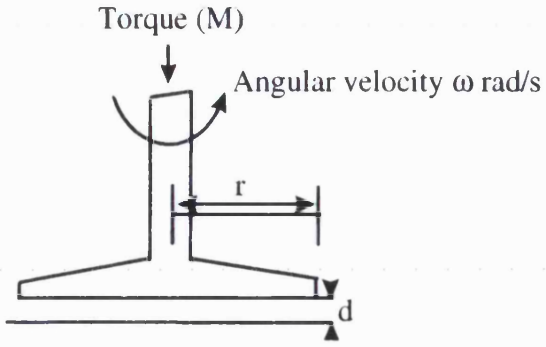

Figure 3.4. Schematic diagram of a parallel plate geometry, where d is the gap between the parallel plates, r is the plate radius and M is the torque.

In order to establish a correlation between the yield stress measured on the electrorheometer and the response in the diffusion cell, a 40 mm diameter stainless steel parallel-plate geometry with a gap of 1.0 mm was chosen. It is generally recommended that a gap of at least ten times the particle size be used for dispersed systems (Nguyen and Boger, 1992). Particularly with low viscosity formulations, a compromise between large gaps and fluid retention must be reached. The main disadvantage of the parallel plate is that the shear rate is not uniform across the entire diameter; the shear rate at a point is proportional to the distance from the centre.

3.4. Methods

3.4.1. Standardised Experimental Procedures for Flow Measurements

Compressed air which was clean, dry and oil-free was supplied to the air-bearing at a pressure of approximately 262 kPa (38.5 p.s.i.). The basic measurement is torque (M) as a function of the angular velocity (ω), from which the fundamental shear stress - shear rate relationship can be established. The angular velocity, the speed at which the plate rotates, is measured by the optical encoder. Temperature control was achieved via a Peltier plate system, which enabled the temperature to be controlled to within $\pm$ 0.1 °C. All experiments were conducted at 37 °C, unless otherwise stated. A continuous shear stress ramp from 0 to 50 Pa was applied to the test fluid. On attaining 50 Pa, the reverse response from 50 to 0 Pa was observed. Shear stress was applied at a rate of 0.1 Pa/s.

All ER fluids were prepared in triplicate (Samples A, B, and C), with five determinations from each sample being performed. Experiments were conducted in a manner avoiding the introduction of bias. The mean and standard deviation for each sample was calculated and an ANOVA test (one way) was carried out to highlight the presence of inter-sample differences. Data were collected via a personal computer using TA Instruments software (Leatherhead, UK) and subsequently processed using Excel 7.0

for the purpose of graphical reproduction (Windows 95, Microsoft Corporation, USA). To aid clarity, every fiftieth measurement, with values being offset for ascending and descending curves, was used to plot the flow rheograms illustrated below.

3.4.2. Flow Behaviour of Electrorheological Fluids in the Absence of an Applied Electric Field

The effect of particle concentration and particle size is known to have an effect on suspension viscosity (Barnes et al., 1989). Einstein's equation predicts that the viscosity of a suspension will increase. The rheological behaviour of our model ER fluids is discussed below. Furthermore, the rheological properties of our model ER fluids with the addition of 0.5 % w/w tacrine was measured.

3.4.2.1. Effect of Particle Concentration

Suspensions of MCC (sieve fraction below 45 μm) in 100 cSt silicone oil were prepared at the following concentrations: 1.0, 2.5, 5.0, 10.0 and 20.0 % w/w in accordance with the method outlined in Section 2.4. In addition, samples were prepared containing the above listed concentrations of MCC (sieve fraction below 45 μm) together with 0.5 % w/w tacrine.

3.4.2.2. Effect of Particle Size

From information provided by particle-size analysis (documented in Section 2.3.1) and SEM photomicrographs (Section 2.3.2 and Appendix Two), together with the true density, the approximate weight for one particle in each sieve fraction was calculated. The true density of MCC, as measured by helium pycnometry, was found to be 1581 kg/m^3 (± 0.002). From SEM photomicrographs, the approximate length of an MCC particle was taken to be 100 μm. The volume was calculated on the assumption that the particles were

approximately cylindrical. All subsequent calculations were based on the equivalent number of particles in a 1.0 % w/w suspension of MCC (sieve fraction below 45 μm) in 25.0 g of silicone oil. The following equation was used to calculate the number of particles present:

$$\text{No. of particles} = \frac{m}{\rho \pi r^2 l}$$

where m is the mass of powder, ρ is the true density of the powder, r is the radius of the particle and l is the length of the particle. The following sieve fractions were investigated: < 45 , 45 - 63, 63 - 75, 75 - 90 and 90 - 125 μm.

3.4.3. Flow Behaviour of Electrorheological Fluids under the Influence of an Applied Electric Field

Several parameters were considered to have an effect on the development of the yield stress, namely temperature, the duration of the applied electric field and the rate at which the shear stress was applied. Power consumption is critical in the development of battery-operated controllable drug-delivery devices. The current was measured using a simple ammeter (Department of Pharmacy and Pharmacology at the University of Bath) capable of measuring up to 100 μA.

As yield stress fluids are generally structured materials whose rheology is dependent on the previous shear history, it has been found that the determination of the yield stress may be sensitive to the duration of measurement (Cheng, 1986). More specifically, in the case of ER fluids, it may well be dependent on the duration of the applied electric field prior to analysis. The rheological properties of a 10.0 % w/w suspension of MCC (sieve fraction below 45 μm) in 100 cSt silicone oil were determined

following an equilibrium period of 0, 5 and 10 min. During the equilibrium period, an applied electric field of 250 V/mm was applied. Furthermore, the rate at which the shear stress is applied has also been investigated on a 10 % w/w suspension of MCC (sieve fraction below 45 μm) in 100 cSt silicone oil at 250 V/mm. The shear stress was applied at rates of 0.05, 0.1 and 1 Pa/s.

The effect of particle concentration on the ER response was investigated. The following suspensions of MCC (sieve fraction below 45 μm) in 100 cSt silicone oil were prepared: 1.0, 2.5, 5.0, 10.0 and 20.0 % w/w. The rheological properties at 250 V/mm were investigated. Particle size is known to have an effect on the ER response (see Section 1.8.2.1) and the series of experiments conducted in Section 3.4.2.1 were repeated at 250 V/mm.

MCC powders of different moisture contents were investigated to establish a relationship between the Bingham yield stress and moisture. A representative sample of MCC (sieve fraction below 45 μm) was dried in the oven (Gallenkemp, Model IH-150, UK) at 60 °C for 48 h. MCC grades with inherently low moisture content (LM50 and XLM90) were sieved according to the procedure outlined in Section 2.2. The moisture content and particle size distribution were measured for all samples (for methods refer to Section 2.2.1 and 2.2.3 respectively). A suspension of 10.0 % w/w MCC (sieve fraction below 45 μm) was prepared in 100 cSt silicone oil and the rheological properties investigated at 250 V/mm. A 10.0 % w/w suspension of MCC (sieve fraction below 45 μm) in 100 cSt silicone oil was prepared and the flow behaviour observed at applied electric fields of 50, 100, 250 and 500 V/mm.

3.4.4. Rheological Behaviour of Three Compartment Electrorheological Fluids

The rheological behaviour of a 0.5 % w/w suspension of tacrine in 100 cSt silicone oil was investigated at 0 V/mm and 250 V/mm. There is a possibility that tacrine may

undergo electrophoresis upon application of an electric field as tacrine carries one positive charge at physiological pH. For this reason, an investigation into the effect of polarity on the rheological behaviour at 250 V/mm was conducted. The charge on the lower electrode plate was altered by switching the power supply polarity.

The rheological properties of tacrine-MCC suspensions under the influence of an applied electric field have also been investigated. The aforementioned experiments investigating the effect of particle concentration, particle size, moisture content and applied electric field were repeated with the addition of 0.5 % w/w tacrine.

3.4.5. Rheological Behaviour of Microcrystalline Cellulose in Super Refined (or BP) Oils

In controlled drug delivery applications, it would be necessary to use approved constituents. For this reason, we observed the ER behaviour of a 10.0 % w/w suspension of MCC (sieve fraction below 45 μm) in different super refined (or BP) oils. Linoleic and oleic acids, as the major components of the chosen super refined oils, were also investigated. The rheological behaviour was investigated at 0 V/mm and 250 V/mm.

3.4.6. Microscopic Observation

Two stainless-steel razors blades were affixed onto a standard microscope slide, such that the gap between them was approximately 1.0 mm. A Zeiss microscope (Germany) was coupled to a JVC TK1270 colour video camera through which the images were captured using the Optimas software (Version 5.2). The distance between the electrodes was accurately measured with the aid of a graticule (Graticules, London, UK). A 2.5 % w/w suspension of MCC (sieve fraction below 45 μm) in 100 cSt silicone oil was used for the microscopy illustrated. The structure formation at higher concentrations and different particle sizes was also investigated. However, at these high concentrations it was difficult to resolve chain formation at the microscopic level. Approximately 1.0 ml of the

ER fluid was placed between the electrodes. The dispersed ER fluid under no field conditions was photographed together with the image after 10 min application of the electric field. The effect of structure formation with respect to time was also investigated by applying the electric field and photographing the resultant structure formation after 0, 5 and 10 min.

3.5. Results and Discussion

3.5.1. Flow Behaviour of Electrorheological Fluids in the Absence of an Applied Electric Field

In general, suspensions of MCC in silicone oil exhibited Newtonian behaviour in the absence of an applied electric field. The following sections outline the effect of particle concentration and size on the suspension viscosity. The Newtonian viscosity of silicone oil at 37 °C was 0.0809 Pa s (± 0.0012). The viscosity provided by the manufacturers at 25 °C was 0.0801.

3.5.1.1. Effect of Particle Concentration

Figure 3.5 shows the flow rheograms of the effect of particle concentration under no applied electric field. Table 3.1 summarises the Newtonian viscosities of different concentration of MCC (sieve fraction below 45 μm) in 100 cSt silicone oil.

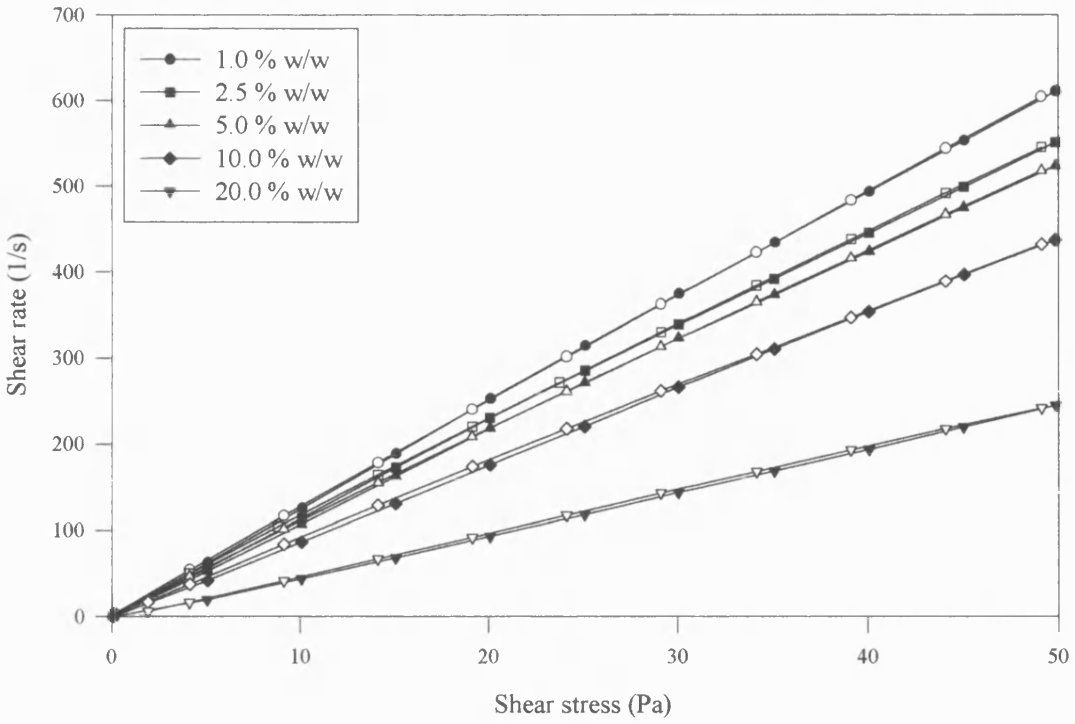

Figure 3.5. The effect of particle concentration on the Newtonian behaviour of MCC (sieve fraction below 45 μm) in 100 cSt silicone oil (Sample A). Open symbols depict the descending curve. Error bars representing the standard deviation are smaller than the symbols used (n = 5).

The Newtonian viscosity was found to increase with particle concentration. For all concentrations, there were no significant differences (t-test; t_{tab} 2.776; $p > 0.05$) between the ascending and descending curves for each sample (Samples A, B and C). At 20.0 % w/w concentration, the flow properties deviated from Newtonian behaviour; the viscosity was observed to decrease with increasing shear rate. The Power law index (n) was calculated using Equation 1.2. The term n, a measure of the degree of non-Newtonian behaviour, was calculated to be 0.934 (± 0.00), indicating a tendency towards shear thinning or pseudoplastic behaviour. Reinforcement of pseudoplastic behaviour is achieved through observation of the descending curve, which exhibited a decreased Newtonian viscosity. This indicated a gradual breakdown of the structure upon reduction

of the shear stress. This type of behaviour is observed to a lesser extent in the 10.0 % w/w suspension.

Concentration	Newtonian viscosity (Pa s)					
% w/w	Sample A		Sample B		Sample C	
	Up	Down	Up	Down	Up	Down
1.0	0.0813 (0.0004)	0.0812 (0.0007)	0.0810 (0.0002)	0.0811 (0.0006)	0.0813 (0.0005)	0.0811 (0.0006)
2.5	0.0897 (0.0042)	0.0896 (0.0022)	0.0898 (0.0030)	0.0896 (0.0024)	0.0897 (0.0022)	0.0896 (0.0019)
5.0	0.0941 (0.0014)	0.0937 (0.0014)	0.0943 (0.0005)	0.0936 (0.0006)	0.0941 (0.0014)	0.0931 (0.0014)
10.0	0.1135 (0.0023)	0.1124 (0.0022)	0.1135 (0.0019)	0.1129 (0.0027)	0.1137 (0.0021)	0.1124 (0.0013)
20.0	0.2079 (0.0048)	0.2037 (0.0048)	0.2080 (0.0022)	0.2034 (0.0014)	0.2079 (0.0048)	0.2037 (0.0048)

Table 3.1. The effect of particle concentration on the Newtonian viscosity at different concentrations of MCC (sieve fraction below 45 μm) in 100 cSt silicone oil. Standard deviation values are shown in brackets (n = 5).

The viscosity of suspensions of solid particles in Newtonian liquids can be predicted by Einstein's equation. Einstein showed that a single particle increased the viscosity of a liquid as a simple function of its phase volume, according to the following equation:

$$\eta = \eta_l (1 + 2.5\phi) \qquad \text{Equation 3.1}$$

where η is the viscosity of the suspension and η_l is the viscosity of the suspending liquid.

The volume fraction was calculated as follows:

$$\phi = \frac{m_p / \rho_p}{(m_l / \rho_l) + (m_p / \rho_p)}$$

where m_p and m_l refer to the mass of powder and liquid used and ρ_p and ρ_l are their respective densities.

Einstein's theory neglects the effects of particle size and position and generally correlation with experimental data is only achieved at low volume fractions, typically below 0.03 (Eirich, 1967; Lee, 1969). Many theoretical and experimental studies have been made to extend Einstein's theory to suspensions of finite concentration and geometrically different particles.

The Newtonian viscosity is plotted against the concentration in Figure 3.6 together with the predicted viscosity calculated using Einstein's equation (Equation 3.1).

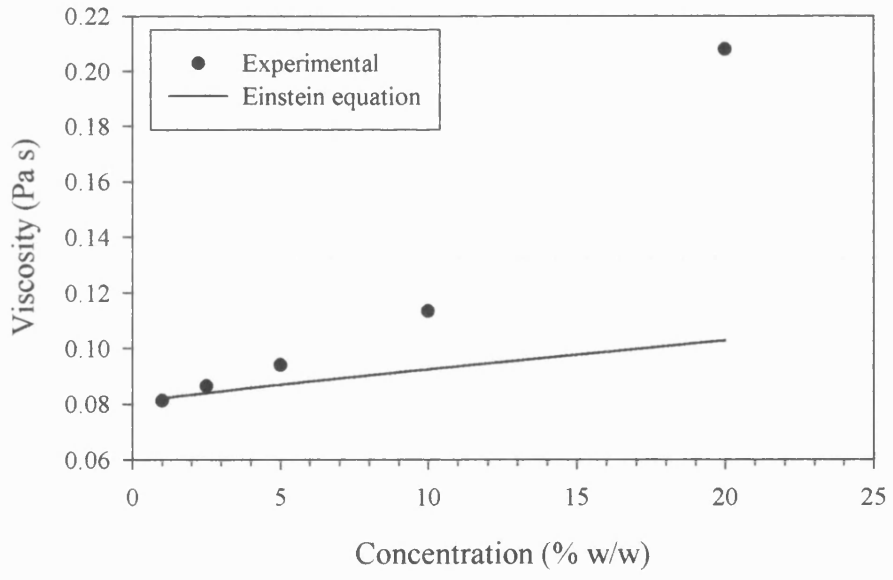

Figure 3.6. Newtonian viscosity of different concentrations of MCC (sieve fraction below 45 μm) in 100 cSt silicone oil. Predicted viscosity calculated using the Einstein equation.

The experimental data for concentrations 5.0 % w/w ($\phi = 0.029$) and below were adequately predicted using Equation 3.1. Eirich (1967) stated that the Einstein equation holds true at volume fractions below 0.03. The influence of particle concentration on the viscosity of concentrated suspensions cannot be accounted for simply by adding the effects of each particle sequentially and is generally determined in relation to the maximum packing fraction (Krieger and Dougherty, 1959; Quemada, 1984). At high concentrations, flow is no longer affected only by hydrodynamic interactions and Brownian motion. Particle asymmetry may also account for the deviation from Einstein's equation at high concentrations. Thus far, the particles in question have been spherical; as such, rotation or orientation of the particles has no influence. In the case of cylindrical particles, orientation, the degree of which will depend on Brownian motion, will interfere with the laminar flow (Reiner, 1960). Figure 3.7 shows the effect of MCC concentration (sieve fraction below 45 μm) in a 0.5 % w/w suspension of tacrine in silicone oil. The Newtonian viscosities are presented in Table 3.2.

Concentration	Newtonian viscosity (Pa s)	
% w/w	Up	Down
1.0	0.0822 (0.0013)	0.0817 (0.0017)
2.5	0.0889 (0.0021)	0.0825 (0.0012)
5.0	0.0927 (0.0021)	0.0919 (0.0023)
10.0	0.1112 (0.0007)	0.1103 (0.0010)
20.0	0.1892 (0.0072)	0.1854 (0.0073)

Table 3.2. The effect of the addition of 0.5 % w/w tacrine in different concentration suspensions on the Newtonian behaviour of MCC (sieve fraction below 45 μm) in 100 cSt silicone oil. Standard deviation values are shown in brackets (n = 5).

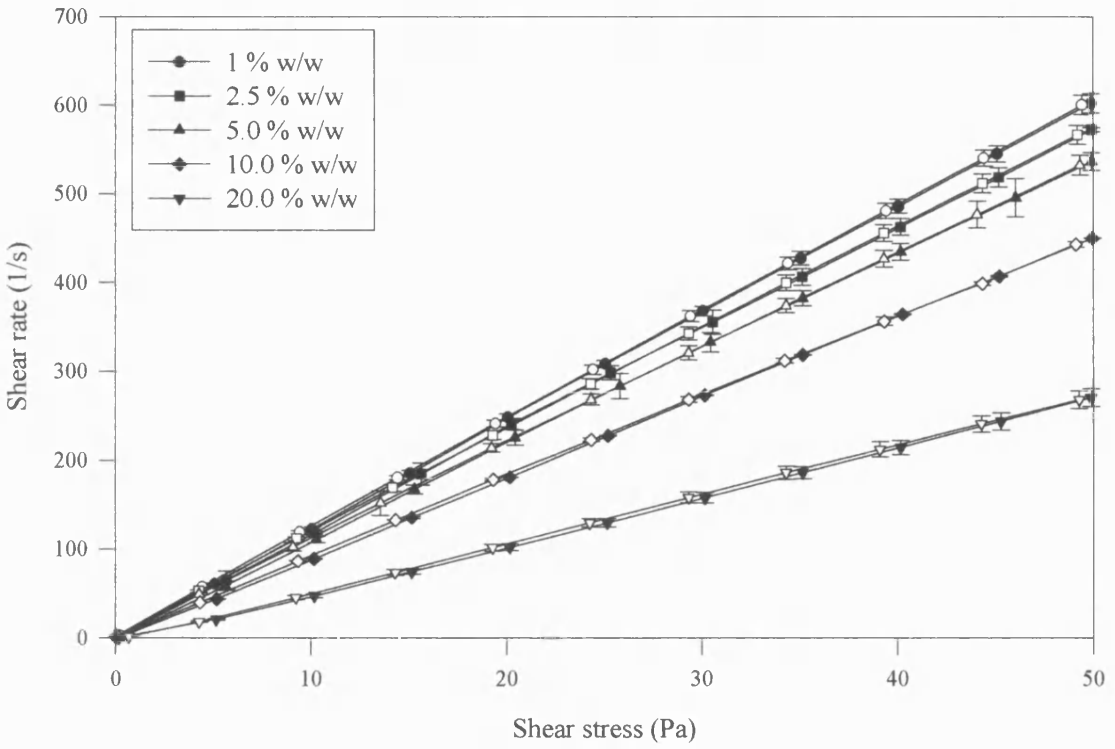

Figure 3.7. The effect of the addition of 0.5 % w/w tacrine in different concentration suspensions on the Newtonian behaviour of MCC (sieve fraction below 45 μm) in 100 cSt silicone oil. Open symbols depict the descending curve; error bars represent standard deviation (n = 5).

The Newtonian viscosity increased with MCC concentration. The addition of tacrine did not result in a significant difference ($p > 0.05$) in the viscosity for concentrations up to and including 10.0 % w/w MCC. A significant difference ($p < 0.05$; $F = 13.87$) was observed after the addition of tacrine to the 20.0 % w/w MCC suspension. The Power law index (n) was calculated to be 0.9190 (± 0.0020), indicating shear thinning behaviour. The Einstein equation successfully predicted the viscosity for suspensions of 5.0 % w/w MCC and below (Figure 3.8). Particle size distribution plays a significant part in the maximum packing fraction (Lee, 1970; Metzner, 1985). The smaller tacrine particles may fill the voids between the larger MCC particles, thereby reducing the maximum packing fraction. The Quemada equation (Equation 3.2) suggests that by

lowering the maximum packing fraction (ϕ_m) the relative viscosity of the suspension (η_r) will decrease at a given volume fraction and indeed this is observed experimentally (Goto and Kuno, 1984; Tsai et al., 1992; Chang and Powell, 1994; Probstein et al., 1994). Farris (1968) estimated the bimodal suspension viscosity by using the product of the individual components computed by the Krienger and Dougherty equation.

$$\eta_r = \left(1 - \frac{\phi}{\phi_m}\right)^{-2} \qquad \text{Equation 3.2}$$

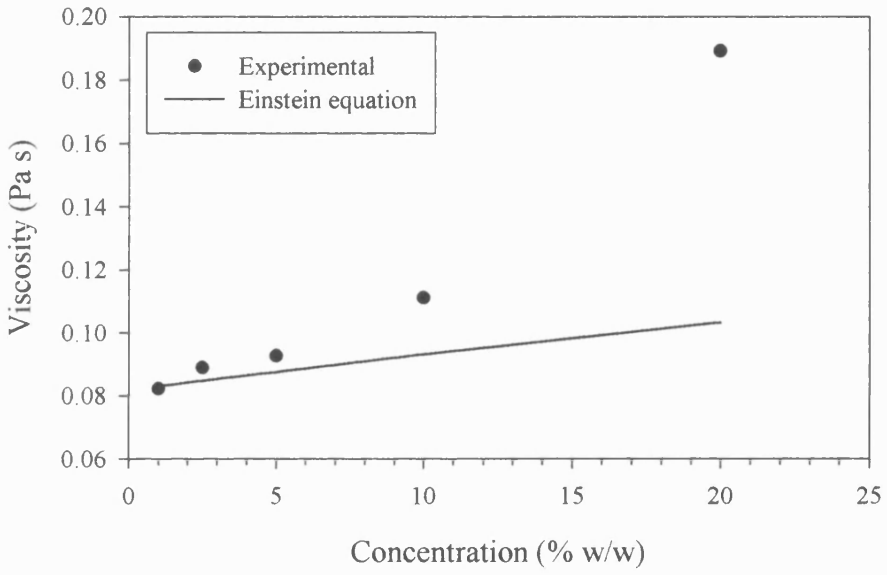

Figure 3.8. Newtonian viscosity of a 0.5 % w/w suspension of tacrine with different concentrations of MCC (sieve fraction below 45 μm) in 100 cSt silicone oil. Predicted viscosity calculated using the Einstein equation.

3.5.1.2. Effect of Particle Size

Figure 3.9 shows the flow rheograms of the effect of particle size under no applied electric field. Table 3.3 summarises the Newtonian viscosities of suspensions of MCC of different sieve fractions in 100 cSt silicone oil.

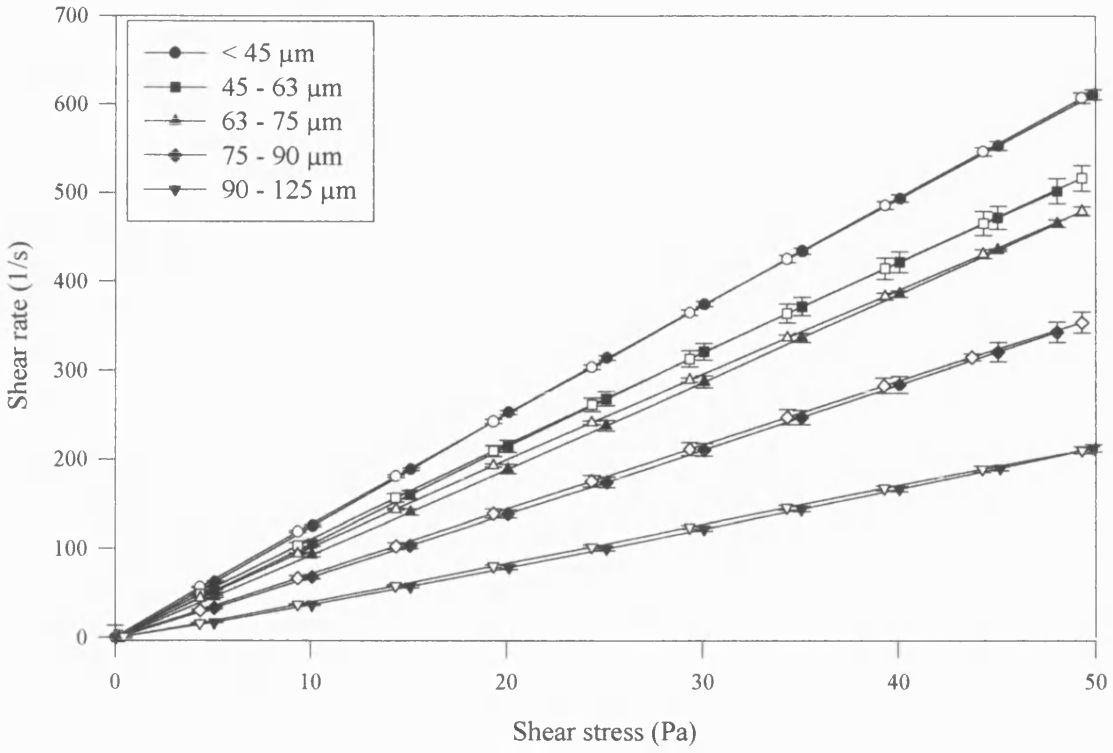

Figure 3.9. The effect of particle size of MCC on the Newtonian behaviour in 100 cSt silicone oil (Sample A). Open symbols depict the descending curve; errors bars represent the standard deviation (n = 5).

Each sieve fraction was prepared to contain an approximately equal number of particles, based on the assumptions that the particles are cylindrical and of equal mean length. The number of particles in a 1.0 % w/w suspension of MCC (sieve fraction below 45 µm) was $1.85 \times 10^7/25$ g. It was found that a 1.0 % w/w suspension of MCC (sieve fraction below 45 µm) contained the optimum particle number, with higher particle numbers resulting in paste-like suspensions when larger sieve fractions of MCC were used. The Newtonian viscosity increased with particle size. For all concentrations, there was no significant difference ($p > 0.05$) between the ascending and descending curves for each sample (Samples A, B and C). For the sieve fraction 90 - 125 µm, the Power law index, n, was calculated and found to be 0.9163 (± 0.0059), indicating shear thinning behaviour.

Sieve fraction	Newtonian viscosity (Pa s)					
μm	Sample A		Sample B		Sample C	
	Up	Down	Up	Down	Up	Down
< 45	0.0809 (0.0007)	0.0807 (0.0007)	0.0808 (0.0006)	0.0807 (0.0005)	0.0809 (0.0007)	0.0807 (0.0006)
45-63	0.0948 (0.0027)	0.0944 (0.0028)	0.0947 (0.0026)	0.0943 (0.0025)	0.0948 (0.0023)	0.0944 (0.0015)
63-75	0.1041 (0.0010)	0.1020 (0.0010)	0.1039 (0.0009)	0.1021 (0.0008)	0.1040 (0.0012)	0.1019 (0.0016)
75-90	0.1449 (0.0013)	0.1421 (0.0013)	0.1448 (0.0015)	0.1420 (0.0011)	0.1450 (0.0012)	0.1419 (0.0009)
90-125	0.2421 (0.0045)	0.2352 (0.0041)	0.2420 (0.0048)	0.2351 (0.0039)	0.2422 (0.0043)	0.2351 (0.0038)

Table 3.3. The effect of particle size of MCC in 100 cSt silicone oil on the Newtonian viscosity. Standard deviation values are shown in brackets (n = 5).

Figure 3.10 shows the relationship between the equivalent volume particle diameter and the Newtonian viscosity together with the estimated Einstein viscosity. Einstein's equation neglects the effect of particle size which results in the poor correlation observed in Figure 3.10. Einstein's equation successfully predicted the viscosity for the suspension containing particles below 45 μm. As the suspensions were formulated to contain approximately equal numbers of particles, the increase in Newtonian viscosity observed must be as a direct result of the particle size.

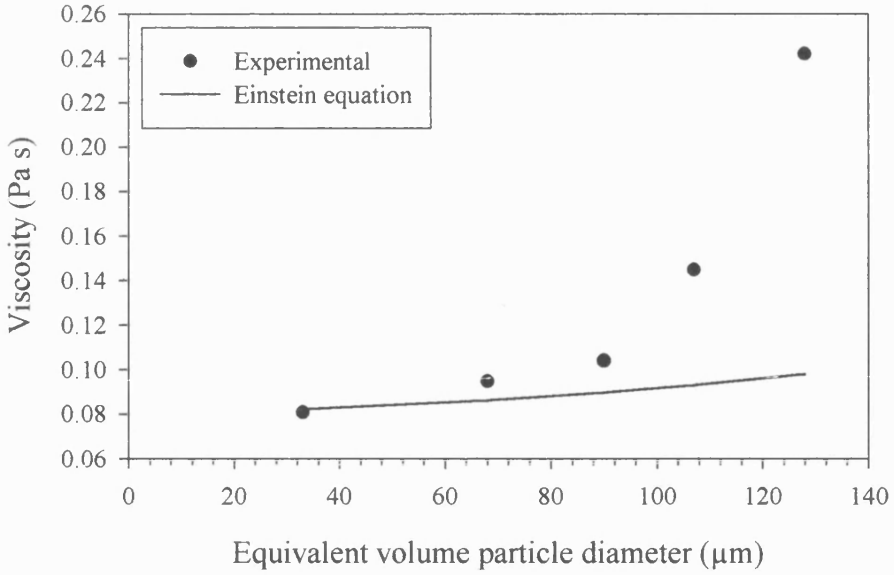

Figure 3.10. Newtonian viscosity of different equivalent volume particle diameters in 100 cSt silicone oil. Estimated values for the viscosity as determined using the Einstein equation are shown.

The effect of particle size of MCC in a 0.5 % w/w suspension of tacrine in 100 cSt silicone oil is illustrated in Figure 3.11. The respective Newtonian viscosities are shown in Table 3.4. The Newtonian viscosity was observed to increase with particle size. The addition of tacrine did not result in a significant change ($p > 0.05$) in the Newtonian viscosity for suspensions containing sieve fractions 63 - 75 μm and below.

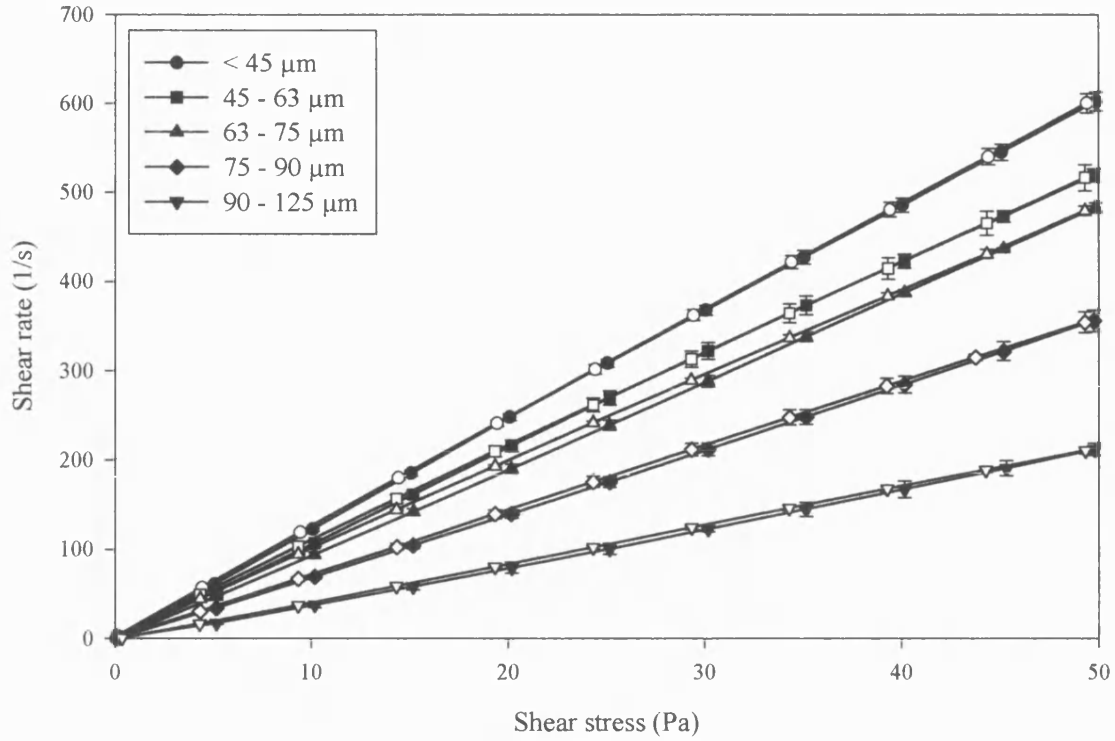

Figure 3.11. The effect of the addition of 0.5 % w/w tacrine in different particle size suspensions on the Newtonian behaviour of MCC (sieve fraction below 45 µm) in 100 cSt silicone oil. Open symbols depict the descending curve; error bars represent standard deviation (n = 5).

Particle size	Newtonian viscosity (Pa s)	
µm	Up	Down
< 45	0.0822 (0.0013)	0.0817 (0.0014)
45 - 63	0.0919 (0.0043)	0.0913 (0.0040)
63 - 75	0.1067 (0.0021)	0.1026 (0.0063)
75 - 90	0.1372 (0.0017)	0.1337 (0.0015)
90 - 125	0.2996 (0.0087)	0.2862 (0.0081)

Table 3.4. Newtonian viscosity values of different size particles of MCC in a 0.5 % w/w suspension of tacrine in 100 cSt silicone oil. Standard deviation values are shown in brackets (n = 5).

3.5.2. Flow Behaviour of Electrorheological Fluids under the Influence of an Applied Electric Field

The yield stress was determined by extrapolating the shear stress-shear rate graph to zero shear rate in accordance with the Bingham model (see Section 1.7.1.1). In general, good correlation (r^2 values typically 0.9999) was observed as the viscosity above the yield stress became shear stress independent. On several occasions, the rheological properties could be described equally well by more than one model and hence could have a different yield stress (Keentok, 1982).

Three distinct regions can be discerned on the flow rheogram and by further analysis of the data. Upon application of the electric field, viscosities of all the fluids tested increased. At shear-stress values below the yield stress (pre-yield region), the shear rate remains constant, despite the increase in shear stress. In terms of structure formation, Asano et al. (1997) and Sprecher et al. (1990) observed an inclination of the particle chains in the direction of the applied shear stress (Figure 3.12b). At the yield stress, there is a sudden increase in the shear rate, corresponding to the breakdown of the fibrous structure (Figure 3.12c). At shear stresses above the yield stress (post-yield region), the response is approximately linear and can be correlated to the Bingham model (Figure 3.12d). As the fluid is sheared and the structure breaks down, the viscosity decreased to zero field viscosity (Figure 3.12d). The linearity of the flow curve was only obtained at high shear stress values, probably because the structure responsible for the yield behaviour may gradually breakdown during shear and its complete destruction may only occur at high shear stress values (Bonnecaze and Brady, 1992). There is some debate as to whether the chains (in Figure 3.12c) undergo a reforming process at shear stresses proceeding the yield stress (Bonnecaze and Brady, 1992).

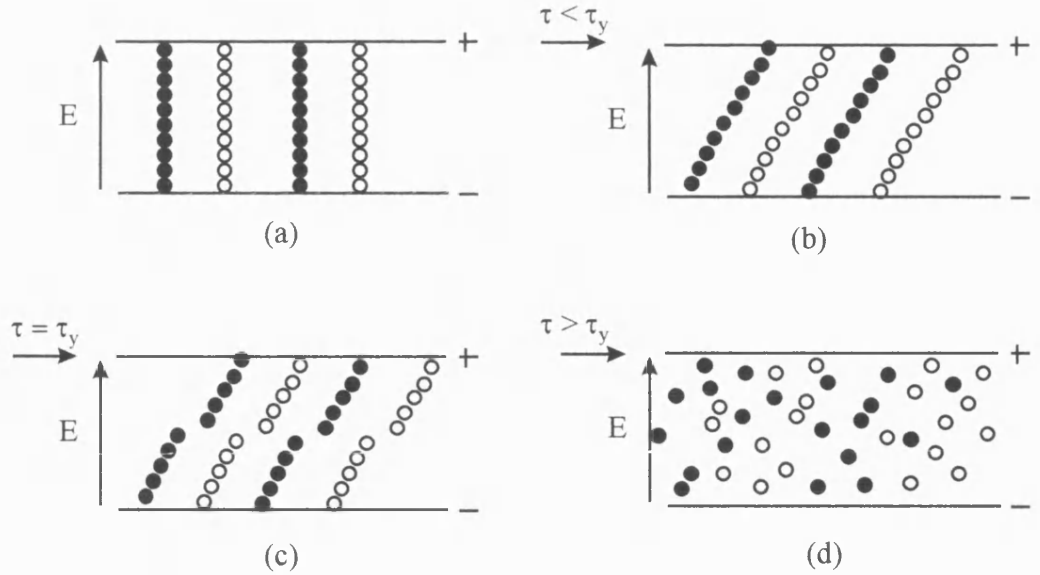

Figure 3.12. Idealised microstructural configurations depicting the effect of applied shear stress (τ) on an ER fluid (a) below the yield stress (b), at the yield stress (c) and above the yield stress (d). For simplicity, the illustration depicts single particle diameter chains with no inter-chain cross-linking. Adapted from Bonnecaze and Brady (1992).

Measurement of the yield stress may produce conflicting values depending on the technique or shear stress range employed, therefore it is often useful to quote the static yield stress. The static yield stress, the point at which the fluid begins to flow, was higher than the dynamic yield stress as measured using the Bingham model. Most of the samples exhibited a hysteresis which may be accounted for by the difference in the original particle arrangement (i.e. Figure 3.12d as opposed to Figure 3.12a). Upon commencement of the descending curve, the structure has been completely destroyed by the previous shear stress history. Approaching the yield stress under the influence of an applied shear stress would mean that the structure would have to form under constant stress. In dilute suspensions, this constant movement of particles may never lead to structure formation.

In general, the power requirements of the ER suspensions tested ranged from 0.5 mW for systems operating at 50 V/mm to 7.5 mW at applied electric fields of 500 V/mm. Pacemakers in use today operate at voltages of approximately 1-3 V with current values in

the region of mA (Wilson Greatbatch Technical Information). The possibility of using ER fluids at physiologically acceptable power requirements is achievable using electric fields below 100 V/mm. The sensitivity of the ammeter did not allow for minor variation on current flow to be detected during the experiment.

3.5.2.1. Pre-treatment Parameters

Figure 3.13 shows the ascending flow rheograms following 0, 5 and 10 min of applied electric field (250 V/mm). Figure 3.14 shows the ascending flow rheograms at applied shear stress rates of 0.05, 0.1 and 1 Pa/s. Table 3.5 summarises the Bingham yield stress values.

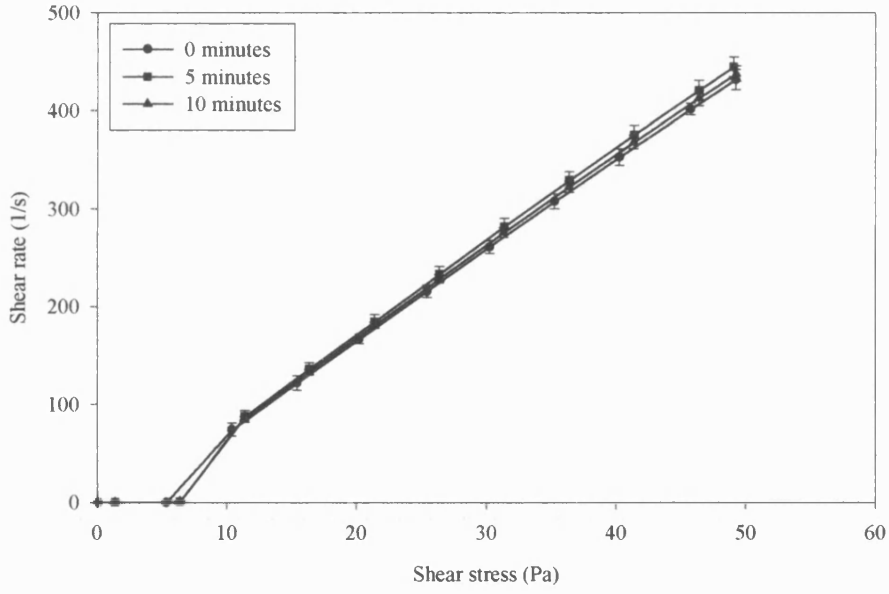

Figure 3.13. Ascending flow rheograms after 0, 5 and 10 min of applied electric field. Error bars represent the standard deviation (n = 5).

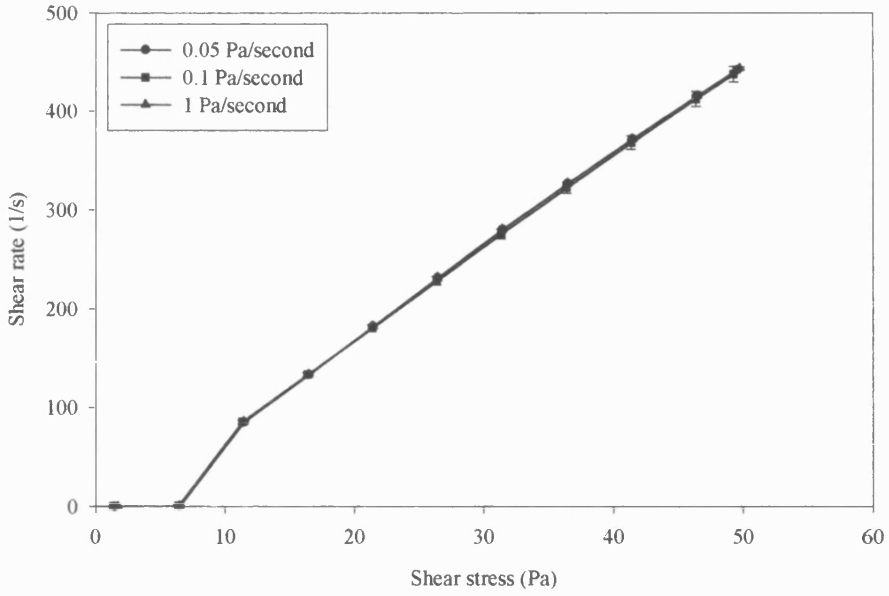

Figure 3.14. Ascending flow rheograms at applied shear stress rates of 0.05, 0.1, 1 Pa/s. Error bars represent the standard deviation (n = 5).

Treatment	Bingham yield stress (Pa)	
Applied electric field	Up	Down
0 min	2.9886 (0.0836)	1.2466 (0.0931)
5 min	3.0104 (0.1782)	0.8912 (0.0327)
10 min	2.9726 (0.0821)	1.1184 (0.0740)
Shear stress rate		
0.05 Pa/s	3.1562 (0.0306)	0.8047 (0.0208)
1 Pa/s	3.7322 (0.2808)	0.6056 (0.0639)

Table 3.5. Pre-treatment parameters investigating the duration of the applied electric field prior to analysis and the rate of application of the shear stress. Standard deviation values are shown in brackets (n = 5). Note: 10 min = 0.1 Pa/s.

The duration of the applied electric field prior to analysis was found to have no significant effect (one-way ANOVA; $p > 0.05$; $F = 0.12$) on the resultant Bingham yield stress. Upon application of an electric field, the ER response is known to occur within milliseconds, although to achieve a full structure may take several seconds (Sprecher et al., 1987; Conrad et al., 1990; Otsubo et al., 1991; Halsey, 1992). The rate at which the shear stress was applied resulted in a significant difference (one-way ANOVA; $p < 0.05$, $F = 27.23$) between the Bingham yield stress values. A Fisher pairwise test indicated that no significant difference occurred between 0.05 Pa/s and 0.1 Pa/s. The initial viscosities of the samples subjected to 1 Pa/s applied stress were significantly higher, indicating the migration of chains into columns.

In light of these results, it was decided to conduct all experiments at a rate of 0.1 Pa/s, following a 10 min temperature equilibration period during which time the electric field was applied.

3.5.2.2. Effect of Concentration

Typical ascending and descending rheograms of shear rate versus shear stress are shown for sample A in Figures 3.15a and 3.15b respectively. Yield stress values, as determined by the Bingham model, are shown in Table 3.6.

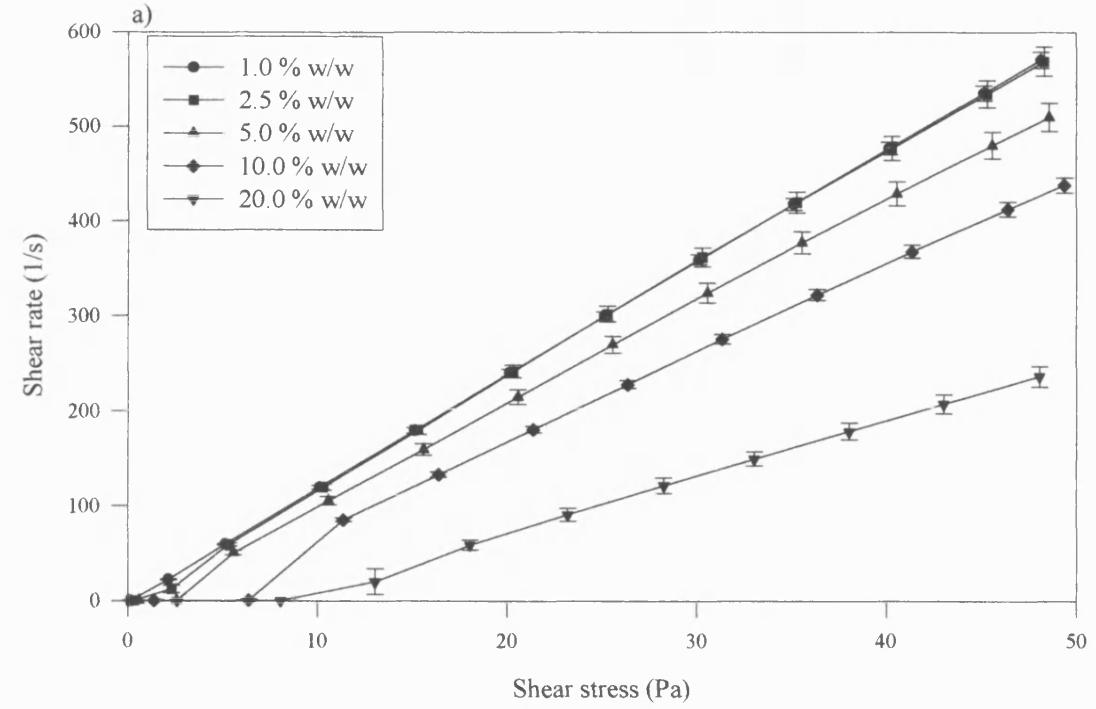

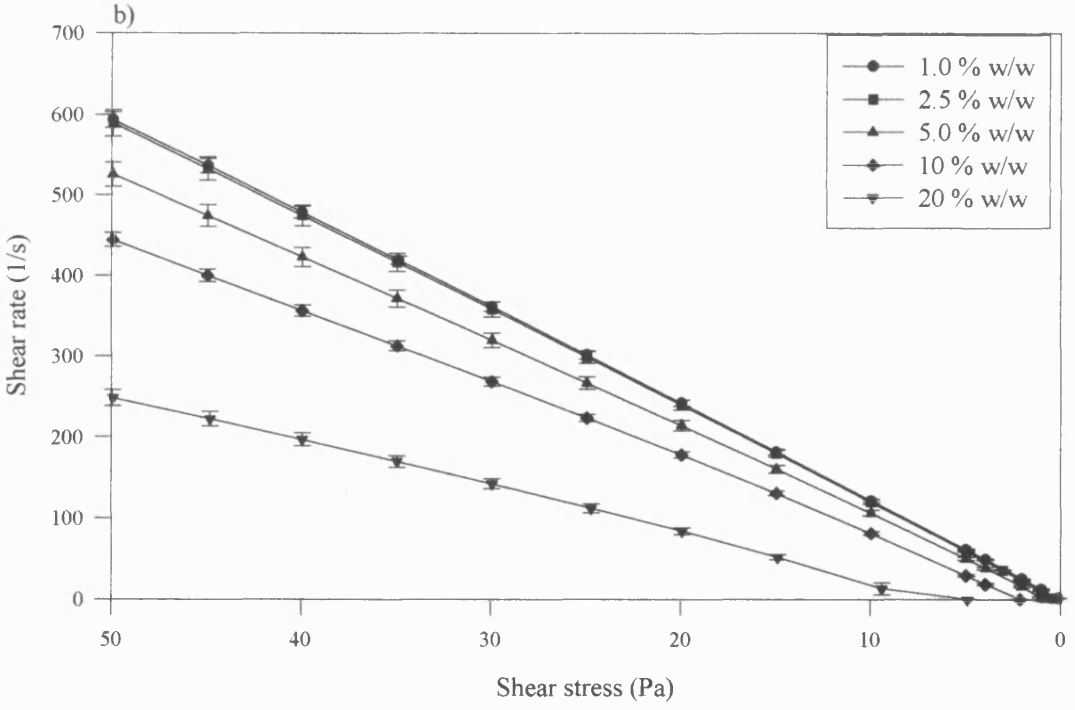

Figures 3.15 (a and b). The effect of particle concentration on the flow properties of MCC (< 45 μm) in 100 cSt silicone oil (Sample A) at an applied electric field of 250 V/mm. Figures 3.15 (a and b) represent the ascending and descending curves respectively; error bars represent the standard deviation (n = 5).

Concentration	Bingham yield stress (Pa)					
% w/w	Sample A		Sample B		Sample C	
	Up	Down	Up	Down	Up	Down
1.0	0.0928 (0.0035)	-0.2634 (0.0060)	0.0921 (0.0257)	-0.2651 (0.0095)	0.0971 (0.0321)	-0.2620 (0.0069)
2.5	0.3440 (0.0209)	-0.1636 (0.0553)	0.3489 (0.0144)	-0.1965 (0.0729)	0.3371 (0.0168)	-0.1902 (0.0163)
5.0	1.0510 (0.0343)	-0.0087 (0.0449)	1.0502 (0.0285)	-0.0375 (0.0370)	1.0556 (0.0176)	-0.0308 (0.0520)
10.0	2.9726 (0.0821)	1.1184 (0.0740)	2.9680 (0.0627)	1.1170 (0.0153)	2.9454 (0.0634)	1.0798 (0.0410)
20.0	7.9610 (0.2269)	5.8836 (0.2682)	7.9798 (0.0460)	5.8802 (0.0826)	8.0284 (0.0834)	5.9478 (0.2097)

Table 3.6. The effect of particle concentration on the Bingham yield stress of different concentrations of MCC (sieve fraction below 45 μm) in 100 cSt silicone oil at 250 V/mm. Standard deviation values are shown in brackets (n = 5).

For each concentration, no significant difference (one-way ANOVA; $p > 0.05$) was found between the Bingham yield stress calculated for ascending curves of samples A, B and C. No significant differences existed between the descending curves of samples A, B and C at concentrations of 10.0 and 20.0 % w/w. However, there was a significant difference (t-test; t_{tab} 2.776; $p < 0.05$) in all samples between the ascending and descending curves. The descending curve produced a lower yield stress and at concentrations of 5.0 % w/w and below the yield stress was negative, indicating possible Newtonian behaviour.

The relationship between Bingham yield stress and concentration was found to be approximately linear (Figure 3.16), with yield stress increasing with concentration. Previous studies investigating the effect of concentration on yield stress have shown a similar linear relationship (Conrad et al., 1992; Sprecher et al., 1992; Yatsuzuka et al.,

1995). The original correlation value (r^2) of 0.98552 was considered low (n = 5). At a concentration of 1.0 % w/w, it is possible that the behaviour exhibited was Newtonian under the influence of an electric field and was therefore omitted from the linear regression analysis. Regression analysis (n = 4) yielded the following equation for the linear relationship (y = mx + c) between Bingham yield stress and concentration:

r^2 : 0.99160

Gradient (SD) : 0.4440 (0.0289)

Intercept (SD) : -1.0755 (0.3331)

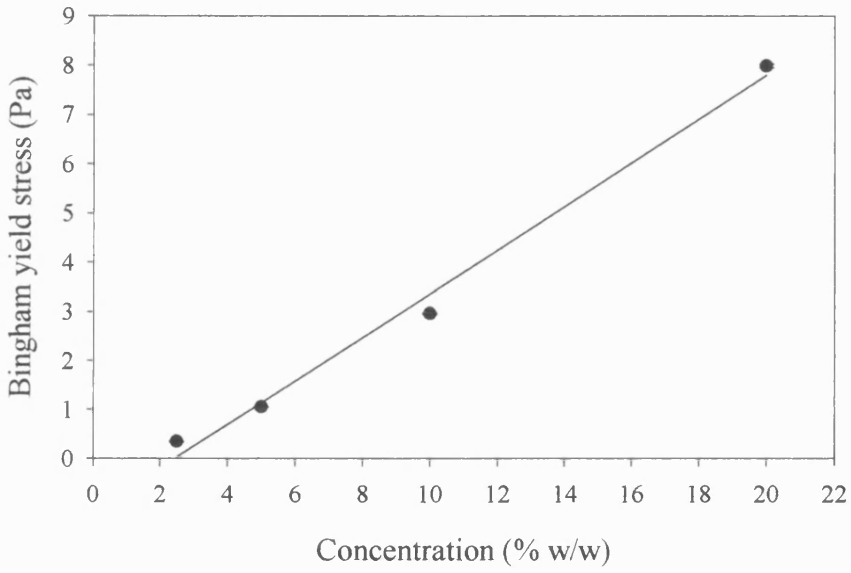

Figure 3.16. Relationship between Bingham yield stress and concentration of MCC (sieve fraction below 45 μm) in 100 cSt silicone oil at 250 V/mm. Data points represent the mean Bingham yield stress of samples A, B and C. Error bars are smaller than the symbols (n = 15).

The number of particle chains is likely to scale linearly with concentration, resulting in a subsequent linear increase in yield stress. Although a linear relationship exists, the function does not pass through the origin, indicating the presence of a more

complex association between concentration and yield stress which can not be accounted for simply by the number of particle chains (Marshall et al., 1989).

It is often stated that there is no ER effect at low concentrations ($\phi < 0.1$ or below 20.0 % w/w MCC) (Klass and Martinek, 1967; Gast and Zukoski, 1989). However, other workers often report the absence of any measurable solidification, whereas the question of whether some field enhancement of the flow resistance may be occurring is generally neither probed nor reported. In the case of the 1.0 % w/w suspension, no rheologically noticeable structure would appear to have developed upon application of the electric field. However, the viscosity at low applied shear stress (approximately 0.5 Pa) increased six-fold (compared to the Newtonian viscosity at 0 V/mm) from 0.1096 Pa s ($\pm$ 9.39 x 10^{-3}) to 4.5084 Pa s ($\pm$ 0.931). Furthermore, the stress at which the fluid was observed to flow (or static yield stress) was in the region of 1.6460 Pa ($\pm$ 0.2027).

Increasing the concentration of the dispersed phase not only increased the yield stress value of the fluid in the presence of an electric field, but also enhanced the zero field viscosity (see Section 3.5.1). Uejima (1972) plotted the ratio of the viscosity under field (η_E) to the viscosity under zero field (η_0) against weight fraction and found a maximum. This points to an optimum concentration that maximises the yield stress whilst maintaining fluidity in the absence of a field. Increasing the particulate concentration can obviously present problems of loss of fluidity, but additionally this state often negates the required effect as contact between the conducting particles may become so extensive as to short the electrodes (Block and Kelly, 1988). The optimum concentration forging the maximum yield stress for MCC (sieve fraction below 45 μm) in 100 cSt silicone oil would be between 5.0 and 10.0 % w/w (Figure 3.17). According to the point-dipole approximation, yield stress values are expected to increase in proportion to the number of particle chains or concentration (Klingenberg et al, 1991b; Ota and Miyamoto, 1993). This saturation occurs at high concentrations, where the particles form columns as opposed to single

particle chains, thereby introducing inter-particle chain interactions (Cerda et al, 1981; Chen et al., 1991; Bonnecaze and Brady, 1992 a and b). At low concentrations, interactions between chains may be considered negligible (Ota and Miyamoto, 1993).

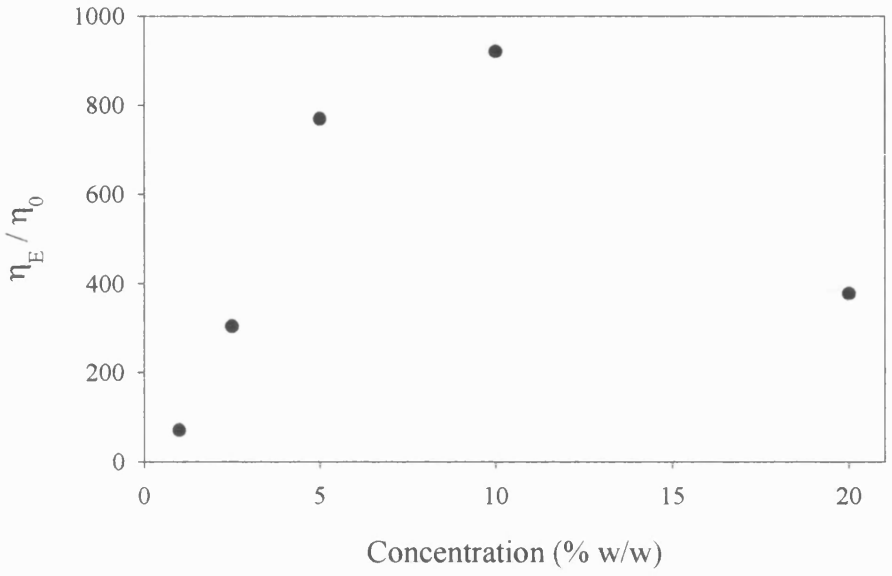

Figure 3.17. Relative viscosity (η_E/η_o) of MCC (sieve fraction below 45μm) at different concentrations in 100 cSt silicone oil. The viscosity ratio was calculated using the viscosity reading at an approximate shear stress of 0.5 Pa. Errors bars representing the standard deviation (n = 15) are smaller than the symbols.

3.5.2.3. Effect of Particle Size

The effect of particle size on the rheological behaviour of MCC in 100 cSt silicone oil under the influence of an applied electric field (250 V/mm) is shown in Figure 3.18. The Bingham yield stress values are found in Table 3.7.

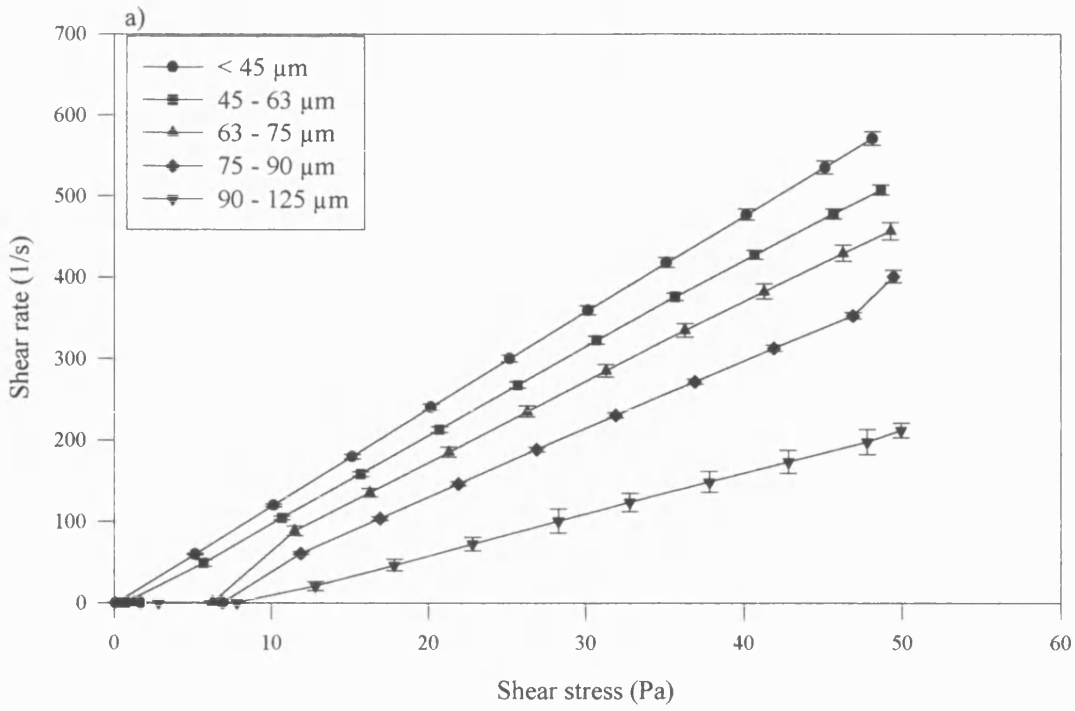

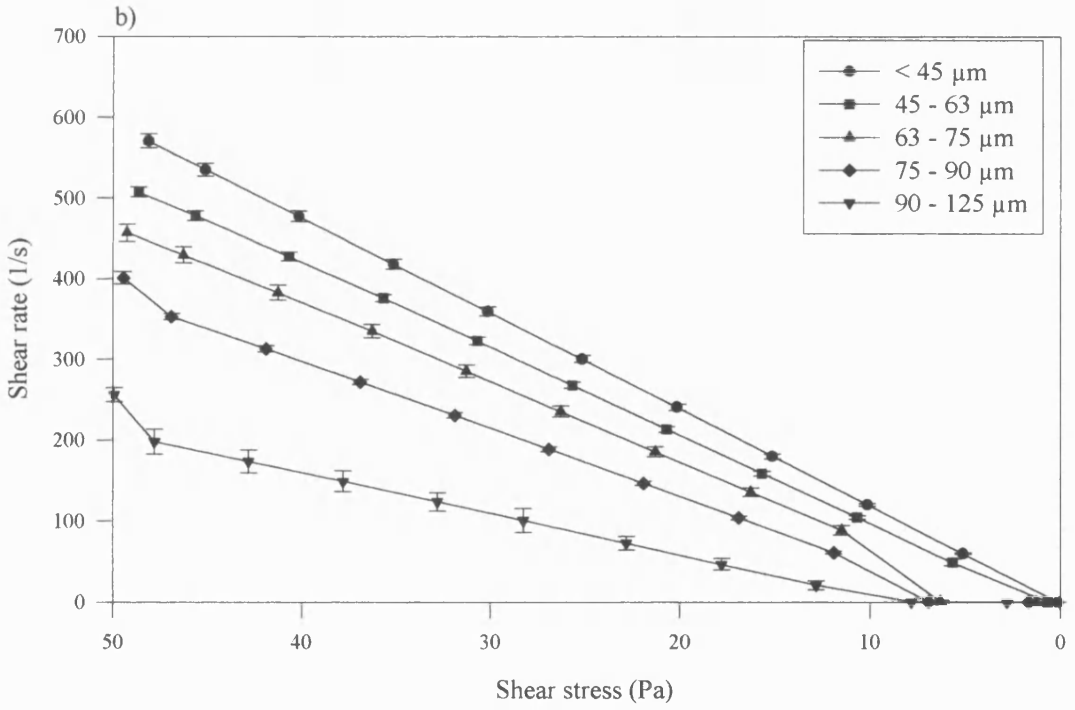

Figures 3.18 (a and b). The effect of particle size on the flow properties of MCC in 100 cSt silicone oil (Sample A) at an applied electric field of 250 V/mm. Figures 3.18 (a and b) represent the ascending and descending curves respectively; error bars represent the standard deviation (n = 5).

Sieve fraction	Bingham yield stress (Pa)					
µm	Sample A		Sample B		Sample C	
	Up	Down	Up	Down	Up	Down
< 45	0.0928 (0.0354)	-0.2634 (0.0061)	0.0927 (0.0245)	0.0459 (0.0025)	0.0930 (0.0125)	0.0758 (0.0052)
45 - 63	1.5818 (0.0821)	0.1547 (0.0411)	1.5821 (0.0745)	0.1552 (0.0126)	1.5820 (0.0753)	0.1546 (0.0231)
63 - 75	3.2762 (0.1050)	1.4158 (0.2201)	3.2764 (0.0998)	1.4158 (0.2078)	3.2763 (0.1064)	1.4157 (0.1985)
75 - 90	4.8308 (0.2622)	3.3632 (0.1773)	4.8304 (0.2302)	3.3628 (0.1812)	4.8305 (0.1998)	3.3632 (0.1728)
90 - 125	8.4081 (0.1456)	7.6613 (0.0224)	8.4083 (0.1321)	7.6614 (0.0125)	8.4081 (0.1235)	7.6613 (0.0598)

Table 3.7. The effect of particle size on the Bingham yield stress of MCC in 100 cSt silicone oil at an applied electric field of 250 V/mm. Standard deviation values are shown in brackets (n = 5).

There was no significant difference ($p > 0.05$) between the determined Bingham yield stress values (for the ascending curve) of sample replicates (n = 5) and batches of samples (A, B and C) for all sieve fractions. The relationship between the equivalent particle diameter and the Bingham yield stress increased exponentially (Figure 3.19) according to the following equation (Equation 3.3):

$y = ab^x$

r^2 : 0.99035

a (SD) : 0.2609 (0.0683)

b (SD) : 1.0275 (0.0022)

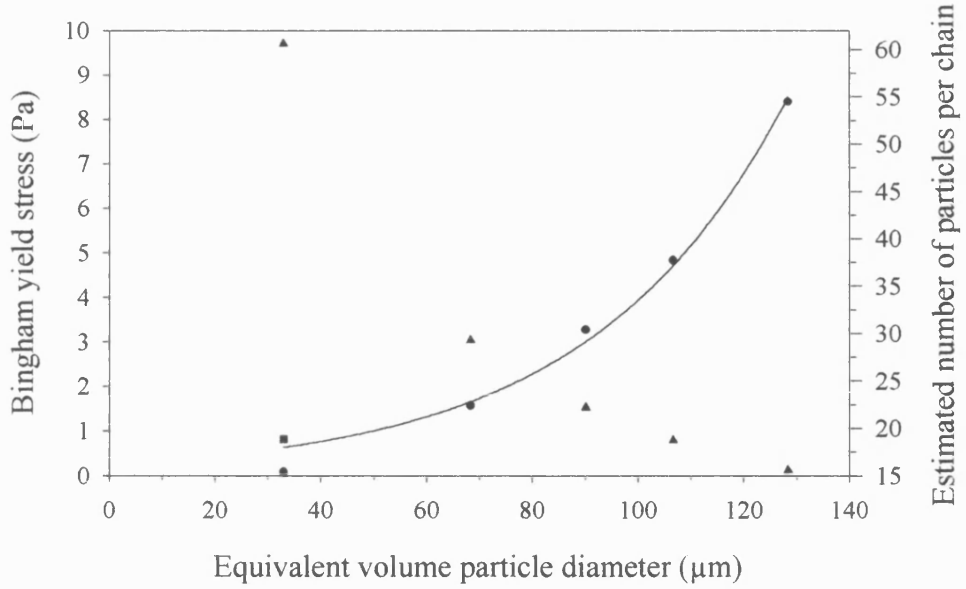

Figure 3.19. Relationship between the equivalent volume particle diameter and the Bingham yield stress (•). The static yield stress value for the sieve fraction below 45 μm is also shown (▪). Errors bars representing the standard deviation (n = 15) are smaller than the symbols. The estimated number of particles per chain for each sieve fraction is given (▲).

The sieving process (outlined in Section 2.2), plays a critical role in determining the nature of MCC particles in each size fraction as particles may transverse the mesh in one of two ways: horizontally or vertically. As the ER fluids were prepared such that all sieve fractions contained approximately equal number of particles (1.85×10^7 particles/25 g), the non-linear relationship may arise as a result of chain diameter or number of particle chains. Microscopic observation, at high magnification, of the particle rearrangement in response to the application of an electric field (see Section 3.5.5) indicated that particles orientated vertically. From SEM photomicrographs (see Section 2.3.2), we observed the presence of particles of similar lengths in all sieve fractions. The calculation for the number of particles was based on the assumption that equilength particles were present in

each sieve fraction. The hypothesis in this case is that the chain diameter was the crucial factor in the development of the yield stress (Figure 3.20a).

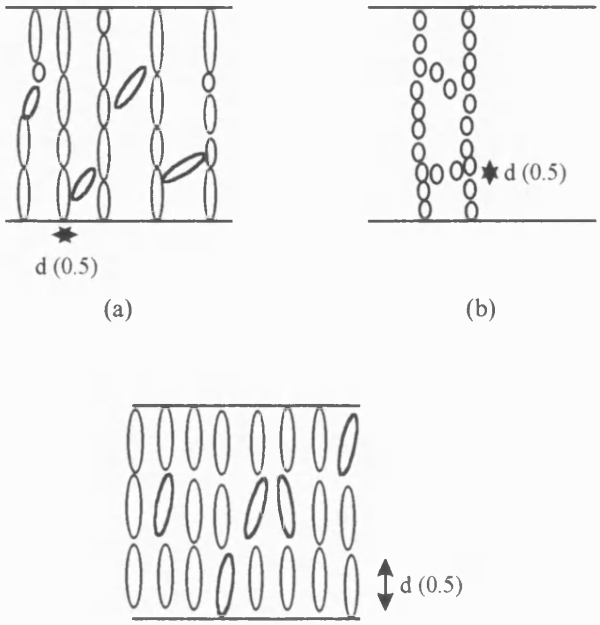

Figure 3.20. Diagrammatic representation of chain formation in ER fluids containing different particle sizes. (a) represents the scenario where the MCC particles transverse the mesh vertically. (b) and (c) represent horizontal transversal through mesh of small and large apertures respectively. Each figure contains the same number of particles.

The number of particles from each sieve fraction required to span the electrode gap was calculated (Figure 3.19). The estimated number of particles, based on the assumption that the powder transverses the mesh horizontally (Figure 3.20 b and c), decreased exponentially. This suggests a correlation between the number of particle chains (related to the estimated number of particles per chain) and the Bingham yield stress (Figures 3.19). Further research is required to provide a definite answer, however, in reality the relationship is likely to arise as a result of a combination of number and diameter of chains. The optimum particle size would dependent on the device design.

3.5.2.4. Effect of Moisture Content

The rheological properties of MCC of different moisture contents in 100 cSt silicone oil are depicted in Figure 3.21 and the Bingham yield stress values are shown in Table 3.8.

Type	Moisture content	Bingham yield stress (Pa)					
	%	Sample A		Sample B		Sample C	
		Up	Down	Up	Down	Up	Down
Dried (50M)	1.77 (± 0.09)	0.8891 (0.0891)	0.3644 (0.0141)	0.8902 (0.0458)	0.3642 (0.0245)	0.8921 (0.0235)	0.3641 (0.0183)
LM50	2.87 (± 0.27)	2.5403 (0.0739)	0.1674 (0.0082)	2.4983 (0.1124)	0.1673 (0.0101)	2.5289 (0.1572)	0.1672 (0.0097)
XLM90	1.69 (± 0.12)	0.8772 (0.119)	0.3624 (0.0141)	0.8698 (0.0987)	0.3621 (0.0099)	0.8725 (0.1324)	0.3626 (0.0153)
50M	4.21 (± 0.06)	2.9726 (0.0821)	1.1184 (0.0740)	2.9680 (0.0627)	1.1170 (0.0153)	2.9454 (0.0634)	1.0798 (0.0410)

Table 3.8. The effect of oven dried MCC (sieve fraction below 45 μm) in a 10.0 % w/w suspension in 100 cSt silicone oil compared with two low moisture grades of MCC on the development of the Bingham yield stress at 250 V/mm. Standard deviation values are shown in brackets (n = 5).

The particle size distributions for sieved LM50 and XLM90 are shown in Table 2.3. The median equivalent volume diameters are 32.99 μm (± 0.83), 26.36 μm (± 1.79) and 35.82 μm (± 1.12) for oven dried MCC, LM50 and XLM90 respectively. The particle-size distribution for LM50 contained 10 % of particles below 5 μm compared with 13.29 μm (± 0.17) and 12.30 μm (± 0.99) for oven dried MCC and XLM90 respectively.

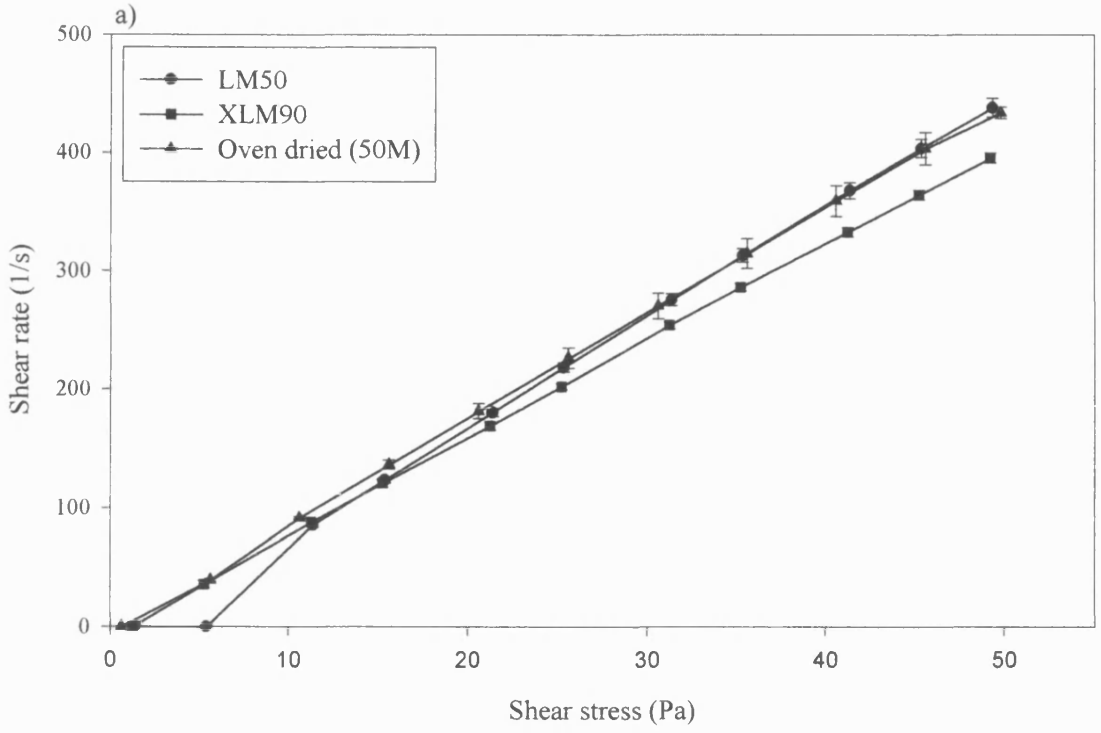

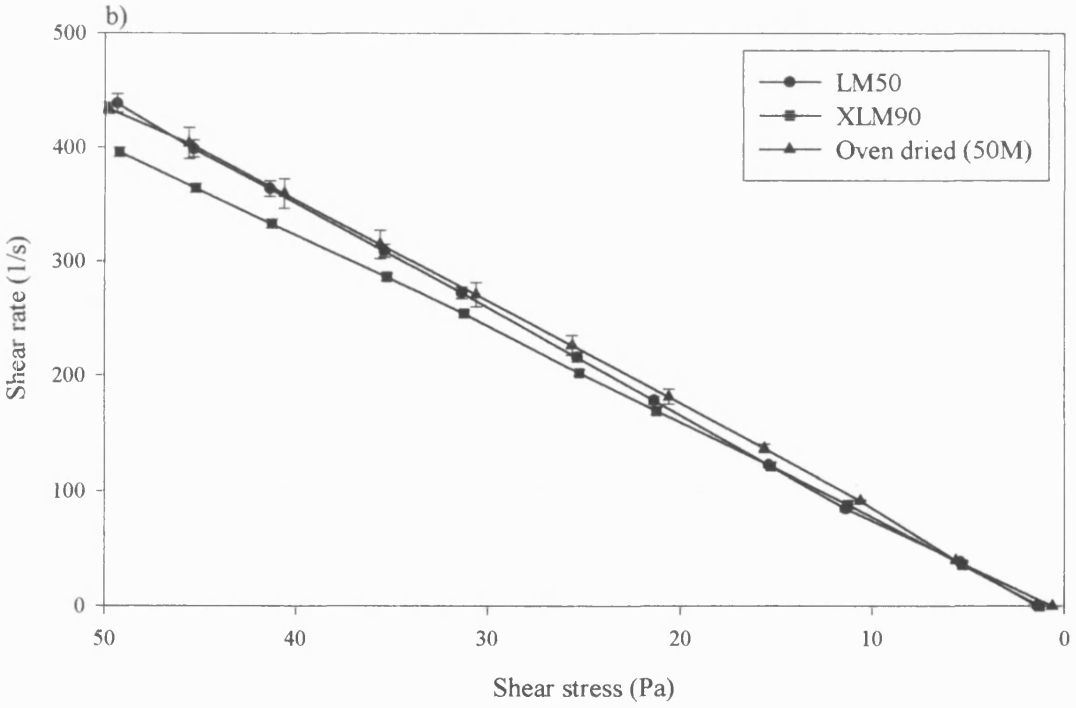

Figures 3.21 (a and b). The effect of moisture content on the flow properties of MCC in 100 cSt silicone oil (Sample A) at an applied electric field of 250 V/mm. Figures 3.21 (a and b) represent the ascending and descending curves respectively; error bars represent the standard deviation (n = 5).

The ER response, at 250 V/mm, was significantly reduced ($p < 0.05$) following the drying process. There was found to be no significant difference ($p > 0.05$) between the extra low moisture MCC grade (XLM 90) and the oven dried MCC. Furthermore, there was a significant difference between the low moisture MCC grade and the standard grade MCC. The role of water in the activation or enhancement of the ER effect is well documented (Winslow, 1949; Klass and Martinek, 1967; Block and Kelly, 1988; Block, 1992). Complete drying of these formulations has been shown to result in the destruction of the ER effect (Deinega and Vinogradov, 1984; Gast and Zukoski, 1989).

3.5.2.5. Effect of the Applied Electric Field

The effect of applied electric field on the rheological properties of MCC (sieve fraction below 45 μm) in 100 cSt silicone oil are shown in Figure 3.22 and Table 3.9.

The Bingham yield stress was found to increase with applied electric field. There was no significant difference between the Bingham yield stress values of samples A, B and C. At high shear stress values the merger of the flow curves indicated the cessation of electric field effects. At high shear stress values, there appears to be a limiting curve corresponding to the viscosity of the non-electrified suspension. This finding provides evidence in support of the rheological behaviour being Bingham, where unrestricted flow occurs after structure destruction.

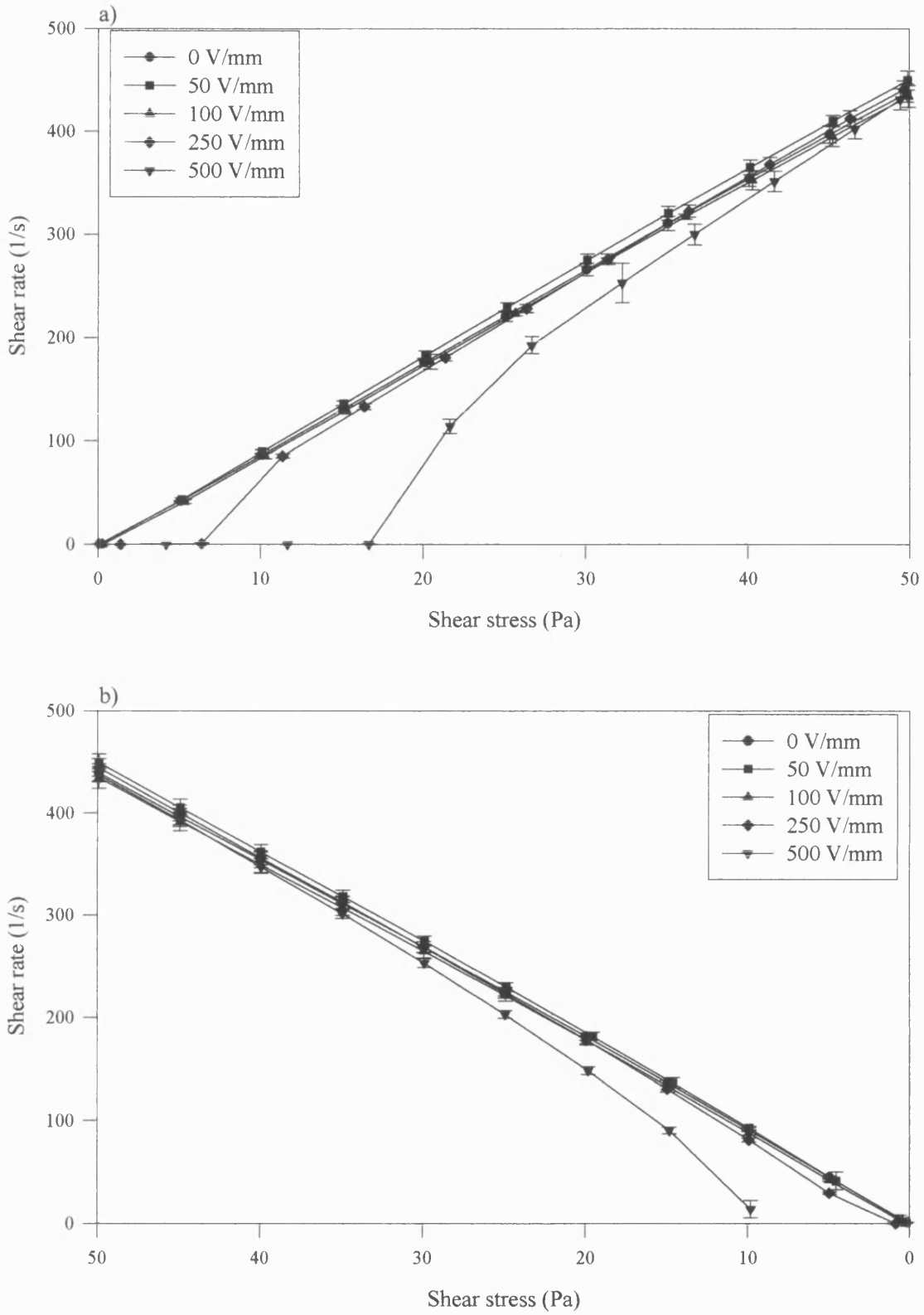

Figure 3.22 (a and b). The effect of applied electric field on the flow properties of 10.0 % w/w MCC (< 45 μm) in 100 cSt silicone oil (Sample A). Figure 3.22 (a and b) represent the ascending and descending curves respectively; error bars represent the standard deviation (n = 5).

Applied electric field	Bingham yield stress (Pa)					
V/mm	Sample A		Sample B		Sample C	
	Up	Down	Up	Down	Up	Down
50	0.3191 (0.0187)	0.1156 (0.0043)	0.3190 (0.0156)	0.1155 (0.0041)	0.3191 (0.0014)	0.1154 (0.0034)
100	0.5743 (0.0472)	0.1147 (0.0032)	0.5744 (0.0451)	0.1146 (0.0012)	0.5742 (0.0312)	0.1146 (0.0024)
250	2.9726 (0.0821)	1.1184 (0.0740)	2.9680 (0.0627)	1.1170 (0.0153)	2.9454 (0.0634)	1.0798 (0.0410)
500	8.7320 (0.3631)	3.0106 (0.3116)	8.7319 (0.2895)	3.0107 (0.3121)	8.7322 (0.3012)	3.0109 (0.2989)

Table 3.9. The effect of the magnitude of the applied electric field on the Bingham yield stress for a 10.0 % w/w suspension of MCC (sieve fraction below 45 μm) in 100 cSt silicone oil. Standard deviation values are shown in brackets (n = 5).

The development of a yield stress below 200 V/mm is questioned by Block and Kelly (1990) and Halsey (1992), however the observed increase in apparent viscosity is indicative of an ER response. At low shear stress under the influence of 50 V/mm electric field, the viscosity increased 15-fold (compared to conditions of no applied electric field), compared to a 75-fold increase at 100 V/mm. Static yield stress values at 50 and 100 V/mm of 4.312 Pa (± 0.541) and 7.822 Pa (± 0.698) respectively provided further evidence for field induced structure formation. The yield stress values obtained in the present study were found to be of a similar magnitude, if not higher in some cases, to previous research carried out at low applied electric fields (Marshall et al., 1989; Gandhi and Thompson, 1992; Lue and Mao, 1997).

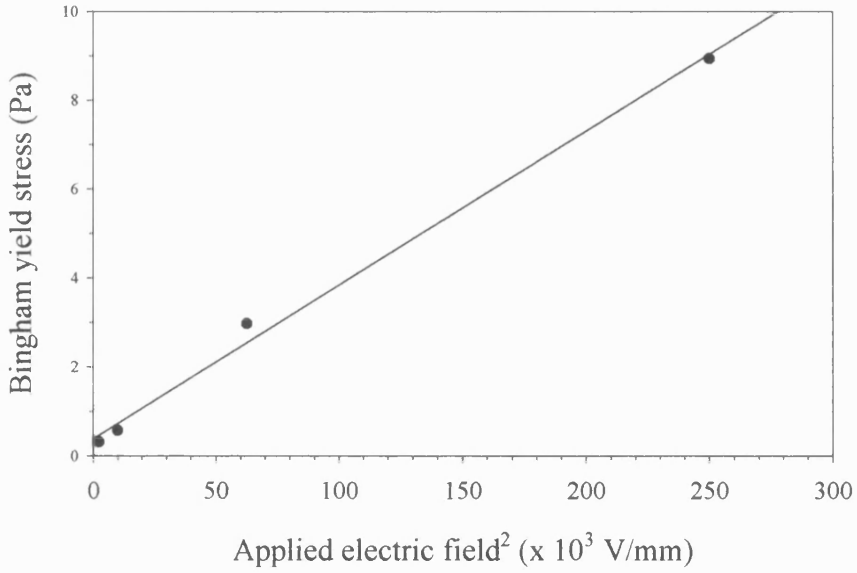

Figure 3.23. The relationship between Bingham yield stress and applied electric field. Errors bars representing the standard deviation (n = 15) are smaller than the symbols.

The yield stress followed a square dependence on the electric field (Figure 3.23), similar to results by other workers experimentally and theoretically (Marshall et al., 1989; Conrad et al., 1991; Klingenberg et al., 1990 and 1991a; Lemaire and Bossis, 1991; Xu and Liang, 1991). This is a common response, though not always the case for hydrous-based ER fluids systems. It follows from the fact that the interaction force for dipoles in an electric field is proportional to the field and many hydrous based fluids have linearly induced dipole moments. The net effect will be that the interaction force and consequently the strength of the fluid are proportional to the square of the electric field; this should hold until the particle's polarisability saturates. At high electric fields, saturation may occur (Winslow, 1949; Uejima, 1972; Stangroom, 1983; Havelka and Pialet, 1996) ultimately leading to electrical breakdown.

3.5.3. Rheological Behaviour of Three-Compartment Electrorheological Fluids

The rheological properties of 0.5 % w/w suspension of tacrine in 100 cSt silicone oil are presented in Figure 3.24 and Table 3.10.

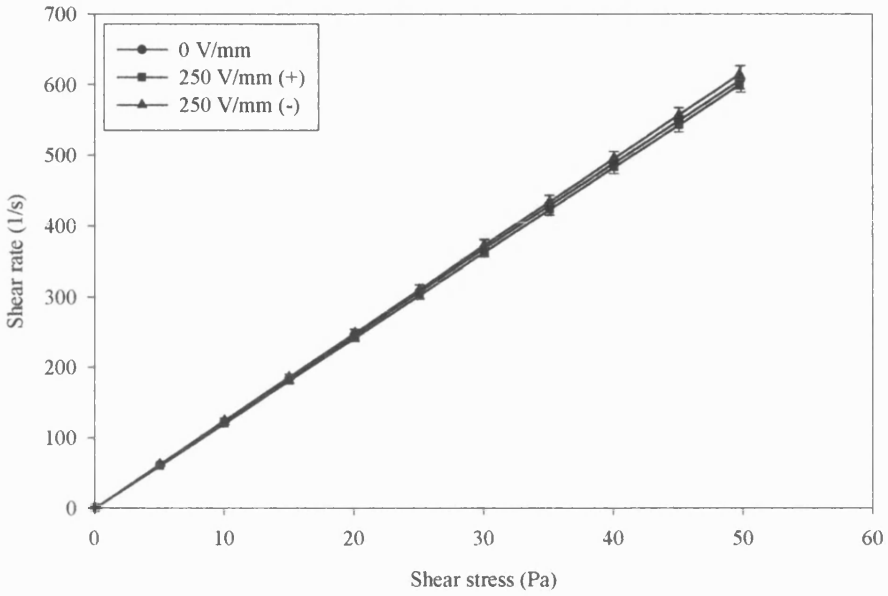

Figure 3.24. Ascending curves for 0.5 % w/w suspensions of tacrine in 100 cSt silicone oil at 0 V/mm and 250 V/mm. Error bars represent the standard deviation (n = 5).

The Newtonian viscosity of a 0.5 % w/w suspension of tacrine in 100 cSt silicone oil was 0.08186 Pa s (± 0.0026) and 0.08129 Pa s (± 0.0027) for the ascending and descending curve respectively. There was no significant difference between the ascending and descending curves ($p > 0.05$).

Conditions	Newtonian viscosity (Pa s)	
	Up	Down
0 V/mm	0.08186 (0.0026)	0.08129 (0.0027)
250 V/mm (+)	0.08290 (0.0017)	0.08206 (0.0015)
250 V/mm (-)	0.08092 (0.0015)	0.08017 (0.0014)

Table 3.10. The rheological behaviour of a 0.5 % w/w suspension of tacrine in 100 cSt silicone oil at 0 V/mm and 250 V/mm. Values for standard deviation are shown in brackets (n = 5).

A 0.5 % w/w suspension of tacrine in 100 cSt silicone oil did not exhibit an ER response at 250 V/mm. In addition, the effect of the upper electrode polarity was investigated. When comparing the Newtonian viscosity for the different treatments, there was no significant difference (one-way ANOVA; $p > 0.05$; $F = 1.98$). After completion of the experiment it was noted that tacrine particles appeared to clump on the lower plate i.e. the negative electrode. When the polarity was reversed and the lower plate became the positive electrode, this pattern was not so prominent. The small particle-size distribution of tacrine (see Section 2.2) may account for the lack of an ER response, however, it is more likely that electrophoresis is occurring owing to the positive charge on the tacrine. Furthermore, microscopic evidence reported in Section 3.5.5 indicated that tacrine particles do not rearrange upon application of an electric field.

Currently, there is little information available on three-compartment ER fluids. Klingenberg et al. (1995) introduced small amounts of protein (≤ 0.1 % by weight) to suspensions of alumina, silica or zeolite A in silicone oil. The response was investigated under ac electric fields up to 1.5 kV/mm. They observed a significant increase in the Bingham yield stress in suspensions containing protein. The proposed mechanism

involved enhanced polarisation of the disperse phase particles owing to the increased number or mobility of the charge carriers.

3.5.3.1. Effect of Particle Concentration

The effects of particle concentration on the rheological properties of MCC in a suspension of 0.5 % w/w tacrine in 100 cSt silicone oil under the influence of an applied electric field (250 V/mm) is shown in Figure 3.25. The Bingham yield stress values are also given below (Table 3.11).

Concentration	Bingham yield stress (Pa)	
% w/w	Up	Down
1.0	0.0945 (0.0278)	-0.1536 (0.0364)
2.5	0.3179 (0.0444)	0.0761 (0.0365)
5.0	1.0619 (0.0289)	0.3008 (0.0240)
10.0	2.8468 (0.2113)	1.4971 (0.1139)
20.0	8.2392 (0.2545)	7.1181 (0.2728)

Table 3.11. Calculated Bingham yield stress values for different concentrations of MCC (sieve fraction below 45 μm) and 0.5 % w/w tacrine in 100 cSt silicone oil (cf. Table 3.6 pp. 78). Standard deviation values are shown in brackets (n = 5).

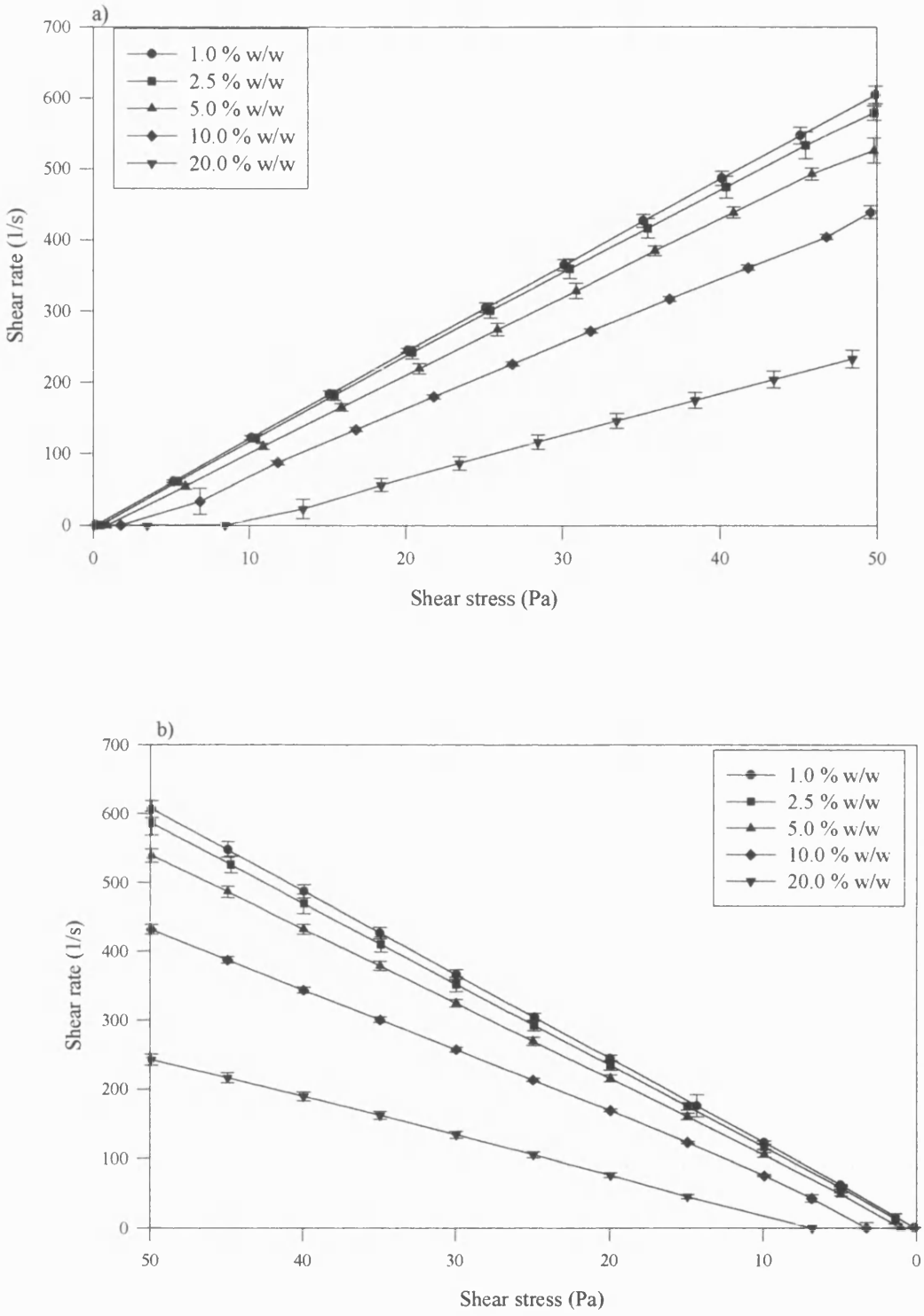

Figure 3.25 (a and b). The effect of the addition of 0.5 % w/w tacrine in different concentration suspensions of MCC (< 45 μm) in 100 cSt silicone oil at an applied electric field of 250 V/mm. Figure 3.25 (a and b) represent the ascending and descending curves respectively; error bars represent standard deviation (n = 5).

The addition of tacrine did not result in a significant difference ($p > 0.05$) in the Bingham yield stress for each concentration investigated. The low concentration of tacrine in the suspension may mean that there is not enough to make any significant difference to the ER response. Similar to the response observed in formulations containing MCC alone, the relationship between the Bingham yield stress and concentration was linear (Figure 3.26). The gradient, as estimated by least square linear regression, was 0.465 (± 0.0345) compared to 0.4440 (± 0.0289). As this is the relationship between the Bingham yield stress and the concentration, the addition of tacrine tended to produce higher yield stress values. In light of this finding, the tendency towards higher yield stresses may be accounted for by adsorption of tacrine to MCC powders producing larger particle sizes (as described in Section 2.9). This hypothesis could not be successfully quantified as the powders were not dry blended prior to the addition of silicone oil resulting in difficulties in the analysis of powder composites within the ER formulation.

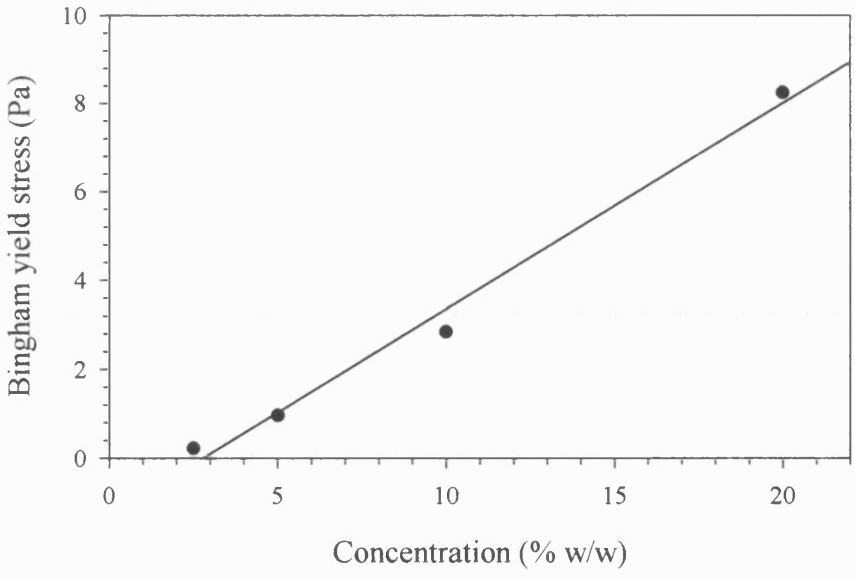

Figure 3.26. Relationship between the Bingham yield stress and the MCC concentration (sieve fraction below 45 µm) in 100 cSt silicone oil at 250 V/mm. Error bars representing the standard deviation are smaller than the symbols used (n = 5).

3.5.3.2. Effect of particle size

The rheological behaviour of 0.5 % w/w tacrine with different particle size MCC powders in 100 cSt silicone oil is shown in Figure 3.27. The Bingham yield stress values are given below (Table 3.12).

Particle size	Bingham yield stress (Pa)	
μm	Up	Down
< 45	0.0945 (0.0278)	-0.1536 (0.0364)
45 - 63	1.5838 (0.1392)	0.2362 (0.0710)
63 - 75	3.2458 (0.0712)	1.7792 (0.0356)
75 - 90	4.8248 (0.1437)	3.6036 (0.0646)
90 - 125	8.7704 (0.2484)	7.4838 (0.4195)

Table 3.12. The Bingham yield stress values for ER fluids comprising of 0.5 % w/w tacrine with different size MCC particles in 100 cSt silicone oil (cf. Table 3.7 pp. 83). Standard deviation values are shown in brackets (n = 5).

There was no significant difference (one-way ANOVA; $p > 0.05$) between the Bingham yield stress values for MCC suspensions with and without the addition of 0.5 % w/w tacrine up to and including the sieve fraction 63 - 75 μm. Large sieve fractions (75 - 90 and 90 - 125 μm) exhibited a significant increase ($p < 0.05$) in the Bingham yield stress values upon addition of tacrine.

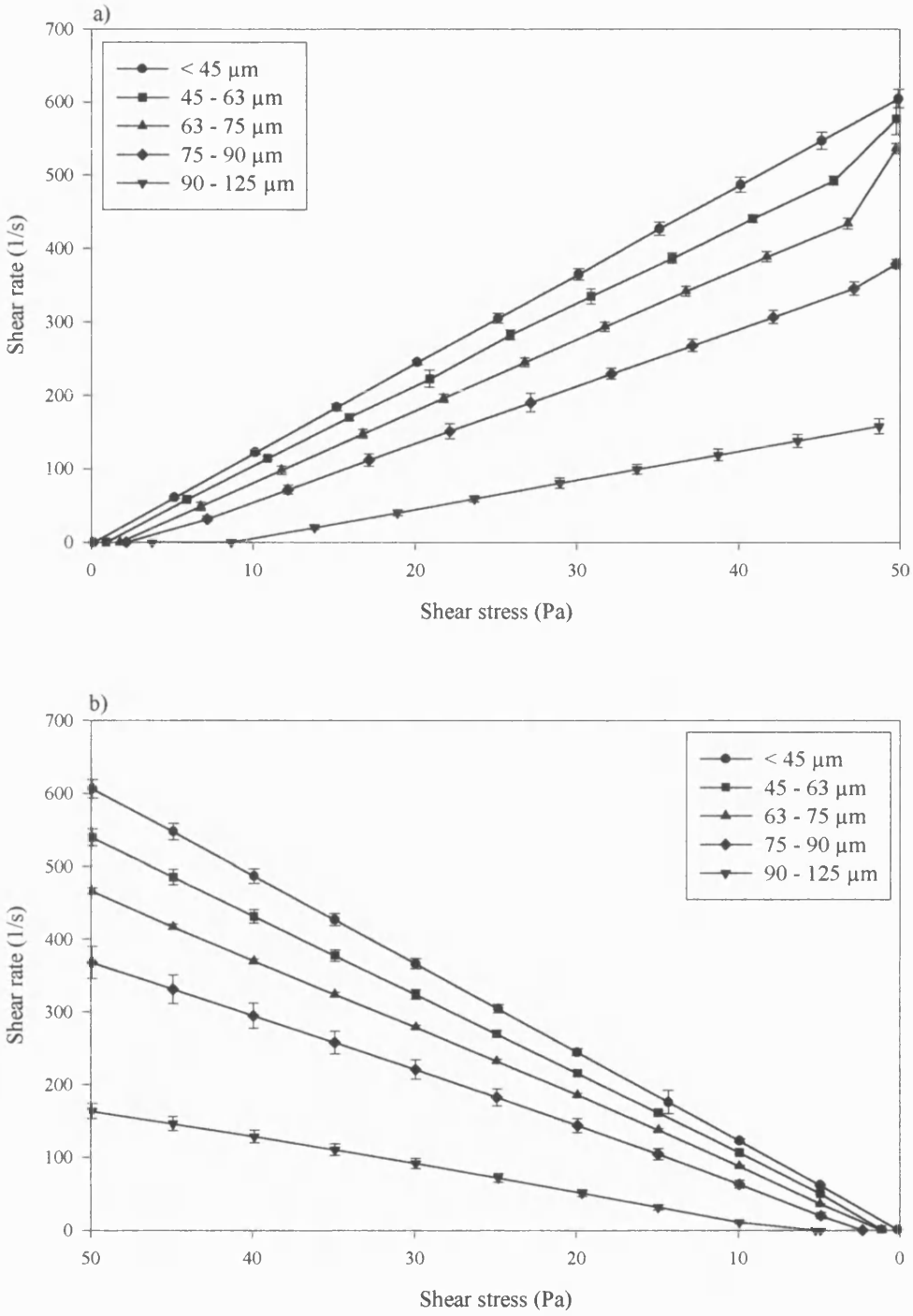

Figure 3.27 (a and b). The effect of the addition of 0.5 % w/w tacrine in different particle size suspensions of MCC (< 45 µm) in 100 cSt silicone oil at an applied electric field of 250 V/mm. Figure 3.27 (a and b) represent the ascending and descending curves respectively; error bars represent standard deviation (n = 5).

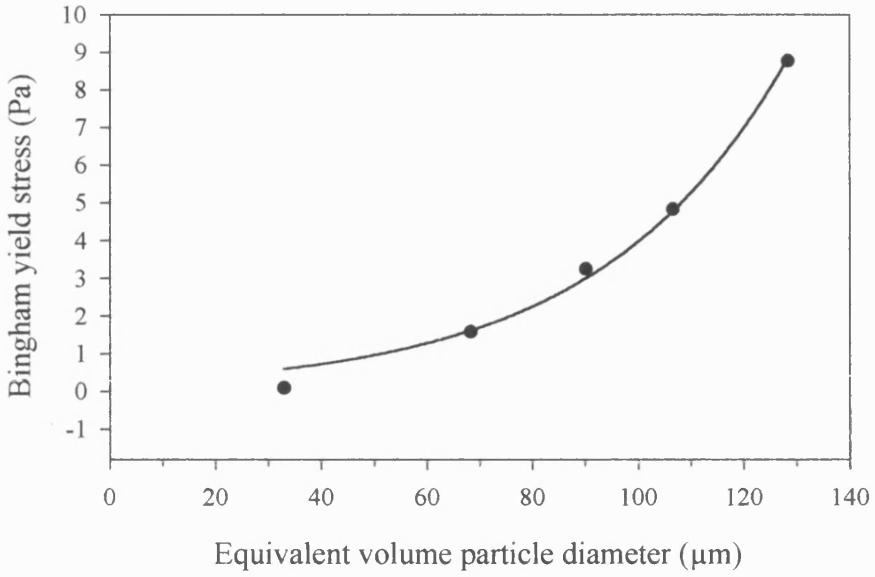

Figure 3.28. Relationship between the equivalent volume particle diameter of MCC and the Bingham yield stress. The suspensions contained equal number of particles (1.85 x 10^7/25 g). Error bars are smaller than the symbols used (n = 5).

The Bingham yield stress values exhibited an exponential increase with equivalent MCC volume diameter. The parameter b as described in Equation 3.3 is related to the equivalent volume particle diameter and remained constant for the regression analysis of Figure 3.28. The addition of tacrine yielded an estimated value for a as 0.2688 (± 0.0076) compared to 0.2352 (± 0.0558), with a regression value (r^2) of 0.99198. Although there was no significant difference ($p > 0.05$) found with the addition of tacrine, regression analysis pointed to a tendency for slightly higher yield stress values.

3.5.3.3. Effect of Moisture Content

The rheological properties of MCC powders of different contents with 0.5 % w/w tacrine in 100 cSt silicone oil are depicted in Figure 3.29 and the Bingham yield stress values are shown in Table 3.13.

Moisture content	Bingham yield stress (Pa)	
	Up	Down
Oven dried	0.8989 (0.1001)	0.3752 (0.0247)
LM50	2.6389 (0.1121)	0.2543 (0.0122)
XLM90	0.9001 (0.0990)	0.8754 (0.0879)

Table 3.13. The effect of moisture content on the development of the Bingham yield stress in suspensions of 0.5 % w/w tacrine with 10 % w/w MCC (sieve fraction below 45 μm) of different moisture contents in 100 cSt silicone oil at 250 V/mm (cf. Table 3.8 pp. 86). Standard deviation values are shown in brackets (n = 5).

The addition of tacrine resulted in a significant increase in the Bingham yield stress values for all moisture contents. The moisture content of tacrine was determined using infrared dryer described in Section 2.4 as 4.09 % (± 0.35). Moisture available as a result of the introduction of tacrine may transfer to the MCC particles.

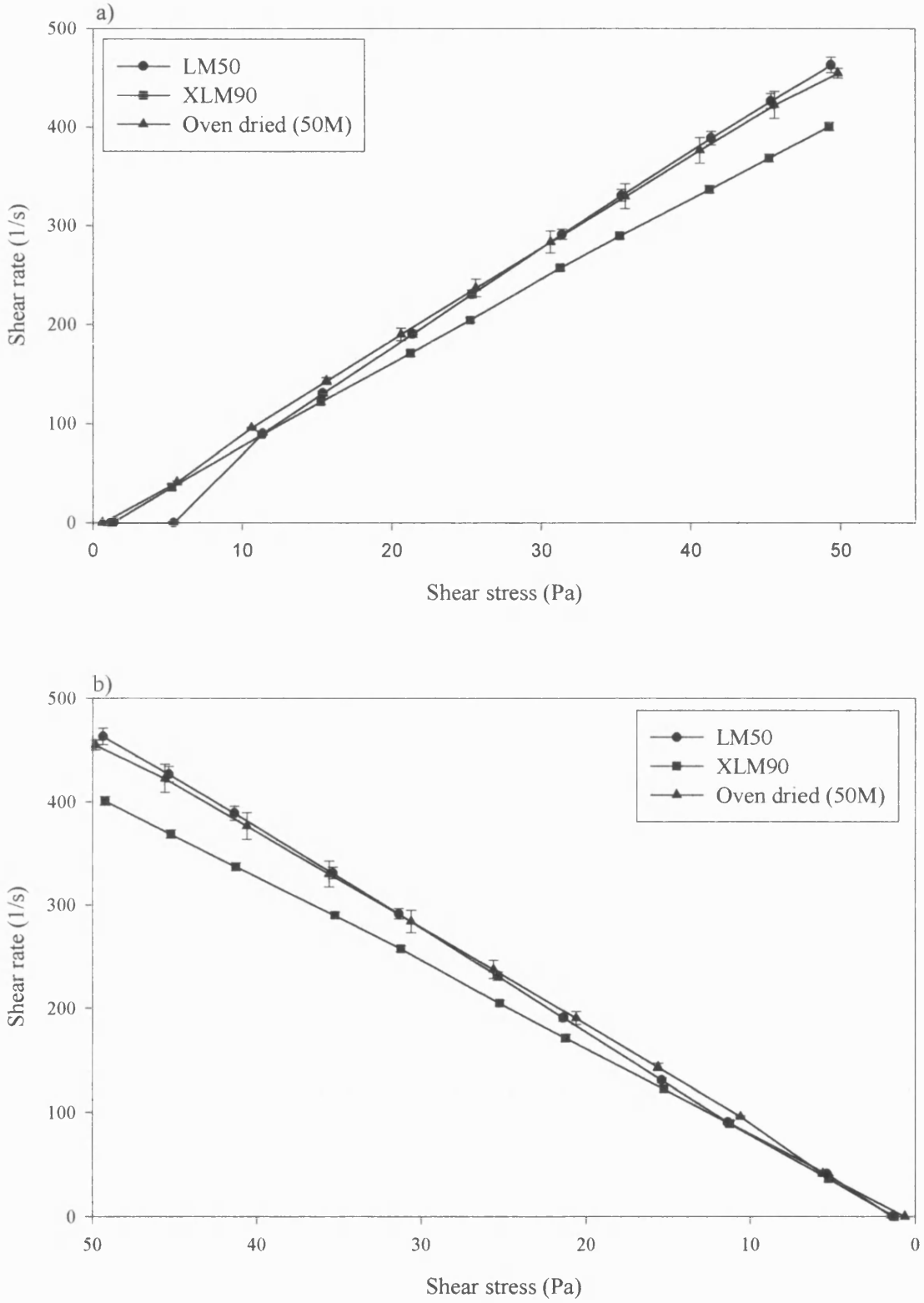

Figure 3.29 (a and b). The effect of the addition of 0.5 % w/w tacrine in different MCC moisture content suspensions in 100 cSt silicone oil at an applied electric field of 250 V/mm. Figure 3.29 (a and b) represent the ascending and descending curves respectively; error bars represent standard deviation (n = 5).

3.5.3.4. Effect of Applied Electric Field

The effect of applied electric field on the rheological properties of MCC (sieve fraction below 45 μm) and 0.5 % w/w tacrine in 100 cSt silicone oil are outlined in Figure 3.30 and Table 3.14.

Applied electric field	Bingham yield stress (Pa)	
V/mm	Up	Down
50	0.4833 (0.1195)	-0.0397 (0.0507)
100	0.6436 (0.0229)	0.0858 (0.0843)
250	3.0068 (0.2113)	1.4971 (0.1139)
500	8.0123 (0.3965)	3.9712 (0.5850)

Table 3.14. The effect of the applied electric field on the ER response of a suspension of 0.5 % w/w tacrine and 10.0 % w/w MCC (sieve fraction below 45 μm) in 100 cSt silicone oil (cf. Table 3.9 pp. 90). Standard deviation values are shown in brackets (n = 5).

A significant increase ($p < 0.05$) in the Bingham yield stress resulted in suspensions of 10.0 % w/w MCC (sieve fraction below 45 μm) containing 0.5 % w/w tacrine at applied electric fields of 50, 100 and 500 V/mm. However, no significant difference was observed with the addition of tacrine at an applied electric field of 250 V/mm. Further evidence for the enhanced effect of tacrine was provided by regression analysis of the relationship between the electric field squared and the Bingham yield stress (Figure 3.30). In the absence of tacrine, the gradient was 0.3919, however, in the presence of tacrine the gradient increased to 0.4804.

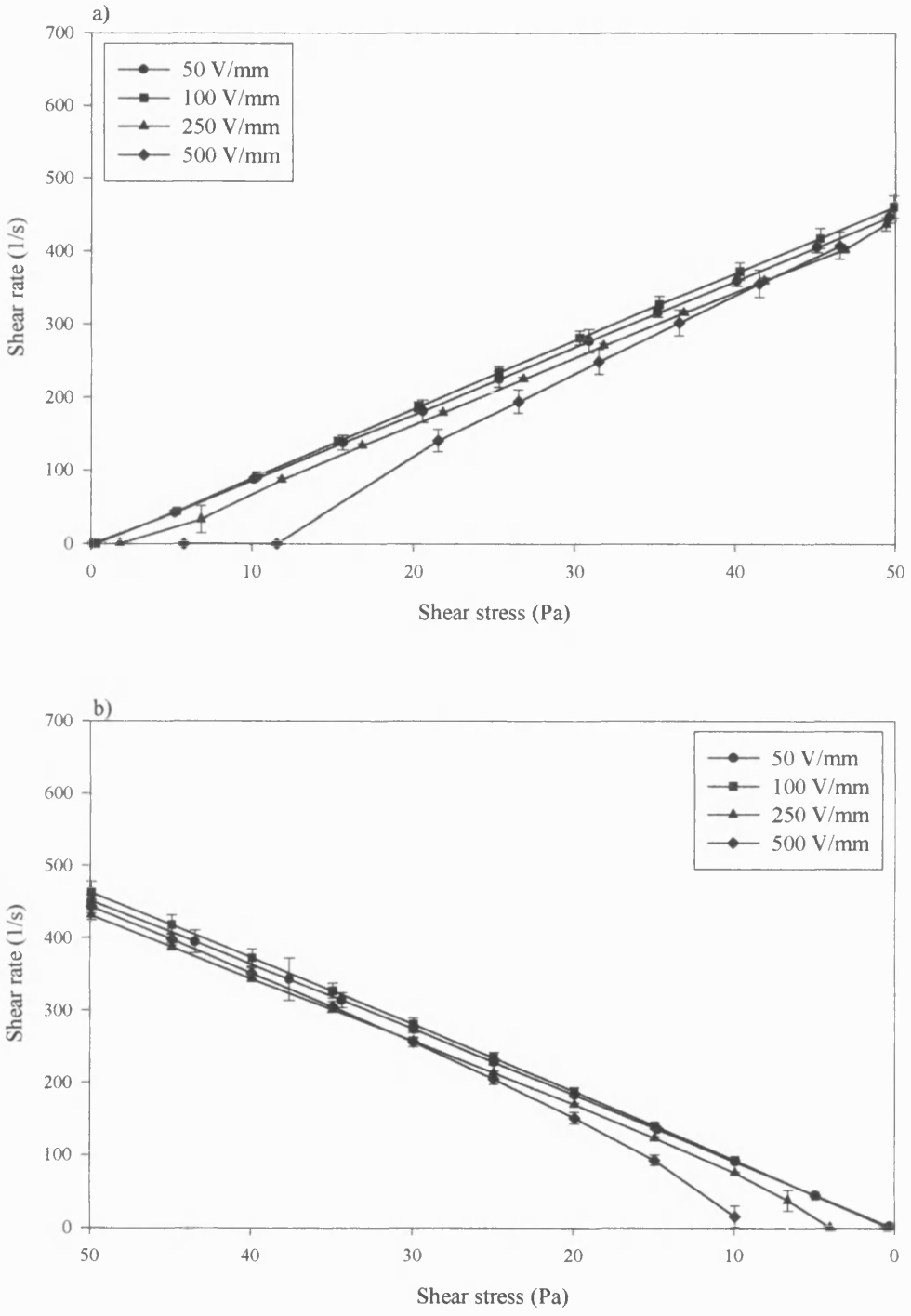

Figure 3.30 (a and b). The effect of the addition of 0.5 % w/w tacrine in a 10.0 % w/w suspension of MCC (< 45 μm) in 100 cSt silicone oil at different applied electric fields. Figure 3.29 (a and b) represent the ascending and descending curves respectively; error bars represent standard deviation (n = 5).

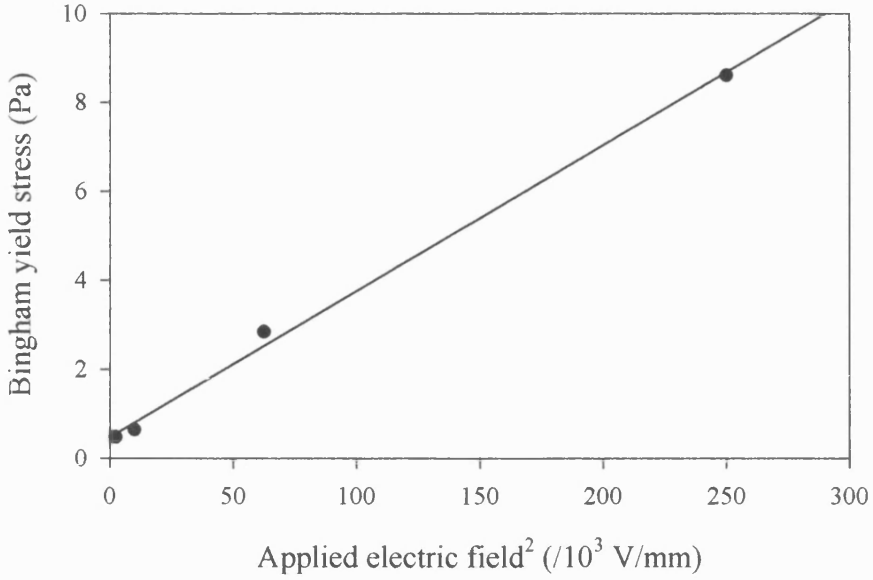

Figure 3.31. The relationship between the Bingham yield stress and the applied electric field on a suspension of 0.5 % w/w tacrine and 10.0 % w/w MCC (sieve fraction below 45 μm) in 100 cSt silicone oil. Error bars representing the standard deviation (n = 5) are smaller than the symbols used.

3.5.4. Rheological Behaviour of Microcrystalline Cellulose in Super Refined (or BP) Oils

Table 3.15 shows the rheological properties of 10.0 % w/w MCC (sieve fraction below 45 μm) in 100 cSt silicone oil under no applied electric field and after application of a 250 V/mm electric field. Figures 3.32 a and b depict the rheological behaviour of 10 % MCC (sieve fraction below 45 μm) with BP oils as substitutes for silicone oil.

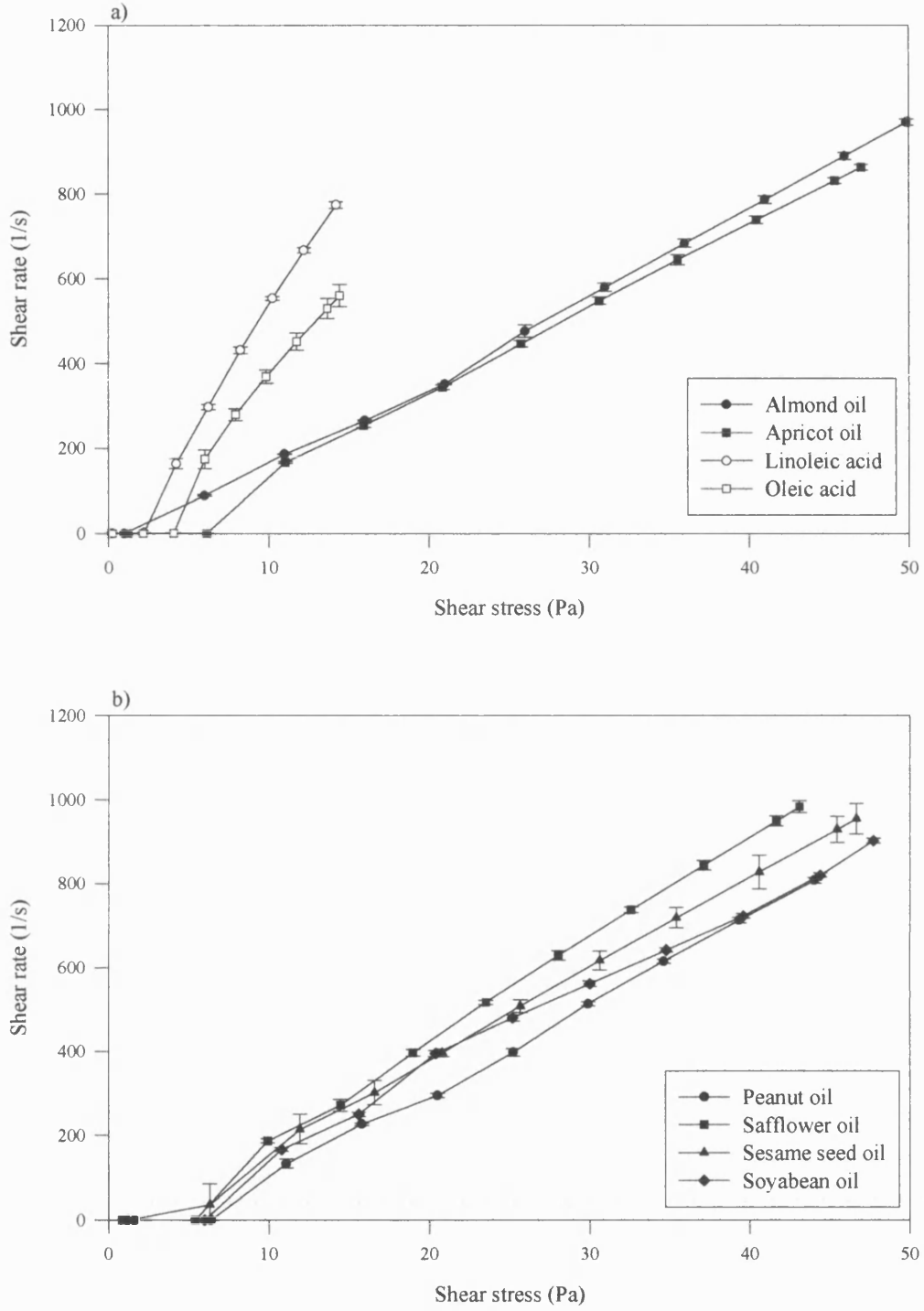

Figure 3.32 (a and b). The use of BP oils as substitutes for silicone oil as the continuous phase. The ER fluids were prepared with 10.0 % w/w MCC (sieve fraction below 45 μm) and the applied electric field was 250 V/mm. Error bars representing the standard deviation (n = 5) maybe smaller than the symbols used.

Super refined oil	Newtonian viscosity (Pa s)		Bingham yield stress (Pa)	
	Up	Down	Up	Down
Almond	0.05079 (1.4571×10^{-3})	0.04997 (1.3661×10^{-3})	2.6177 (0.1066)	1.7223 (0.1654)
Apricot	0.04778 (1.3973×10^{-3})	0.04794 (6.1102×10^{-5})	4.4883 (0.1388)	1.7597 (0.0987)
Linoleic	-	-	1.4832 (0.0901)	-
Oleic	-	-	2.3861 (0.2088)	-
Peanut	0.05329 (1.0024×10^{-3})	0.05256 (1.0492×10^{-3})	6.0577 (0.4471)	5.5785 (0.3104)
Safflower	0.04734 (1.0128×10^{-3})	0.04665 (1.0080×10^{-3})	3.3732 (0.1755)	1.4783 (0.1040)
Sesame seed	0.04503 (1.5454×10^{-3})	0.04414 (1.4434×10^{-3})	3.5433 (0.1607)	1.5897 (0.0870)
Silicone oil	0.0809 (0.0012)	0.00809 (0.0011)	2.9726 (0.0821)	1.1184 (0.0740)
Soyabean	0.04404 (2.0602×10^{-4})	0.04313 (8.1851×10^{-5})	3.5431 (0.1706)	1.544 (0.0891)

Table 3.15. Rheological properties of 10 % MCC (sieve fraction below 45 μm) in 100 cSt silicone oil and BP oils at 0 and 250 V/mm. Standard deviation values are shown in brackets (n = 5).

In general, the super refined oils afforded a higher Bingham yield stress, typically greater than 3.5 Pa compared to 2.5 Pa. Using the ANOVA test (one way), it was found that there were significant differences ($p < 0.05$) between the oils. A Fisher analysis was carried out to highlight where the difference occurred. No significant difference was found between almond and silicone oil. Safflower, sesame seed and soyabean oils were

also found not to be significantly different from each other In light of these findings, we conclude that super refined oils which have glycerides of oleic acid as the major constituents have generally have higher yield stress values compared with super refined oils having glycerides of linoleic acid as their major constituent. Further investigation using a 10.0 % w/w suspensions of MCC in the constituent acids confirmed that oleic acid as the base fluid produced a higher yield stress. In terms of the dielectric constants for the super refined oils, peanut oil with a dielectric constant of 3.51 (at 12 Hz) produced the highest yield stress at 6.0577 Pa. Generally, the higher the dielectric constant the greater the yield stress. The ER response is thought to arise through a mismatch in dielectric constants between the powder and the base fluid (Klingenberg et al., 1989; 1991a and b).

3.5.5. Microscopic Observation

The field-induced rheological changes described earlier are accompanied by equally dramatic changes in the suspension structure. It is now generally accepted that upon application of an electric field the particles align in the direction of the field forming a chain-like or fibrous structure (Winslow, 1949; Klingenberg and Zukoski, 1990).

Poor resolution of particle rearrangement presented difficulties when investigating concentrated suspensions. For this reason the photographs reproduced in the following section are representative of the images obtained using a 2.5 % w/w suspension of MCC (sieve fraction below 45 μm) in silicone oil. The field-induced structure formation in the quiescent fluid, at applied electric fields of 50, 100, 250 and 500 V/mm are illustrated in Figures 3.33 b, d, f, i. respectively. The corresponding fluids prior to electric field application are depicted in Figures 3.33 a, c, e, h respectively. A quantitative method using image analysis to determine the approximate column diameter was investigated. The loading process together with the tendency of the electrodes to behave as a capacitor after the removal of the electric field resulted in the particle clumping near the electrodes.

Subsequent analysis of the chain diameter resulted in poorly reproducible results. The general trends in the chain width are discussed in the following sections.

Particle rearrangement occurred at applied electric fields as low as 50 V/mm. The particles under the influence of a 50 V/mm electric field rearranged to form incomplete structures, typically in the middle of the electrode gap. This is in agreement with the sparse chain density calculated by Sakai et al. (1997) using a suspension of approximately 32 % corn starch in a insulating oil at 50 V/mm. At 100 V/mm single particle diameter chains spanning the electrode gap were observed. At these low applied electric fields, many of the clumps or loosely woven structures appear not to span the entire gap. Chains which are not parallel with the electric field are likely to be cross-links rather than individual chains formed at an angle to the electrodes. As the structures were allowed to develop over a 10 min period, there is a possibility that as gravity acts normal to the microscope slide that sedimentation would occur. In these circumstances, there is necessity for the forces involved in the chain formation to overcome gravity, possibly providing explanation for the incomplete chain formation observed at these low voltages. However, preliminary experiments carried out with the electric field application immediately after sample loading showed similar structure patterns, therefore negating the effects of gravity.

Figure 3.33 f depicts the structure formation at 250 V/mm. The removal of the electric field, caused the fibrils to breakdown resulting in a disordered fluid similar to the original arrangement (Figure 3.33 g). At 500 V/mm, the chains appear to no longer be composed of single particle thickness chains. The thickening of the particle fibrils with increasing applied electric field, could provide an explanation as to the increase in the Bingham yield stress. If the yield stress is defined as the stress which must be exceeded before the fluid flows, it stands to reason that enhanced chain formation would require a higher stress to disrupt and subsequently destroy it.

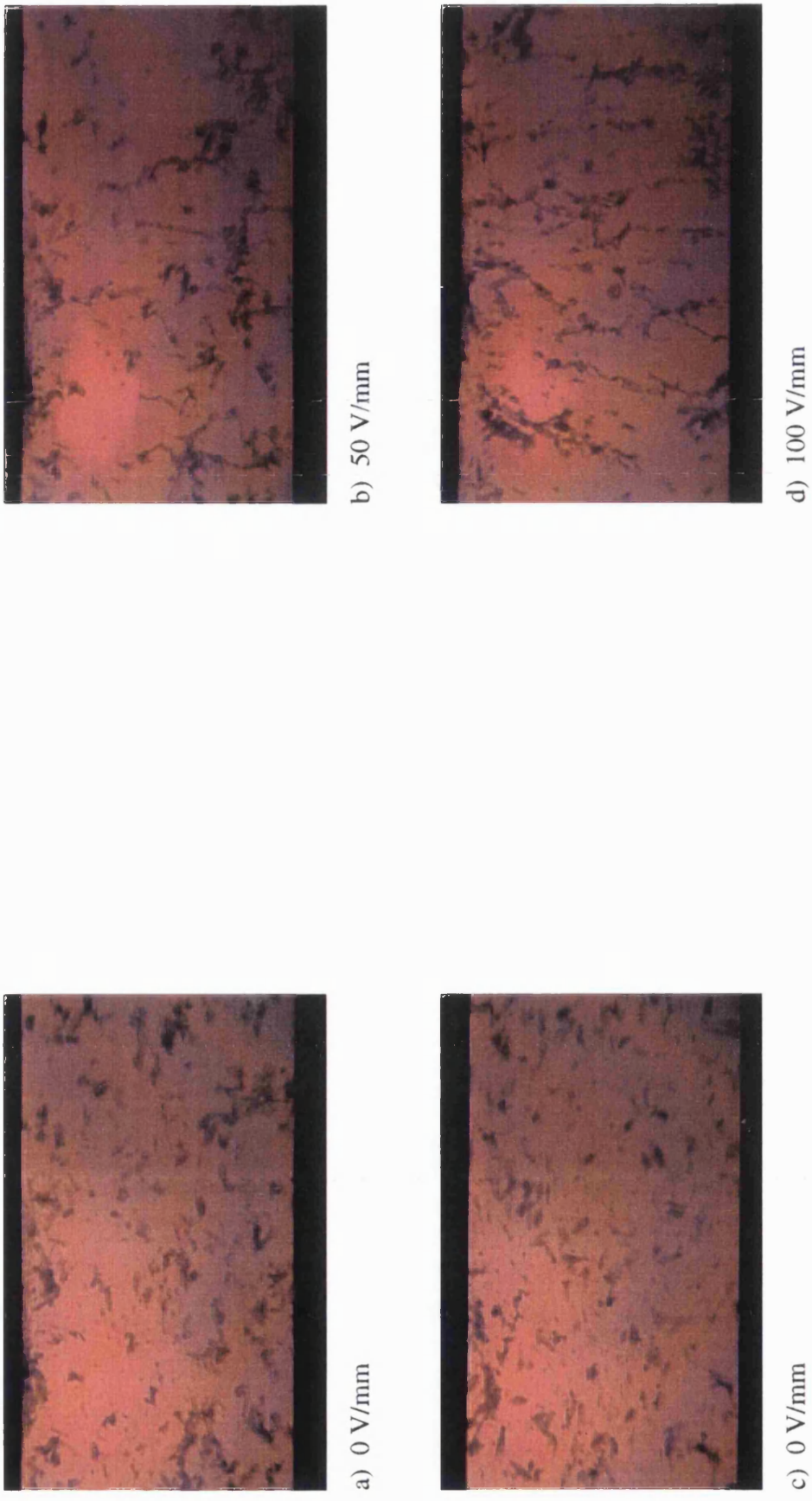

Figure 3.33 (a-d). Field-induced structure formation at applied electric fields of 50 (b), 100 (d). (a) and (c) are the corresponding zero-field images.

f) 250 V/mm

g) Removal of the applied electric field

e) 0 V/mm

Figure 3.33 (e-g). Field-induced structure formation at an applied electric field of 250 V/mm (f). (e) are the corresponding zero-field images.

i) 500 V/mm

h) 0 V/mm

Figure 3.33 (h and i). Field-induced structure formation at an applied electric field of 500 V/mm (i). (h) is the corresponding zero-field images.

The dominant features o' the chain formation were evident immediately upon application of the electri field (Figure 3.34 a). Photographic evidence has reinforced the conclusion that the duraton of tie applied electric field prior to analysis had no significant effect on the Bingham yield stres. Continuous readjustment of the particles occurred over the 5 min time period folowingthe initial stucture formation. Wen et al. (1999) concluded from their wok on the gereral structure kinetics that an initial change followed by contnuous adjustmens over an extendedtime period occurred. The chains are observed to coalesce ove the long time period, leading to a coarsening of the fibrous structue (Figure 3.34 c). Clear zones can beclearly distinguished at this stage. There appeared to be no furtherchain earrangement after 5 min.

At low concentraions, the microstructure consisted mainly of incomplete or isolatec chains of a singl partice width. Asthe concentration increased, the number densityof the chains increased vithout muchincrease in the average width At high concentrations, the structure consisted of thick clusters. Structures consisting of bundles rather than isolated chains are lilely to have an increased strength arising from the increased particle contactpoints. This hypothesis is substantiated by the high yield stressesobserved with concentraed suspensions. At sufficiently high enough concentations, the columns became indiscernible under the light microscope.

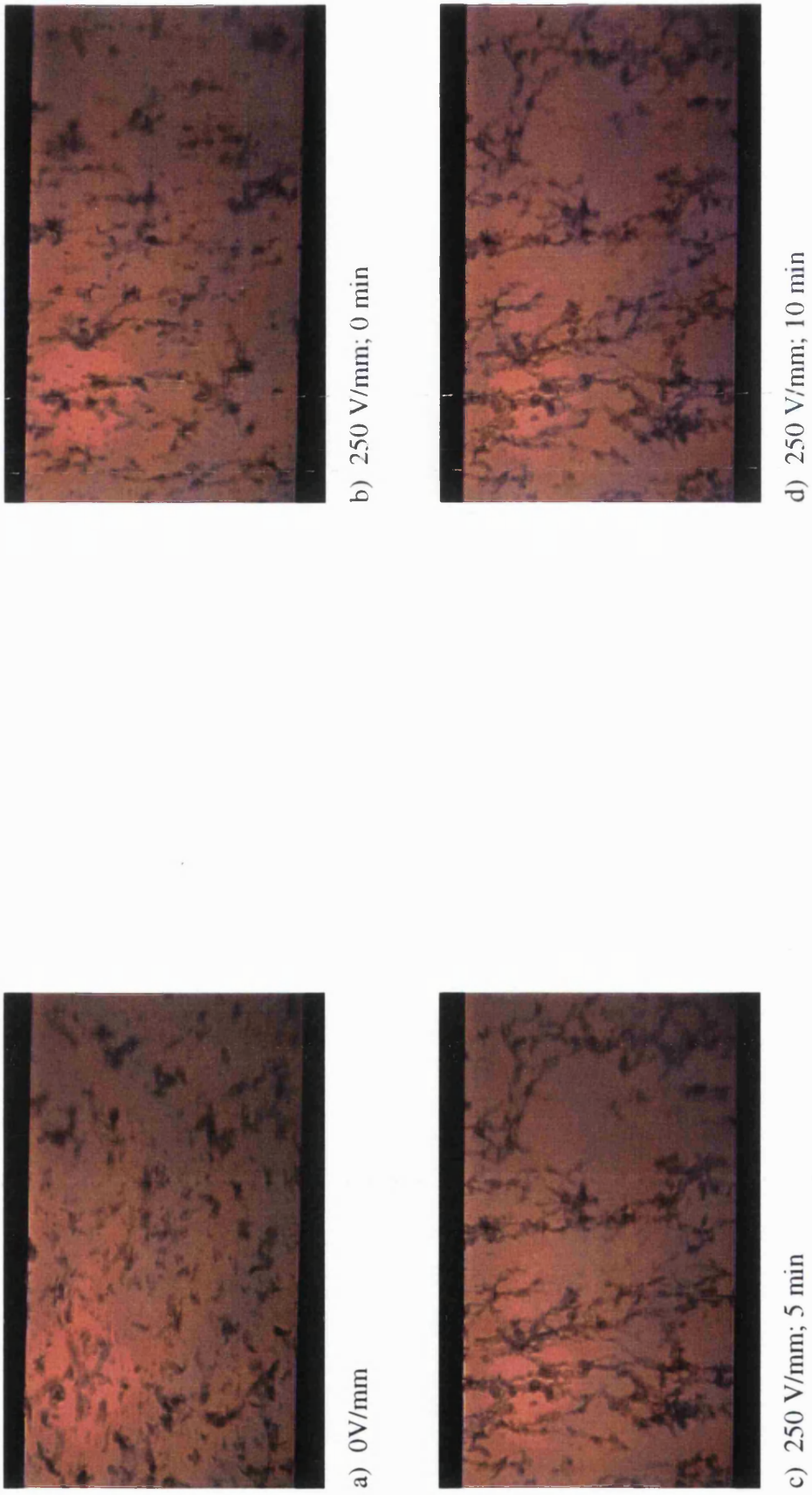

Figure 3.34 (a-d). Field-induced structure formation, immediately (b), 5 min (c) and 10 min (d) after application of an electric field of 250 V/mm.

3.6. Conclusions

We have demonstrated the presence of a yield stress at physiologically acceptable low applied electric fields. Particle concentration, size and moisture content were found to increase the Bingham yield stress value. For example, increasing the concentration from 1.0 to 10.0 % w/w resulted in a yield stress of 7.96 Pa (± 0.23) compared to 0.09 Pa (± 0.004); a similar increase was observed for particle size. The moisture content in MCC was found to have a significant effect on the ER behaviour; oven dried and very low moisture grades of MCC (XLM90) exhibited a decrease in the Bingham yield stress from approximately 3.0 Pa to 0.9 Pa. Low moisture grades of MCC (LM50) were found to have no effect on the Bingham yield stress value, possibly as a result of the particle-size distribution, indicating that particle-size effects may overcome the decreased moisture content. The relationship between the magnitude of the applied electric field and the Bingham yield stress was approximately linear, with an yield stress increase from 0.32 Pa (± 0.02) to 8.73 Pa (± 0.36) at 50 and 500 V/mm respectively. The ER response at 50 V/mm resulted in a power consumption of 0.5 mW, therefore within the order of magnitude stated for pacemaker batteries.

High yield stress values can be obtained by the judicious choice of parameters. The yield stress values obtained in the present study were found to be of similar magnitude, if not higher in some cases, to previous research carried out at low applied electric fields (Marshall et al., 1989; Chen et al., 1991; Gandhi and Thompson, 1992; Malins and Lacey, 1994; Parthasarathy and Klingenberg, 1996).

Typically, microscopic observations has provided evidence for particle alignment upon application of an electric field at fields as low as 50 V/mm. Although chains spanning the entire electrode gap do not appear until 250 V/mm, a noticeable increase in the apparent viscosity was observed below this level. It is likely that even pre-chain completion, agglomerates influence fluid structure in a manner which affects the flow.

The creep and recovery behaviour of ER fluids will be investigated in Chapter Four. Typically, creep experiments are conducted in the linear viscoelastic region, where the strain is proportional to the applied stress. Analysis in the viscoelastic region is designed not to destroy the structure, thereby providing information on the intermolecular and inter-particle forces within the structure. The creep and recovery behaviour will be investigated using the factors described above, namely particle concentration, size and moisture content, together with the magnitude of the applied electric field.

Chapter Four

Creep Behaviour of Electrorheological Fluids

4.1. Introduction

Flow experiments have provided information on the yield stress and strength of ER fluids. Creep and recovery experiments are intended to complement these findings and enhance our understanding of the structure-formation process. As in the flow experiments (Chapter Three), several factors, namely particle size, particle concentration and the magnitude of the applied electric field will be investigated.

The process of creep may be defined as the slow and progressive deformation of a material with time, under a constant stress. Creep experiments are usually conducted in the linear viscoelastic region, where the strain is proportional to the applied stress. Investigations carried out in this region are designed to be rheologically non-destructive, thereby providing information on the intermolecular and interparticle forces within the structure (Barry, 1974). The results of such experiments may then be interpreted using linear viscoelastic theory as the Boltzmann principle is obeyed (Ferry, 1970). The material, initially at rest, is subjected to a constant shear stress (σ_o). The shear strain (γ) is monitored as a function of time. The stress is removed and the rate and extent to which the sample recovers its original dimensions are measured. The total creep compliance (J_t) is the strain (γ) divided by the stress (σ_o):

$$J_t = \frac{\gamma}{\sigma_o}$$

Mechanical models comprising of springs and dashpots, arranged in parallel or in series, provide a popular method of describing linear viscoelastic behaviour. In mechanical models, Newtonian flow is represented by a dashpot (where the force is proportional to the rate of extension) (Figure 4.1a), whilst Hookean deformation is represented by a spring (where the force is proportional to extension) (Figure 4.1b). The

individual elements can be combined, in series or in parallel to describe complex viscoelastic behaviour, for example, the Maxwell model consists of a dashpot in series with a spring. A Voigt unit comprises of a spring of compliance J_o and a dashpot of viscosity η_o mounted, in parallel, on a rigid frame (Figure 4.1c).

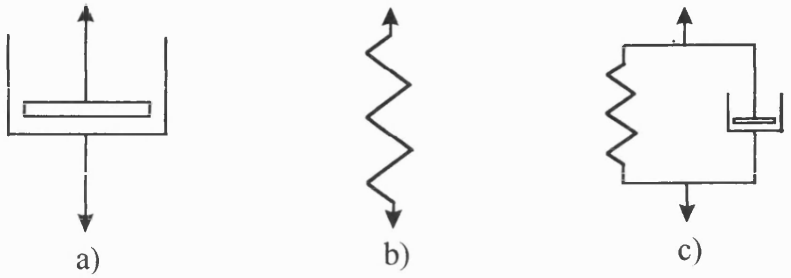

Figure 4.1. Mechanical representation of a viscous liquid (a), an elastic solid (b) and a Voigt unit (c).

A typical creep and recovery curve is illustrated in Figure 4.2. According to convention, the curve is in units of compliance (strain/stress) versus time, thus the same curve is produced regardless of the magnitude of the applied stress provided the test is in the linear viscoelastic region.

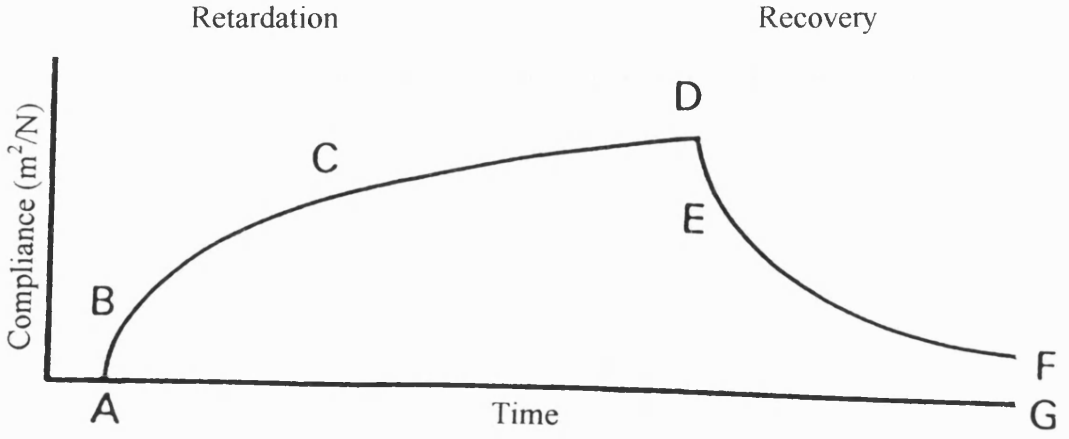

Figure 4.2. Typical creep compliance and recovery curve for a viscoelastic material.

The creep compliance and recovery curve can be divided into three regions. The initial region (A-B) is characteristic of the instantaneous compliance associated with the elastic component. B-C is representative of the time-dependent retarded elastic behaviour exhibited by a single Voigt unit. The existence of additional Voigt units is accounted for by the summation of each individual unit (Equation 4.1). C-D is the linear region of Newtonian compliance indicative of the residual viscous flow or viscosity of the dashpot fluid. On removal of the stress, the recovery curve is represented by D-F. There is an instantaneous elastic recovery (D-E) of the same magnitude as A-B, followed by a retarded elastic recovery (E-F) equivalent to the region B-C. The latter portion of the creep curve is not recoverable as the bonds are irreversibly ruptured in the region represented by C-D. The creep compliance curve enables the spring compliance (J_o) and zero-shear viscosity (η_o) to be determined from the regions A-B and C-D respectively. The total compliance (J_t) for a viscoelastic material may be described mathematically as:

$$J_t = J_o + \sum_{i=1}^{i} J_i \left[1 - \exp\left(-\frac{t}{\lambda}\right) + \frac{t}{\eta_o} \right]$$

where J_o is the compliance of the elastic spring and η_o is the residual shear viscosity of the dashpot liquid. The compliance associated with the Voigt units is calculated by the summation of the individual elements:

$$J_t = \sum_{i=1}^{i} J_i \left[1 - \exp\left(-\frac{t}{\lambda}\right) \right] \qquad \text{Equation 4.1}$$

The development of the mathematical theory of linear viscoelasticity is based on the assumption that the response (strain) at any time is directly proportional to the value of the initiating signal (stress). Thus, in linear viscoelastic theory, the differential equations are linear. In addition, the coefficients of time are constant, thereby enabling the prediction of material parameters such as spring compliance (J_o) and zero-shear viscosity (η_o). Compared to linear theory, characterisation of the non-linear response of a material is much more complex. There is no specific generalised constitutive equation that is universally acknowledged and which is capable of predicting the mechanical behaviour of different types of non-linear viscoelastic material. Several constitutive equations have been developed for describing the non-linear behaviour of viscoelastic materials (Green and Rivlin, 1957, 1960; Tervoort, 1996; Drozdov, 1997).

4.1.1. Creep Behaviour of Electrorheoloigcal Fluids

ER fluids have been shown to exhibit Bingham behaviour under the influence of an electric field (Chapter Three). In terms of the mechanical models described above, a material exhibiting a yield stress can be represented by the addition of a slider corresponding to the stress which must be overcome prior to flow initiation (Figure 4.3).

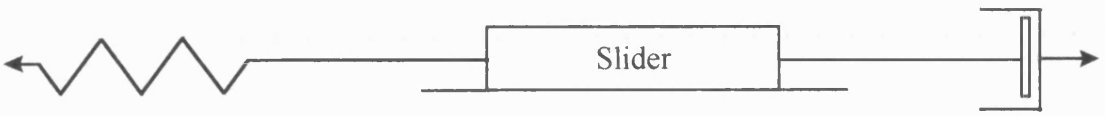

Figure 4.3. Diagrammatic representation of ideal Bingham fluid behaviour.

At shear-stress values below the yield stress, the fluid is expected to behave as an elastic solid, the strain increases with time towards a constant value and a complete strain recovery may be observed upon the removal of the stress (Nguyen and Boger, 1992). At

stresses above the yield stress, the strain increases indefinitely with time and a steady rate of shear indicating viscous flow will be attained.

The development of yield stress in steady-state shear stress experiments can be derived from the single-chain model in which the particles all align into fully developed chains. According to the single-chain model, under the influence of an electric field, ER behaviour is characterised by Voigt units (Otsubo and Edamura, 1994, 1995, 1996). The elastic modulus is derived from the chains and the viscosity component from the suspending fluid. Several researchers (Conrad et al., 1991; Gamota and Filisko, 1991) have shown the existence of viscoelastic behaviour in ER fluids at shear-stress values approaching the yield stress. However, viscoelastic experiments have produced contradictory information on the relationship between the rheological behaviour and magnitude of the applied electric field (Klingenberg, 1993). Furthermore, the rheological behaviour expressed by a given sample is dependent on the applied stress, applied electric field and, in the case of oscillatory experiments, the frequency and magnitude of the applied stress.

The failure of creep and indeed oscillation experiments to verify the predicted model particularly at high particle concentration, stems from the coalescence of primary structures into columns or clumps (Gamota and Filisko, 1991). Otsubo and Edamura (1994, 1995, 1996) have published a series of articles on the creep and recovery behaviour of ER fluids. The creep and recovery behaviour fell into three distinct categories, depending on the applied stress in relation to the predicted yield stress. These creep and recovery responses will be described below in detail in Section 4.4.2. The static yield stress estimated from the viscous flow transition was approximately 70 % of the static yield stress predicted from the steady flow curve (Otsubo and Edamura, 1994).

4.2. Materials and Methods

ER fluids were prepared using sieve fractions of MCC (Emcocel 50M, LM50 and XLM90) and 100 cSt silicone oil as previously described in Section 2.1. A 0.1 % w/w aqueous solution of potassium chloride was used as the electrolyte for all ER measurements.

Several factors have been shown to influence the Newtonian viscosity (0 V/mm) and the development of the Bingham yield stress under the influence of an electric field (see Chapter Three). The following parameters will be investigated to establish the creep and recovery behaviour of ER fluids with and without the application of electric field: particle concentration, particle size and the magnitude of the applied electric field. The role in moisture content in the creep and recovery behaviour will not be investigated owing to the hygroscopic nature of MCC. The preparation of ER fluids is outlined above in Section 2.4, with specific details relating to particle concentration and particle size in Sections 3.4.2 and 3.4.3.

In order to achieve consistent and reproducible results from creep experiments, it is important to ensure that the material under test is in a completely relaxed state. The loading of the sample is critical and it is usual to leave the sample to stand for several hours prior to the experiment. In the case of suspensions, sedimentation is likely to occur over such time scales, as gravity acts normal to the parallel plate. As the application of an electric field has been shown to induce particle rearrangement (Section 3.5.5), it was considered unnecessary to ensure a completely relaxed state prior to experiment commencement. Preceding assessment of the creep and recovery response, a simple but effective test was conducted to determine the linear viscoelastic range for each sample, both in the non-electrified and electrified states. The applied stress is increased until the strain is observed to increase gradually indicating the attainment of the linear viscoelastic region.

The electrorheometer used in these studies is described in Section 3.3. Prior to initiating the experiment, all samples were subjected to an applied stress of 1.0 Pa for 5 min, and then electrified, in the quiescent state, for a further 10 min. The initial pre-shear of the test fluid was found to reduce errors associated with failure to ensure a completely relaxed state. Subsequently, the stress was applied and maintained for 2 min, after which time the stress was removed and the rate and extent to which the sample recovered were monitored for 2 min. A parallel-plate geometry of 40.0 mm diameter was chosen for the experiments with a gap of 1.0 mm (see Section 3.3). All measurements were conducted at 37 °C (± 0.1 °C). Samples were prepared in triplicate (Samples A, B and C) with five determinations at each stress being performed.

Data were collected via a personal computer using TA Instruments software and subsequently processed using Excel 7.0 for the purpose of graphical reproduction (Windows 95, Microsoft Corporation, USA). In all cases, the graphs reproduced are for Sample A and are entirely representative of the responses observed for Samples B and C. The standard deviation values are represented by error bars (n = 5), which may in some cases be smaller than the symbols used. Circles (•) represent the creep response, whilst square symbols (▪) represent the recovery behaviour.

4.3. Results and Discussion

4.3.1. Creep and Recovery Responses under no Applied Electric Field

The experiments were carried out in the linear viscoelastic region, where the strain is proportional to the stress, for all samples investigated under no applied electric field. Upon application of the stress, the compliance was observed to increase at a constant rate which is inversely proportional to the zero-shear viscosity. Upon removal of the applied stress, no recovery was observed. The combined creep and recovery response is typical of

a viscous or Newtonian fluid. The strain was observed to increase as a constant rate in response to the application of a uniform stress and may be fitted to the following equation:

$$\eta_o = \frac{\sigma}{\gamma} = \frac{1}{[dJ(t)/dt]}$$

where η_o is the zero-shear viscosity of the sample, which can be calculated from the reciprocal of the slope:

$$J_t = \frac{t}{\eta_o} \qquad \text{Equation 4.2}$$

Table 4.1 shows the viscosity of different MCC concentrations (sieve fraction below 45 μm) in 100 cSt silicone oil as measured by the reciprocal of the retardation slope. Furthermore, for comparison, the viscosity as determined using the flow technique is presented (Section 3.5.1.1). In Figures 4.4, 4.5 and 4.6, the responses observed under a constant stress of 1.0 Pa and 2.5 Pa for 20.0 % w/w MCC concentration (retardation) and after removal of the stress (relaxation) are shown as creep and recovery curves.

There was no significant difference (one-way ANOVA; $p > 0.05$) observed between samples (A, B and C) of each concentration. However, significant differences (one-way ANOVA; $p < 0.05$) were observed between the predicted viscosity values determined by the reciprocal of the slope and the steady-state flow method for concentrations greater than and equal to 5.0 % w/w. The viscosity predicted using the reciprocal of the creep curve is indicative of the zero-shear viscosity of the sample, and therefore reflects the absolute-viscosity value.

Concentration	Viscosity ($1/\eta_o$)			Newtonian viscosity
(% w/w)	Sample A	Sample B	Sample C	(Pa s)
1.0	0.0813 (0.0017)	0.0824 (0.0026)	0.0819 (0.0021)	0.08090 (0.0005)
2.5	0.0894 (0.0012)	0.0900 (0.0010)	0.0901 (0.0005)	0.08981 (0.0023)
5.0	0.1021 (0.0025)	0.1031 (0.0016)	0.1027 (0.0014)	0.0941 (0.0010)
10.0	0.1404 (0.0023)	0.1397 (0.0019)	0.1400 (0.0012)	0.1136 (0.0018)
20.0	0.3840 (0.0301)	0.3844 (0.0292)	0.3846 (0.0283)	0.02079 (0.0036)

Table 4.1. The viscosity of MCC (sieve fraction below 45 μm) at different concentrations in 100 cSt silicone oil. The standard deviation is shown in brackets (n = 5).

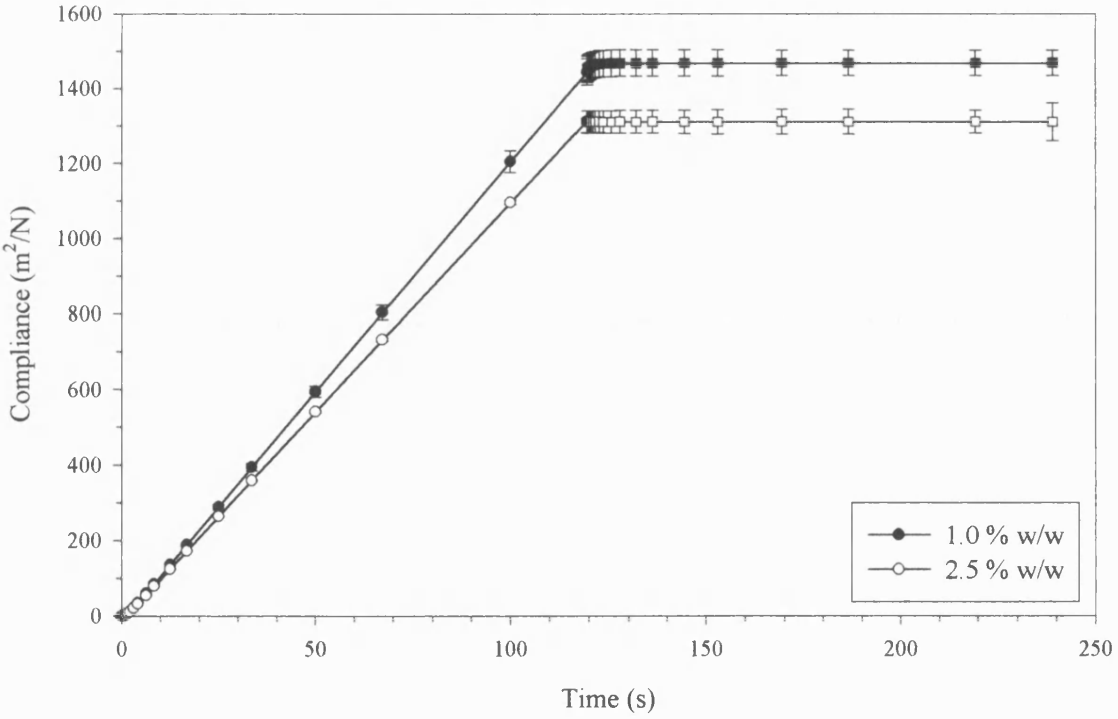

Figure 4.4. Creep (•) and recovery (■) curves for 1.0 and 2.5 % w/w suspensions of MCC (sieve fraction below 45 μm) in 100 cSt silicone oil at an applied stress of 1.0 Pa.

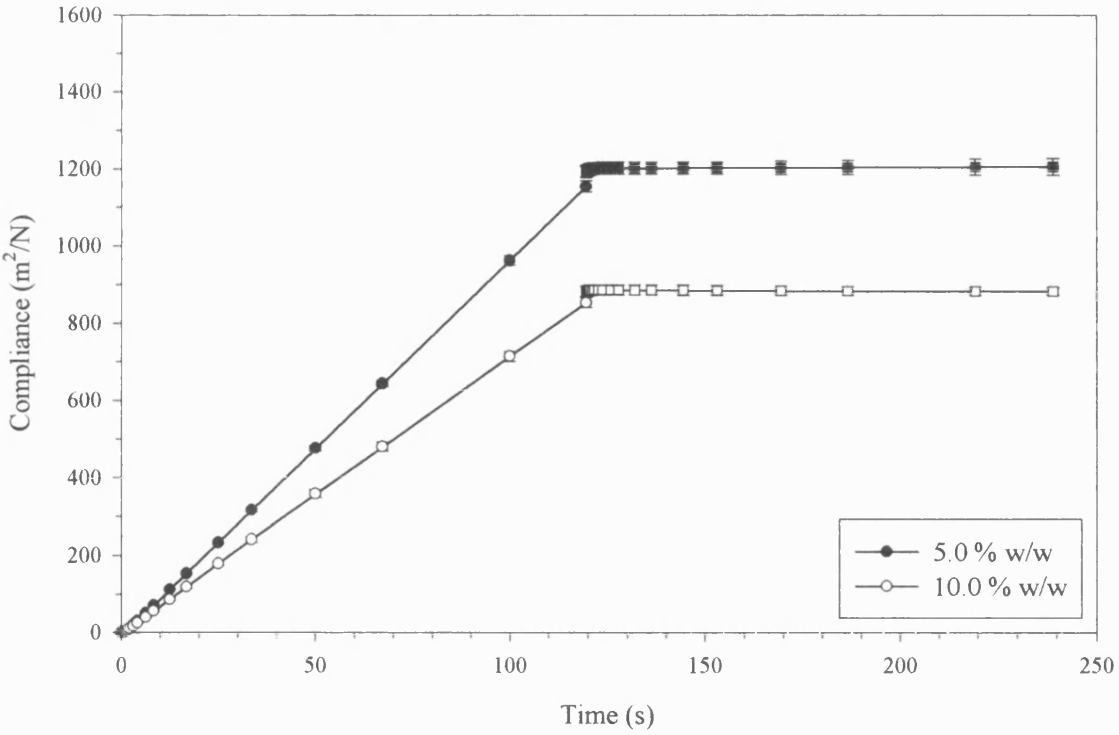

Figure 4.5. Creep (•) and recovery (■) curves for 5.0 and 10.0 % w/w suspensions of MCC (sieve fraction below 45 μm) in 100 cSt silicone oil at an applied stress of 1.0 Pa.

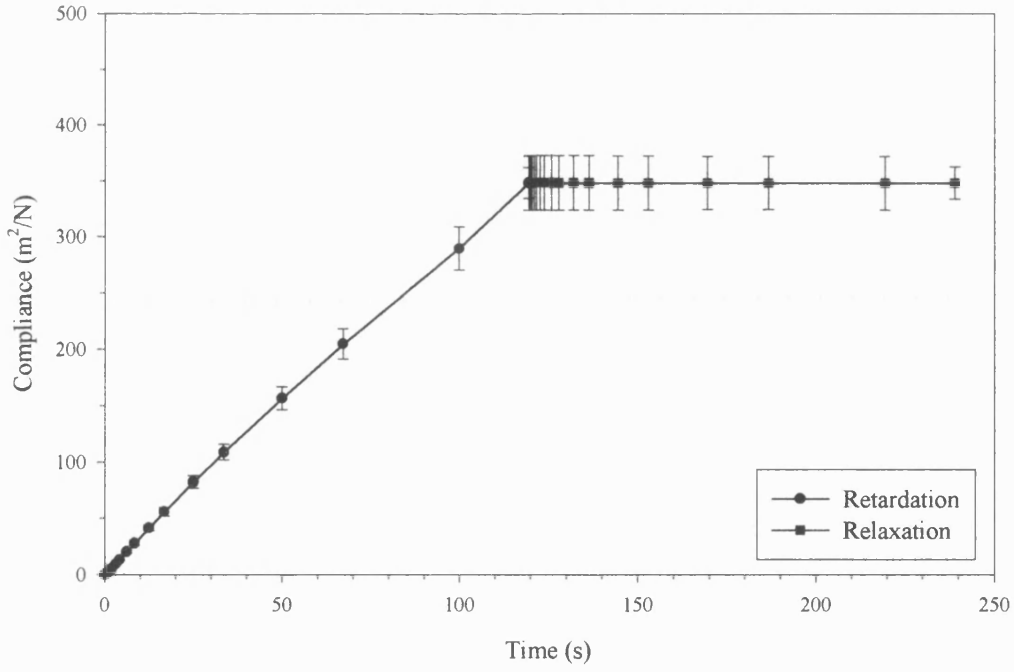

Figure 4.6. Creep (•) and recovery (■) curve for a 20 % w/w suspension of MCC (sieve fraction below 45 μm) in 100 cSt silicone oil at an applied stress of 2.5 Pa.

The creep response was measured in the linear viscoelastic region, enabling the zero-shear viscosity to be estimated (Equation 4.2) for MCC suspensions containing particles of different sieve fractions. The determined viscosity values of different sieve fractions of MCC in silicone oil are tabulated below (Table 4.2). In Figures 4.7 and 4.8, the creep and recovery curves are illustrated.

Sieve fraction (μm)	Viscosity ($1/\eta_o$)			Newtonian viscosity (Pa s)
	Sample A	Sample B	Sample C	
< 45	0.0813 (0.0017)	0.0824 (0.0026)	0.0819 (0.0021)	0.08090 (0.0005)
45 - 63	0.0958 (0.0021)	0.0961 (0.0025)	0.0967 (0.0031)	0.0949 (0.0009)
63 - 75	0.1208 (0.0089)	0.1212 (0.0048)	0.1202 (0.0065)	0.1041 (0.0012)
75 - 90	0.1545 (0.0067)	0.1551 (0.0050)	0.1545 (0.0029)	0.1449 (0.0023)
90 - 125	0.3690 (0.0121)	0.3684 (0.0097)	0.3692 (0.0111)	0.2421 (0.0015)

Table 4.2. The viscosity of different sieve fractions of MCC in 100 cSt silicone oil. The standard deviation is shown in brackets (n = 5). For reference the mean Newtonian viscosity (n = 15) as determined in Section 3.5.1.2 is included. The equivalent particle density for all samples is 1.85×10^6 particles/25 g.

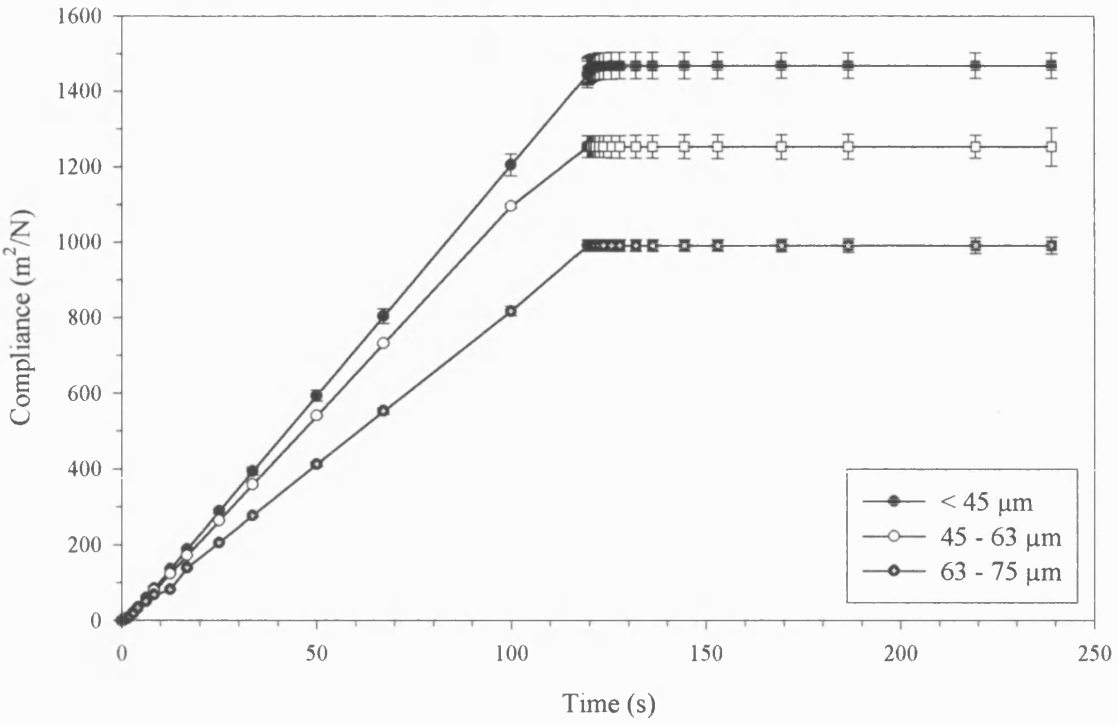

Figure 4.7. Creep (•) and recovery (■) curves for sieve fractions of MCC below 45 µm, 45 - 63 µm and 63 - 75 µm in 100 cSt silicone oil at an applied stress of 1.0 Pa.

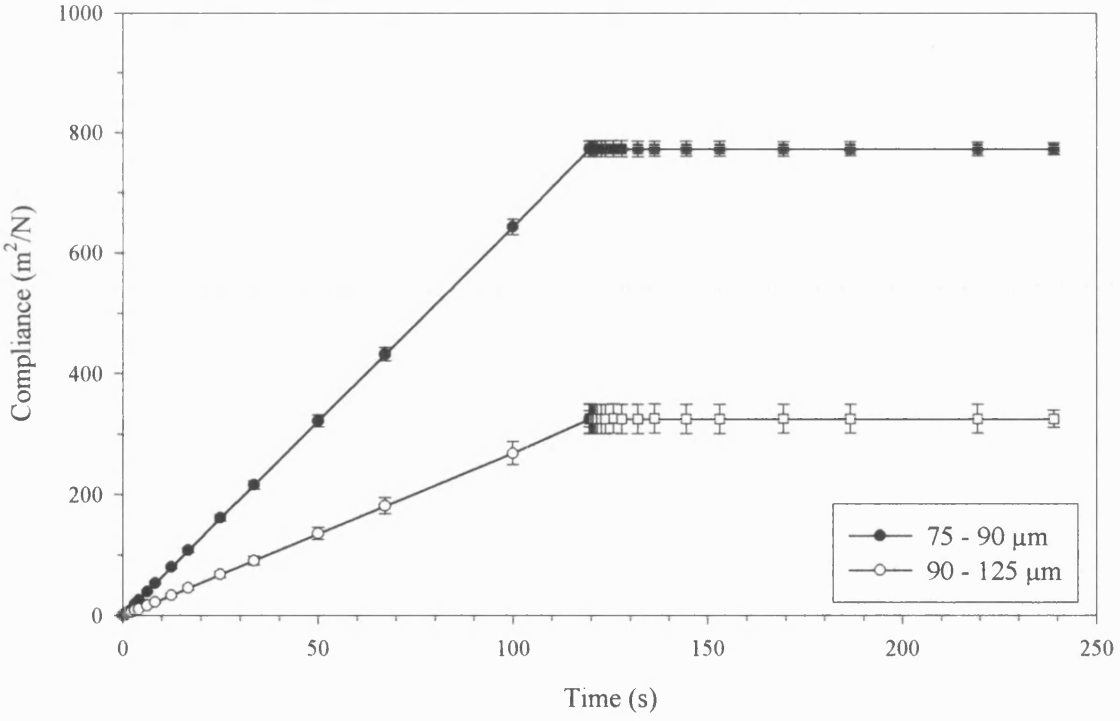

Figure 4.8. Creep (•) and recovery (■) curves for sieve fractions of MCC 75 - 90 µm and 90 - 125 µm in 100 cSt silicone oil at applied stresses of 1.0 Pa and 2.5 Pa respectively.

The zero-shear viscosity was significantly different (one-way ANOVA, $p < 0.05$) from the predicted shear stress-shear rate viscosity (see Section 3.5.1.2). There was no significant difference, except for suspensions of sieve fraction 63 - 75 μm, between the prepared samples (A, B and C). The existence of the inter-sample variation for the aforementioned sieve fraction may simply be as a direct result of poor loading. The theoretical explanation for the increase in viscosity observed with concentration and sieve fraction has been discussed in Chapter Three.

4.3.2. Creep and Recovery Behaviour of ER Fluids under the Influence of an Applied Electric Field

Theory predicts that as the elastic modulus is derived from the chains and the viscosity from the suspending fluid, an ER fluid under the influence of an applied electric field will exhibit simple Voigt properties (Conrad et al., 1991; Gamota and Filisko, 1991; Otsubo and Edamura, 1994). Deviation from theory has been observed, particularly at high particle concentration (Otsubo and Edamura, 1994, 1995, 1996) where the creep and recovery behaviour could not be quantified using linear viscoelastic components. The complexities of non-linear viscoelastic responses have prevented the calculation of quantitative data from the creep and recovery curves. Nonetheless, the creep and recovery curves have provided valuable information on chain formation and the development of yield stress. Typically, three distinct creep and recovery responses were observed depending on the magnitude of the applied stress in relation to the predicted yield stress.

a) Pre-yield stress

At low stresses, the creep curves were found to be composed of instantaneous elastic, retarded elastic and viscous regions. The behaviour, however could not be described using typical linear viscoelastic components. Preliminary observation of the

resultant creep curves indicated the presence of a large elastic modulus that is not recovered upon removal of the stress. At the longest times, the compliance was observed to increase linearly with time. This constant-rate strain was due to viscous flow and was not recovered.

The application of the stress resulted in an increase in the viscosity of ER fluids with time. The formation of particle chains upon application of an electric field has been illustrated in Chapter Three. Imperfections in the chain structure, cross-linking and single particles are known to occur particularly at low concentrations. The application of the stress may provide additional momentum resulting in single particle contribution to the primary chain structures or the rupture of cross-links and the subsequent coalescence of single chain structures. These weakly associated particles or structures may be bought together by collision during shear. The formation of a more favourable structure results in an increase in viscosity. Otsubo and Edamura (1996) extended the single-chain model to account for particle chain aggregation. Tao and Sun (1991) have shown theoretically that the ideal structure of ER under an electric field is a body-centred tetragonal lattice. In this configuration, repulsion forces act on particles directly approaching the chain structure. When the chain structure is strained, the existence of attractive forces within the columns maintains the arrangement. It is believed that at a critical strain value, the column structure changes from a body-centred tetragonal lattice to another metastable configuration (Otsubo and Edamura 1996). The existence of such a configuration provides an explanation for the failure of elastic recovery.

b) Yield stress

The generally accepted model for an ER fluid is that when the material is subjected to an electric field, the particles align themselves, forming a fibrous structure. Furthermore, it has been suggested that the yield phenomena may be related to the

destruction of the chains (Shulman et al., 1989). At stresses just below the yield stress, samples underwent instantaneous deformation and reached equilibrium without viscous flow and subsequently showed no recovery after removal of the stress. It is considered unlikely that this response was a result of inertia or drift owing to the high viscosity of the sample under question. This is comparable to the response typically exhibited by thixotropic materials, where structures takes time to respond to the stress (Barnes, 1997).

The yield-stress value determined by creep analysis was generally lower than the estimated static-yield stress from flow data. For example, the Bingham yield stress for a 10 % w/w suspension of MCC in 100 cSt silicone oil at 250 V/mm was 1.05 Pa. The static-yield stress, which is described as the stress at which flow occurs was 3.81 Pa, compared to a yield stress between 2 and 3 Pa as determined by creep analysis (cf. Table 3.6 pp. 78).

c) Post-yield

This region is characterised in steady state by the material shearing continuously at a constant rate in response to a shear stress. At stresses above the predicted yield stress the suspensions behaved as viscous fluids. When the stress was placed on to the sample, the strain increased at a constant rate which was inversely proportional to the zero-shear viscosity of the liquid (η_o). When the stress was removed, the sample stopped deforming with no subsequent recovery.

Gamota and Filisko (1991) proposed a mechanical analogy to represent qualitatively the dynamic behaviour observed. The mechanical model for a Bingham material (Figure 4.3) is essentially composed of a frictional element, simulating the field dependent yield stress, sandwiched between a dashpot and spring. Gamota and Filisko (1991) proposed the addition of a Voigt unit between the slider and spring, representing the linear viscoelastic behaviour observed in pre-yield deformation.

The figures reproduced below (4.9 - 4.13) illustrate the effect of particle concentration on the creep and recovery behaviour. Typically, three types of behaviour, depending on the magnitude of the applied stress to the predicted stress, were observed. The effect of particle concentration is discussed in detail below. The creep and recovery curves shown (Figures 4.9 - 4.13) demonstrate the general trends in behaviour exhibited by all test fluids; graphs illustrating the effect of particle size and applied electric field magnitude are not included.

d) Concentration

Figures 4.9 through 4.13 illustrate the creep and recovery behaviour of MCC suspensions of different concentrations (1.0, 2.5, 5.0, 10.0 and 20.0 % w/w respectively) at applied stress values below the yield stress, at the yield stress and above the yield stress (cf. Table 3.6 pp. 78). Creep analysis has provided valuable information on the existence of structure even at low concentrations. The responses observed at low MCC concentrations (1.0 and 2.5 % w/w) are indicative of solid behaviour. In general, the creep and recovery behaviour below the yield stress could not be described using linear viscoelastic principles. However, a detailed assessment of the creep and recovery responses observed with a 1.0 % w/w MCC suspensions under an applied stress of 0.5 Pa provided the following information on the viscoelastic components. The compliance (J_o) was calculated to be 1.27 m^2/N (± 0.15), whilst the Newtonian viscosity, predicted at long times, was 2259 Pa s (± 343). A single Voigt unit described the intermediate region of the creep curve with a retardation time of 329 s (± 25).

At high MCC concentration (≥ 5.0 % w/w), the compliance was observed to respond almost instantaneously and reach equilibrium without viscous flow. This response was more typical of an elastic solid, possibly indicating the formation of fully developed chains between the electrode gap. Unexpectedly, the suspensions showed no elastic

recovery upon removal of the stress. The degree of movement observed under these experimental conditions is but slight, typically 0.01 radians. A possible explanation is the rearrangement of MCC particles resulting from the removal of an opposing stress. It has previously been shown (Chapter Three) that the degree of particle chain development is concentration dependent. The creep and recovery response at applied stress values above the yield stress is representative of viscous behaviour. The zero-shear viscosity (Table 4.3.), for Sample A, was calculated from the reciprocal of the creep slope (Equation 4.2).

Concentration (% w/w)	Viscosity (Pa s)
1.0	0.1008 (0.0095)
2.5	0.1072 (0.0114)
5.0	0.1263 (0.0135)
10.0	0.2444 (0.0178)
20.0	9.7547 (0.7456)

Table 4.3. Table showing the zero-shear viscosity of different concentration MCC (sieve fraction below 45 μm) suspensions under the influence of an electric field (250 V/mm) at applied stress values above the predicted yield stress (cf. Table 3.1 pp. 63). Standard deviation values are shown in brackets (n = 5).

The zero-shear viscosity values determined from the reciprocal of the creep curve under the influence of an electric field are significantly higher than the estimated zero-shear viscosity values without the application of an electric field (cf. Table 4.1 pp. 125). The increased zero-shear viscosity may be as a result of chain formation upon application of an electric field. It seems reasonable to assume that even under an applied stress, ER fluids are capable of structure formation; the degree of chain formation is dependent on the applied stress.

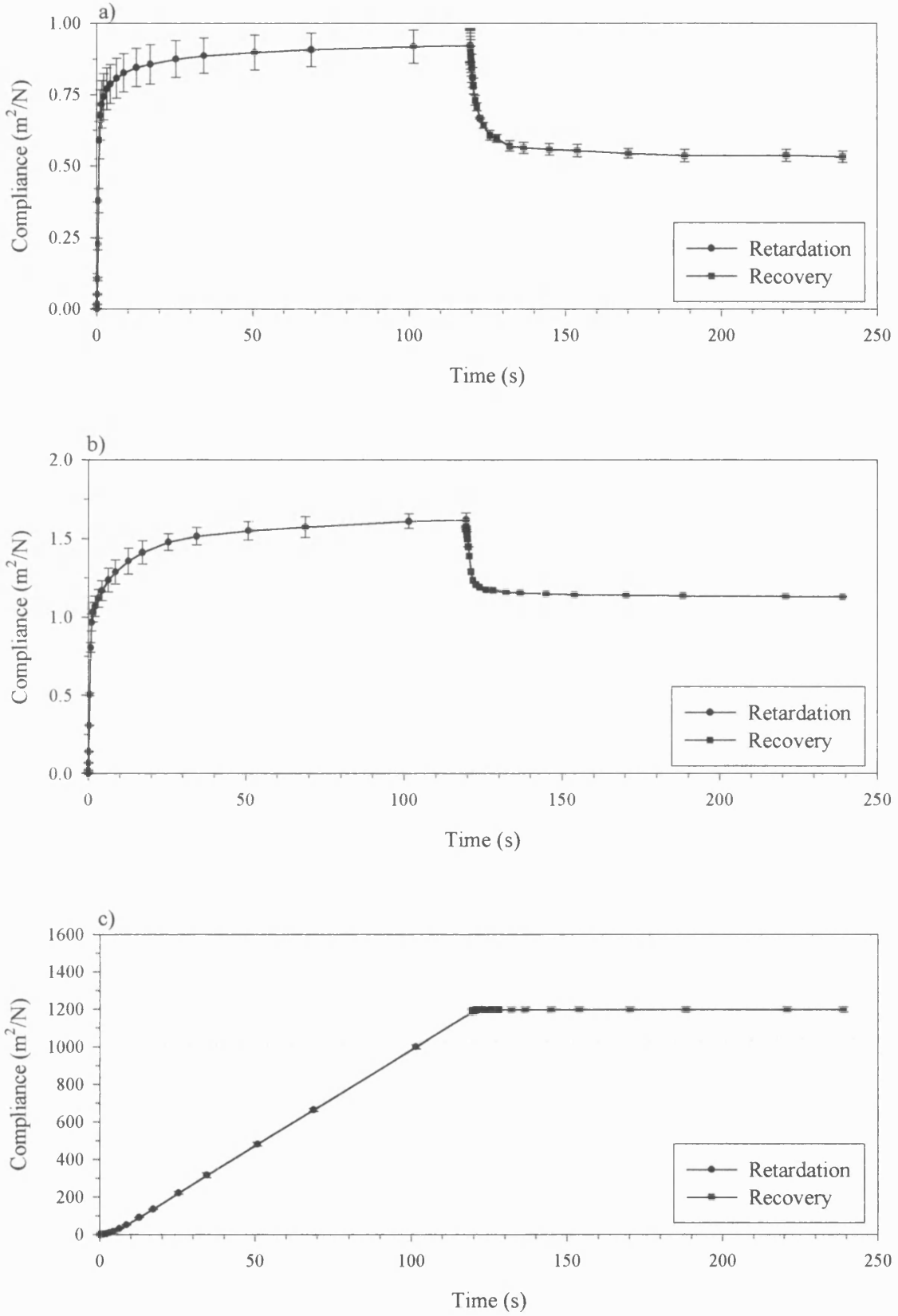

Figure 4.9. Creep (•) and recovery (■) behaviour for a 1.0 % w/w suspension of MCC in 100 cSt silicone oil under the influence of an electric field (250 V/mm) at applied stress values of 0.25 (a), 0.5 (b) and 0.75 (c) Pa respectively.

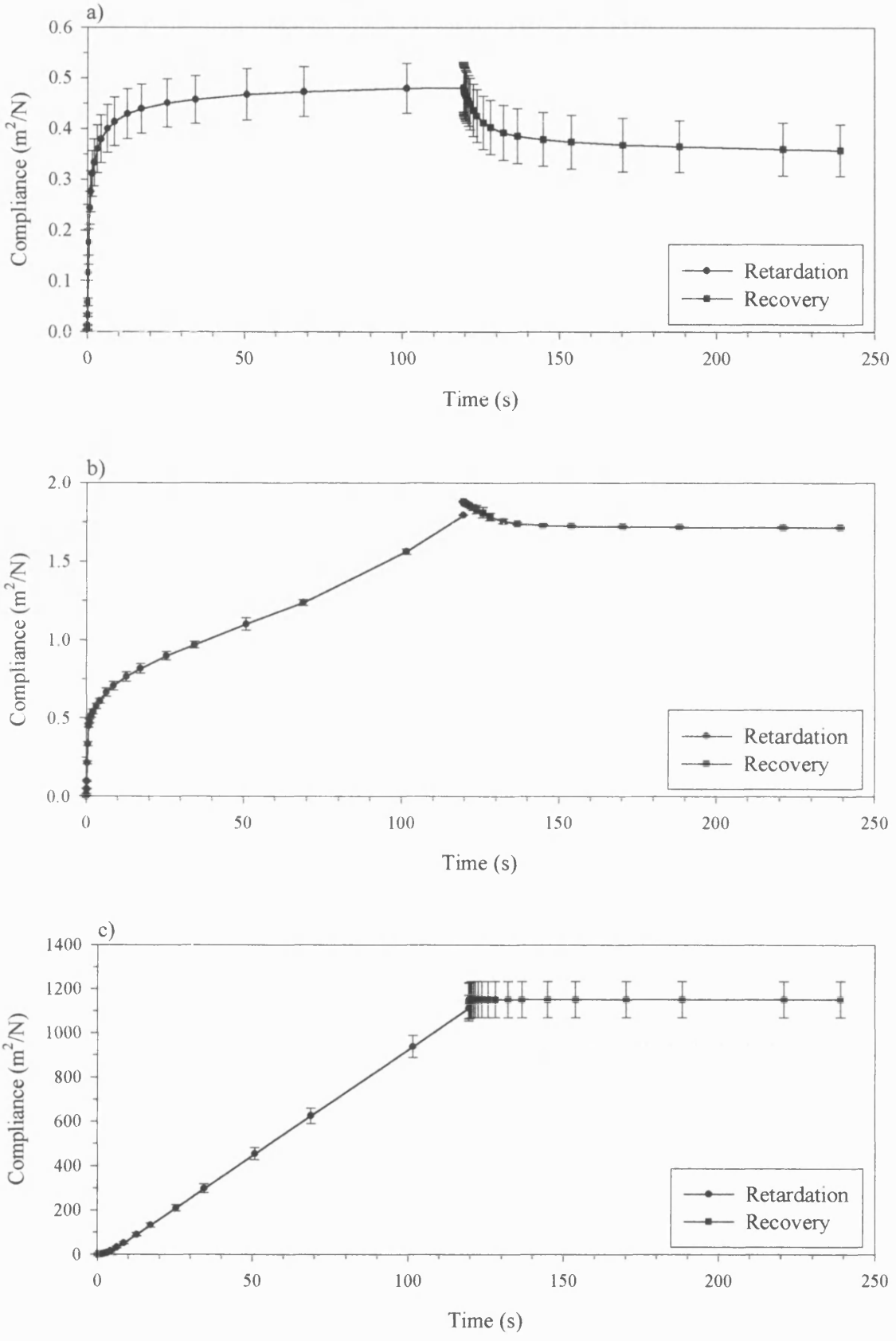

Figure 4.10. Creep (•) and recovery (■) behaviour for a 2.5 % w/w suspension of MCC in 100 cSt silicone oil under the influence of an electric field (250 V/mm) at applied stress values of 0.5 (a), 1.0 (b) and 2.0 (c) Pa respectively.

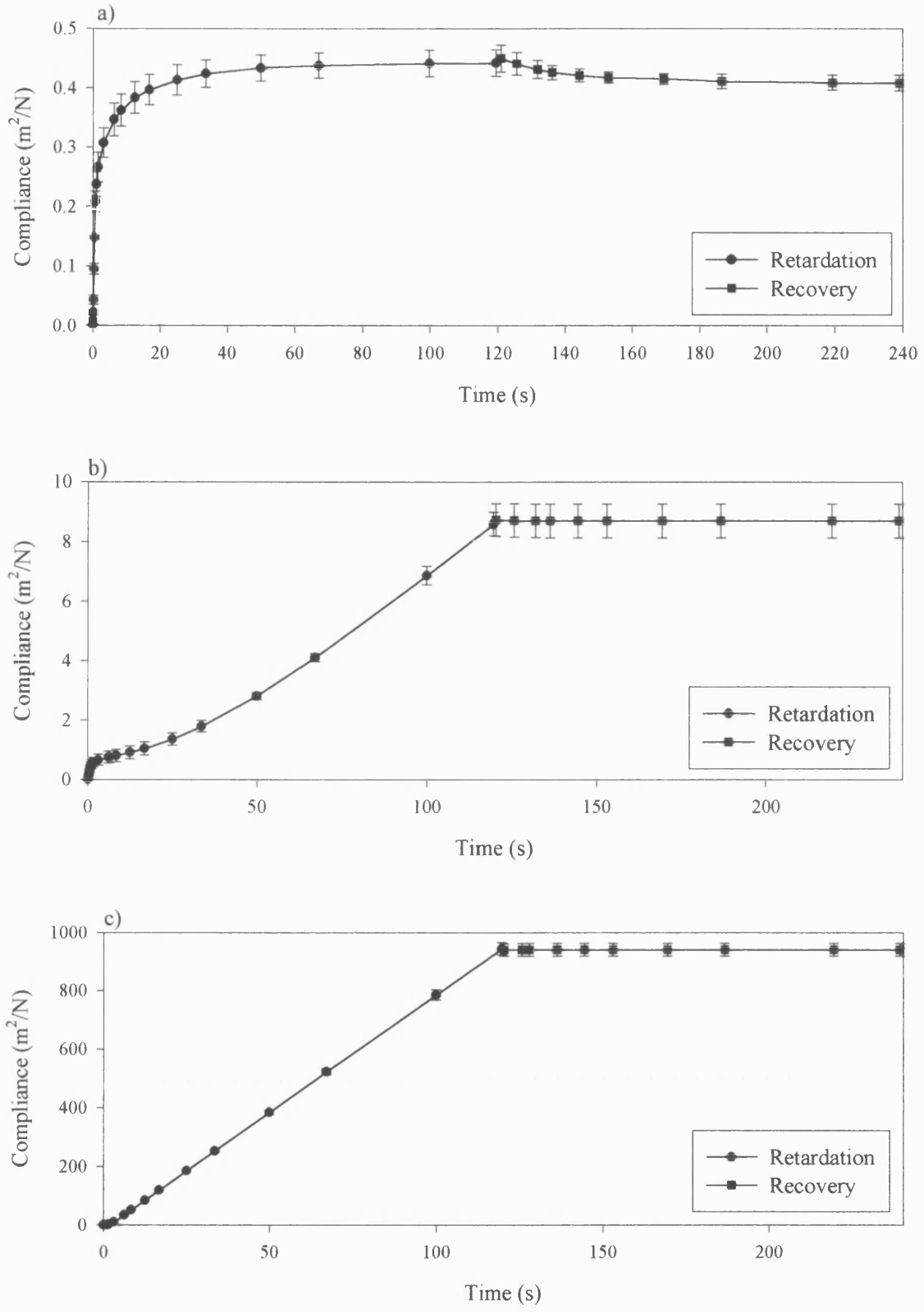

Figure 4.11. Creep (•) and recovery (■) behaviour for a 5.0 % w/w suspension of MCC in 100 cSt silicone oil under the influence of an electric field (250 V/mm) at applied stress values of 1.0 (a), 2.0 (b) and 3.0 (c) Pa respectively.

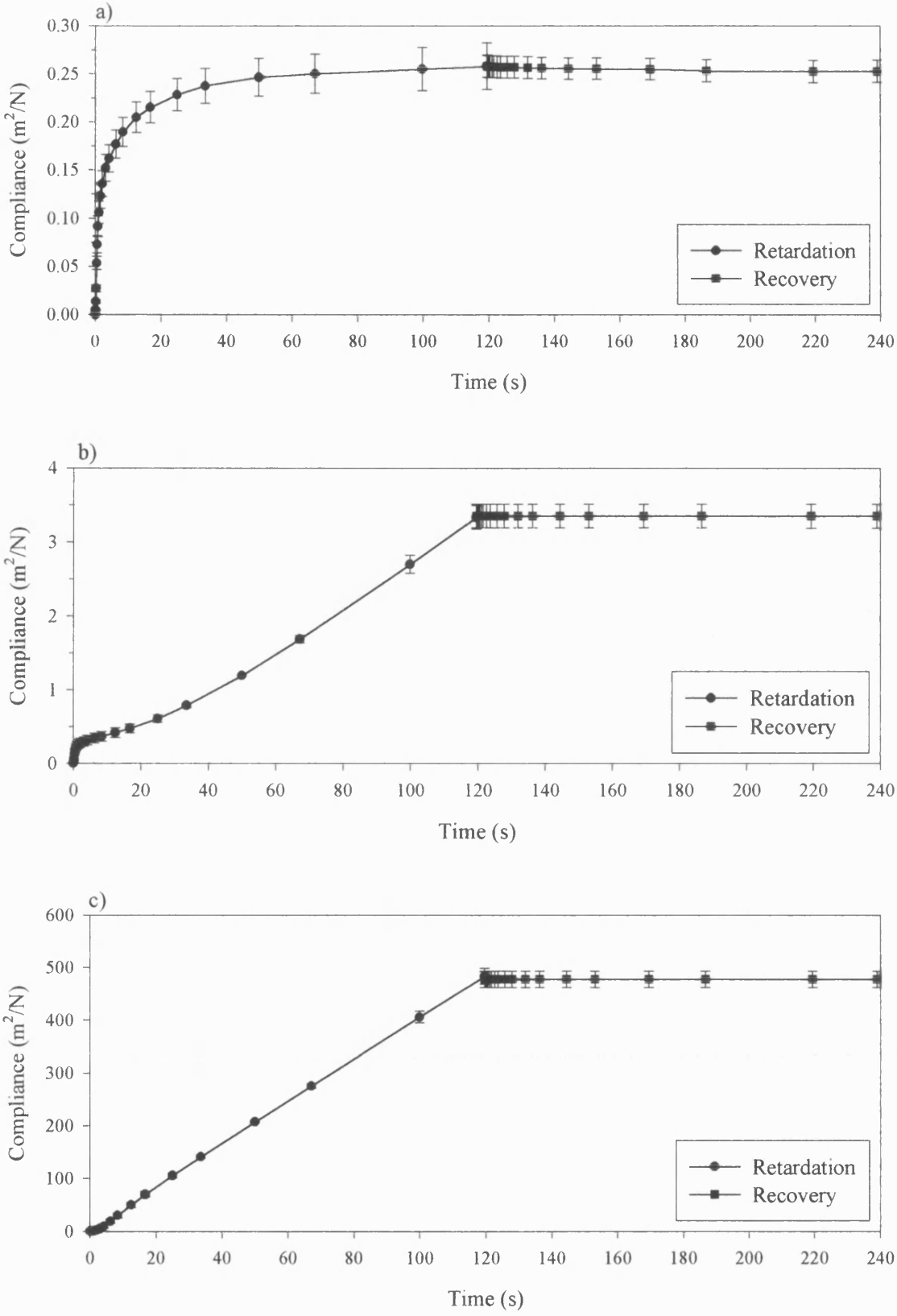

Figure 4.12. Creep (•) and recovery (■) behaviour for a 10.0 % w/w suspension of MCC in 100 cSt silicone oil under the influence of an electric field (250 V/mm) at applied stress values of 2.5 (a), 3.5 (b) and 4.5 (c) Pa respectively.

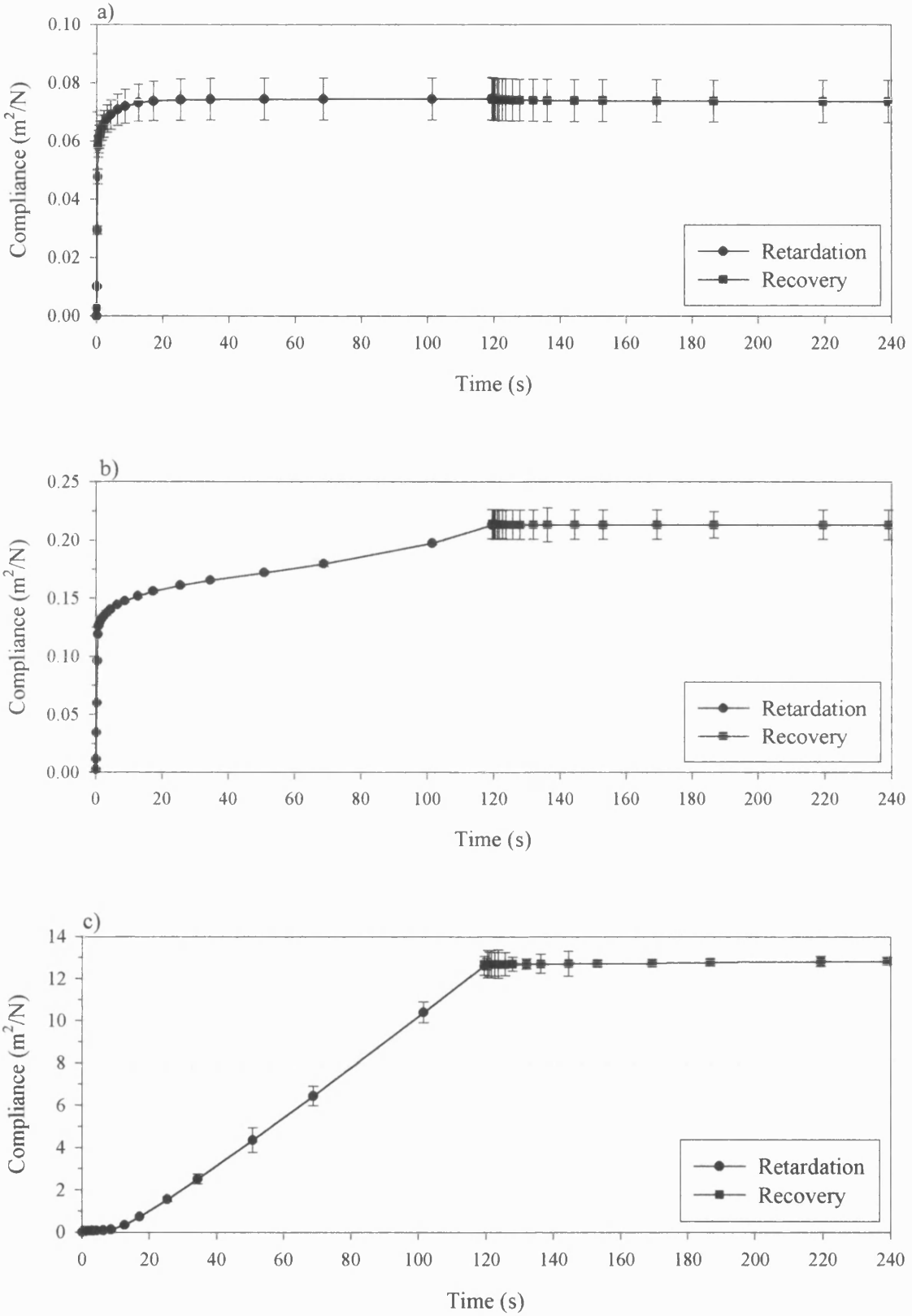

Figure 4.13. Creep (•) and recovery (■) behaviour for a 20.0 % w/w suspension of MCC in 100 cSt silicone oil under the influence of an electric field (250 V/mm) at applied stress values of 10.0 (a), 12.0 (b) and 13.0 (c) Pa respectively.

e) Particle size

Similar patterns of response were observed in MCC suspensions prepared with different particle sieve fractions. Each suspension contained an equal number of MCC particles (approximately 1.85 x 10^6 particles/25 g) as described in Chapter Three. Table 4.4 shows the zero-shear viscosity of MCC suspensions (Sample A) prepared with different sieve fractions under the influence of an electric field (250 V/mm).

Particle sieve fraction (μm)	Viscosity (Pa s)
< 45	0.1008 (0.0095)
45 - 63	0.1145 (0.0987)
63 - 75	0.1454 (0.0159)
75 - 90	0.1897 (0.0115)
90 - 125	11.0112 (0.9754)

Table 4.4. The zero-shear viscosity and standard deviation (n = 5) calculated from the reciprocal of the creep curve at applied stress values above the yield stress for suspensions prepared with different MCC sieve fractions (cf. Table 3.3 pp. 69). The applied electric field was 250 V/mm.

f) Applied electric field

Figure 4.14 illustrates the creep and recovery response of a 10.0 % w/w MCC suspension (sieve fraction 45 μm) under the influence of an applied electric field (50 V/mm).

The shape of the creep and recovery curve under an applied electric field of 500 V/mm at a shear stress below the predicted yield stress was similar to the 20.0 % w/w suspension at 250 V/mm (Figure 4.13). The zero-shear viscosity for the 10.0 % w/w

suspension (sieve fraction below 45 μm) under the influence of a 500 V/mm electric field was 12.5601 Pa s(± 0.1300).

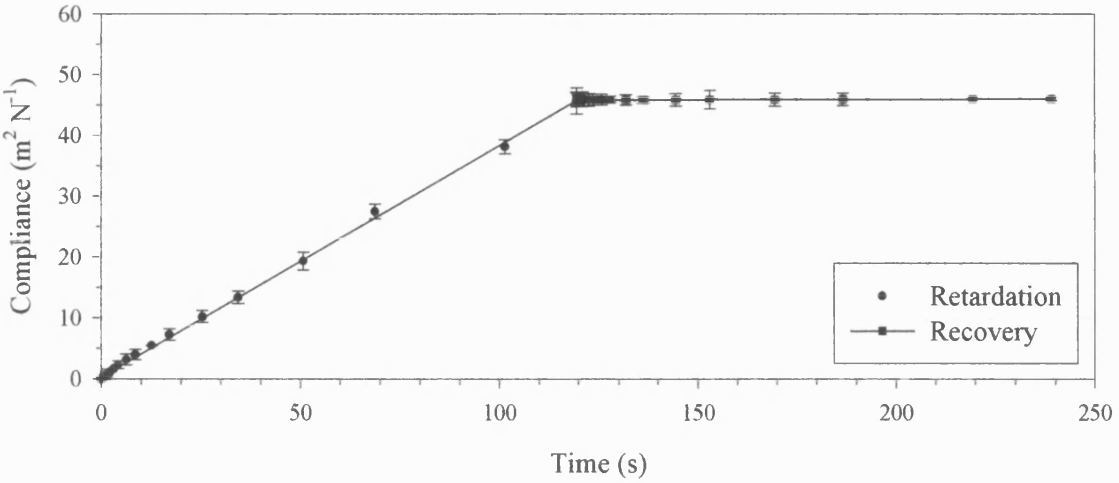

Figure 4.14. Creep (•) and recovery (■) behaviour of a 10 % w/w suspension of MCC in 100 cSt silicone oil under an applied electric field of 50 V/mm. The linear regression analysis is shown for the retardation (creep) behaviour.

The applied stress (0.05 Pa) utilised in this experiment was at the limits of the CSL^2 rheometer. The resultant response was indicative of a viscous liquid. It was unlikely that under these experimental conditions, no chain formation has occurred. However, the reciprocal of the slope was 2.63 Pa s which was significantly higher than the predicted zero-shear viscosity without the application of the electric field. The observed increase in zero-shear viscosity points to the presence of structure. Observation using a light microscope (Chapter Three), at 50 V/mm, indicated the presence of incomplete chains at this concentration (10.0 % w/w), providing an explanation of the increased zero-shear viscosity observed, but the failure, under these experimental conditions, of the creep analysis to detect structure formation.

4.4. Conclusions

From our flow data (Chapter Three), the development of a yield stress could be quantified by the Bingham constitutive equation, and provided a method for the determination of the particle chain strength and structure. Creep and recovery experiments conducted in this Chapter, indicate that ER fluids are much more complex in properties than we previously concluded. The development of the pre-yield region described above is not accounted for in the Bingham model. The consistent and reproducible creep and compliance responses observed cannot be as a result of instrument artefacts. Typically, the behaviour followed the characteristic three-stage response depending on the magnitude of the applied stress in relation to the predicted yield stress. Such complex properties for ER fluids are also supported by recent literature reports (Gamota and Filisko, 1991; Otsubo and Edamura, 1994, 1995, 1996).

The Newtonian viscosity predicted from the reciprocal of the creep slope was higher than previously calculated values from flow data (Chapter Three). Post-yield, the Bingham model predicts a complete structure breakdown, however, predicted viscosity values for this region on the flow curve are significantly higher than the Newtonian viscosities, indicating the presence of residual particle structures.

Prior to investigating the release kinetics of tacrine from ER fluids (Chapter Six), a modified diffusion cell was constructed and validated for use with these low viscosity formulations (Chapter Five). A diffusion cell, based on a traditional Franz cell, will be used to determine the release rates of tacrine from 100 cSt silicone oil in the non-electrified state through several mesh apertures. In addition, the effects of stirring rate, receptor fluid volume and temperature will be investigated. A possible release mechanism will then be defined using literature models of drug release, primarily taken from the fields of oral and transdermal drug delivery.

Chapter Five

Validation of a Modified Diffusion Cell

5.1. Introduction

The purpose of *in vitro* diffusion studies is to gain an understanding of the release mechanism and expected release rates of tacrine, as our chosen drug, from silicone oil. It is envisaged that the classic diffusion cell will require modification for use with such low viscosity formulations. Mathematical modelling of the drug release process is of considerable importance in the prediction of the release behaviour and in the investigation of parameters which may affect the release process.

Tacrine hydrochloride is a drug which may be a suitable candidate for a controlled drug-delivery device. Tacrine, a reversible cholinesterase inhibitor, is used for the treatment of mild to moderate Alzheimer's disease (e.g. Forsyth et al., 1989; Small, 1992). Conventional dosage forms are not entirely satisfactory due to low bioavailability and variability in plasma levels within individuals due to extensive first pass metabolism (e.g. Hartvig et al., 1990; Sathyan et al., 1995). Ideally, a delivery route avoiding the hepatic circulation would thus be preferable.

5.1.1. Diffusion

Diffusion is the process by which matter is transported from one part of a system to another as a result of random molecular motions. The rate of transfer of the diffusing substance through unit area of a section is proportional to the concentration gradient measured normal to the section and can be described by Fick's first law of diffusion:

$$J_d = -D \frac{dC}{dx}$$

where J_d is the rate of transfer per unit area of section, C is the concentration of the diffusing substance, x is the distance of movement perpendicular to the surface of the barrier and D is the diffusion coefficient. The negative sign indicates that the flux is in the

direction of decreasing concentration. The equation assumes that the driving force of diffusion is the concentration gradient. In order to acknowledge the fact that the concentration depends not only on the rate of transfer (x), but also on time, Fick's law is often expressed as a differential equation. Fick's second law states that the rate of change in concentration in a volume element within a diffusional field (dC/dt) is proportional to the rate of change in concentration at that point in the field (d^2C/dx^2) as stated below:

$$\frac{\partial C}{\partial t} = D\frac{d^2C}{dx^2}$$

Fick's second law is a general equation which has many complex solutions depending upon the boundary conditions being considered (Crank, 1975).

Mathematical modelling is used extensively in the literature to describe diffusion-controlled release from oral polymeric systems such as monolithic (or matrix) and reservoir devices. Such diffusion controlled systems are dependent on a rate-limiting process, either a polymer membrane (reservoir devices) or a polymer network (matrix systems). The kinetics of drug release from matrix devices containing uniformly dispersed or dissolved drug are well documented (e.g. Langer, 1980; Langer and Peppas, 1981; Cardinal, 1984). A simple mathematical model for the prediction of diffusion of a drug suspended in a polymeric matrix above its solubility limit was presented by Higuchi (1961), who extended his work concerned with drug delivery from ointments. For systems containing dispersed drug, where the drug loading per unit volume (A) is greater than the drug solubility in the matrix (C_s), the drug release kinetics (Q) can be analysed by the Higuchi equation (Higuchi, 1961):

$$Q = \left[C_s \left(2A - C_s\right) Dt\right]^{1/2}$$

The above equation is based on the following assumptions: (1) the drug is uniformly suspended, (2) the total amount of drug present per unit volume is substantially greater than the solubility of drug per unit volume in the matrix, (3) the release medium is a perfect sink and there are no boundary layer effects, (4) the polymer remains of constant dimensions and (5) diffusion through the polymer is the rate-limiting step.

Higuchi (1962) deduced the following equation for the amount of drug released from one side of an ointment layer in which the drug is initially uniformly dissolved:

$$Q = hC_o\left[1-\frac{8}{\pi^2}\sum_{m=0}^{\infty}\frac{1}{(2m+1)^2}\exp\left(-\frac{D(2m+1)^2\pi^2 t}{4h^2}\right)\right] \qquad \text{Equation 5.1}$$

where Q is the amount of drug released per unit area, h is the thickness, C_o is the initial concentration, D is the diffusion coefficient, t is the time after application and m is an integer. The main assumptions in Equation 5.1 are that D remains constant with respect to time, depletion of vehicle components does not occur and that sink conditions prevail in the receptor compartment (Higuchi, 1962). Equation 5.1 can be simplified at release rates below 30 % (Higuchi, 1962) to:

$$Q = 2\,C_o\left(\frac{Dt}{\pi}\right)^{1/2} \qquad \text{Equation 5.2}$$

Fickian diffusion from a plane sheet may be expressed using Equations 5.1 and 5.2. Furthermore, Korsmeyer et al. (1983) and Peppas (1985) have presented a simple equation which can be used to analyse controlled-release data, from a plane sheet, under perfect sink conditions. For short times ($M_t/ M_\infty < 0.6$), Fickian-diffusion release can be described using the following equation:

$$\frac{M_t}{M_\infty} = kt^n \qquad \text{Equation 5.3}$$

where M_t is the amount of solute released at time t, M_∞ is the amount of solute released at infinite time, theoretically corresponding to the total amount of active agent incorporated into the formulation, k is a constant incorporating structural and geometric characteristics of the controlled release device and n is the release exponent, indicative of the mechanism of drug release.

Such a mathematical model may be used to predict solute release rates and elucidate the physical mechanisms of solute transport by comparison of the data to mathematical models. Investigations into whether the drug diffusion process is Fickian or non-Fickian, can be conducted by fitting the release data to the above equation (Equation 5.3). The exponent (n) may take a range of values depending on the transport mechanism (Sinclair and Peppas, 1984; Peppas, 1985) (Table 5.1).

Release exponent (n)	Drug transport mechanism
0.5	Fickian or Case I
$0.5 < n < 1.0$	Anomalous (non-Fickian) transport
1.0	Case II transport
$n > 1.0$	Super Case II transport

Table 5.1. Interpretation of diffusional release mechanisms applicable to drug release data from thin polymeric films (Peppas, 1985).

5.1.2. In Vitro Drug Diffusion Measurements

As there are no general directives in the pharmacopoeias regarding the diffusion cell design, researchers have designed their own (for example, Rolland et al., 1992; Parera Morell et al., 1996), although there does exist a general series of considerations which must be taken into account to guarantee reliability of release results. The rate of diffusion depends, among other factors, on the temperature at which the test is performed and the type of membrane employed, particularly important in transdermal applications. The receptor solution must be maintained in sink conditions with respect to the drug (Higuchi, 1961; Higuchi,1962) and it is advisable for it to be stirred at an adequate speed to ensure removal of the drug from the boundary layer (Higuchi, 1961; Higuchi, 1962). These theoretical requirements stem from Fick's first law of diffusion.

Two techniques have been adopted in studying the drug transport, the infinite-dose technique and the finite dose technique (Franz, 1975). In the infinite-dose technique, the donor compartment contains a solution of drug under study, and the build up of drug in the receptor is monitored during the experiment course. Generally, the concentration in the donor remains constant during the experiment and the receptor acts as an effective sink, thus in the case of skin permeability experiments, after an initial lag period, steady-state diffusion would prevail. The finite dose technique involves the application of the drug to the donor side exposed to ambient conditions. During the course of the experiment, the flux rises to a peak then falls as the concentration on the exposed site decreases.

In this Chapter, we detail our diffusion cell design and its validation by preliminary experiments at 0 V/mm. The traditional Franz cell has been modified for use with low viscosity formulations by incorporation of an interchangeable mesh support, a rubber o-ring and a glass lip. Stainless steel square wire mesh cloths, complying to BS and ISO specifications of 45, 90 and 180 μm aperture and 34 % open area were chosen as inert supports (Endecotts, London, UK).

5.2. Diffusion cell design

Conceptional designs for the diffusion cell were based either on vertically or horizontally orientated electrodes. Vertically orientated electrodes posed several problems, not least formulation retention between the electrodes under no applied electric field and sedimentation. Furthermore, the magnitude of the applied electric field negated the total submersion of the electrodes into the receptor fluid. The diffusion cells constructed and validated in this study are based on a Franz cell design (Franz, 1975; Nugent and Wood, 1980; Barry, 1983) (Figure 5.1). The open diameter of 40.0 mm was chosen to correspond to the parallel plate diameter (see Chapter Three). The diffusion cell is composed of a donor compartment and a receptor compartment. Square mesh woven wire cloths were chosen as an inert support on to which the sample was loaded (Endecotts London, UK). The mesh was manufactured from stainless steel and conformed to ISO and BS standards. Table 5.2 outlines the mesh apertures used throughout these studies. The open area is expressed as a percentage of all mesh openings in relation to the total cloth area, where w is the aperture size (μm) and the wire diameter is d (μm):

$$F_o = \frac{w^2 * 100}{(w+d)^2}$$

Aperture size (μm)	Wire diameter (μm)	Open area (%)
45	32	34
90	63	34
180	125	34

Table 5.2. Aperture size, wire diameter and percentage open area for the stainless steel mesh supports used in the diffusion cell work. Reference source: Endecotts literature on BOPP woven wire cloth (Endocotts, London, UK).

The cells were designed to satisfy the following criteria according to theoretical and experimental requirements. Firstly, stirring must be adequate and constant in order to minimise boundary layers and to give reproducible analysis of diffusion results (Gummer et al., 1987. Sink conditions must prevail to ensure valid application of Fick's first law of diffusion (Higuchi, 1962). The membrane should be chemically inert, permeable to the drug concerned and should not be the rate-limiting step in the release process (Corbo et al., 1993). Three prototype diffusion cells are described, each building on the previously exposed design flaws; prototype C is described in Chapter Six.

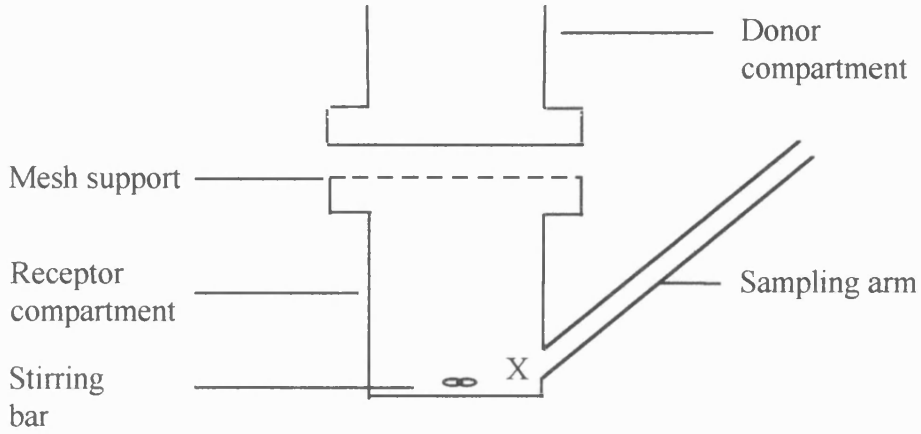

Figure 5.1. Schematic diagram of prototype A.

5.2.1. Prototype A

Prototype A, based on the classic Franz cell design described, was used in preliminary studies to assess the general performance of horizontally oriented electrodes (Figure 5.1). Several criteria were addressed in these initial experiments, namely suitability of design in terms of formulation retention and a measurable degree of drug release. The cell comprised of donor and receptor compartments, with a ground glass interface. The stainless steel mesh was sandwiched between the donor and receptor compartments and the cell clamped together. The open diameter, measured using internal callipers at five points, was 39.58 mm (± 0.98) resulting in an effective diffusional area of

12.30 cm^2. The diffusion cell was not thermostatically controlled, therefore experiments were conducted at ambient temperatures (21.0 °C ± 0.2). The withdrawal of the receptor medium was achieved, using a long needle 500 µL syringe (SGE, UK), via the sampling arm at point X. Several problems were highlighted during work with this prototype which were subsequently addressed in prototype B.

5.2.2. Prototype B

In order to overcome the problem of poor fluid retention, encountered in prototype A, a glass lip was secured around the donor compartment (Figures 5.2 and 5.3). In addition, prototype B was built with an integral fluid jacket which extended to the level of the mesh support, enabling temperature controlled experiments to be conducted. The mean open diameter, measured using internal callipers, and was found to be 38.40 mm resulting in an open area of 11.58 cm^2. The mean receptor height was 32.55 mm, resulting in a receptor volume of 35.54 ml. The calculated receptor volume did not take into account the volume of receptor fluid within the sampling arm.

A rubber o-ring was fixed to the mesh using silicone rubber compound (RS Components, Northants, UK), resulting in a surface area of 10.92 cm^2 and an estimated formulation loading volume of 1.15 cm^3. The upper plate was cut from 500 µm thickness copper sheet to a diameter of 50.0 mm. The separation of the two electrodes was maintained constant throughout all the experiments, at a distance of 1.02 mm. The electrode assembly was secured with a glass weight, to ensure flatness.

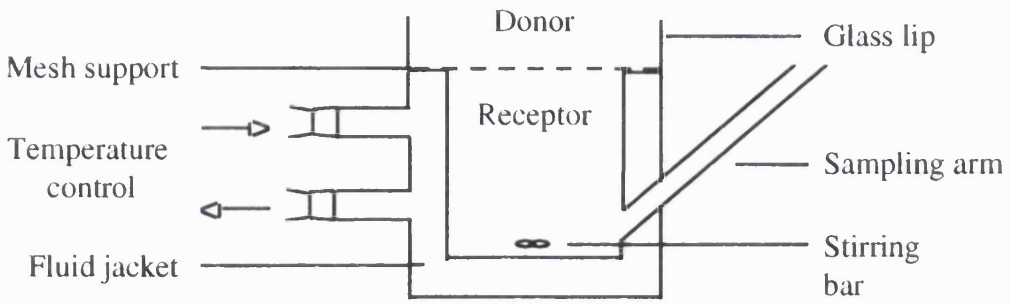

Figure 5.2. Schematic diagram of prototype B.

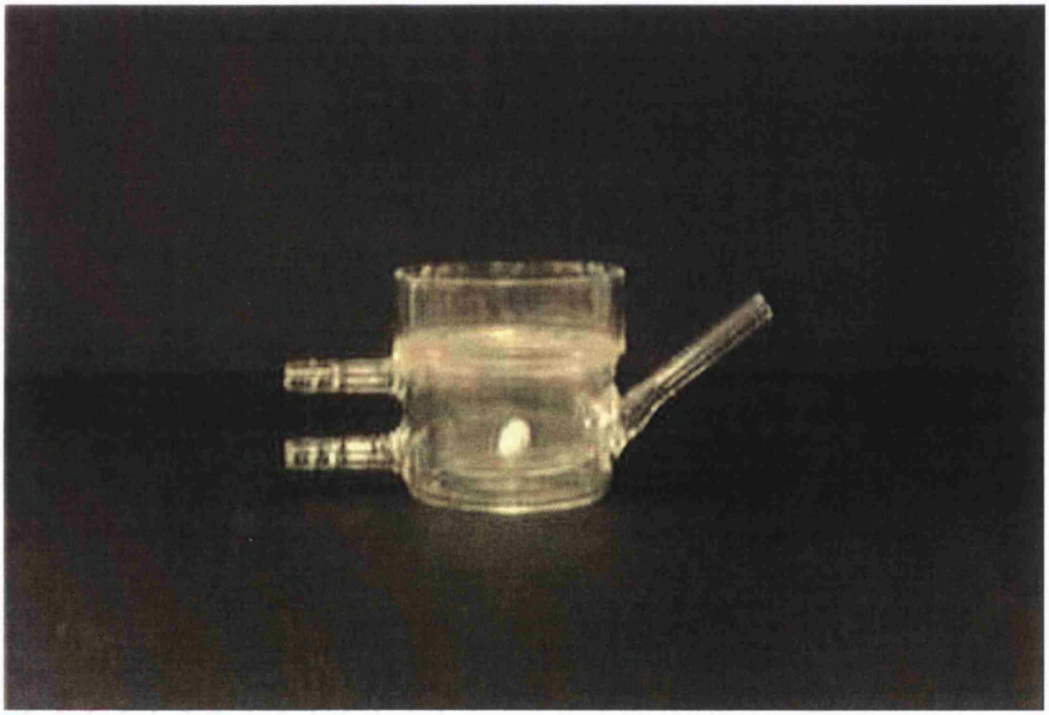

Figure 5.3. Photograph of prototype B.

5.3. Materials

Tacrine and silicone oil as previously described (Section 2.1). Distilled water, which was degassed (using helium) for 30 min, was chosen as the receptor fluid. Distilled water was elected for the receptor fluid for several reasons, specifically the solubility of tacrine in distilled water ensured adequate sink conditions over the course of the experiment and the determined oil/water partition coefficient (Sections 2.2.6 and 2.3.5). Degassed distilled water was used to minimise poor reproducibility experienced by other researchers (for example Gummer et al., 1987; Parera Morell, 1996). Propan-2-ol was of HPLC grade (Fisons Scientific Equipment, Loughborough, UK).

5.4. Methods

5.4.1. Determination of Excipient Interference in the Assay of Tacrine by UV Spectrophotometry

The possibility of MCC and silicone oil interference in the previously measured UV calibration curves (Section 2.10) is addressed in this section. Primarily, each of the formulation constituents (MCC and silicone oil) was scanned, against the appropriate blank, over the range 190 to 390 nm (Perkin Elmer, Beaconsfield, UK). MCC insolublity in the chosen solvents was addressed by dispersion and subsequent equilibration in the appropriate solvent over 24 h, prior to the scan being performed. Calibration curves were constructed at 324 nm in distilled water and propan-2-ol, over the concentration range 1.0 to 25 μg/ml, with the addition of MCC and silicone oil. MCC and silicone oil were introduced at the maximum concentrations enlisted in the ensuing experiments (Chapter Six). In addition, the silicone rubber glue (RS Silicone Rubber Compound, RS Components, Northants, UK) used to fix the rubber spacer to the mesh apertures was left in water and propan-2-ol for 24 h before being spectrophotometrically assessed in the wavelength range 190 to 390 nm.

5.4.2. Evaluation of Tacrine Recovery from Silicone Oil

Tacrine (~ 5.0 mg) dispersed in silicone oil (~ 1.5 g) was accurately weighed into single use vials (n = 10) and the total amount of drug recovered assessed using a UV spectrophotometric method. The vials were sonicated for two periods of 15 min and then washed with propan-2-ol into a 250 ml volumetric flask. The amount of tacrine in the volumetric flask was determined at 324 nm.

5.4.3 Drug Diffusion Determination using Prototype A

The cell was prepared by firstly smearing a thin layer of vacuum grease onto the interfacial ground glass joints of the donor and receptor compartments. A magnetic stirrer bar was placed into the receptor compartment, together with 52.0 ml of distilled water. The level of water in the receptor compartment was just below the mesh aperture; formulation seepage resulted thereby ensuring the existence of negligible air space. The stirring rate was maintained at a low, but constant speed over the experiment (Heidolph MR3000 stirrer, Germany). The 45 μm aperture mesh was sandwiched between the donor and receptor compartments which were then clamped together, prior to the sample being uniformly loaded onto the mesh support. The cell had one sampling arm through which 1.0 ml was manually withdrawn by syringe after 24 h. The sampling arm aperture was covered with Nescofilm™ (Nippon Shoji Kaisha Ltd, Osaka, Japan).

The preparatory experiments were conducted using a concentrated formulation of tacrine (~ 250 mg) in 5.0 g silicone oil weighed into a single-use vial. The amount of tacrine remaining in the vial was determined spectrophotometrically, in order to calculate accurately the concentration of tacrine embodied in the diffusion cell formulation. At the cessation of the experiment, the cell was carefully dismantled and the mesh support washed using propan-2-ol into a 250 ml volumetric flask; subsequent dilution was needed.

The amount of tacrine released together with the vial and mesh washings, yielded the total drug recovery.

5.4.4. Standardisation of Experimental Procedures in Prototype B: Temperature Maintenance, Stirring Rate and Turbulence

Prototype B comprised of an integral water jacket for conducting temperature controlled experiments (Figure 5.2). An investigation into the temperature of the fluid jacket required to maintain an internal receptor fluid temperature of 37.0 °C was carried out. In addition, temperature fluctuations over 12 h were assessed (n = 5). It was envisaged that water evaporation may occur over the course of the experiment. The diffusion cell was assembled, according to the method described below, with and without a layer of silicone oil and the weight monitored at 30 min intervals over 12 h (n = 5).

Three stirring rates were measured over a 1 min period, together with ability of the stirrer to maintain constant speed over 12 h. Five reading were taken for each method and the mean stirring rate calculated. Slow and/or incomplete stirring is often cited as a cause of irreproducible results (Gummer et al., 1987). In order to ensure adequate stirring in the modified Franz cell, the degree of dispersal of potassium permanganate from a silicone oil-based formulation was qualitatively assessed in relation to the mesh aperture and stirring rate. The end-point was taken as the time after loading when even colouration, extending up the sampling arm, was observed. The colouration in the receptor compartment, using a 45 μm mesh aperture and stirring rate of 62 rpm, was photographed at 1.5 s intervals.

The use of sesame seed oil in sustained-release intramuscular injections and in the preparation of subcutaneous injections, promoted a feasibility study into its use in ER drug-delivery devices (Chapter Three). A UV scan, indicated that sesame seed oil absorbed at λ 324 nm. At high stirring rates, turbulence in the formulation layer beneath the mesh aperture, may result in the formation of an oil-in-water emulsion.

The degree of turbulence, at three stirring rates (62, 100 and 150 rpm), was assessed over 8 h using sesame seed oil (n = 5). The receptor fluid was pumped through the UV detector at a rate of 0.6 ml/min (± 0.02) and readings taken every 30 min.

5.4.5. Assembly of Prototype B and General Experimental Procedures

The assembly of the prototype B diffusion cell (Figure 5.4) and preparatory experimental details are outlined below.

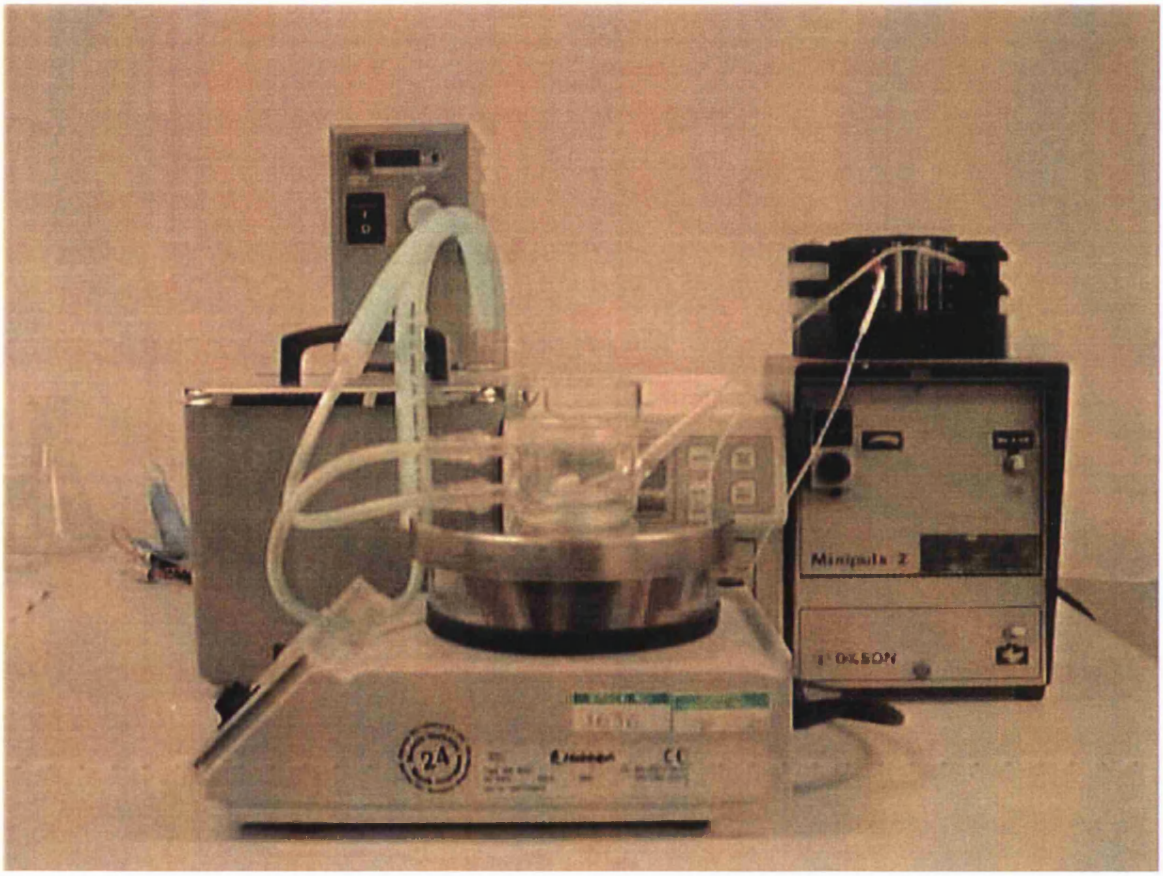

Figure 5.4. Photograph showing the experimental apparatus used in the determination of tacrine release from ER fluids.

The fluid jacket temperature (Grant Y6 circulating water bath, BDH, UK) was allowed to equilibrate for 1 h. The temperature of the modified Franz cell was maintained at 37.0 °C (± 0.2 °C), unless otherwise stated. During this time, the UV spectrophotometer was zeroed using distilled water as the blank; this procedure ensured removal of contaminants in the peristaltic tubing. The degassed distilled water was weighed into a measuring cylinder and poured into the diffusion cell; temperature equilibration of the receptor medium was conducted for a further 30 min. Previous experiments established that no detectable water evaporation occurred over this time period. The flow-through tubing was inserted into the sampling arm avoiding the scenario where the outflow is in direct contact with the sampling tube. The sampling arm aperture was sealed with Nescofilm™ to minimise water evaporation over the coarse of the experiment. The diffusion cell was agitated using a stirring bar. The ground glass surface of the donor compartment was smeared with a thin layer of vacuum grease and the mesh support secured in place. The formulation was uniformly distributed on the mesh aperture and the upper plate carefully lowered on top. A glass weight was lowered into place, to ensure flatness of the electrode assembly.

The diffusion characteristics were determined by monitoring the concentration of tacrine in the receptor compartment by UV analysis. The receptor cell solution was pumped at a rate of 0.6 ml/min (± 0.02) (Gilson Minipuls 2, Anachem, Luton, UK) into the flow-through UV detector (Jasco UV-975, Jasco, UK) and the outflow returned to the receptor cell. Although the principle absorption peak is 240 nm, an alternative λ of 324 nm had a more convenient extinction coefficient ($\varepsilon_{240} = 3.7 \times 10^4$ L/mole/cm and $\varepsilon_{324} = 1.1 \times 10^4$ L/mole/cm) at the concentrations employed in these experiments. The UV detector was calibrated at weekly intervals by analysing a number of solutions of known concentration. The absorbance measurements were taken manually at 2 min intervals for the first h and then every 15 min thereafter for 7 h. The release profiles were determined

five times for each experimental condition, with runs conducted in a fashion that avoided the introduction of bias.

The volume of distilled water required is a balance between the attainment of sink conditions and the assurance of adequate receptor fluid stirring. All volumes used in the present study ensured the maintenance of sink conditions, as defined by Corbo et al. (1993). The solubility was determined in Section 2.2.6 to be 82 mg/ml (± 0.36), which is considerably higher than ten times that of the maximum achievable concentration during the course of the experiment (approximately 0.13 mg/ml).

Suspensions of 0.5 % w/w tacrine (~ 7.5 mg) in 100 cSt silicone oil (~ 1.5 g) were prepared in single-use vials and sonicated for two periods of 15 min. After sample loading, the single use vial was washed with propan-2-ol into a 250 ml volumetric flask prior to spectrophotometric evaluation at 324 nm. The decision was taken not to conduct the spectrophotometric assay at the major peak wavelength due to the possibility of interference of silicone glue at the lower wavelength (see below). The mesh support was carefully removed at the end of the experiment and washed, with propan-2-ol, into a 500 ml volumetric flask. The samples were sonicated for 2 min, prior to UV determination. Sample centrifugation was not necessary to displace the quantities of silicone oil present. The UV spectrometer was zeroed using propan-2-ol as the blank solution, with each unknown solution assayed at 324 nm, in triplicate, and the mean absorbance recorded.

The cleaning of the diffusion cell at the cessation of an experiment was carried out in three stages to ensure removal of trace amounts of silicone oil. The diffusion cell was soaked for 2 h in an aqueous solution of Decon®, prior to rinsing with concentrated Decon® in the hard to reach areas, particularly at the intersection of the ground glass with the lip. The diffusion cell was thoroughly rinsed in distilled water before drying at 50 °C.

5.4.6. Validation of Prototype B: The Effect of Mesh Aperture, Stirring Rate, Receptor Fluid Volume and Temperature on the Release of Tacrine from Silicone Oil

Several factors which may influence the diffusion profile, namely mesh aperture, stirring rate, receptor fluid volume and temperature were investigated. Unless otherwise stated, the temperature was maintained at 37.0 °C, the receptor fluid volume was 37.0 ml and the mesh aperture was 45 μm. The effect of stirring rate on the tacrine release rate was studied at four stirring rates (0, 62, 100 and 150 rpm). Three mesh apertures, each with the same open area, were chosen (see Section 5.2) and the release rate assessed at low stirring rates (62 rpm). The effect of receptor fluid volume on tacrine release through a 45 μm mesh aperture was investigated at low stirring rates (62 rpm). In order to ensure accuracy of measurement, the equivalent weight corresponding to each volume was determined. The equivalent volumes were 36.5, 37.0 and 37.5 ml. The effect of temperature on the release properties of tacrine from 100 cSt silicone oil was determined. Experiments were conducted at 25.0 and 37.0 °C, through a mesh aperture of 45 μm, with a receptor fluid volume of 37.0 ml stirred at 62 rpm. The effect of temperature on the density of distilled water was taken into account.

5.5. Results and Discussion

5.5.1 Determination of Excipient Interference in the Assay of Tacrine by UV Spectrophotometry

Silicone oil was found to have a peak absorbance in water and propan-2-ol at approximately 210 nm, enabling the conclusion to be drawn that no interference would prevail upon addition of silicone oil. Furthermore, no absorbance was detected with MCC in either solvent, probably owing to the insoluble nature of MCC. The silicone glue soaked in distilled water produced a similar absorbance profile to silicone oil, with a peak at approximately 210 nm. A gradual increase in the absorbance commencing at 300 nm was observed for silicone glue soaked in propan-2-ol culminating in a peak at approximately 203 nm. In light of these findings, the vial and mesh washings were analysed at 324 nm to avoid the possibility of interference.

Calibration plots for tacrine in distilled water and propan-2-ol together with the addition of MCC and silicone oil were linear (Figures 5.4 and 5.5) and it was therefore considered that analysis by UV detection was appropriate over the concentration range examined. In both figures, the curves shown with and without (Section 2.3.8) the addition of silicone oil and MCC are dilution A1. Statistical analysis was carried out to determine whether any difference occurred between the calibration curves with and without the addition of silicone oil and MCC. No significant difference (one-way ANOVA; $p > 0.05$) in absorbance was noted with the addition of MCC and silicone oil and it was therefore concluded that any dissolved excipients did not interfere with the assay. The respective combined calibration curves calculated in Section 2.3.8 were used for the analysis of all unknown samples.

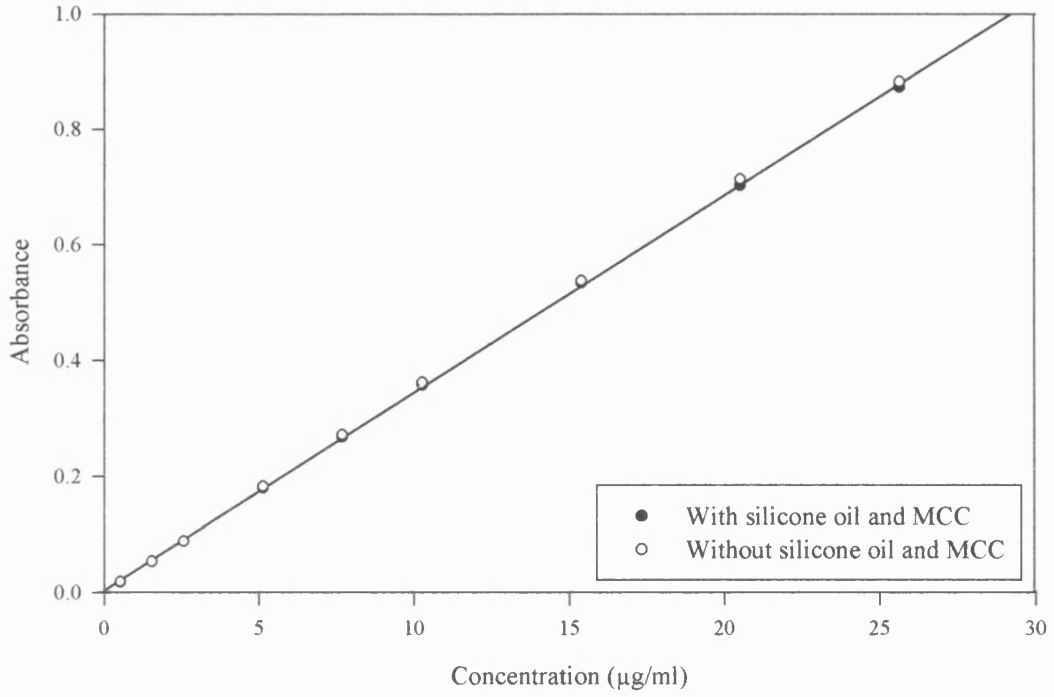

Figure 5.4. Calibration curve for tacrine, in distilled water at 324 nm, with and without the addition of silicone oil and MCC.

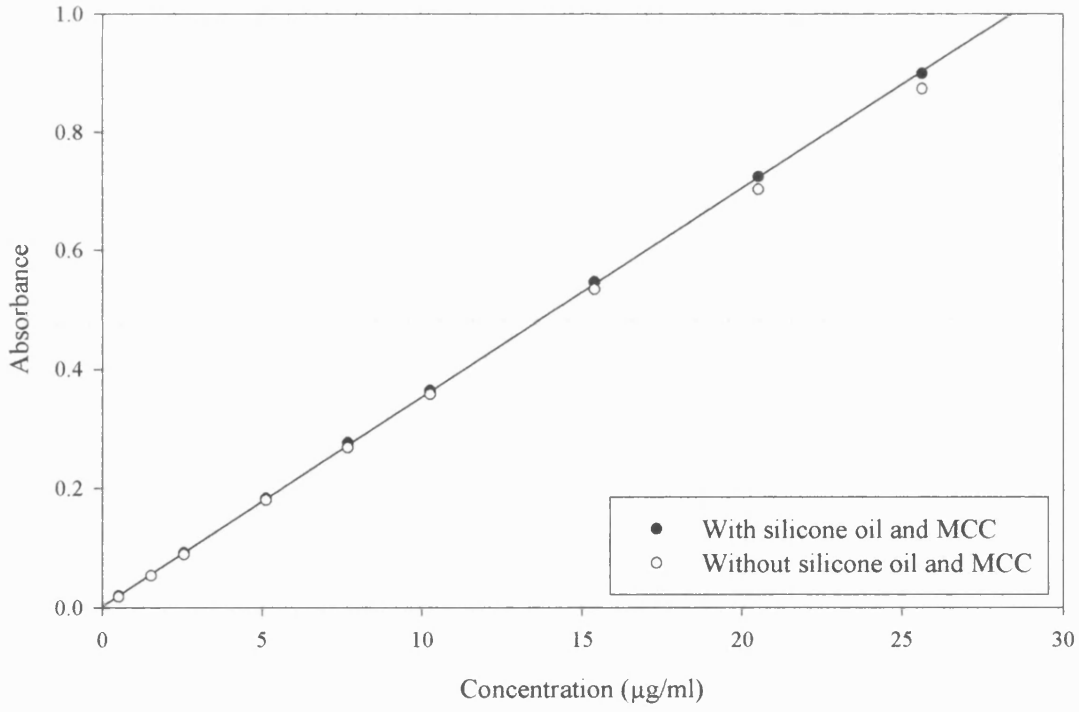

Figure 5.5. Calibration curve for tacrine, in propan-2-ol at 324 nm, with and without the addition of silicone oil and MCC.

5.5.2. Evaluation of Tacrine Recovery from Silicone Oil

The total amount of tacrine recovered from the formulation was 97.60 % (± 5.62). The amount of tacrine recovered indicated that the method installed for the analysis of drug content provided an acceptable outcome.

5.5.3 Drug Diffusion Determination using Prototype A

The principle aim of prototype A was to assess the feasibility of a horizontally oriented diffusion cell for the determination of release profiles from ER fluids. The total tacrine release was 0.54 % (approximately 1.35 mg) after 24 h. The percentage recovery was 89.59 % (± 15.91). The poor recovery can be explained by the seepage of the formulation from the donor and receptor cell interface. Prototype A yielded valuable information with regard to the suitability of diffusion cells in these experiments. Furthermore, design flaws such as the loss of formulation were addressed in prototype B.

5.5.4. Standardisation of Experimental Procedures in Prototype B: Temperature Maintenance, Stirring Rate and Turbulence

In order to ensure a temperature that is essentially constant and close to 37.0 °C, it was experimentally determined that the water circulating around the fluid jacket be heated to 37.5 °C. It was found that within 15 min the receptor fluid was at 37.0 °C and the temperature was maintained within 0.2 °C ($n = 5$) over the 12 h. Water evaporation was found to occur over 12 h, with a significant reduction in volume occurring after 2 h. It was found that once silicone oil had been place on top of the mesh aperture, water evaporation was (not unexpectedly) reduced, resulting in no significant change in volume occurring over the course of the experiment ($n = 5$).

The stirring rates used during this work were 62 rpm (± 2.0), 100 rpm (± 1.0) and 150 rpm (± 2.0). There was no significant change ($n = 10$; $p > 0.05$) in the stirring rate at

each speed over the 12 h. The choice of 62 rpm was taken as this was the lowest achievable stirring rate. Figure 5.6 (a - h) illustrates the receptor compartment appearance immediately after potassium permanganate loading on to the 45 μm mesh aperture and the subsequent progression over one min. Immediately after loading, a stream of potassium permanganate was observed to form towards the apex of the stirring bar. Subsequent observations indicated that the stream of potassium permanganate initiated from different areas, suggesting the presence of a clump of solid. Within 60 s, complete colouration extending up the side arm was achieved. As the mesh aperture increased, the time taken to achieve complete colouration decreased from approximately 35 s to 15 s for the 90 and 180 μm meshes respectively. The degree of dispersal was considered unacceptable under conditions of no stirring, with patchy potassium permanganate colouration observed. An homogeneous distribution of potassium permanganate was not achieved even after 10 min, indicating the possibility of irreproducible release rates.

The UV spectrum of sesame seed oil made it an ideal candidate for these studies. It was found that at low stirring rates (≤ 100 rpm), there was no deviation from the base line, indicating that the sesame seed oil was not being mixed with the receptor fluid. At high stirring rates (150 rpm), there was a significant move away from the base line and visual examination upon completion of the experiment, showed the receptor fluid was an emulsion. These high revolutions resulted in receptor medium turbulence and possibly alterations to the mesh support-receptor solution interface not normally visibly appreciated. For this reason, the stirring rates investigated in the study were 62 and 100 rpm.

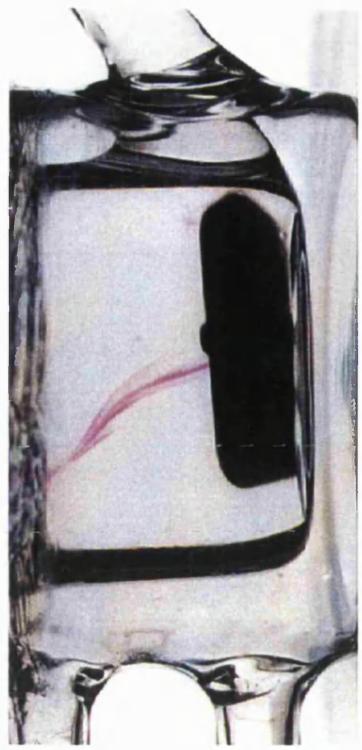

b) 4.5 seconds

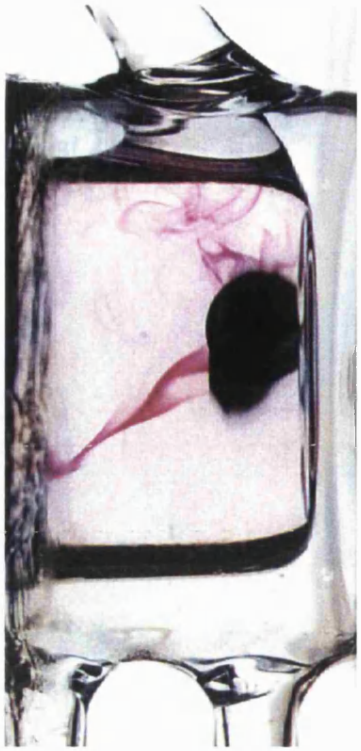

d) 18 seconds

a) 0 seconds

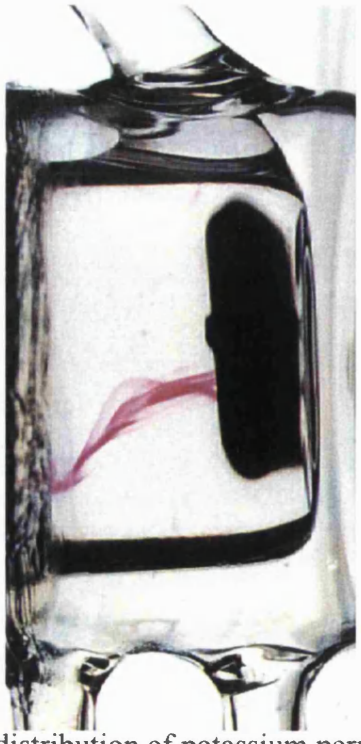

c) 9 seconds

Figure 5.6 (a-d). Receptor compartment distribution of potassium permanganate after release from 100 cSt silicone oil using a 45 μm mesh aperture and a stirring rate of 62 rpm.

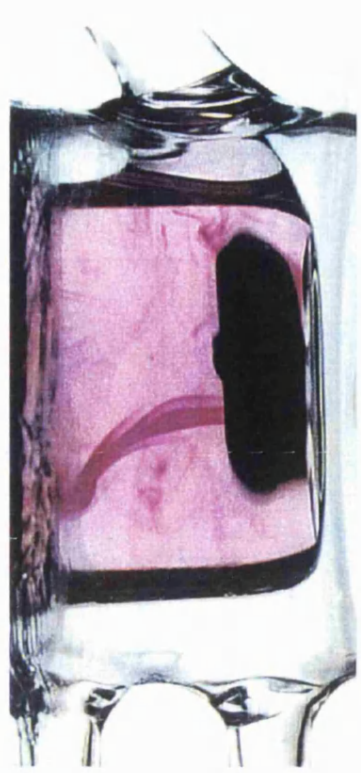

e) 27 seconds

f) 36 seconds

g) 45 seconds

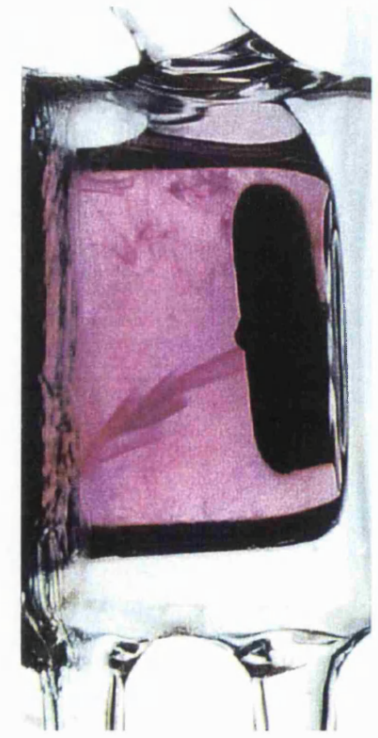

h) 54 seconds

Figure 5.6 (e-h). Receptor compartment distribution of potassium permanganate after release from 100 cSt silicone oil using a 45 μm mesh aperture and a stirring rate of 62 rpm.

5.5.5. Assembly of Prototype B and General Experimental Procedures

The total percentage drug recovery for all experiments conducted was 97.68 % (± 2.02). The total percentage tacrine recovery from the diffusion was comparable to the value quoted in Section 5.5.2, although some formulation loss occurred during cell disassembly.

The cumulative percentage of tacrine in the receptor compartment was plotted against the time in minutes. The reproducibility was considered to be acceptable, with relative standard deviation values within 12.0 %. After the first data point was plotted, subsequent recordings were plotted every 10 min for the first hour and then every 15 min for 7 h. The error bars represent the standard deviation (n = 5), which in some cases are smaller than the symbols used. An investigation into the mechanism involved in the drug diffusion process (Fickian or non-Fickian) was carried using the release data. In order to be able to quantify the release kinetics from ER fluids, the data were analysed according to various models. As can be seen from the release profiles shown, the zero-order model does not apply, as the release was not linear with time. As all the drug release profiles obtained conformed to the pattern of apparently exponential decreasing cumulative drug release with increasing time, it was decided to analyse the data according to first order and square root time models. Furthermore, the exponent value (n) was determined for all release profiles (Equation 5.3).

5.5.6. Validation of Prototype B: The Effect of Mesh Aperture, Stirring Rate, Receptor Fluid Volume and Temperature on the Release of Tacrine from Silicone Oil

i) Stirring Rate

The effect of receptor fluid stirring rate on the cumulative percentage release of tacrine from 100 cSt silicone oil is shown in Figure 5.7. The cumulative percentage release over 8 h is tabulated below (Table 5.3).

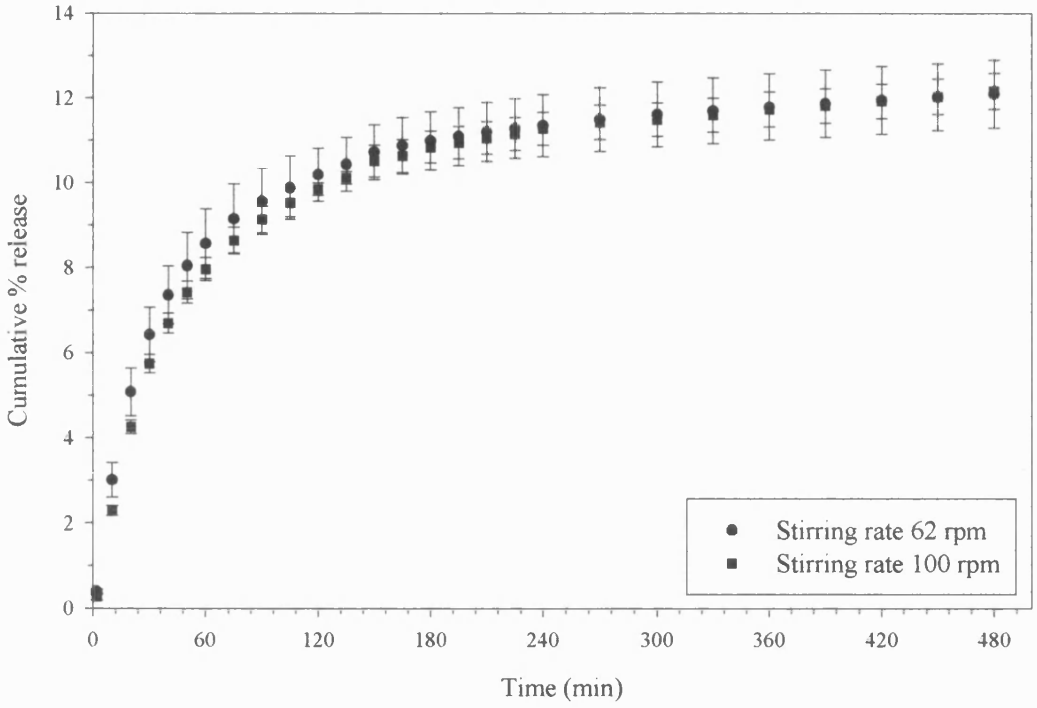

Figure 5.7. The effect of stirring rate on the cumulative percentage release of tacrine from 100 cSt silicone oil using a 45 µm mesh aperture support at 37.0 °C.

Stirring rate (rpm)	Cumulative % release after 8 h	Standard deviation (RSD)
0	-	-
62	12.10	0.80 (6.61 %)
100	12.16	0.43 (3.55 %)

Table 5.3. The effect of stirring rate on the cumulative percentage release of tacrine from 100 cSt silicone oil using a 45 µm mesh aperture support at 37.0 °C.

A Student's t-test was conducted to determine the effect of stirring rate on the cumulative percentage release. The degrees of freedom was 4 (n - 1) and the tabulated t value was 2.776 at the 95 % significance level. There was no significant difference ($t_{critical}$ = 0.12) in the cumulative percentage tacrine release when the receptor fluid was stirred at

62 and 100 rpm. Under conditions of no stirring, the diffusion of tacrine was erratic and irreproducible. The cumulative percentage release validation experiments have reinforced evidence observed in previous studies (Section 5.5.6), where the failure to produce an homogenous distribution of potassium permanganate led to the conclusion that the degree of distribution was unacceptable under conditions of no agitation. Furthermore, the conclusions drawn with respect to formulation turbulence at high stirring rates (≥ 150 rpm) (see Section 5.5.5) have been strengthened with the aid of these validation studies. A stirring rate of 150 rpm resulted in a higher than expected initial burst of tacrine release indicative of agitation of the formulation layer beneath the mesh support. On cessation of the experiment, the receptor fluid compartment resembled an oil in water emulsion.

The general shape of the release profiles obtained suggested that either first-order or a square root of time relationship existed. The release data were analysed according to a first-order kinetics using the following equation:

$$\text{Log}_{10}M = - \frac{kt}{2.303} + \text{Log}_{10}M_o \qquad \text{Equation 5.4}$$

where k is the first-order rate constant, M is the mass of drug remaining at time t and M_o is the initial mass of drug in the formulation. For drug release to occur according to this model, a plot of $\log_{10}$ M versus time would produce a straight line with a slope -k/2.303. Data were plotted according to this relationship except that the percentage remaining was used in place of mass remaining. A plot showing the general relationship over the entire experimental time is shown in Figure 5.8, together with an expanded long time plot (t ≥ 165 min).

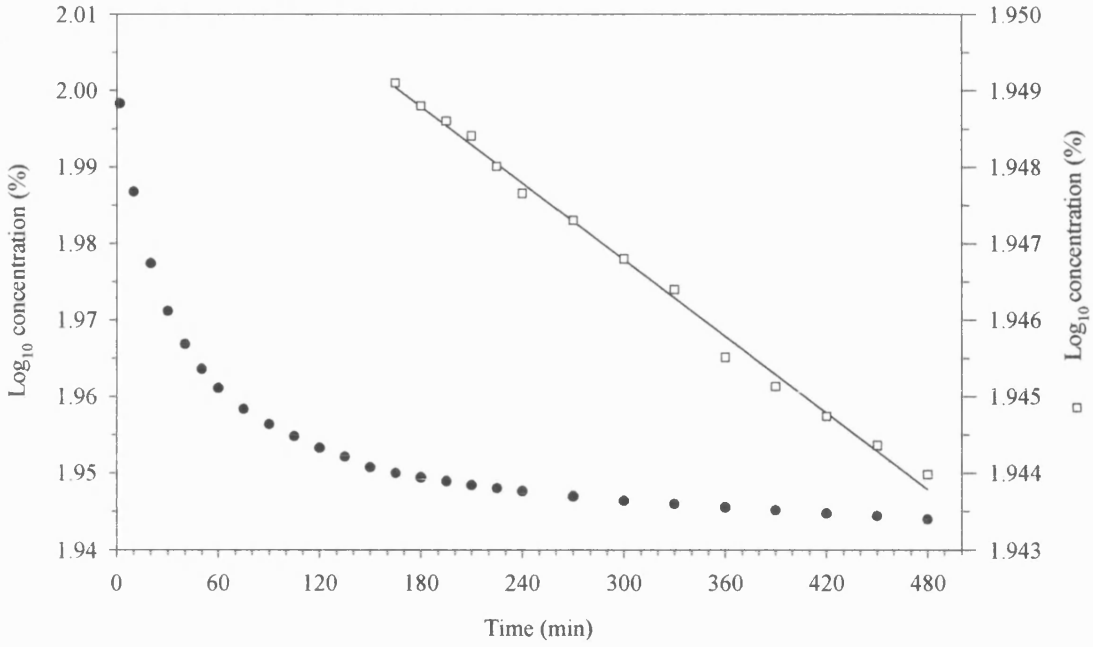

Figure 5.8. Plot of $\log_{10}$ percentage original drug concentration remaining versus time for the aforementioned formulation stirred at 62 rpm using a 45 µm mesh aperture support at 37.0 °C (Symbol •). An expanded plot ($t \geq 165$ min) is shown together with the calculated linear regression analysis curve (Symbol □; right hand side y-axis).

Analysis of the first-order plot indicated two distinct regions, with the long-time region ($t \geq 165$ min) being approximately linear ($r^2 = 0.99503$). The sample loading in horizontally oriented diffusion cells, will inevitably result in the seepage of formulation through the mesh support (Figure 5.9), forming a thin layer on top of the receptor fluid.

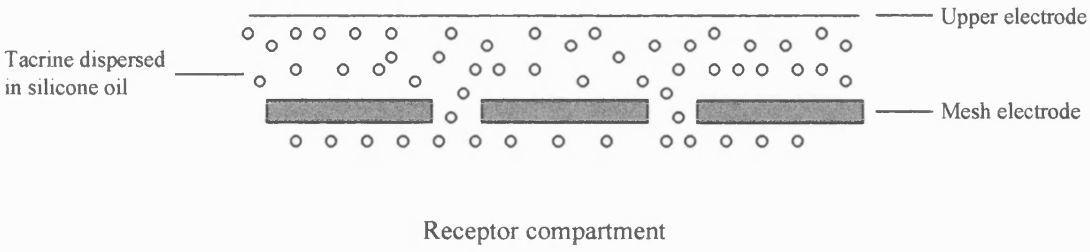

Figure 5.9. Post-loading formulation distribution as a result of seepage through the mesh support.

Although likely to create a rate-limiting barrier, sesame seed oil measurements (Section 5.5.5) indicated that this layer does not become involved in the receptor fluid at the stirring rates used in these studies (≤ 100 rpm). The initial rapid release (or "burst" effect) may be as a direct result of drug release from this layer. In the diffusion cell arrangement, there was no rate-limiting barrier between the formulation and the receptor fluid, resulting in the rapid drug release observed. An analogy to the boundary layer effects described for membrane-controlled reservoir devices may be drawn to explain the decrease in release rate observed at long time periods. The boundary layer offers significant resistance to mass transfer resulting in the constant release rate observed during the early times, with a later transition to first-order release at long times. It seems likely from this initial mechanism investigation, that the release was biphasic, with a short time oil/water partitioning process and a long time oil/oil diffusion controlled release. The drug was first removed from the formulation layer beneath the mesh aperture, after this layer has been depleted replenishment was initiated from the formulation layer retained by the mesh aperture. The time quoted (165 min) appeared to describe the transition point from "burst" release to possible first-order release kinetics.

Biphasic drug delivery is not a novel concept. Reservoir devices in which the drug is surrounded by a polymeric membrane (e.g. Langer, 1980; Langer and Peppas, 1981; Peppas, 1985), typically silicone based (Blackshear, 1979; Lee et al., 1997) or ethylene vinyl acetate copolymer (EVAc) (Siegel et al., 1989; Edelman et al., 1996) sometimes exhibit a "burst" of drug release associated with the saturation of the rate controlling membrane (Park et al., 1984). The release from matrix systems, were the active agent is homogeneously dissolved or distributed throughout the polymer matrix (e.g. Langer, 1980; Narasimhan and Langer, 1997), is diffusion controlled and governed by Fick's first law of diffusion. However, low drug loading matrix systems are often seen to exhibit a two phase release profile, the "fast" phase corresponding to the release of drug from the pore network

adjacent to the surface and a "slow" phase possibly corresponding to the diffusion of drug through the polymer matrix (Siegel et al., 1989; Brachais et al., 1998; Kikkinides et al., 1998). Historically, most drug models fail to predict the initial burst (Rhine et al., 1980) however, Narasimhan and Langer (1997) have recently developed a mathematical model which quantitatively accounts for the burst effect observed with polymeric hemispheres.

In an attempt to provide further support for the aforementioned hypothesis, the release data were fitted according to the square root of time model (Equation 5.3 when n is equal to 0.5). A plot of the amount of drug remaining against $t^{1/2}$ should yield a linear plot with a slope k. Figures 5.10 and 5.11 show the square root of time plots over the entire release period and at long times ($t \geq 165$ min) respectively. The curve depicted previously in Figure 5.8 was likely to comprised of two regions, an initial non-linear section proceeding a linear region at long times. The linearity of the long time region ($t \leq 165$ min) of the curve was assessed using least square regression analysis (Figure 5.11). The cumulative percentage released is used instead of mass.

Figure 5.11 indicated a good linear regression correlation ($r^2 = 0.98651$). The linearity of the square root of time plot indicated that Fickian diffusion is the predominant mechanism of release at long times.

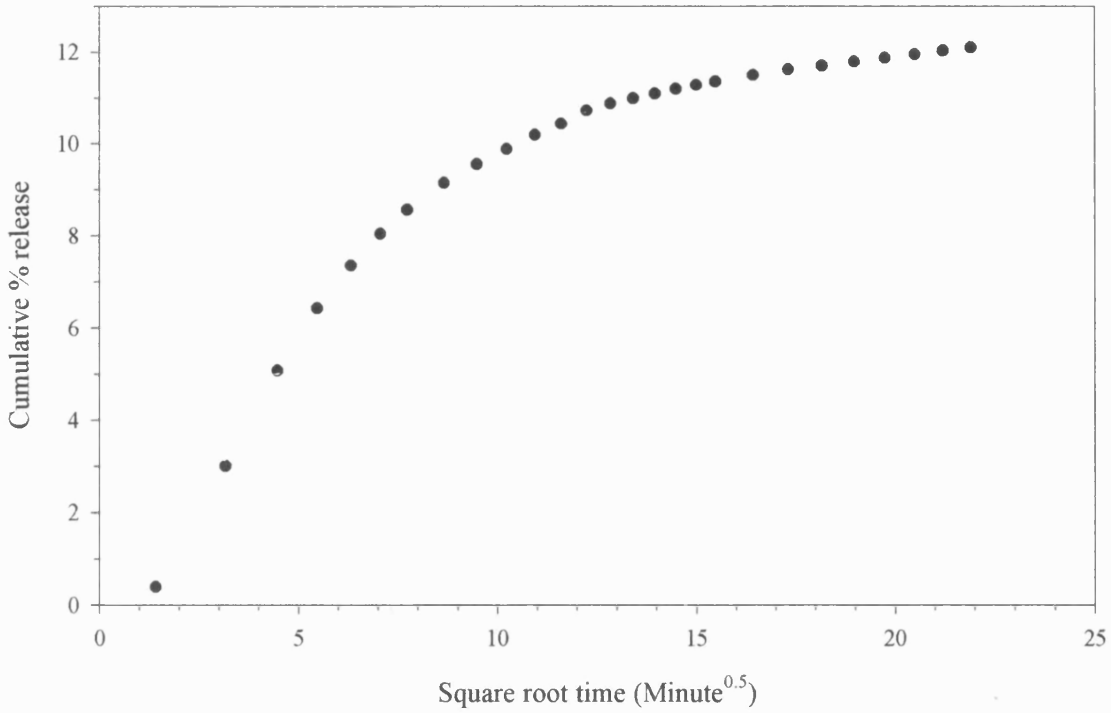

Figure 5.10. Graph showing the cumulative percentage tacrine release versus square root of time for a suspension of 0.5 % w/w tacrine in 100 cSt silicone oil stirred at 62 rpm using a 45 μm mesh aperture support at 37.0 °C.

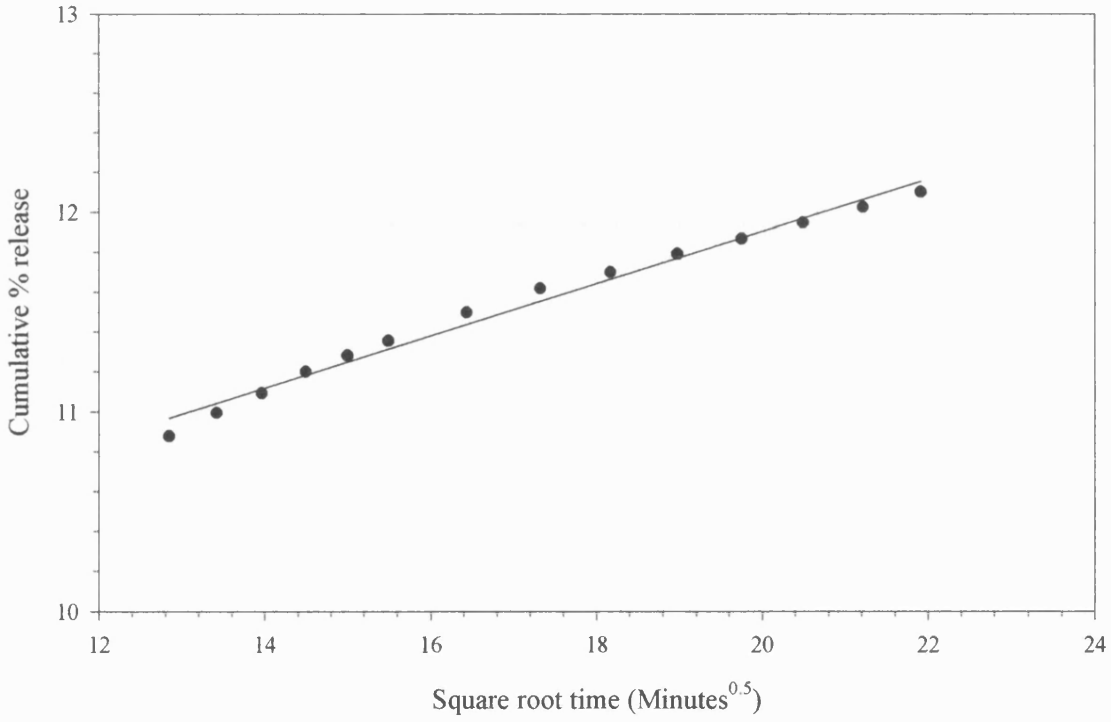

Figure 5.11. Expanded linear regression analysis curve ($t \geq 165$ min) of Figure 5.10.

The mechanisms involved in the drug diffusion process were further investigated by fitting the release data to Equation 5.3. The significance of the magnitude of the power term has been discussed in Section 5.1. The power term values (n) predicted for each stirring rate (62 and 10 rpm) were 0.25 and 0.28 respectively, indicating neither zero nor first-order kinetics were obeyed. In both cases, the correlation between the drug release profile and the model was in the region of 0.9000. Peppas (1985) concluded that the exponent (n) may take values greater than or equal to 0.5, with smaller values indicative of a statistical analysis problem. Korsmeyer and co-workers (1983) further proposed the use of Equation 5.3 for drug diffusion through polymeric structure. The analysis of drug release from porous systems is likely to lead to exponent (n) values below 0.5 as a result of a combination mechanism for example diffusion through the swollen matrix and water filled pores will result in small values of n (Korsmeyer et al., 1983; Peppas, 1985). The exponent values predicted are indicative of a complex release mechanism, possibly composed of several routes of diffusion. This provides strength for the biphasic release mechanism proposed earlier.

The initial portion of the curve ($M_t/M_\infty \leq 0.60$) was analysed to determine the exponent (n) value (Figure 5.12). The total amount of drug released after infinite time, M_∞, was taken to be the value at which the release curve reached an asymptote. The exponent (n) value calculated for stirring rates of 62 and 100 rpm were 0.69 ($r^2 = 0.9820$) and 0.71 ($r^2 = 0.9847$), signifying anomalous or non-Fickian transport mechanisms.

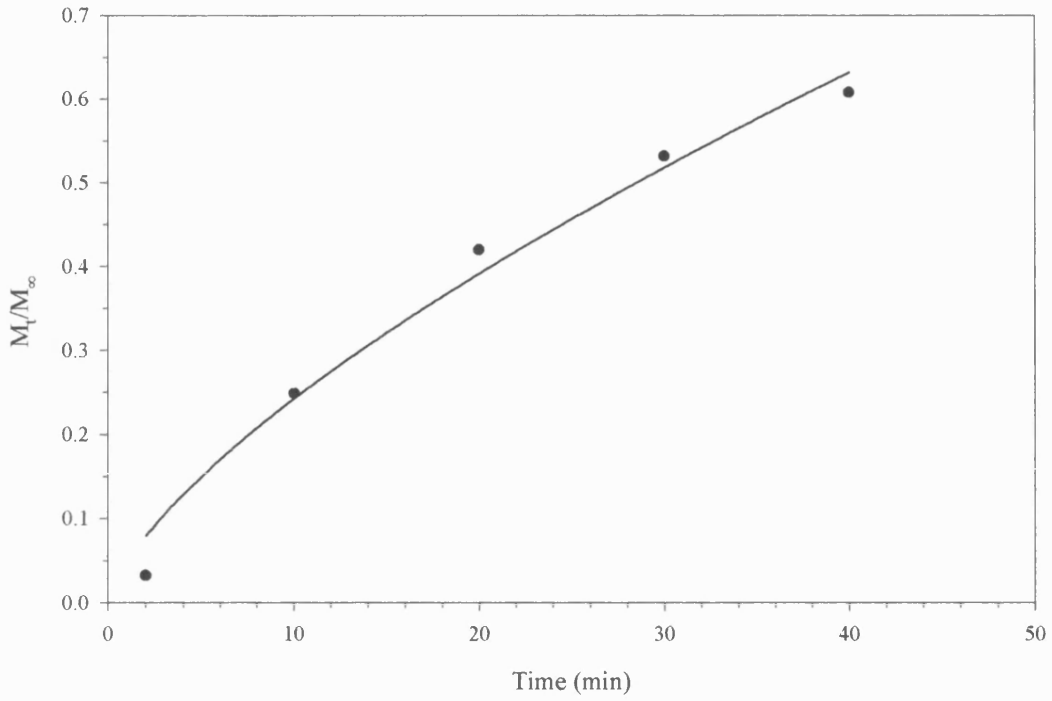

Figure 5.12. Determination of the exponent (n) value for the initial portion of the release curve ($M_t/M_\infty < 0.60$).

ii) Mesh Aperture

The effect of mesh aperture on the release of tacrine from 100 cSt silicone oil is reproduced in Figure 5.13 (a and b). The total cumulative percentage release after 8 h is shown in Table 5.4.

Mesh aperture (μm)	Cumulative % release after 8 h	Standard deviation (RSD)
45	12.10	0.80 (6.61 %)
90	18.58	0.39 (2.10 %)
180	34.83 *	1.07 (3.07 %)

Table 5.4. The effect of mesh aperture on the cumulative percentage release of tacrine (0.5 % w/w) from 100 cSt silicone oil with a stirring rate of 62 rpm at 37.0 °C. (* over 1 h).

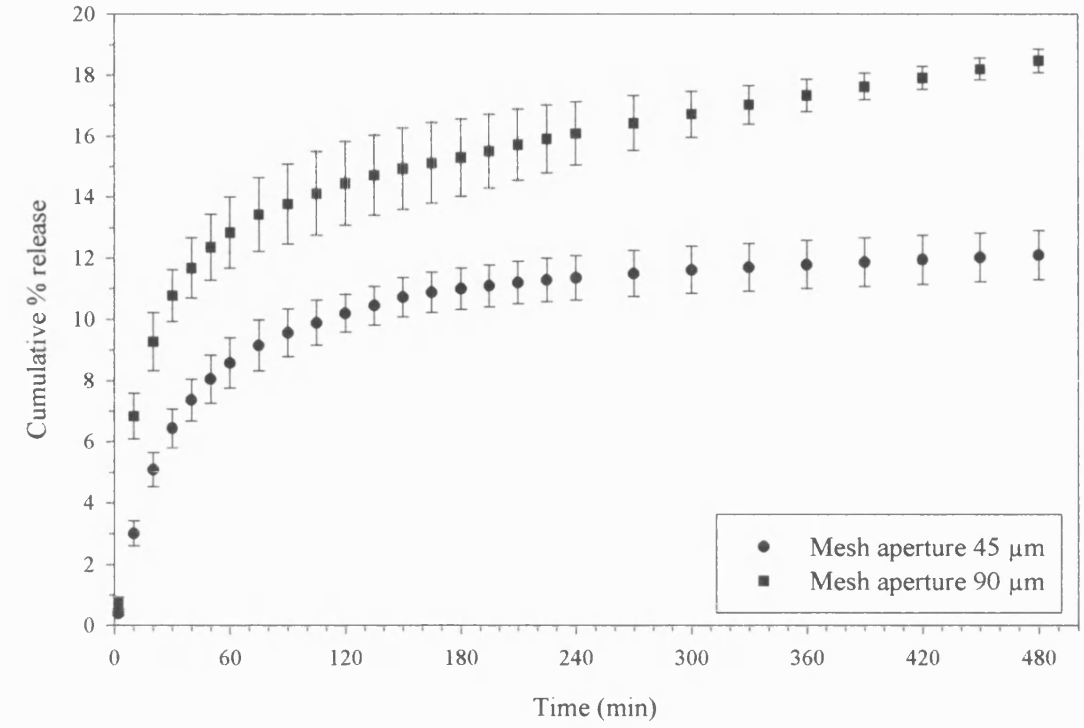

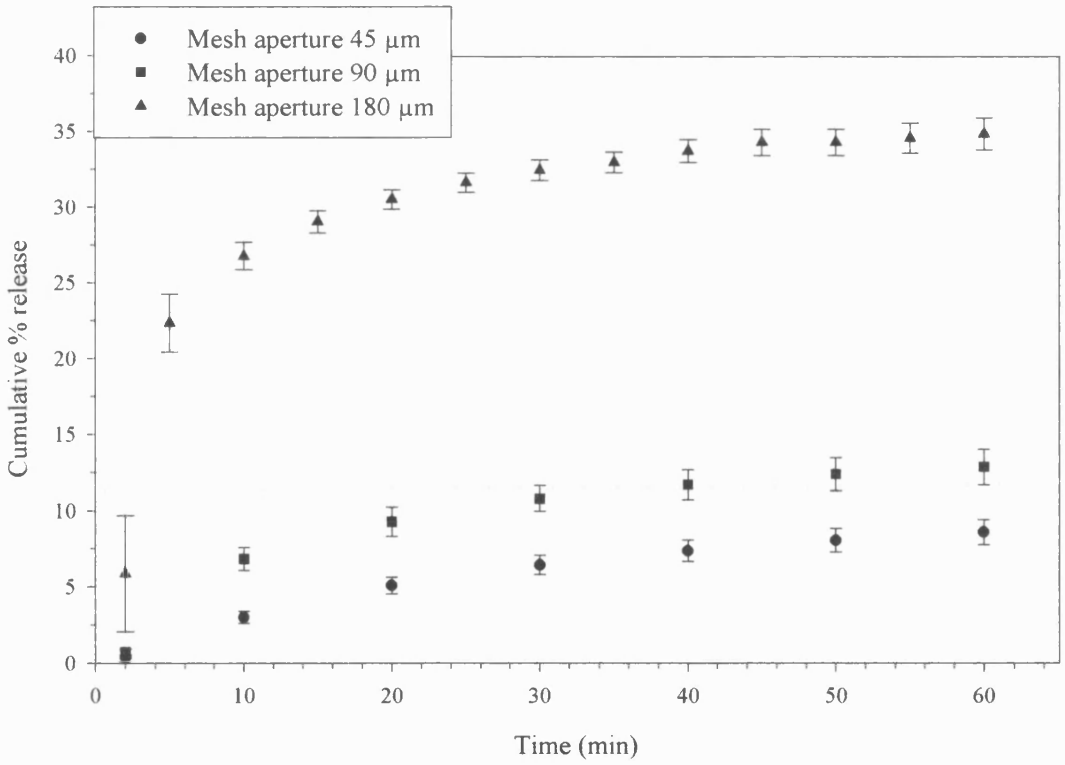

Figure 5.13 (a and b). The effect of mesh aperture (45, 90 and 180 µm) on the cumulative percentage release of tacrine (0.5 % w/w) from 100 cSt silicone oil with a stirring rate of 62 rpm at 37.0 °C.

The mesh aperture was found to have a significant effect ($p < 0.05$) on the release of tacrine from silicone oil, with an increase observed from 12.10 % (± 0.80) to 18.58 % (± 0.39) for 45 and 90 μm respectively. The tacrine release through the 180 μm mesh was rapid, with 34.83 % (± 1.07) released over 1 h. The basal rate of release from the formulation could, therefore, be controlled through the appropriate choice of mesh aperture. The first-order release kinetics were obeyed at long times ($t \geq 165$ min) for mesh apertures of 45 and 90 μm (calculated r^2 values were 0.99503 and 0.99708 respectively). The first-order rate constants (k) for mesh apertures of 45 and 90 μm are 3.85 and 12.74 min^{-1} respectively. With regard to the release profile using the 180 μm mesh support, first-order kinetics were obeyed after approximately 30 min ($r^2 = 0.99221$) (Figure 5.14). The relationship between square root time and cumulative percentage release was analysed for the 180 μm mesh aperture over the same period (Figure 5.15).

The power terms in Equation 5.3 were calculated using least square regression analysis to be 0.25, 0.23 and 0.26 for mesh apertures of 45, 90 and 180 μm respectively. Although these values do not predict the mechanism of tacrine release from silicone oil, the closeness of the value indicates that similar processes are occurring regardless of the mesh aperture utilised.

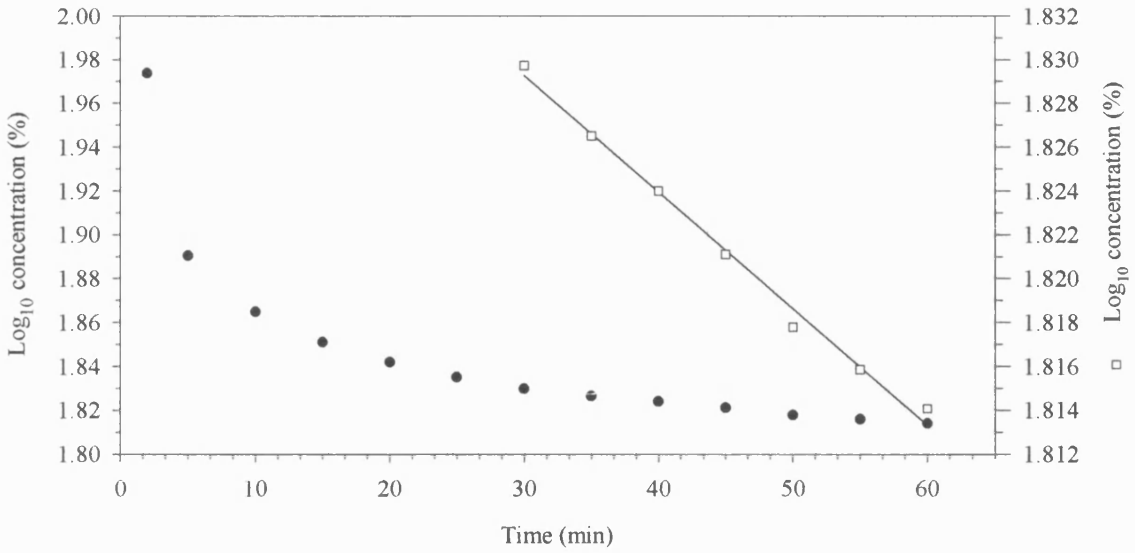

Figure 5.14. Plot of $\log_{10}$ percentage original drug concentration remaining versus time for a 0.5 % w/w suspension of tacrine in 100 cSt silicone oil stirred at 62 rpm using a 180 µm mesh aperture at 37.0 °C (Symbol •). An expanded plot ($t \geq 30$ min) is shown together with the calculated linear regression analysis curve (Symbol □; RHS y-axis).

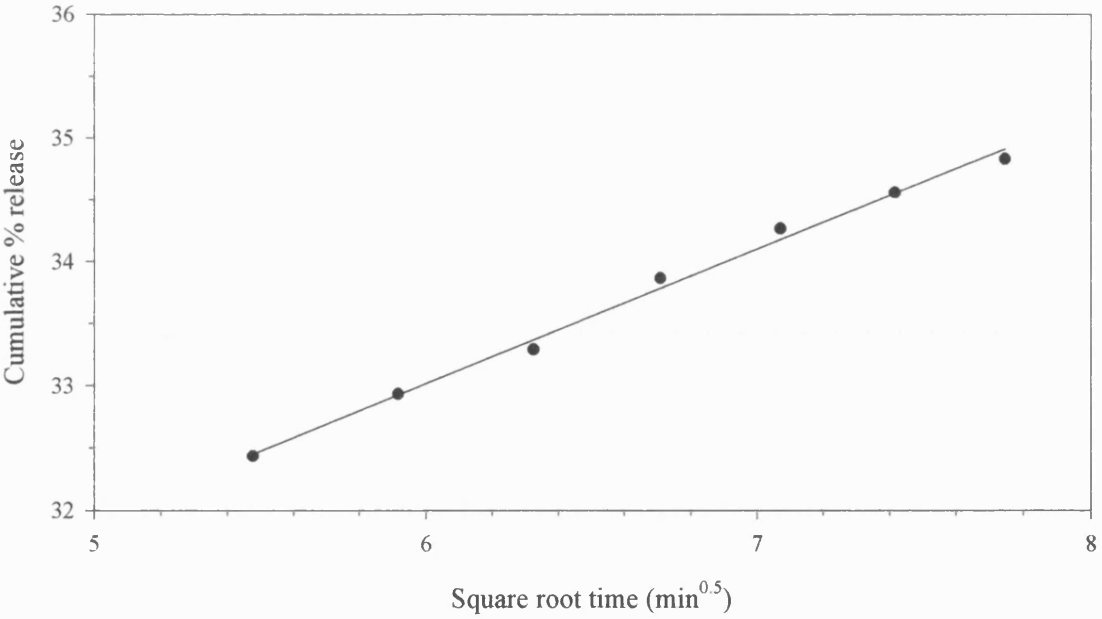

Figure 5.15. Expanded linear regression analysis curve ($t \geq 30$ min) for a 0.5 % w/w suspension of tacrine in 100 cSt silicone oil stirred at 62 rpm using a 180 µm mesh aperture support at 37.0 °C.

The hypothesis proposed in the previous section alludes to a biphasic release profile originating from the seepage of formulation through the mesh aperture and consequently forming a layer on top of the receptor compartment medium. Reinforcement of this hypothesis would ensue, but for the fact that the mesh apertures were specifically chosen with equal open areas. The receptor fluid volume in each case was approximately 37.0 ml, thereby negating the possibility of formulation thickness variations beneath the mesh support. However, there is a significantly higher initial tacrine release associated with the mesh aperture of 180 μm; indeed the burst effect release increased with increasing mesh aperture. The differences observed may be as a result of an increased amount of water in the immediate vicinity of the formulation for drug dissolution. Furthermore, the hypothesis may be further extended to incorporate the effect of convection flow within the mesh openings; convection being greatest with the 180 μm mesh aperture. The increased drug release may simply be explained by the ease of drug diffusion through large apertures, without the obstacle of small openings.

iii) Receptor Fluid Volume

The effect of receptor fluid volume on the release of tacrine from 100 cSt silicone oil is reproduced in Figure 5.16. The total percentage release over 8 h is shown in Table 5.5.

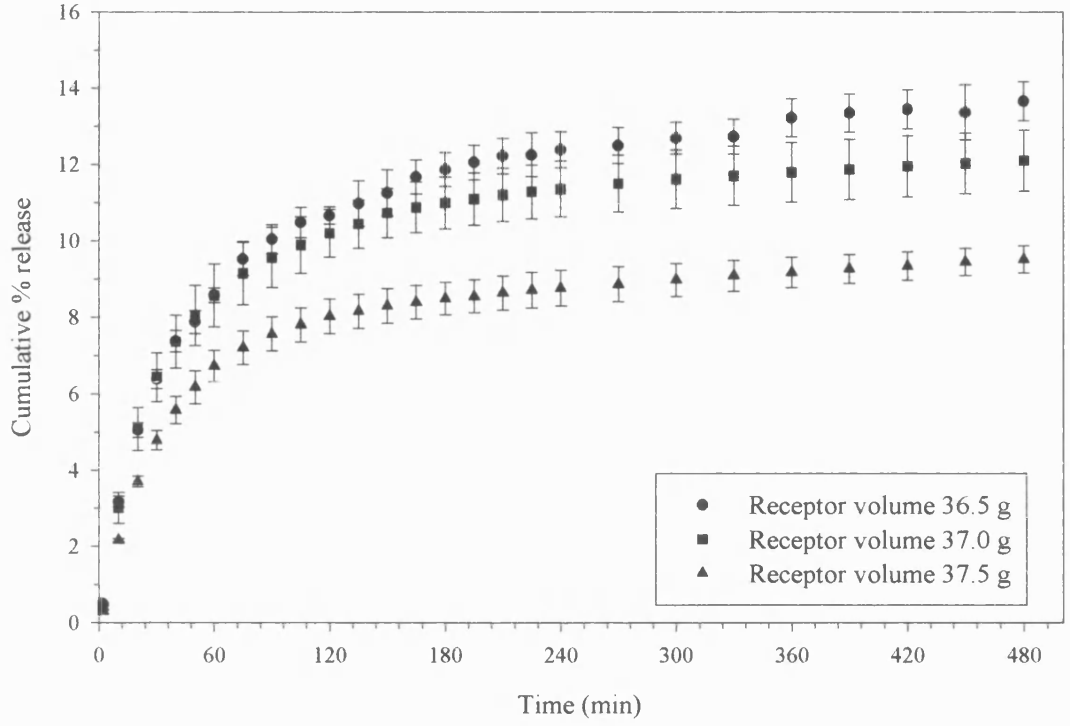

Figure 5.16. The effect of receptor fluid volume on the cumulative percentage release of tacrine (0.5 % w/w) from 100 cSt silicone oil with a mesh aperture of 45 μm and a stirring rate of 62 rpm at 37.0 °C.

Receptor fluid volume (g)	Cumulative % release after 8 h	Standard deviation (RSD)
36.5	13.67	0.52 (3.80 %)
37.0	12.10	0.80 (6.61 %)
37.5	9.52	0.35 (3.68 %)

Table 5.5. The effect of receptor fluid volume on cumulative percentage release of tacrine (0.5 % w/w) from 100 cSt silicone oil using a 45 μm mesh aperture and a stirring rate of 62 rpm at 37.0 °C.

For reasons of accuracy, the receptor fluid was weighed (by difference) into the receptor compartment as opposed to measuring the volume. The receptor fluid volume had a significant effect (one-way ANOVA; $p < 0.05$) on the release of tacrine from 100 cSt silicone oil with an increase from 9.52 % (± 0.35) to 13.67 % (± 0.52) for 37.5 ml and 36.5 ml respectively. The observed increase in cumulative percentage drug release with decreasing receptor fluid volume has strengthened the hypothesis previously proposed. The effluence of formulation through the mesh aperture was suggested for the initial burst of drug release observed in the profiles. With decreasing receptor fluid volume, the layer beneath the mesh support increases. The first 20 min of each run yields comparable drug release, indicating the time scale for the establishment of the water/oil equilibrium.

In subsequent experiments (Chapter Six), conducted under the influence of an applied electric field, care was needed with respect to the amount of distilled water in the receptor compartment. Although, a decrease in the tacrine release was observed at receptor volume of 37.5 ml, indicating a minimal amount of formulation seepage through the mesh support, problems arising from power surges negated the use of this volume; instead 37.0 ml was added to the receptor compartment .

iv) Temperature

The effect of receptor fluid temperature on the release of tacrine from 100 cSt silicone oil is shown in Figure 5.17. The total percentage release over 8 h is shown in Table 5.6.

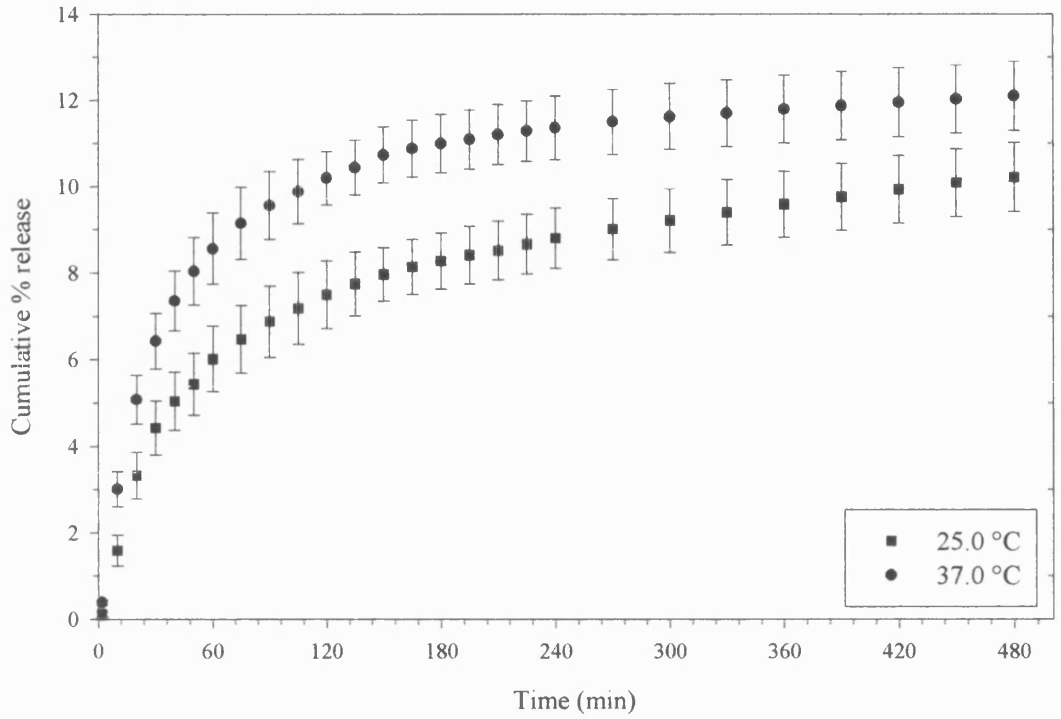

Figure 5.17. The effect of temperature on the cumulative percentage release of tacrine (0.5 % w/w) from 100 cSt silicone oil with a mesh aperture of 45 μm, a stirring rate of 62 rpm and a receptor volume of 37.0 ml.

Temperature (°C)	Cumulative % release after 8 h	Standard deviation (RSD)
25	10.21	0.80 (7.85 %)
37	12.10	0.80 (6.61 %)

Table 5.6. The effect of receptor fluid temperature on the cumulative percentage release of tacrine (0.5 % w/w) from 100 cSt silicone oil with a mesh aperture of 45 μm, a stirring rate of 62 rpm and a receptor volume of 37.0 ml.

The percentage release of tacrine from silicone oil significantly increased (one-way ANOVA; $p < 0.05$) from 10.21 % (± 0.80) to 12.10 % (± 0.80) for experiments conducted at 25.0 and 37.0 °C respectively. The observed increase in tacrine release with

temperature was to be expected. The release profile obtained at 25.0 °C is of a similar shape to those obtained previously. The mechanism of release was evaluated using previously described models. The first order rate constant was calculated from the linear plot of $\log_{10}$ M against time at long time periods ($t \geq 165$ min) to be 7.28 min^{-1}. At long times ($t \geq 165$ min), good correlation was observed (r^2 values 0.99178 and 0.99917 respectively) when fitting the release data to first order kinetics and the square root of time relationship. The exponent value (n) was determined over the experiment duration to be 0.32 compared to 0.25 at 37.0 °C. The initial burst effect ($M_t/M_\infty < 0.6$) yielded an exponent value (n) of 0.66 ($r^2 = 0.97055$), indicating anomalous or non-Fickian behaviour as described previously.

5.6. Estimation of Diffusion Coefficient

The diffusion coefficient (D) in a liquid of viscosity η can be calculated according to Stokes-Einstein equation:

$$D = \frac{RT}{6\pi\eta\, a\, N_a} \qquad \text{Equation 5.5}$$

where R is the gas constant (8.314 x 10^7 erg/deg/mole), T is the temperature (Kelvin), η is the medium viscosity (Poise or g/cm sec), a is the radius of the diffusing particle (cm) (cf. Table 2.2 pg179) and N_a is Avogadro's number (6.0221 x 10^{23} $mole^{-1}$). Values are given in cgs units as the diffusion coefficient is usually defined in cm^2/sec.

The estimated diffusion coefficients are 1.01 x 10^{-11} cm^2/sec (37.0 °C) and 9.75 x 10^{-12} cm^2/sec (25.0 °C). The main assumption is that the tacrine particle is spherical. As D increases, the cumulative percentage of drug released increases. This relationship is

perhaps most useful for predicting the value of D in ER fluids (Chapter Six) with and without the application of an electric field. According to this equation, the diffusion rate will decrease in ER fluids upon application of an electric field as the apparent viscosity is known to increase significantly. The predicted diffusion coefficient fails to account for the initial burst of release observed. The amount of drug released during the burst period is likely to be independent of the drug diffusion coefficient. Drug released during this burst episode is a function of formulation seepage and subsequent partition with the receptor medium. The burst effect is therefore probably controlled by the drug solubility in the receptor compartment.

5.7. Conclusions

The classic diffusion cell has been modified for use with these low viscosity formulations with the addition of a mesh support and a glass lip to aid retention. The modified diffusion cell has been validated and several factors, namely mesh aperture, receptor fluid volume, stirring rate and temperature have been investigated. It was concluded from the general shape of the profile obtained that either first-order or a square root of time model would possibly describe the release process and the data were therefore fitted to these models. These simple mathematical models did not describe the tacrine release data obtained over the entire experimental duration. It was hypothesised that there was a biphasic release profile; after an initial period of rapid release, the curve approached a quasi-equilibrium followed by a slow approach to final equilibrium. The initial rapid and major release of tacrine was as a result of formulation seepage through the mesh aperture. An increase in mesh aperture and a decrease in receptor fluid volume confirmed this hypothesis. When the mesh aperture was increased from 45 μm to 90 μm, the cumulative percentage release rate was increased from 12.10 (± 0.80) to 18.58 (± 0.39). In addition, an increase in mesh opening is likely to enhance convection movements and

increase the water content for solubility. The cumulative percentage release was significantly decreased with increased receptor fluid volume from 13.67 (± 0.52) to 9.52 (± 0.35) for 36.5 and 37.5 ml respectively.

Electrorheologically controllable drug release is discussed in the final Chapter. The simple, precise and reliable method developed above will be used in the determination of drug release from ER fluids. MCC will be added to the tacrine formulation to provide the scaffolding matrix envisaged to hinder or halt drug release from ER fluids. The work will be conducted in accordance with the yield stress results obtained and discussed in Chapter Three.

Chapter Six

In-Vitro Model of an Electrorheological Fluid Based Drug-Delivery Device

6.1. Introduction

The formation of particle chains under the influence of an applied electric field was extensively discussed in Chapter Three, and the conclusion drawn that the magnitude of the yield stress value provided information as to the extent and relative strength of these chains. It is envisaged that the electrorheologically controlled diffusion of tacrine under an applied electric field would, in part, be dependent on the degree of chain formation and the resultant tortuosity of the diffusion pathway. The existence of a correlation between the yield stress and the rate of diffusion is investigated below. In this Chapter, the feasibility of an ER controlled drug-delivery device is examined. The ability of this type of device to deliver a model drug, tacrine, to a delivery site in a fully controlled and predictable manner is investigated. The purposes of this work are twofold: (1) to investigate the effect of structural characteristics of ER fluids on tacrine release, and (2) to establish guidelines for development of controlled release formulations with the ultimate goal of achieving a feedback-controlled delivery system.

The *in vitro* device examined in the present study is based on the previously validated diffusion cell (Chapter Five). Throughout this study, the lower electrode uses different mesh apertures (45, 90 and 180 μm). The formulations were chosen to represent the extremes of behaviour, in terms of the Bingham yield stress, exhibited by each factor (particle size, particle concentration and applied electric field) as discussed above in Chapter Three. A finite element modelling scheme is used to predict the electric field response around an isolated wire. A solution of Gauss' flux theorem is provided. The effect of mesh aperture on the development of the Bingham yields stress is investigated in an attempt to correlate cumulative percentage release data with ER fluid strength. The possibility of tacrine adsorbance onto MCC was investigated in Chapter Three and found to be a potential problem. Therefore, we have also investigated the amount of tacrine recoverable from the ER fluid formulation.

6.2. Diffusion Cell Design

A schematic diagram of the diffusion cell used in this study is shown in Figure 6.1, together with a photograph in Figure 6.2. The diffusion cell was further modified by the addition of an extra side arm enabling separation of the input and output UV detector tubes (prototype C).

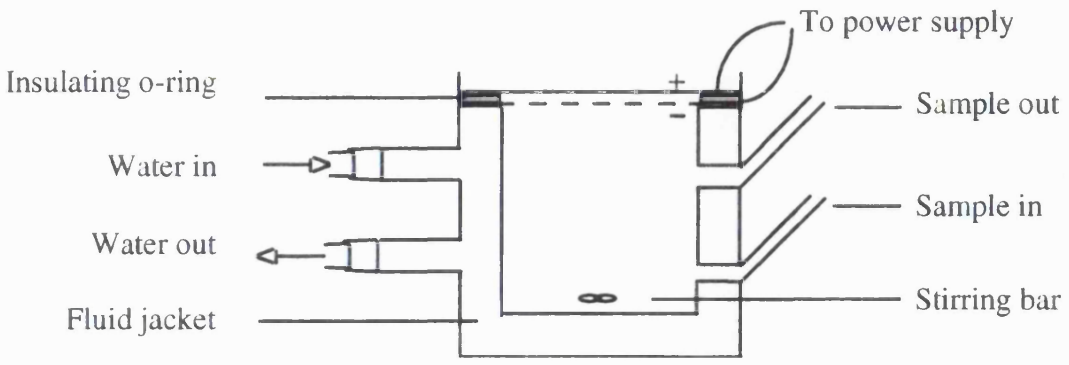

Figure 6.1. Schematic diagram of the diffusion cell.

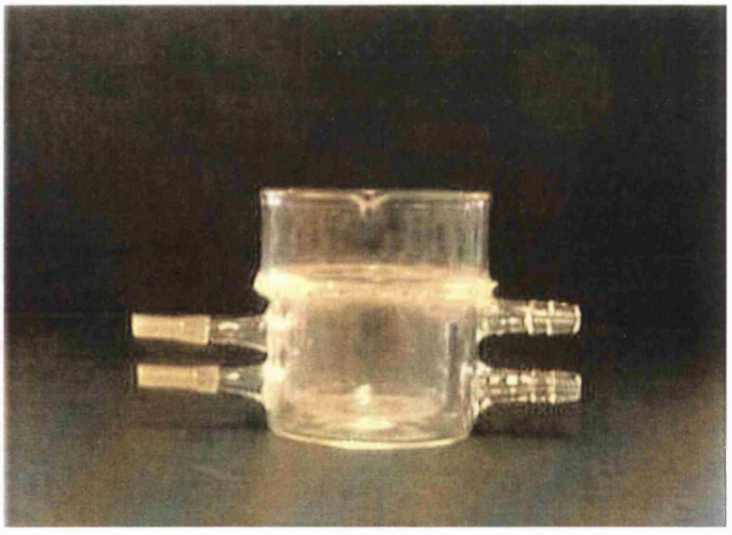

Figure 6.2. Photograph of the diffusion cell developed in this study (prototype C).

The electrode assembly, comprising a lower mesh cloths electrode (Section 5.2) and an upper flat plate electrode of approximately 0.90 mm in thickness and 50.0 mm in diameter (Figure 6.3 and 6.4), was placed horizontally in the diffusion cell. The choice of material for the electrodes would ideally have been platinum as it is generally considered to be inert. Limitations of cost and more specifically the lack of choice in mesh apertures for platinum electrodes negated its use in this study.

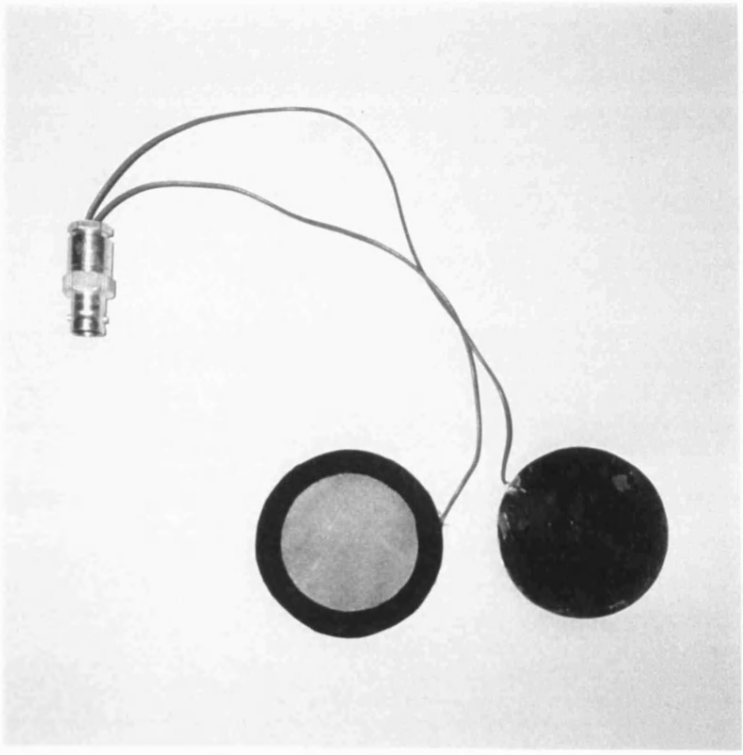

Figure 6.3. Photograph of the electrode design.

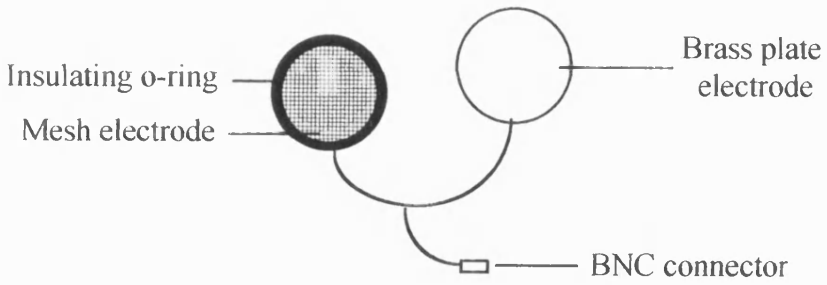

Figure 6.4. Schematic diagram of the electrode design.

6.2.1. Electric field Distortion using Mesh Electrodes

The device utilised in these studies is analogous to a parallel-plate capacitor. In the traditional capacitor design, the electrodes would both be flat plates, thereby resulting in a uniform electric field. The capacitance being defined as the ratio between the charge magnitude and the potential difference existing between the plates. The addition of a dielectric material between two parallel plates increases the capacitance by a dimensionless factor, ε, or the dielectric constant (see Equation 2.1; Section 2.9).

Electric field lines provide a qualitative description of the electric field. The number of electric field lines is proportional to the magnitude of the charge on the positive electrode and is termed electric flux. The electric field lines for a parallel-plate capacitor reveals that the field is uniform in the central region between the plates, but exhibits distortion at the edges. In the situation where one of the electrodes was a mesh, the electric field lines may not simply run perpendicular to the plates. In a simple model, the lower electrode is an open-weave parallel plate. In this situation, the effect on the electric field would simply be the percentage reduction as a result of the open area. For example, if the applied electric field was 250 V/mm, then the voltage experienced by the test fluid would be approximately 165 V (i.e. 66 % of 250 V/mm). In reality the situation is probably more complex, but can be modelled as a series of parallel plate capacitors representing the wire between the gaps (Figure 6.5).

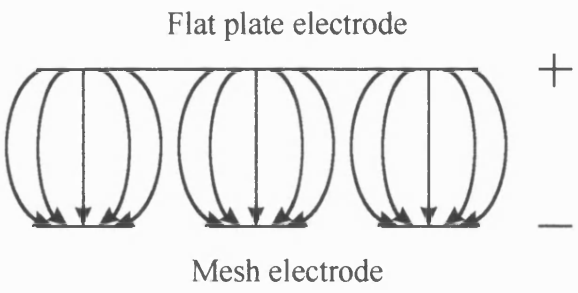

Figure 6.5. Hypothetical electric field lines for a mesh electrode parallel plate capacitor. The diagram is not drawn to scale.

The electric field response was predicted using a finite element modelling scheme (Department of Electrical and Electronic Engineering at the University of Bath). In a simplified 2D model of the electrode design, the lower electrode is represented by an isolated wire of diameter 125 μm (corresponding to a mesh aperture of 180 μm). The predictions were carried out using a hypothetical applied electric field of 500 V/mm and an electrode gap of 1.0 mm. The accuracy of the electric field response could be enhanced by accounting for the dielectric constant of the test material. The dielectric constant was predicted to be 3.54 for a 10.0 % w/w suspension of MCC (sieve fraction below 45 μm) in silicone oil (see Section 2.10). Figure 6.6 illustrates the predicted electric field response around the isolated wire. The voltage is represented using a colour coded scale.

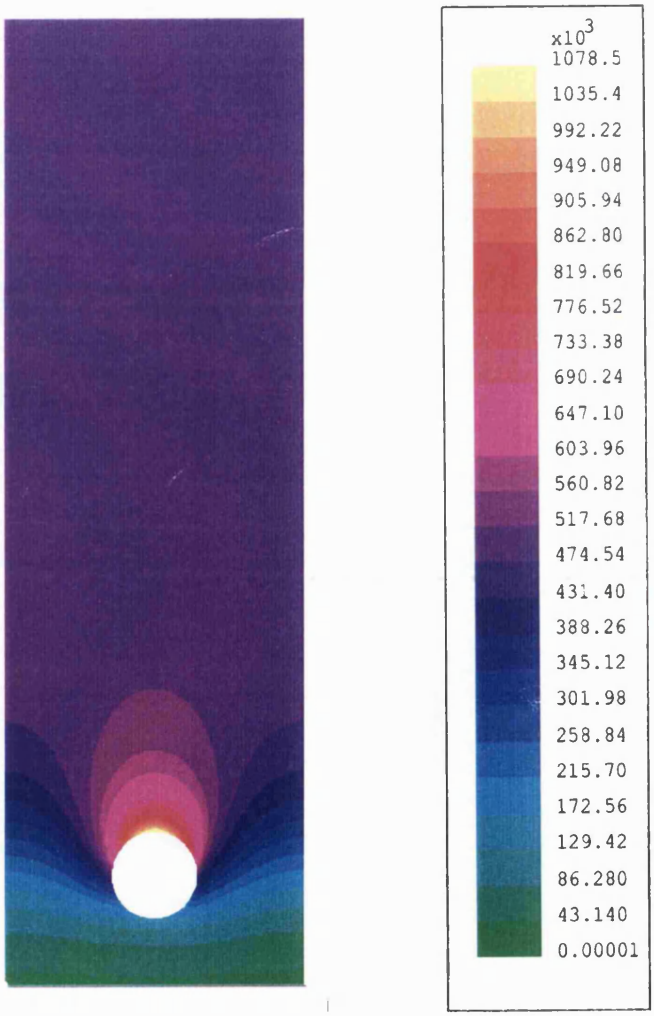

Figure 6.6. Diagrammatic representation of the electric field strength surrounding a wire.

The area immediately below the wire was found to possess a residual voltage in the region of 170 V. At an unknown distance from the underside of the wire, the voltage is zero. The predicted voltage at the wire apex was in the region of 1078 V. The voltage experienced by the wire is more than double the applied electric field.

In Figure 6.7 the arrows are representative of the electric field lines; the number of lines per unit area is proportional to the strength of the electric field in that region. The closeness of the arrows at the wire apex compared to the region at the top of the diagram, is indicative of a region of high voltage.

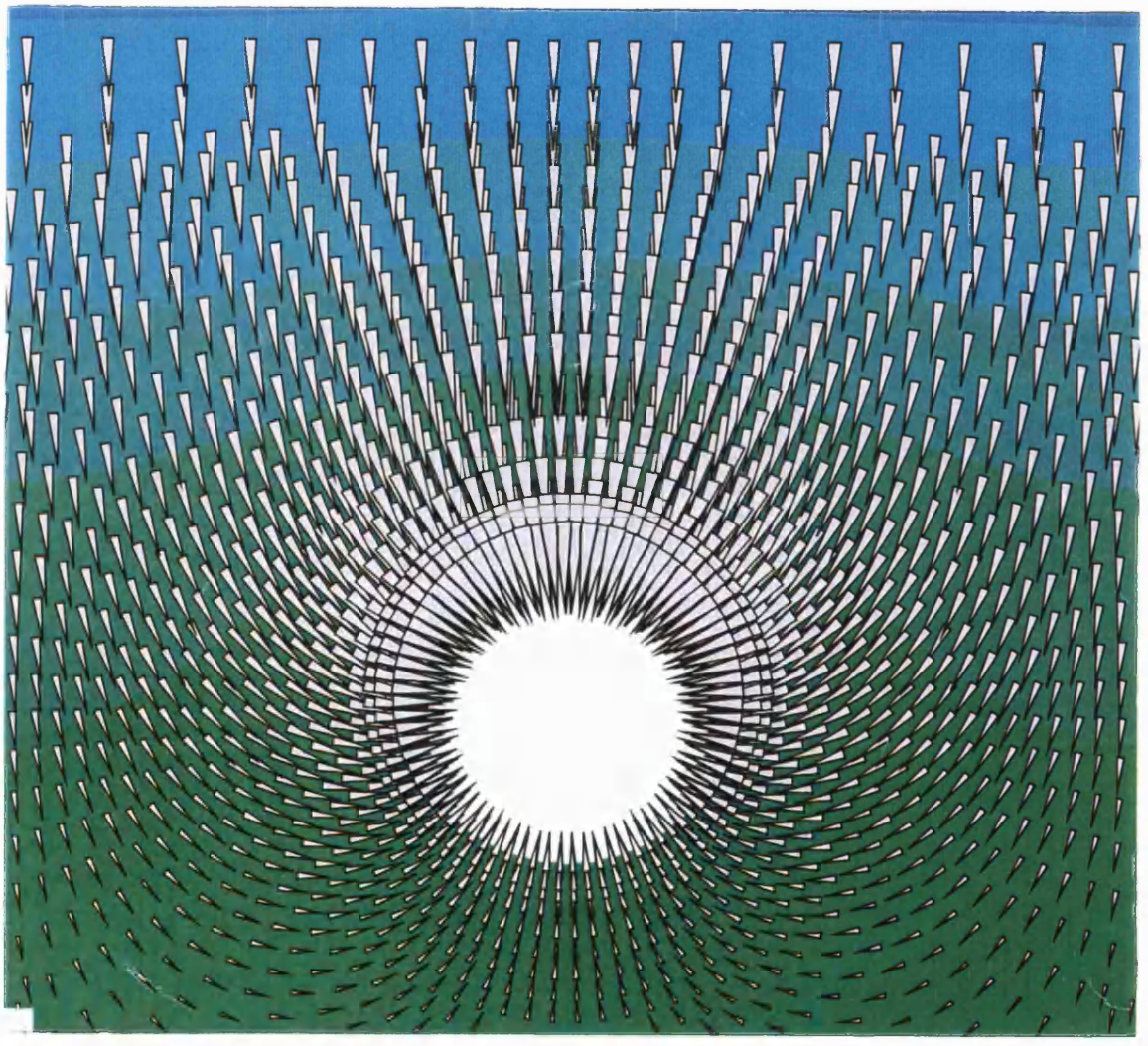

Figure 6.7. Diagrammatic representation of the electric field strength in the immediate vicinity of the wire. The size and frequency of arrows are indicative of the electric field strength.

The 3D representation in Figure 6.8, simulates the wire overlap. The uppermost edge of the wire experiences approximately 1040 V, whilst the underside of the lower wire is at approximately 40 V. As before, at an unknown distance from the lower wire, the voltage was zero. The finite modelling scheme did not predict electric field variations as a result of the wire diameter and dielectric constant modifications discussed above.

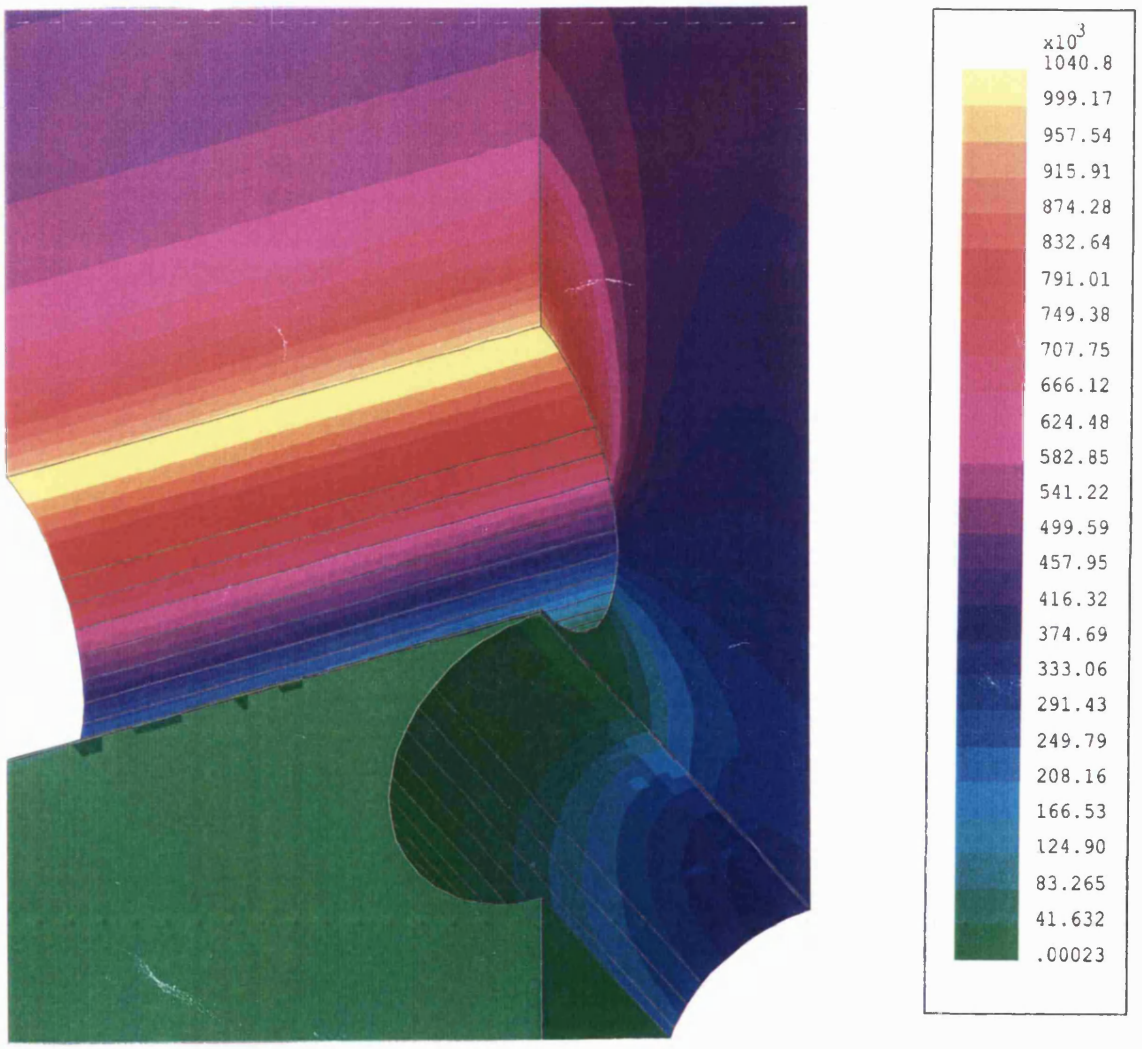

Figure 6.8. 3D representation of the electric field strength around two interwoven wires. A colour scale has been used to represent the voltage

Gauss' flux theorem can be used to predict the voltage experienced by the isolated wire. The electric flux (Φ) is a measure of the number of electric field lines penetrating a plane of area A and can be defined as follows:

$$\Phi = \oint E.dA = \frac{q}{\varepsilon_o} \qquad \text{Equation 6.1}$$

where E is the electric field strength, ε_o is the permittivity of space and q is the charge enclosed by the surface. This equation is a surface integral, which must be evaluated over the hypothetical surface in question. The equation holds true when evaluating the flux through a closed surface, known as the gaussian surface. Gauss' theorem relates the flux through a closed surface to the charge enclosed by the surface. In the context of an isolated wire, Gauss' flux theorem can be used to predict the electric field response, as the system is closed. The simplest gaussian surface, in this situation, is a cylindrical surface of radius r and length *l* (Figure 6.9).

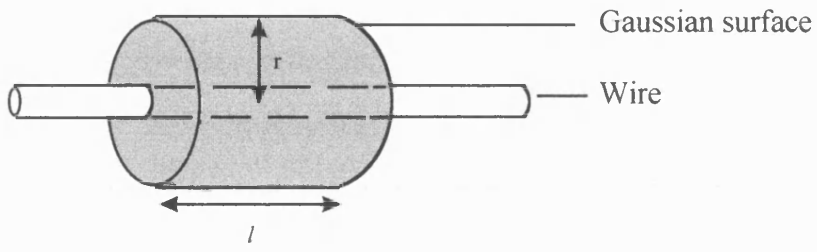

Figure 6.9. Gaussian surface used for the prediction of the electric field response.

The total charge inside the gaussian surface is $l\lambda$, where *l* is the length of the cylinder and λ is the charge per unit length. The electric field strength is constant in magnitude and perpendicular to the wire surface at each point. The electric flux is

predicted using Gauss' law (Equation 6.1), where the area of the surface is $A = 2\pi rl$. Therefore:

$$E = \frac{\lambda}{2\pi \varepsilon_o r} = 2k\frac{\lambda}{r}$$

where k is the Coulomb constant (8.99×10^9 Nm^2/C^2).

This expression for the calculation of the electric field strength holds true for points close to the wire and far from the ends. For a given radius, the electric field doubles. Gauss' flux theorem has successfully predicted the electric field response for an isolated wire. The effect of wire diameter or mesh aperture cannot be predicted using Gauss' flux theorem. The theory, however, cannot be extended to the whole lower electrode, as the surface is not closed. These predictions do, however, yield valuable information on the response of the electric field.

The traditional Franz cell design has been modified with the addition of a glass lip and an electrode assembly, comprising of an interchangeable mesh support. Throughout these studies, three prototype diffusion cells have been used, each building upon the previously exposed design flaws. Prototypes B and C encompassed fluid jackets and enabled UV flow-through detection of tacrine in the receptor compartment. Flow measurements, together with microscopic observations, of ER fluids have provided an insight into the structure formation upon application of an electric field. It is envisaged that this matrix, may hinder or halt the diffusional pathway of tacrine.

6.3. Materials and Methods

Tacrine, MCC (Emcocel 50M) and silicone oil as previously described (Section 2.1). ER fluids were prepared by weighing each component into a single use vial. The vial was sonicated for two periods of 15 min. The suspensions contained approximately 1.50 g of silicone oil.

6.3.1. Release Kinetics of Tacrine from ER fluids with and without the Application of an Electric Field

The development of a yield stress has been shown to provide quantitative information on the strength and to some extent the morphology of chain formation. The particle size, particle concentration and the magnitude of the applied electric field enhanced the development of the yield stress, whilst a decrease in moisture content significantly reduced the Bingham yield stress (Chapter Three). The formation of chain-like structures were observed under the light microscope and the hypothesis proposed that not only the number, but also the chain diameter played a role in the magnitude of the yield stress. Such variations in chain evolution may directly influence the tortuosity of the diffusion pathway, thereby halting or hindering drug release.

In the development of a correlation between the yield stress and the degree of tacrine release, the aforementioned factors were investigated in accordance with Table 6.1. The effect of moisture content was not investigated. The concentration of tacrine in each suspension was 0.5 % w/w. Each experimental factor was assessed with and without the application of an electric field (250 V/mm, unless otherwise stated). In addition, the sieve fraction used was below 45 μm, unless otherwise stated. As previously described (Chapter Three), the number of particles used in the investigation of the effect of particle size was approximately equal for each sieve fraction. The cumulative percentage release over 4 h was determined (n = 5).

Concentration (% w/w)	Size (μm)	Applied electric field (V/mm)
10.0	90 - 125	250
2.5	63 - 75	50

Table 6.1. Variables investigated in the tacrine release from ER fluids.

The possibility of an electrophoretic mechanism governing tacrine release under the application of an electric field was investigated. A 0.5 % w/w suspension of tacrine was prepared and the release profiles assessed over 4 h with and without the application of an electric field (250 V/mm unless otherwise stated). In addition, the polarity of the electrodes were altered.

The assembly and preparatory experimental details for the diffusion cell are described in Chapter Five. All experimental procedures were conducted at 37 °C (± 0.2). The receptor fluid volume was 39.0 ml. In addition, filter paper (Size 1, Whatman, UK) was soaked in distilled water prior to insertion below the mesh electrode. Early experiments in which the distilled water was in direct contact with the lower electrode resulted in a current surge and subsequent electrical breakdown. The possibility of excipient interference was assessed in Chapter Five. From our initial experiments reported above (Chapter Five), the flow-through UV detector was set at a wavelength of 324 nm. Calibration curves utilised in the determination of tacrine concentration in distilled water and propan-2-ol are given in Section 5.5.1 (Figures 5.3 and 5.4 respectively). The single-use vial and the electrode assembly were washed with propan-2-ol (Section 5.4.8).

The current drawn through the device was constantly monitored throughout the experiment. The potential difference across the electrodes was measured upon commencement and cessation of each run (Digital Voltmeter BM8035, Megger AVO International Ltd, Kent, UK).

6.3.2. Flow Behaviour of MCC, Tacrine and Silicone Oil Suspensions using Mesh Electrodes

Pertinent to these studies is the effect mesh electrodes will have on the development of MCC particle chains under the influence of an electric field. Estimation of the electric field response provided no definite figure for the voltage experienced by the test sample. An investigation into the yield stress development in the suspensions assessed in this Chapter has been conducted using mesh electrodes. The influence of a non-uniform electric field on the ER response has not received much attention in the literature. Monkman (1991) attached a layer of cotton to the clutch plate and observed a significant increase in the measured torque under dc fields. Abu-Jdayil and Brunn (1995) coated electrodes with polyvinyl chloride (PVC) foil of low electrical conductivity. In order to produce a non-uniform electric field, a series of holes, approximately 5.0 mm in diameter, were punched in the PVC foil coatings. Depending on the symmetry of the punched holes, the ER effect ranged from negligible, for unsymmetrical aligned holes, to a fraction of the response exhibited by the non-coated electrodes, for symmetrical aligned holes. Otsubo (1997) demonstrated an increase in the yield stress associated with a honeycomb electrode compared to a parallel plate electrode. The ER response exhibited in non-uniform electric fields is, therefore, dependent on the electrode design.

In order to simulate the electrode assembly, an attachment which fitted over the peltier plate was manufactured (TA Instruments, Leatherhead, UK) (see Section 3.3). The plate, of approximately equal dimensions to the diffusion cell (diameter 41.1 mm), was designed to enable the mesh aperture to be changed by unscrewing the sleeve (Figure 6.10). In a manner similar to the diffusion cell design, an (insulating) o-ring was secured to the mesh aperture to aid sample retention.

The temperature of the plate was maintained, through heat conduction, at approximately 37.0 °C (± 1.0) by setting the peltier plate at 55.0 °C. Prior to sample loading, the temperature of the plate was checked and adjusted accordingly. The test fluids were prepared in single use vials in accordance with Table 6.1. In order to avoid potential damage of the upper plate at high shear stress values, the experiments were conducted over the range 0 to 25 Pa at a rate of 0.1 Pa/s. The experiments were conducted in a similar manner to the procedure outlined in Section 3.4. Each experimental variable was assessed five times and the mean Bingham yield stress predicted by extrapolation to the shear-stress axis. The reproduced graphs are plotted using six data points, with error bars representative of the standard deviation (n = 5).

Figure 6.10. Photograph showing the plate used in the assessment of mesh aperture on the electric field and the development of the yield stress.

6.4. Results and Discussion

The total mean recovery for all test fluids was 96.35 % (± 8.69). Generally, the results indicated that tacrine adsorption on to MCC particles was negligible. However, suspensions prepared with the sieve fraction 90 - 125 μm resulted in a lower than expected total recovery of 89.45 % (± 2.36), indicating a degree of tacrine adsorption on to the MCC particles. Our decision not to dry blend the two powder components prior to mixing with silicone oil stemmed from the possibility of tacrine adsorption on to MCC. The total amounts recovered in similar preliminary experiments carried out using dry blended powders (MCC sieve fraction 90 - 125 μm) were significantly lower, with values in the region of 79.56 % (± 6.02). The silicone oil may form a protective barrier surrounding the powder particles thereby minimising adsorption.

6.4.1. Release Kinetics of Tacrine from ER fluids with and without the Application of an Electric Field

The investigation into the release kinetics of tacrine from ER fluids is divided into two sections: a) basal drug delivery in the non-electrified state (0 V/mm) and b) tacrine release under the influence of an applied electric field. The cumulative percentage release values are provided in the tables below (6.4.1b), however, the release profiles and trends in basal drug delivery are now discussed.

a) Basal Drug Delivery

Typically, the response did not follow the zero-order model, as release was not linear with respect to time. It was concluded from the general shape of the profiles that either a first order or a square root of time model could possibly describe the release process. In the previous Chapter, a biphasic release mechanism was proposed and indeed it was likely that basal drug delivery followed a similar pattern. The characteristic initial

burst of release explained by formulation seepage through the mesh aperture. With a subsequent decline in release at long times as a direct result of tacrine diffusion within the formulation.

Basal drug delivery was found to be higher in the current study, an observation explained be the necessity to reduce the amount of water in the diffusion cell. Several modifications were necessary in order to reduce the risk of current surges and subsequent electrical breakdown observed in preliminary experiments conducted under the influence of an electric field. The distilled water level in the receptor compartment was lowered to minimise such risks, but also to prevent electrochemical reactions occurring at the electrodes. A reduction in the receptor fluid volume resulted in enhanced formulation seepage through the mesh electrode, resulting in a higher than predicted cumulative percentage release.

The effect of mesh aperture (45, 90 and 180 μm), at a given concentration (2.5 or 10.0 % w/w), on the cumulative percentage release was statistically assessed using a one-way ANOVA test. In addition, t-tests were carried out to compare the effect of concentration on the cumulative percentage tacrine release through each mesh aperture. The degrees of freedom was 4 (n - 1), resulting in a tabulated t value of 2.776 at the 5 % significance level. The cumulative percentage tacrine release was found to significantly increase ($p < 0.05$) at a given concentration with mesh aperture. The basal drug delivery was found to decrease with MCC concentration (sieve fraction below 45 μm) through mesh apertures of 45 and 90 μm ($t_{critical}$ 0.45 and 0.18 respectively). A possible explanation for this may be the adsorption of tacrine on to MCC particles. The recovery values calculated indicated that in the presence of silicone oil, there is limited and in some cases negligible tacrine adsorption on to MCC. The differences observed may be due to the increase in viscosity associated with an increased concentration, resulting in a reduced leakage of formulation through the mesh aperture. In addition, the diffusional pathway

may be hindered in concentrated suspensions, as the medium viscosity has been shown to influence the diffusion coefficient (D) according to Stokes-Einstein equation (Equation 5.5 pp 181). Values are given in cgs units as the diffusion coefficient is usually defined in cm^2/s. The suspension viscosity and the median equivalent tacrine diameter are reproduced in Table 6.2 (Sections 3.5.1.1 and 2.2 respectively). The calculated diffusion coefficients for tacrine in 2.5 and 10.0 % w/w suspensions of MCC (sieve fraction below 45 μm) are 9.34×10^{-12} cm^2/s and 7.47×10^{-12} cm^2/s respectively. Despite the assumption that tacrine particles are spherical, the calculated diffusion coefficients predict a significant reduction in the diffusion rate of tacrine in the concentrated suspension.

The t-test ($t_{critical}$ - 0.89) revealed no significant difference between the cumulative percentage release of tacrine at an MCC concentration of 2.5 and 10.0 % w/w using the 180 μm mesh aperture. It has been proposed, in this work, that a large aperture minimises vortex movements enabling the free passage of formulation through the opening (see Chapter Five).

Statistical analysis comparing the effects of mesh aperture (one-way ANOVA) and particle size (t-test) were conducted. Basal drug delivery was significantly reduced in suspensions of the sieve fraction 90 - 125 μm compared with the sieve fraction 63 - 75 μm. In comparing the cumulative percentage release using the 180 μm mesh aperture, the total amount delivered reduced from 49.77 % (± 1.91) for the sieve fraction 63 - 75 μm to 3.62 % (± 0.16) for the sieve fraction 90 - 125 μm ($t_{critical}$ 0.08). The median equivalent particle diameter for the sieve fraction 90 - 125 μm was 128.34 μm (± 4.56). The mesh aperture is similar in size to the MCC particles, suggesting a potential for blockage of the mesh opening. In addition, the increase in viscosity associated with suspensions prepared with the 90 - 125 μm sieve fraction may account for the small cumulative percentage release.

The diffusion coefficients calculated using Equation 5.5 are 7.78 $x10^{-12}$ and 2.77 $x10^{-12}$ cm^2/s for suspensions prepared with the sieve fractions 63 - 75 and 90 - 125 μm respectively. Suspension viscosity may not be the only factor affecting tacrine diffusion. Comparison of the cumulative percentage release rates for suspensions composed of 10.0 % w/w MCC (sieve fraction below 45 μm) and the sieve fraction 63 - 75 μm have similar diffusion coefficients, however, the release rates through the 45 and 90 μm mesh apertures are significantly different ($t_{critical}$ 1.56 and 0.99 respectively). Such a discrepancy may provide further evidence for the proposed "mesh blockage" theory. Furthermore, no significant difference ($t_{critical}$ -2.781) in the cumulative percentage release was observed between the aforementioned suspensions through the 180 μm mesh aperture. An anomalous behaviour was observed in the release profile from suspensions containing the sieve fraction 90 - 125 μm through the 90 μm mesh aperture (Figure 6.11). Linear regression analysis of the data indicated a relatively good fit ($r^2 = 0.98946$). However, the release profile would however appear to be biphasic, with a slight inflection at approximately 90 min prior to a surge in release after approximately 140 min. The "mesh blockage" theory holds true in this situation, where the diameter of the MCC particle, in this case, is larger than the mesh aperture. As the release profile exhibits a small initial burst response, we concluded that little formulation seepage has occurred. In this situation, diffusion within the formulation may be the predominant mechanism in tacrine release, resulting in the near zero-order release profile exhibited.

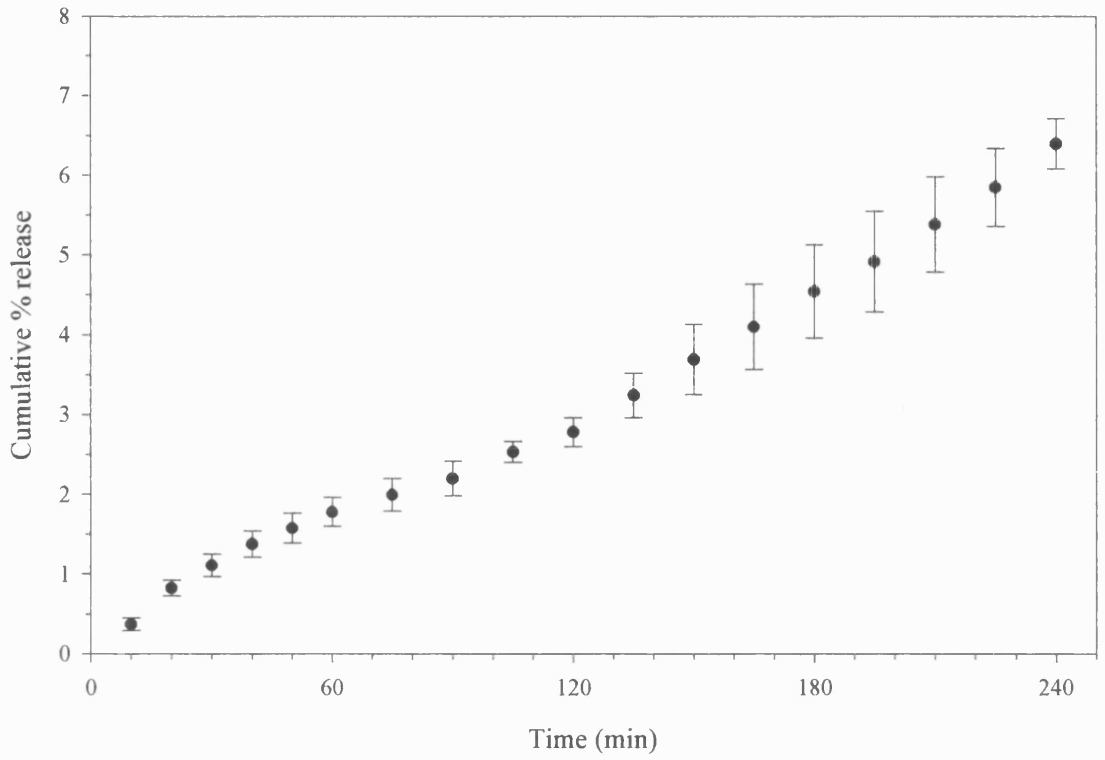

Figure 6.11. The tacrine release profile from a suspension of MCC (sieve fraction 90 - 125 μm) through a 90 μm mesh aperture.

In summary, basal drug delivery was found to be formulation dependent. The suspension viscosity had an effect on the cumulative percentage release of tacrine. In addition, the particle size in conjunction with the mesh aperture was shown to influence the release profile. Two factors affecting the ability of ER fluids to control the release of tacrine have been proposed, namely the formulation viscosity and formulation seepage through the mesh aperture, particularly for low viscosity formulations.

b) Drug release profiles under the influence of an applied electric field

Chain formation under the influence of an applied electric field plays a fundamental role in the controlled release of tacrine from ER fluids. The ability to form and subsequently sustain chains may be fundamental in the control of tacrine release from ER fluids. In Chapter Three, particle size, particle concentration and the magnitude of the applied electric field were shown to influence the strength and possibly the structure of the chains. The validation of the diffusion cell in Chapter Five introduced the possibility of formulation seepage through the mesh aperture. The void space beneath the mesh electrode remained constant irrespective of the mesh utilised, however, the degree of seepage was found to be dependent on the mesh aperture and the formulation viscosity. The reality of formulation seepage is likely to result in a reduction of MCC particles available for chain formation.

Extensive preliminary investigations highlighted the following experimental limitations on the test sample and the diffusion cell assembly requirements:

1) High viscosity suspensions (≥ 20 % w/w) were difficult to load.

2) For reasons of safety, electric fields above 250 V/mm were not used.

3) Experiment duration was reduced to 4 h to minimise current surge and electrical breakdown.

4) Receptor fluid volume was reduced to prevent electrochemical reactions at the electrodes and current surge. The introduction of a filter paper beneath the mesh electrode minimised the void volume.

The power consumption (P) of the ER fluid based drug-delivery devices was calculated from the following relationship: $P = IV$, where I is the current (amperes) and V is the potential difference (volts). It follows from Ohm's law, $V = IR$, that $P = I^2R$ and therefore the power levels are sensitive to the square of the currents employed. Typically, the initial power requirements at constant potential differences of 50 V and 250 V were 0.75 and 3.75 mW respectively (the current drawn through the system is 15 μA). The difference in power requirements for individual formulations was negligible. The current was observed to increase steadily over the duration of the experiments resulting in a maximum power consumption of 2.75 mW and 13.75 mW for constant potential differences of 50 V and 250 V respectively. The increased current requirements may result from particle chain rearrangement during the experiment.

Depending on the battery composition, the operating voltage of implantable drug-delivery devices and pacemaker batteries is in the region of 3.0 V, with a current demand in the milliampere (mA) range. The power requirements for these batteries (i.e. implantable drug-delivery devices and pacemakers) are in the mW range. Although calculated power requirements are within the range of commercially available battery systems, currently these batteries do not address the voltage requirements of our ER fluid based drug-delivery device even when operating at its lowest voltage (50 V/mm). They certainly cannot supply the potential difference for more traditional ER fluids used e.g. in clutches (5 kV/mm) where a typical electrode gap is in excess of 10 mm. However, the current drawn through our ER fluid based drug-delivery system is 1000-times lower than the equivalent current requirements in the aforementioned implantable batteries.

A table summarising the median equivalent volume particle diameters and suspension viscosity for the samples is given below (Table 6.2). The mesh apertures chosen for this study were woven using different wire diameters. The wire diameters are 32, 63 and 125 μm for mesh apertures of 45, 90 and 180 μm respectively.

Formulation	Median equivalent particle diameter (μm)	Newtonian viscosity (Pa s)
2.5 % w/w	32.99 (0.83)	0.0889 (0.0021)
10.0 % w/w	32.99 (0.83)	0.1112 (0.0007)
63 - 75 μm	90.12 (1.23)	0.1067 (0.0021)
90 - 125 μm	128.34 (4.56)	0.2996 (0.0087)

Table 6.2. Summary table showing the median equivalent particle diameters (s.d.) and Newtonian viscosities (s.d.) of the test suspensions. Methods of determination are given in Chapters Two and Three respectively.

The following section of work is constructed to enable the development of a theory for the controlled release of tacrine from ER fluids. For clarity, the number of data points plotted has been reduced as described in Section 5.5.7. In all cases, errors bars represent the standard deviation (n = 5). Throughout, data points representing basal (0 V/mm) tacrine release are black (filled symbols), whilst data points representing the response under an applied electric field are white (open symbols).

i) Particle Concentration

Table 6.3 shows the cumulative percentage release after 4 h of tacrine from MCC suspensions (sieve fraction below 45 μm) of different concentrations. Figure 6.12 depicts the release profiles over 4 h, with and without the application of an electric field, through mesh apertures of 45 and 90 μm respectively. The release profiles from MCC suspensions of 2.5 and 10.0 % w/w through mesh apertures of 90 μm (6.13a) and 180 μm are shown in Figure 6.13. Figures 6.13b and 6.13c represent the release rates at MCC concentrations of 2.5 % and 10.0 % w/w respectively.

Mesh aperture	Cumulative % release after 4 h (Standard deviation)			
	2.5 % w/w		10.0 % w/w	
	0 V/mm	250 V/mm	0 V/mm	250 V/mm
45 µm	24.00 (1.04)	25.49 (1.45)	8.21 (1.49)	9.15 (0.62)
90 µm	36.94 (2.30)	35.38 (1.72)	21.41 (0.88)	18.20 (0.77)
180 µm	49.07 (1.96)	48.65 (0.98)	53.18 (1.08)	49.24 (0.94)

Table 6.3. The effect of particle concentration (sieve fraction below 45 µm) on the cumulative percentage release after 4 h through mesh apertures of 45, 90 and 180 µm with and without the application of an electric field (250 V/mm).

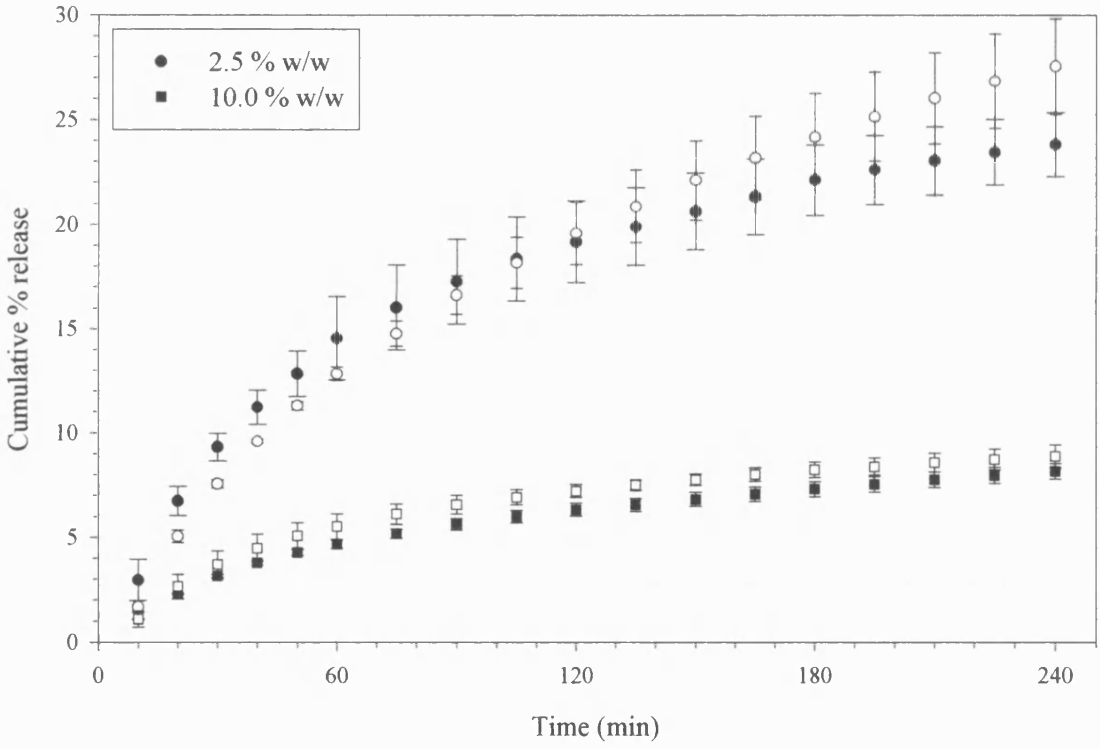

Figure 6.12. Release profiles from MCC suspensions of 2.5 and 10.0 % w/w (sieve fraction below 45 µm) in 100 cSt silicone oil through a 45 µm mesh aperture. Open symbols represent basal drug delivery. Closed symbols represent drug delivery under the influence of an electric field.

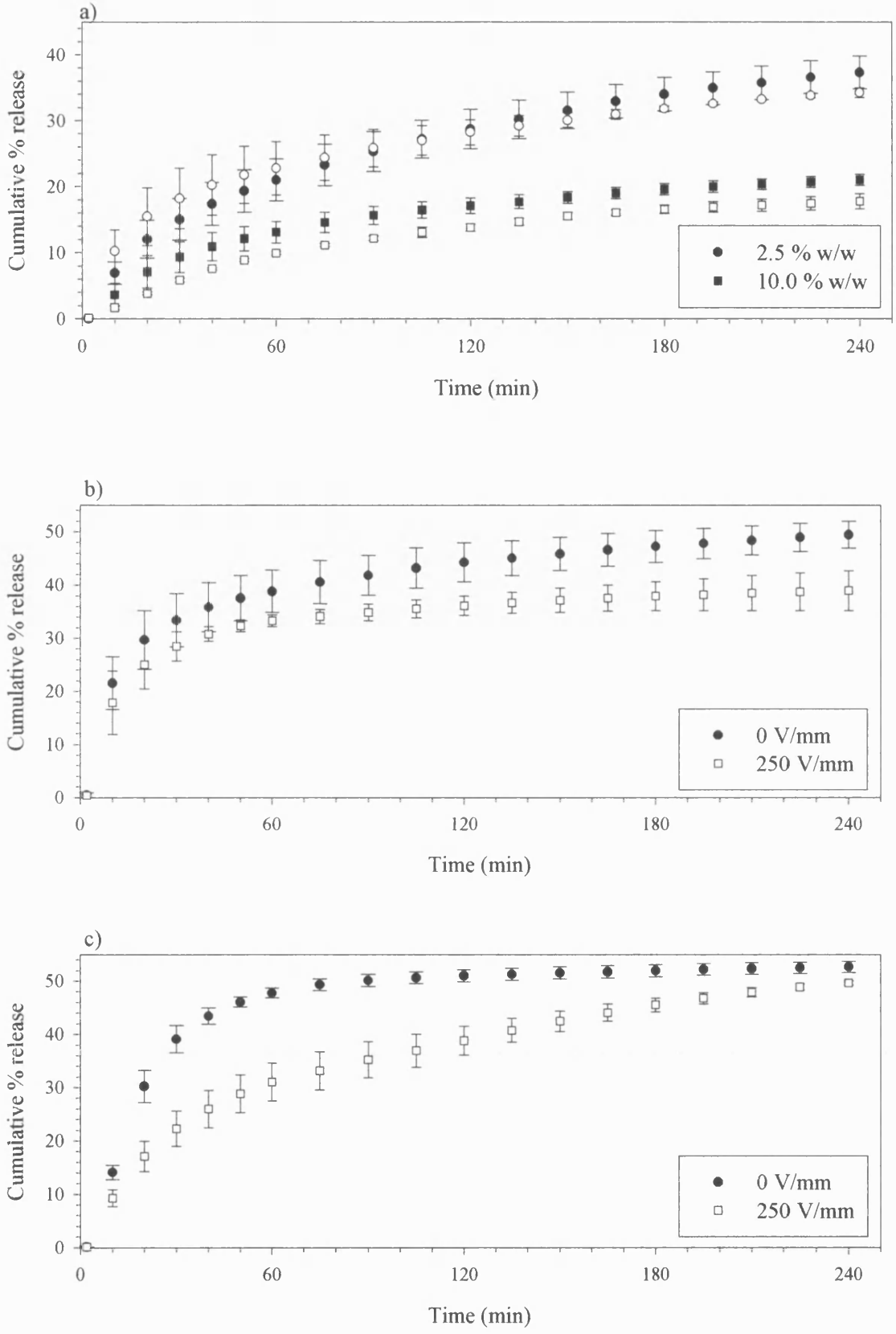

Figure 6.13 (a-c). Release profiles from suspensions of 2.5 and 10.0 % w/w MCC (sieve fraction below 45 μm) in 100 cSt silicone oil through a mesh aperture of 90 (a) μm and 180 μm (b 2.5 % w/w; c 10.0 % w/w) respectively.

The existence of a linear relationship between the yield stress and concentration (cf. Table 3.11 pp. 94), predicts a four-fold increase in the number of particle chains in a 10.0 % w/w suspension compared to a 2.5 % w/w suspension. According to the hypothesis, the basal delivery rate from the 10.0 % w/w suspension is more likely to be reduced upon application of an electric field. The effect of mesh aperture on the degree of particle-chain development can be estimated from the Bingham yield stress values (Figure 6.14). For each of the test formulations, mesh aperture was found to significantly reduce the Bingham yield stress, compared to parallel-plate measurements (Chapter Three). Paired Student's t-tests were conducted on the cumulative percentage release rates with and without the application of an electric field . The degrees of freedom was 4 (n - 1) resulting in a tabulated t value of 2.776 at the 5 % significance level.

For each of the mesh apertures (45, 90 and 180 μm), tacrine release from a 2.5 % w/w suspension remained unchanged upon application of the electric field ($t_{critical}$ - 1.51, 1.00 and 1.18 respectively). The Bingham yield stress values for each of the mesh apertures (45, 90 and 180 μm) were 0.0881 Pa s (± 0.0129), 0.0799 Pa s (± 0.0102) and 0.0890 Pa s (± 0.0268) respectively (Figure 6.14). The incomplete particle-chain formation predicted by the small yield stress values is unlikely hinder the diffusional pathway of tacrine within the formulation (i.e. at long times).

The cumulative percentage release from a 10.0 % w/w suspension of MCC (sieve fraction below 45 μm) significantly decreased under the influence of an electric field for mesh apertures of 90 and 180 μm ($t_{critical}$ 12.06 and 4.73 respectively). However, there was no significant difference between release rates through the 45 μm mesh aperture from the 10.0 % w/w suspension in the non-electrified and electrified states ($t_{critical}$ - 1.56). The predicted Bingham yield stresses for mesh apertures of 45, 90 and 180 μm (Figure 6.14) are 0.0904 Pa s (± 0.0301) 0.5923 (± 0.0817) and 1.0092 (± 0.1296) respectively. The inability of MCC to structure effectively, despite the suspension concentration, on the

45 μm mesh aperture is apparent from the yield stress value. The introduction of a second variable, the wire diameter, was required to provide a possible explanation for this anomalous behaviour. The wire diameter being approximately equal to the median equivalent particle diameter (Table 6.1) may be unable to support the formation of MCC particle chains.

The apparent viscosity is known to increase upon application of an electric field (Winslow, 1949; Block and Kelly, 1988). The apparent viscosities under low shear stresses were 19.6 (± 2.3) and 84.5 Pa s (± 5.9) for suspensions of 2.5 and 10.0 % w/w respectively. These values are approximate, as the rheometer was unable to resolve the viscosity at such low shear stress values. However, the calculated diffusion coefficients (Equation 5.5) for suspensions of 2.5 and 10.0 % w/w under the influence of an electric field are 4.24×10^{-14} cm/s and 9.83×10^{-15} cm/s. In comparison to the basal diffusion rate, the Stokes-Einstein equation predicted a decrease in the diffusion rate upon application of the electric field. As discussed above, the possibility of incomplete or negligible structure formation at low concentration and associated with the narrow diameter wire mesh is not addressed in these calculations.

In general, these findings are consistent with the proposed hypothesis of tacrine entrapment within MCC particle chains. Although, the possibility of chain development cannot be ruled out, it is unlikely that the degree of chain formation is able to hinder tacrine release from the 2.5 % w/w suspension. Basal tacrine delivery from 10.0 % w/w MCC suspensions was significantly reduced through the 90 and 180 μm mesh apertures. This reduction in cumulative percentage release could be explained by the high particle density, possibly as a result of low formulation seepage, producing chain-like structures capable of tacrine entrapment upon application of the electric field. Although, the open area is the same for each mesh cloth, the wire diameter varies and may influence the ability of ER fluids to form chains.

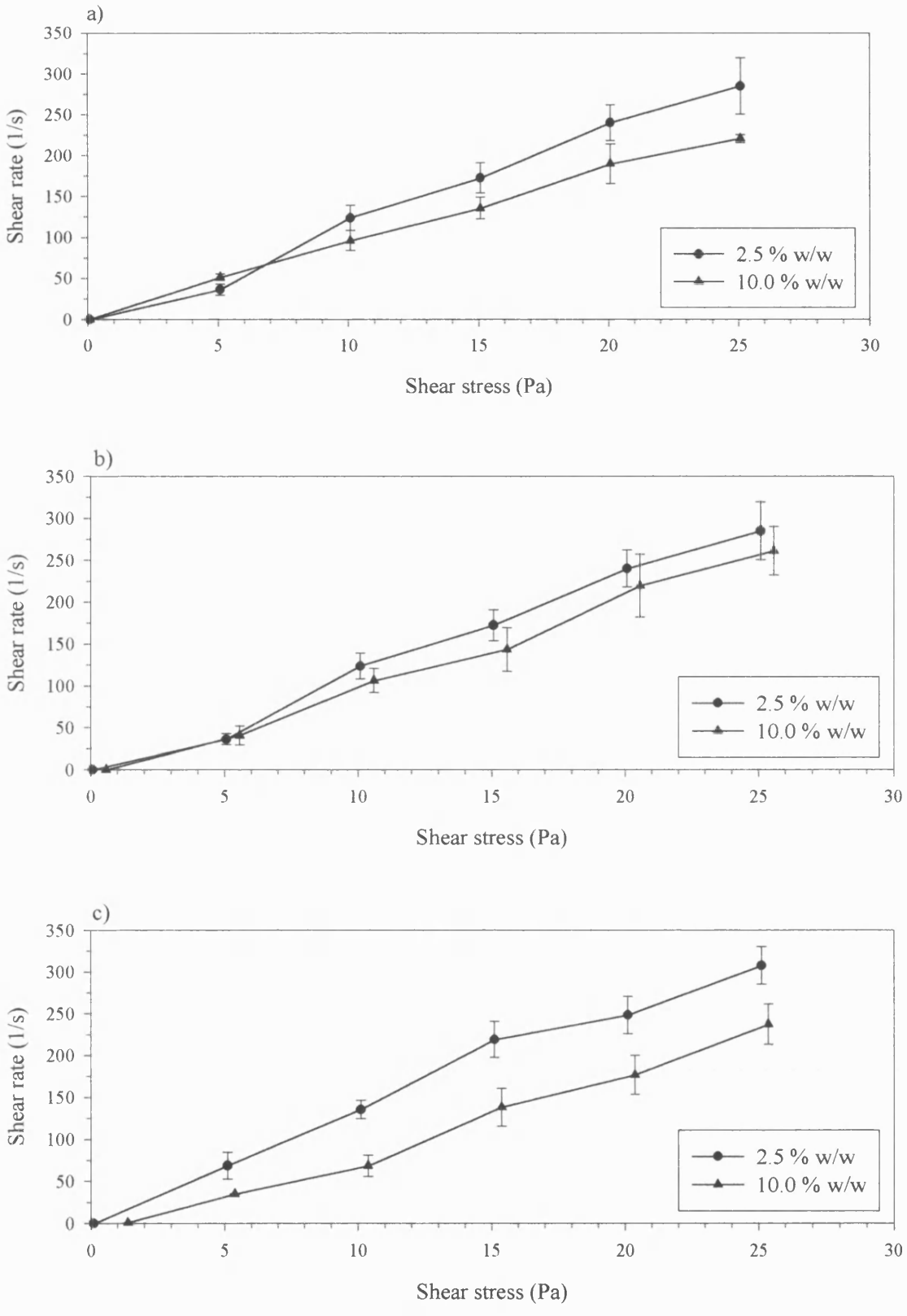

Figure 6.14. The effect of MCC (sieve fraction below 45 μm) concentration on the development of the Bingham yield stress using mesh apertures of 45 (a), 90 (b) and 180 (c) μm. The applied electric field was 250 V/mm.

ii) Particle Size

Table 6.4 shows the effect of mesh aperture on the cumulative percentage release for the sieve fractions 63 - 75 and 90 - 125 μm. Figure 6.15 illustrates the tacrine release profiles from suspensions containing MCC particles of the sieve fraction 63 - 75 μm using mesh apertures of 45 and 90 μm (a) and 180 μm (b).

Mesh aperture	Cumulative % release after 4 hours (Standard deviation)			
	Sieve fraction 63 - 75 μm		Sieve fraction 90 - 125 μm	
	0 V/mm	250 V/mm	0 V/mm	250 V/mm
45 μm	13.39 (1.12)	12.19 (0.94)	2.98 (0.11)	1.60 (0.20)
90 μm	20.60 (0.73)	16.80 (1.53)	6.39 (0.32)	0.14 (0.00)
180 μm	49.77 (1.91)	31.13 (3.13)	3.62 (0.16)	2.45 (0.31)

Table 6.4. The effect of particle size on the cumulative percentage release after 4 h through mesh apertures of 45, 90 and 180 μm with and without the application of an electric field (250 V/mm).

Paired t-tests were conducted on cumulative percentage release data with and without the application of an electric field for the sieve fraction 63 - 75 μm. There was no significant difference ($t_{critical}$ 1.54) observed in the cumulative percentage release through the 45 μm mesh aperture. However, significant differences ($t_{critical}$ 8.39 and 12.65 respectively) were observed for the mesh apertures 90 and 180 μm.

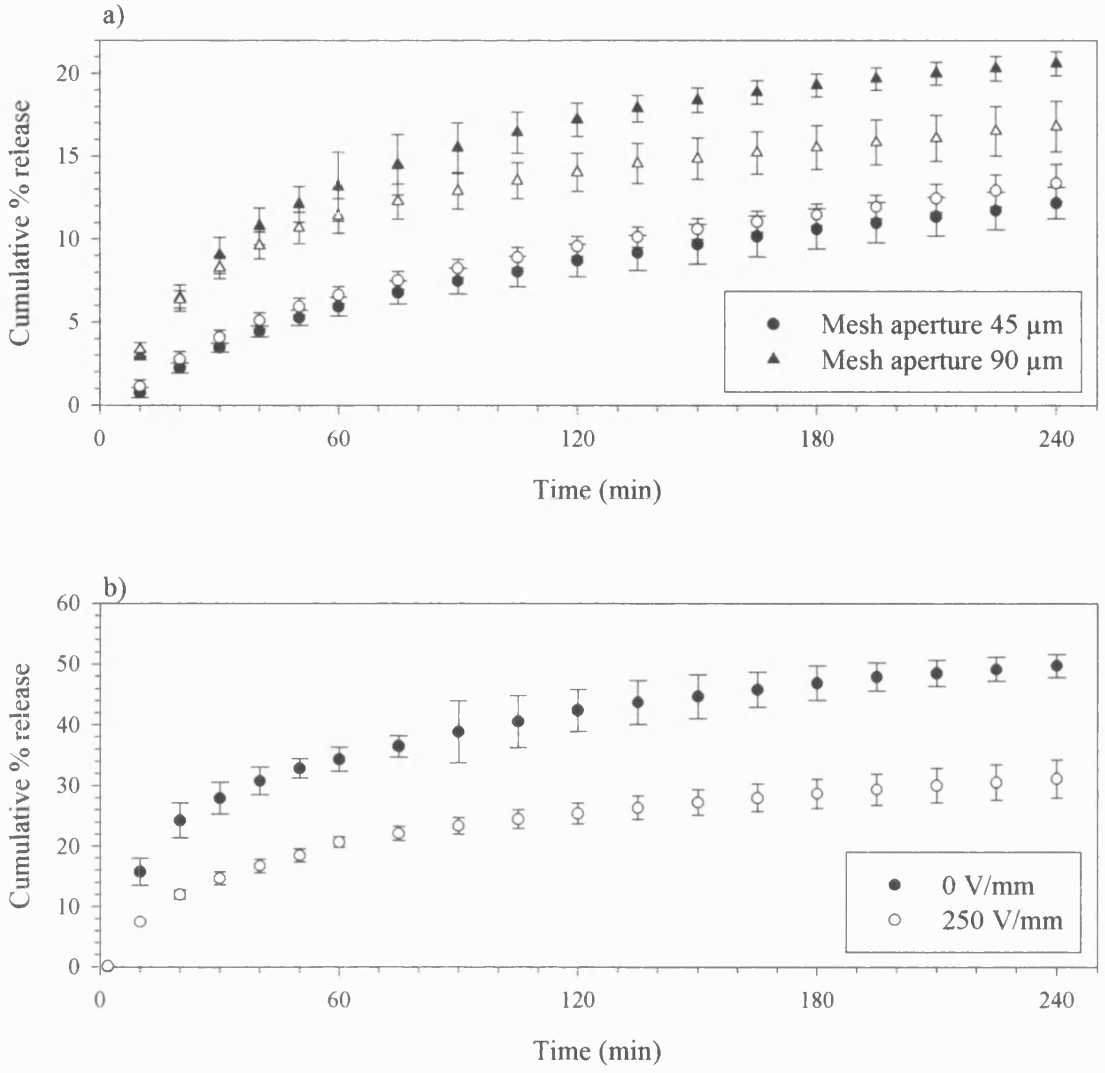

Figure 6.15. Release profiles from suspensions prepared with the sieve fraction 63 - 75 µm in 100 cSt silicone oil with (250 V/mm) and without the application of an electric field through mesh apertures of 45 (a), 90 (a) and 180 (b) µm.

The proposed hypothesis predicts that suspensions prepared with the sieve fraction 63 - 75 µm, with a predicted Bingham yield stress of 0.1067 Pa s (± 0.0021) (Table 6.2), would hinder the release of tacrine upon application of the electric field. These findings from the cumulative percentage release through the mesh apertures 90 and 180 µm have provided evidence in support of the proposed hypothesis. The predicted yield stress values on mesh apertures of 90 and 180 µm are 0.7128 Pa s (± 0.1092) and 1.0499 Pa s (± 0.1325) respectively. The anomalous behaviour exhibited using the 45 µm mesh aperture

would indicate that the diameter of the wire may play a role in the development of particle chains on mesh cloths.

Figure 6.16 illustrates the release profile exhibited in MCC suspensions (sieve fraction 90 - 125 μm) through mesh apertures of 45, 90 and 180 μm with and without the application of an electric field. The cumulative percentage release values for MCC suspensions (sieve fraction 90 - 125 μm) for all mesh apertures are provided in Table 6.4 above.

Basal drug delivery was significantly reduced ($t_{critical}$ 5.48) through the 180 μm mesh aperture upon application of an electric field. The release profile was similar in shape to those previously described. The Bingham yield stress for this mesh aperture is 1.4092 Pa s (± 0.1325) (Figure 6.17c) and is indicative of a highly structured system, comprising of complete particle chains spanning the electrode gap. The chain diameter in such formulations will be high, possibly resulting in little or no inter-chain voids. This may provide an explanation for the decrease in basal drug delivery observed. In addition, the viscosity of the formulation is high, therefore, resulting in low formulation seepage through the mesh electrodes.

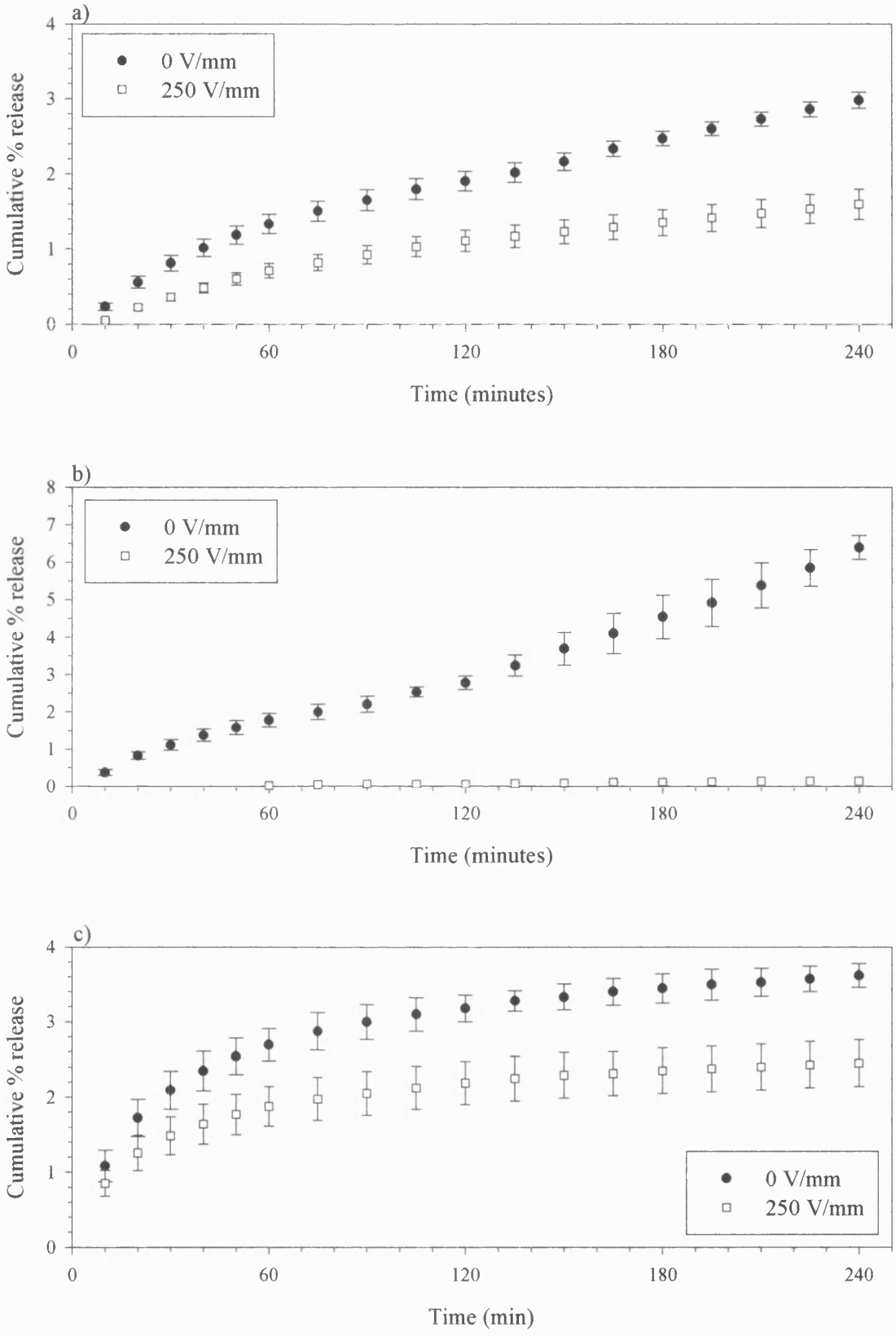

Figure 6.16 (a-c). Release profiles through the 45 (a), 90 (b) and 180 (c) μm mesh apertures of MCC suspensions (sieve fraction 90 - 125 μm) with (250 V/mm) and without the application of an electric field.

Significant differences in the cumulative percentage release over 4 h were observed through the 45 and 90 μm mesh apertures. An anomalous pattern of behaviour was described for the release through these mesh apertures without the application of an electric field. In these circumstances, formulation seepage may be completely prohibited by the inability of MCC particles to transverse the mesh, resulting in diffusion predominating the release mechanism. Assessment of the release profiles with and without the application of an electric field through the 45 μm mesh aperture revealed a significant decrease in the cumulative percentage release values. Previously, the inability of the 45 μm mesh aperture to support chain formation has been proposed and indeed equally applies in this situation. The viscosity of the suspensions may result in little or no formulation loss through the small mesh opening, thereby resulting in a high MCC particle concentration. The Bingham yield stress, under these experimental conditions, was 1.1926 Pa s (± 0.1123) (Figure 6.17a).

Formulations prepared with the sieve fraction 90 - 125 μm and the release assessed through the 90 μm mesh aperture resulted in an almost complete cessation of tacrine release throughout the 4 h period. Previously, we concluded that the basal drug delivery followed approximately zero order release kinetics. Furthermore, there was little or no formulation seepage detected. Under these experimental conditions, MCC particles are likely to structure (i.e. the possibility of at least partial chain formation as evidenced by the development of a yield stress) upon application of the electric field, as the Bingham yield stress value of 2.8954 Pa s (± 0.6129) demonstrated (Figure 6.17b). This combination of mesh aperture and formulation provided optimum conditions for the cessation of tacrine release under an applied electric field.

Figure 6.17 shows the rheological behaviour of tacrine suspensions with MCC of sieve fractions 63 - 75 and 90 - 125 μm using mesh apertures of 45, 90 and 180 μm.

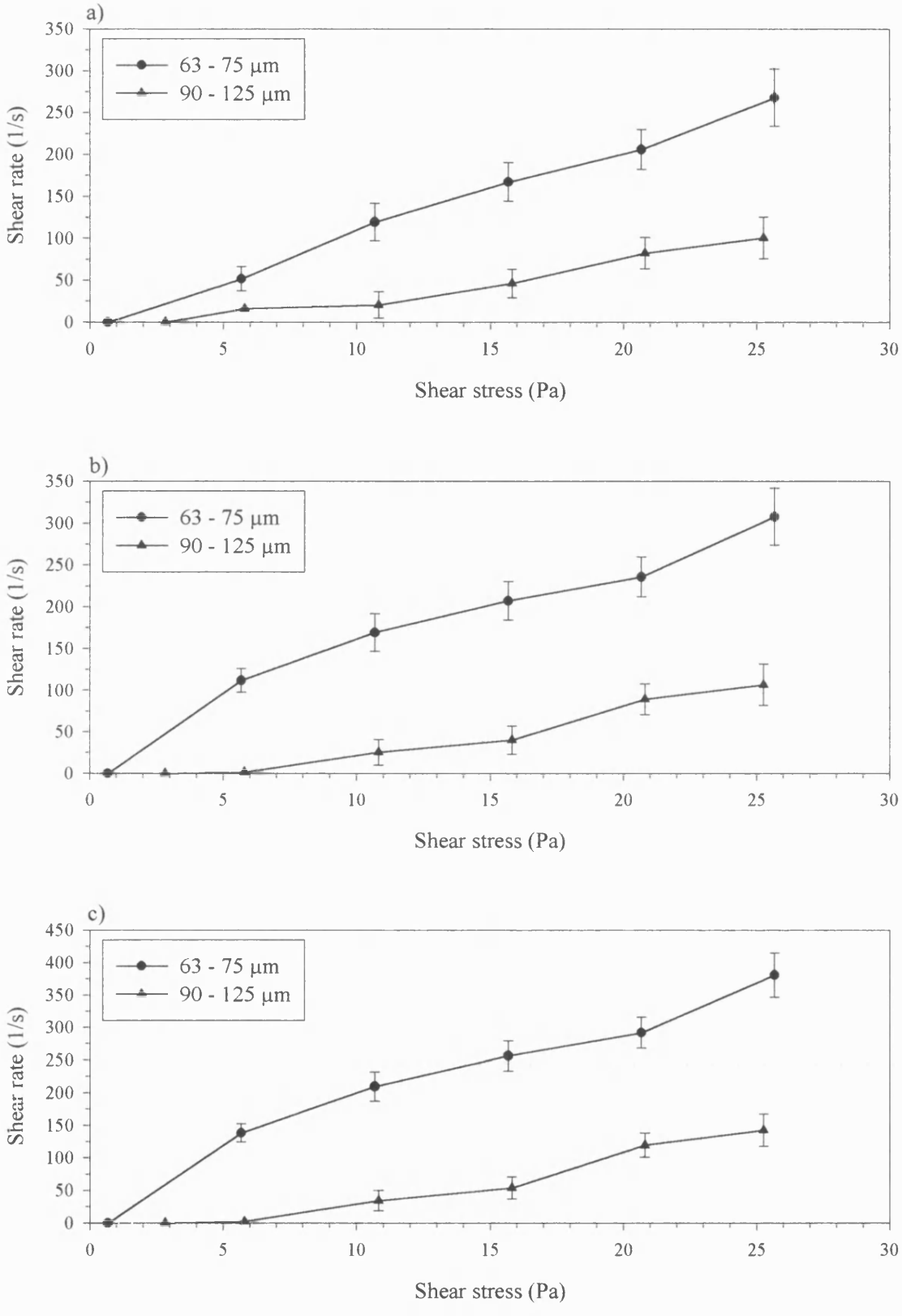

Figure 6.17. The effect of MCC particle size on the development of the Bingham yield stress using mesh apertures of 45 (a), 90 (b)and 180 (c) µm. The applied electric field was 250 V/mm. The suspensions contained approximately equal number of particles.

iii) Applied electric field

The cumulative percentage releases, with and without the application of an electric field (50 V/mm), through mesh apertures of 45, 90 and 180 μm are shown in Table 6.5. Figure 6.18 shows the release profile from a 10.0 % w/w MCC suspension (sieve fraction below 45 μm) through mesh apertures of 45, 90 and 180 μm with (50 V/mm) and without the application of an electric field.

Mesh aperture	Cumulative % release after 4 h (Standard deviation)	
	0 V/mm	50 V/mm
45 μm	8.21 (1.49)	8.49 (0.59)
90 μm	21.41 (0.88)	17.87 (2.08)
180 μm	53.18 (1.08)	52.97 (0.38)

Table 6.5. Cumulative percentage release after 4 h from a 10.0 % w/w MCC (sieve fraction below 45 μm) suspensions in 100 cSt silicone oil with and without the application of an electric field (50 V/mm) using mesh apertures of 45, 90 and 180 μm.

The effect of mesh aperture (45, 90 and 180 μm) on the cumulative percentage release under an applied electric field of 50 V/mm was statistically assessed using a one-way ANOVA test. In addition, t-tests were carried out to compare the effect of application of an electric field (50 V/mm) on the cumulative percentage tacrine release through each mesh aperture. The degrees of freedom was 4 (n - 1), resulting in a tabulated t value of 2.776 at the 5 % significance level. There was no significant difference between the cumulative percentage release values through each mesh aperture with and without the application of an electric field (50 V/mm). At the 99 % significance level, cumulative percentage release through the 90 μm mesh aperture was found to decrease significantly.

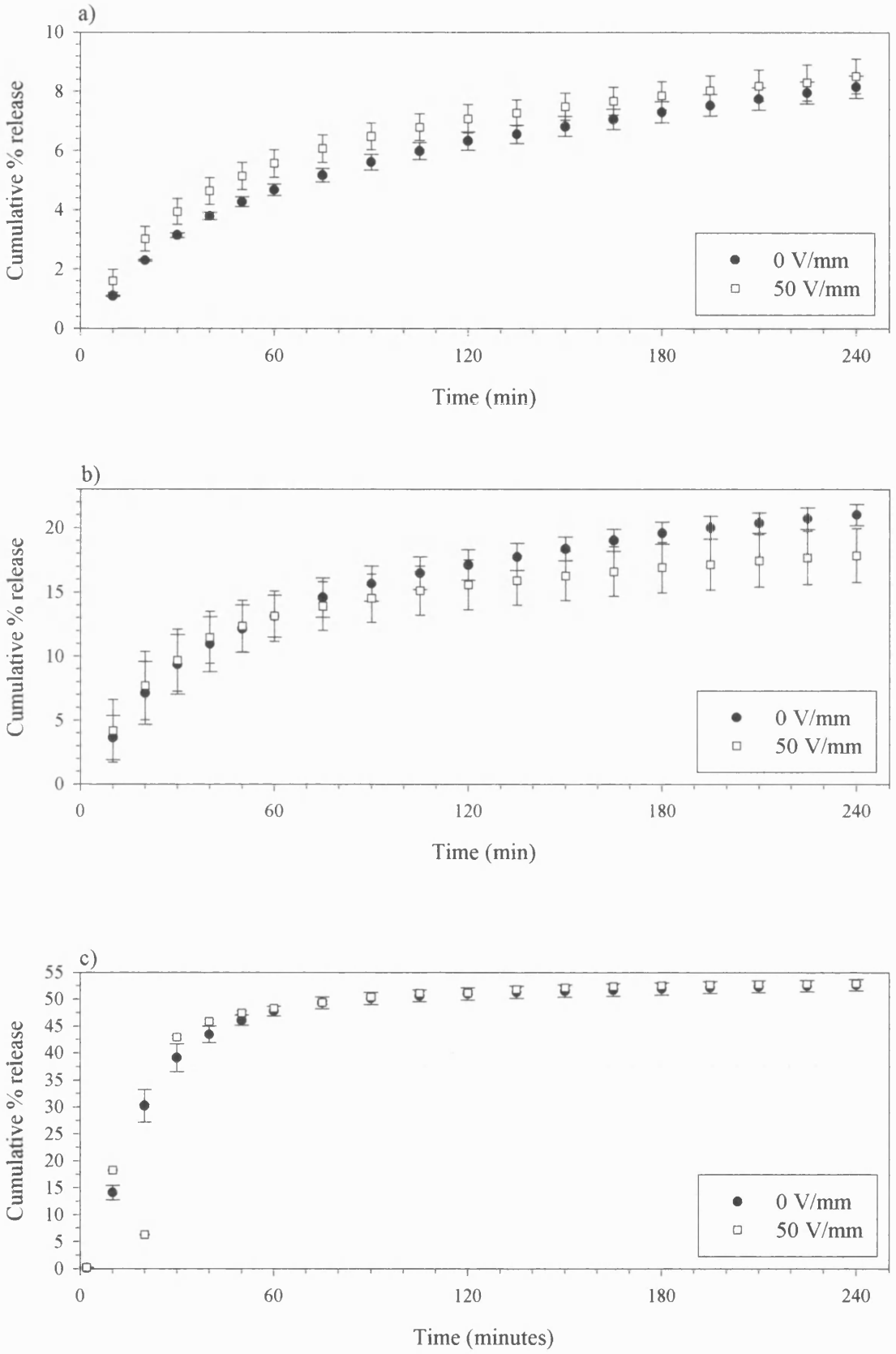

Figure 6.18. Release profiles exhibited by a 10.0 % w/w MCC (sieve fraction below 45 µm) suspension in 100 cSt silicone oil with (50 V/mm) and without the application of an electric field using mesh apertures of 45 (a), 90 (b) and 180 (c) µm.

The Bingham yield stress values for each of the mesh apertures (45, 90 and 180 μm) were 0.0845 Pa s (± 0.0101), 0.1012 Pa s (± 0.0864) and 0.0954 Pa s (± 0.0099) respectively. Figure 6.19 shows the rheological properties at 50 V/mm.

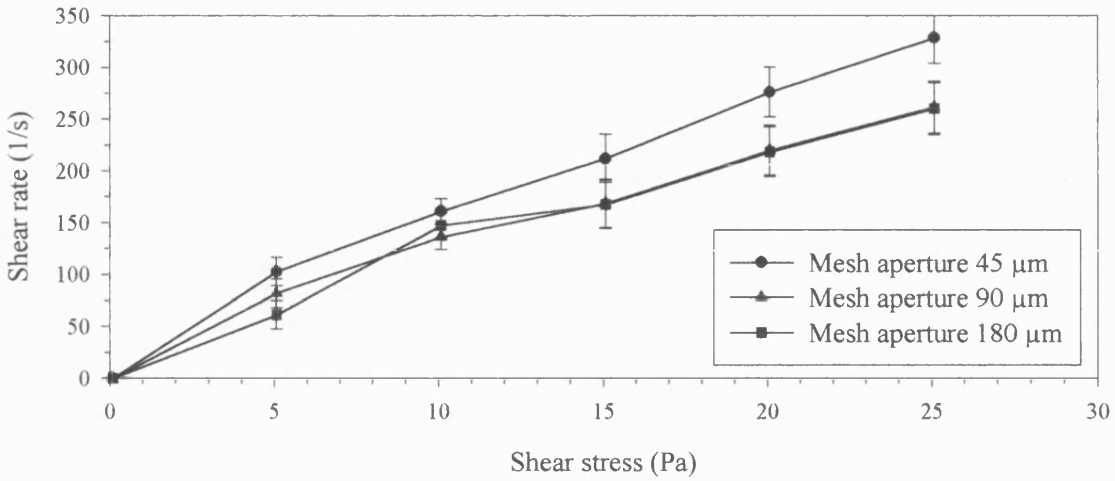

Figure 6.19. Rheological behaviour of a 10.0 % w/w suspensions of MCC (sieve fraction below 45 μm) at an applied electric field of 50 V/mm using mesh apertures of 45, 90 and 180 μm.

iv) Electrophoretic Effect

The proposed chain formation hypothesis does not account for the possibility of electrophoresis under the influence of an applied electric field. Indeed, the mechanism of hindered tacrine release under the influence of an electric field may be as a direct result of electrophoresis. An investigation into the possibility of electrophoresis has been conducted using suspensions of 0.5 % w/w tacrine in 100 cSt silicone oil. The cumulative percentage tacrine release from 100 cSt silicone oil after 4 h through mesh apertures of 45, 90 and 180 μm is shown in Table 6.6 and Figure 6.20. The polarity of the upper electrode was reversed (i.e. negative polarity) and the cumulative percentage release measured. This is denoted in Table 6.6 and in Figure 6.20 as (-).

Mesh aperture	Cumulative % release after 4 hours (Standard deviation)		
	0 V/mm	250 V/mm (+)	250 V/mm (-)
45 μm	19.12 (1.56)	22.12 (2.30)	24.50 (1.19)
90 μm	34.35 (2.15)	30.62 (2.84)	30.52 (2.36)
180 μm	38.79 (1.24)	35.01 (1.25)	37.25 (1.25)

Table 6.6. Cumulative percentage release through mesh apertures of 45, 90 and 180 μm from a 0.5 % w/w tacrine suspensions in 100 cSt silicone oil with and without the application of an electric field (250 V/mm). In addition, the effect of polarity on the cumulative percentage release is shown.

A one-way ANOVA test was carried out to determine the existence of statistical difference between the cumulative percentage release rates with and without the application of an electric field. There was no significant difference observed at the 95 % confidence level, however a significant difference was observed for all mesh apertures at the 99 % confidence level.

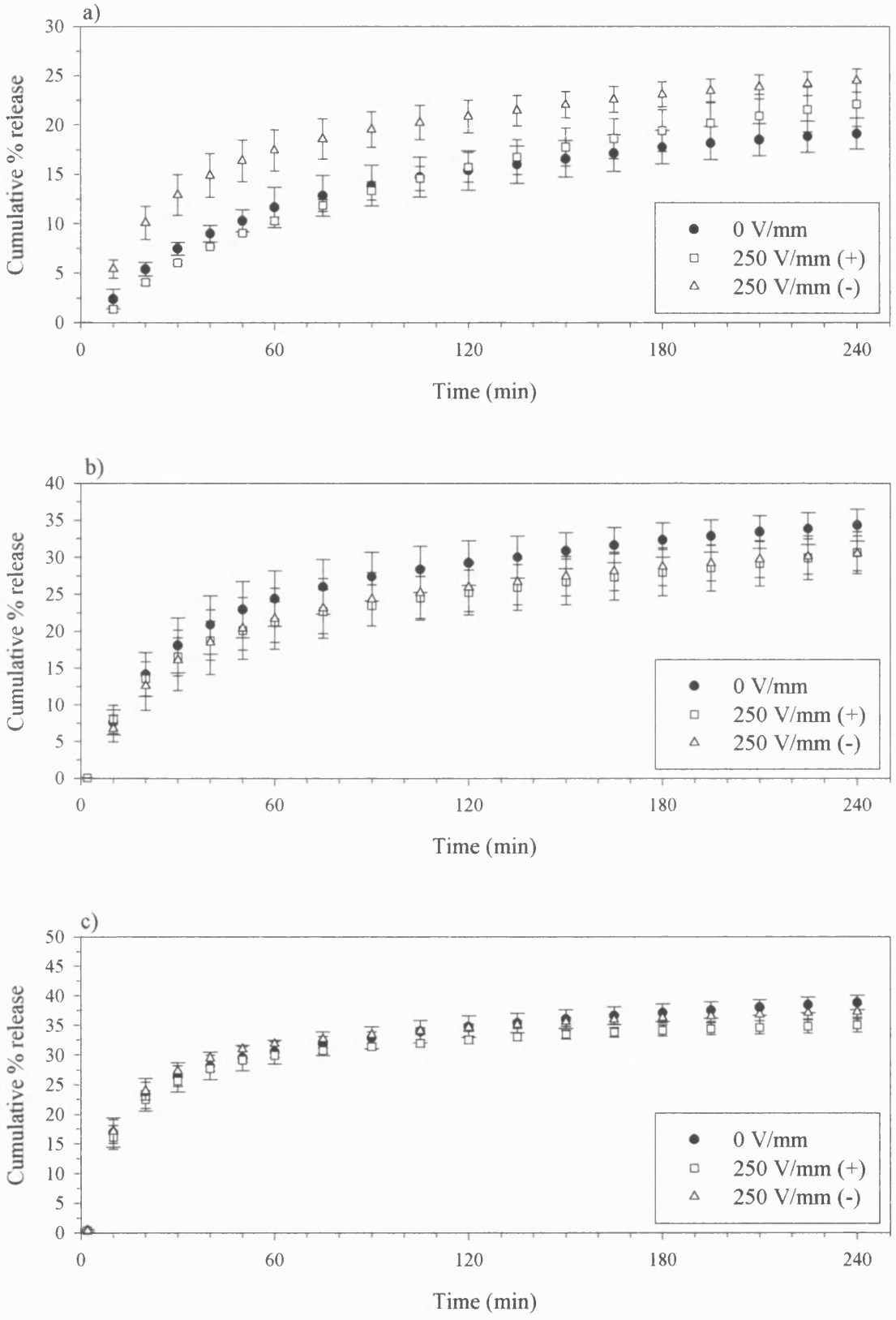

Figure 6.20 (a-c). Release profiles exhibited by a 0.5 % w/w tacrine suspension in 100 cSt silicone oil with (250 V/mm) and without the application of an electric field using mesh apertures of 45 (a), 90 (b) and 180 (c) µm respectively.

The possibility of electrophoresis cannot be discounted as a factor influencing the reduction in tacrine release observed under the influence of an electric field. Fluorescence microscopy was conducted in ER fluids prepared with tacrine and MCC particles (sieve fraction below 45 μm) in an attempt to map the movement of tacrine particles under the influence of an electric field. The movement of tacrine was observed to follow the chain formation patterns described in Chapter Two. The evidence was inconclusive as the intense fluorescence nature of tacrine resulted in single MCC particles being indistinguishable.

6.5. Conclusions

Gauss' flux theorem enabled the prediction of the electric field response for an isolated wire. A prediction of the electric field response for the mesh as a whole was not carried out due to the complexity of the calculations. In order to address the possibility of alteration of the chain formation patterns described in Chapter Three, the Bingham yield stress values were calculated using a specially designed lower electrode enabling the interchange of mesh apertures. The release profiles were determined for a range of formulations with and without the application of an electric field. In addition, the formulation properties may affect the chain formation.

In the absence of an electric field, a basal level of drug release will occur which may be modulated in a controllable manner by altering the magnitude of the electric field. Furthermore, the degree of modulation may be altered by the initial choice of formulation. Basal drug delivery was found to follow a similar pattern to the biphasic response described in Chapter Five. Anomalous behaviour was observed with suspensions prepared with the sieve fraction 90 - 125 μm, particularly with mesh apertures of 45 and 90 μm. The formulation viscosity, together with the mesh opening were found to play a role in the release profile observed. The reduction of the cumulative percentage release with the

application of an electric field was found to correlate with the high Bingham yield stress values calculated. The tacrine release was halted through the mesh aperture 90 μm from suspensions containing the sieve fraction 90 - 125 μm.

Three possible mechanisms for controlled drug release are illustrated in Figure 6.21.

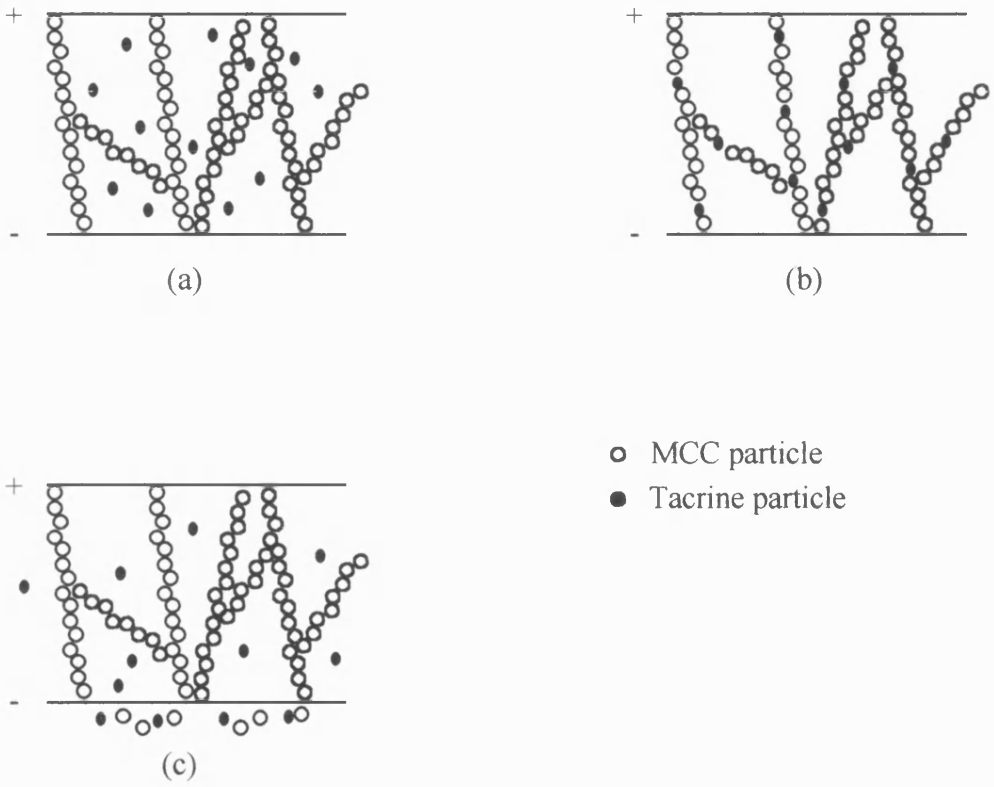

Figure 6.21. Three possible mechanisms for the controlled release of tacrine from electrorheological fluids: (a) entrapment of tacrine particles, (b) electrophoretic control and (c) formulation seepage.

The entrapment of tacrine particles within the chain structure may lead to the reduced release rates observed. The adsorption of tacrine onto MCC particles was previously discussed and may result in reduced tacrine availability. This mechanism would, however, result in little differences between the responses observed with and without the applied electric field. The second mechanism is electroporation and involves

attraction of tacrine to the negatively charge electrode. The third mechanism is the seepage of formulation through the mesh; upon application of an electric field, the formulation viscosity will increase resulting in reduced formulation seepage.

The use of ER fluids in controllable drug-delivery devices has been demonstrated at power requirements of similar magnitude to existing pacemaker and implantable-device battery technologies (i.e. typically mW). This *in vitro* model of an ER fluid based drug-delivery device is a prototype for future research in this area.

In this thesis, creep and recovery behaviour, together with flow response data have been used synergistically to develop our understanding of the ER response at low applied electric fields. We have demonstrated the development of dynamic yield stresses, in our model ER fluids, at low applied electric fields ($\leq$ 500 V/mm) under conditions of flow. Upon application of an electric field, MCC particles were observed to form particle chains spanning the electrode gap. Chains of different structures and densities formed depending on the magnitude of the electric field. The development of such particle chains is the probable cause of the yield stress; the degree of which is dependent on several established factors, namely particle size, particle concentration, moisture content and the magnitude of the applied electric field. It was envisaged that these particle chains could entrap the tacrine particles, thereby hindering or halting tacrine release under the influence of an electric field.

A traditional Franz cell was modified for use with low viscosity formulations by the addition of a glass lip, an insulating o-ring and an interchangeable mesh support that acted as the lower electrode. The modified diffusion cell was validated in Chapter Five using tacrine in 100 cSt silicone oil. The degree of drug release from ER fluids was assessed in relation to three factors, namely particle concentration, particle size and magnitude of the applied electric field.

Future experimental work in this field may involve the use of platinum electrodes, possibly coated on the underside of the lower electrode to overcome problems encountered with current surges. Basal tacrine release at long times was slow, resulting in the small differences observed upon application of an electric field. In future work, a drug of choice may exhibit a high partition coefficient and low lipophilicity, thereby resulting in higher basal drug delivery rates. Nevertheless, we have designed and developed ER fluids from pharmaceutically acceptable materials, operating at less than 1 kV/mm.

Appendices

Appendix One

The following distributions are representative of the particle size distributions of Emcocel and tacrine powders used in the present study.

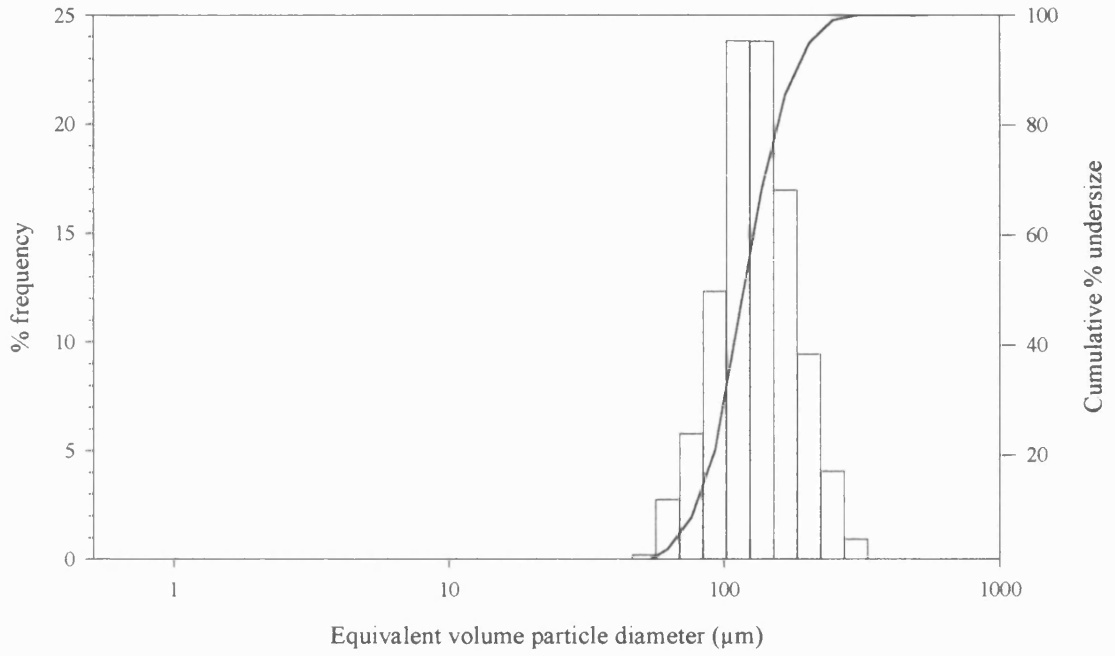

A 1.1. Particle size distribution of Emcocel 50M (sieve fraction 90 - 125 μm).

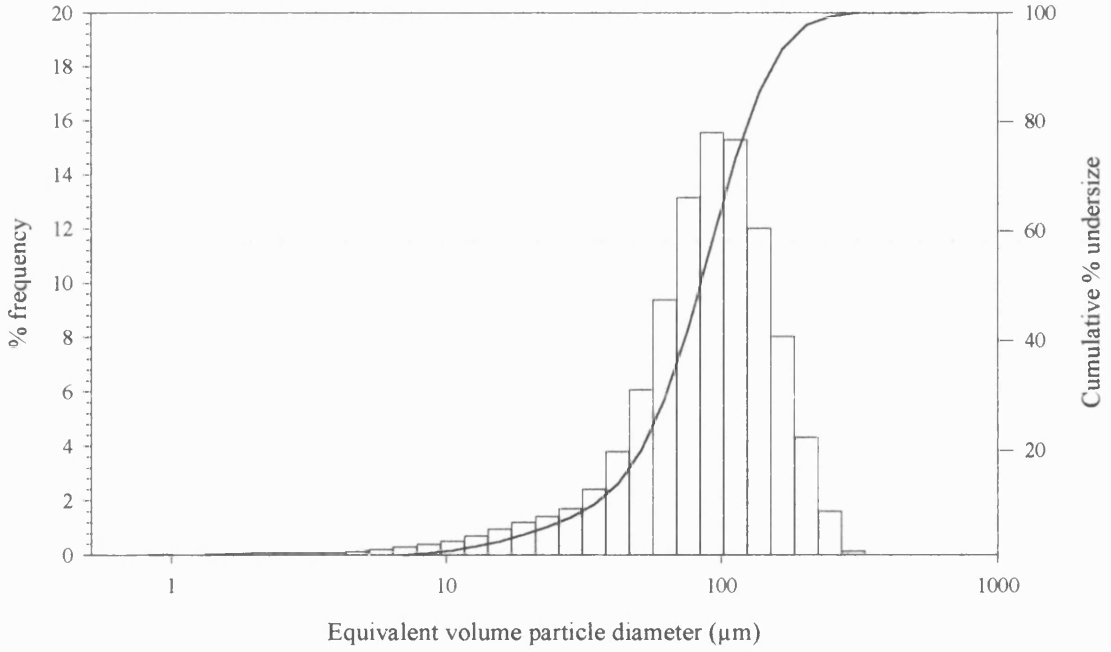

A 1.2. Particle size distribution of Emcocel 50M (sieve fraction 75 - 90 μm).

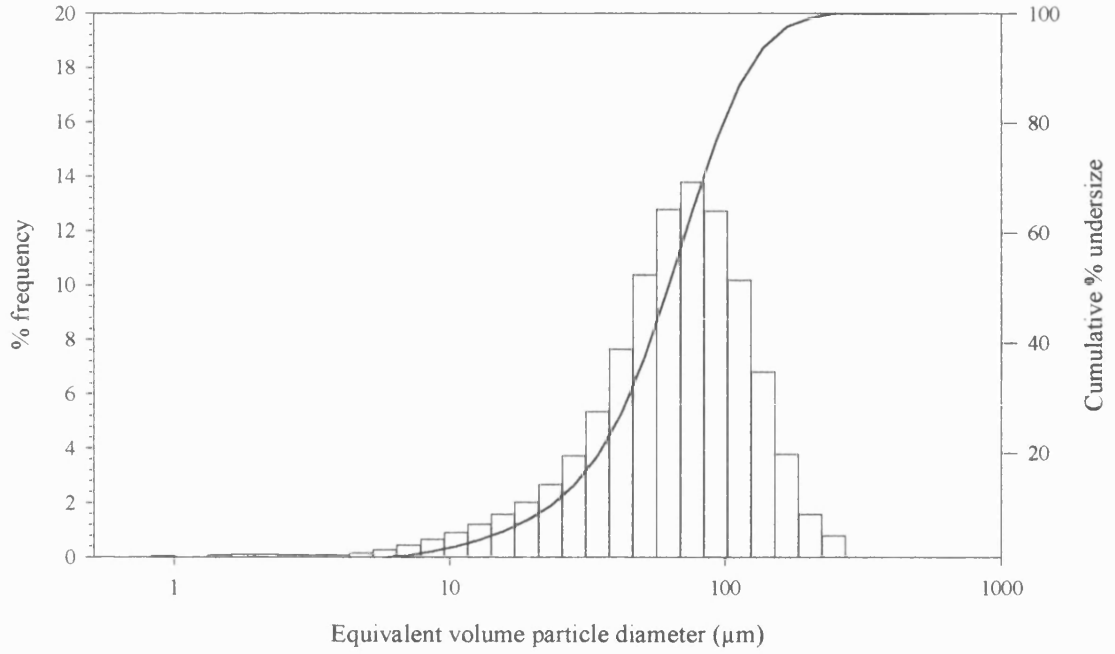

A 1.3. Particle size distribution of Emcocel 50M (sieve fraction 63 - 75 μm).

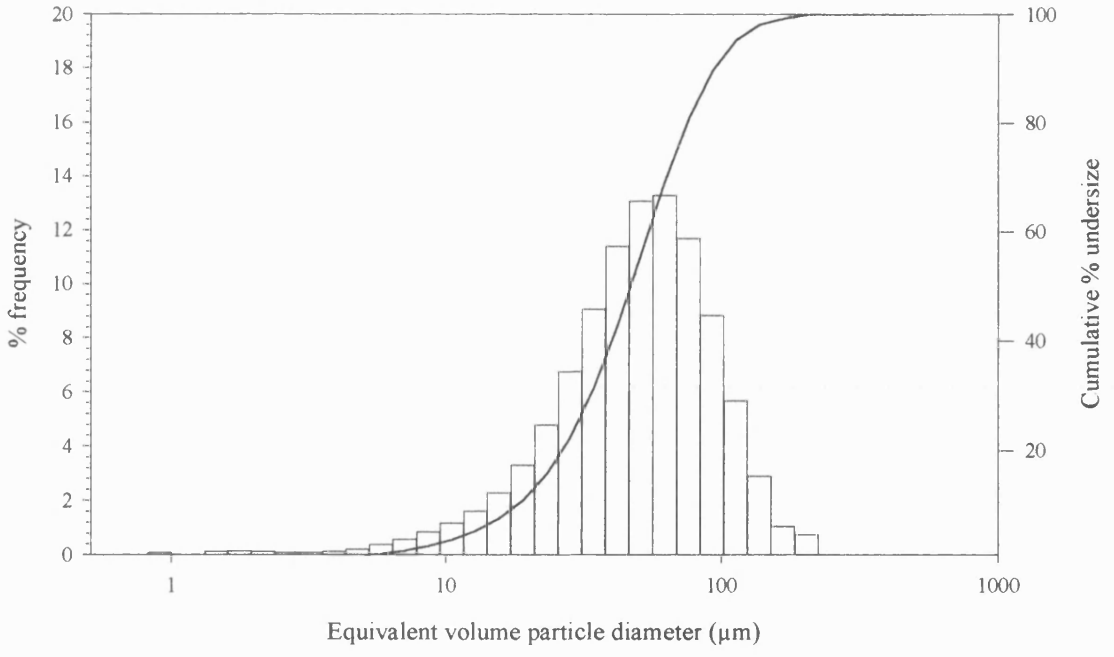

A 1.4. Particle size distribution of Emcocel 50M (sieve fraction 45 - 63 μm).

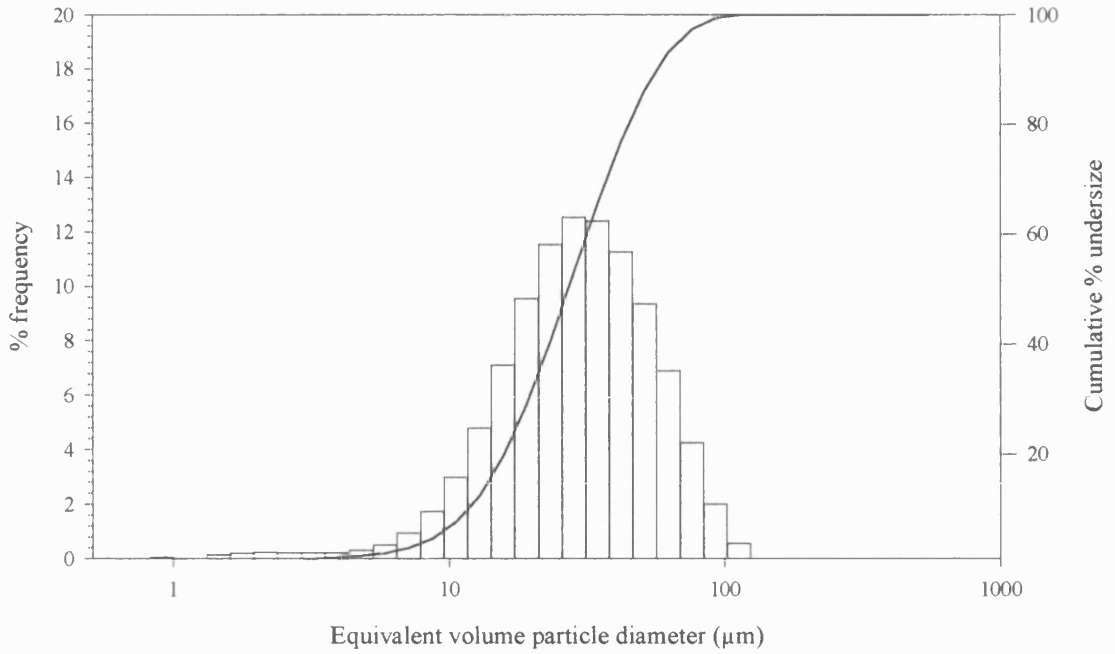

A 1.5. Particle size distribution of Emcocel 50M (sieve fraction below 45 µm).

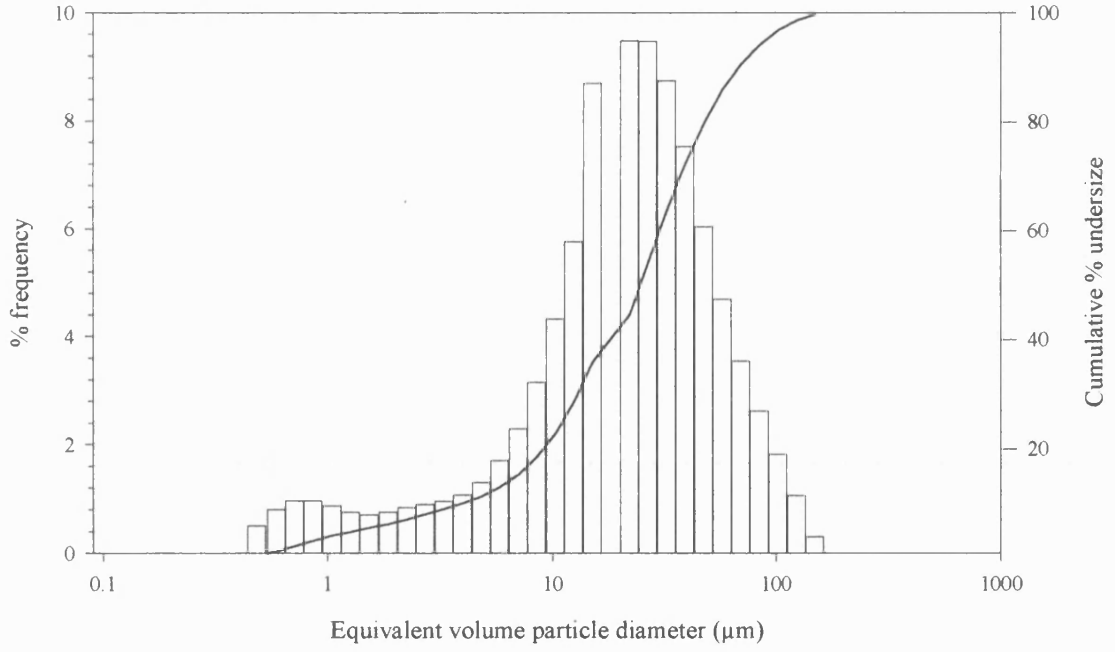

A 1.6. Particle size distribution of Emcocel LM50 (sieve fraction below 45 µm).

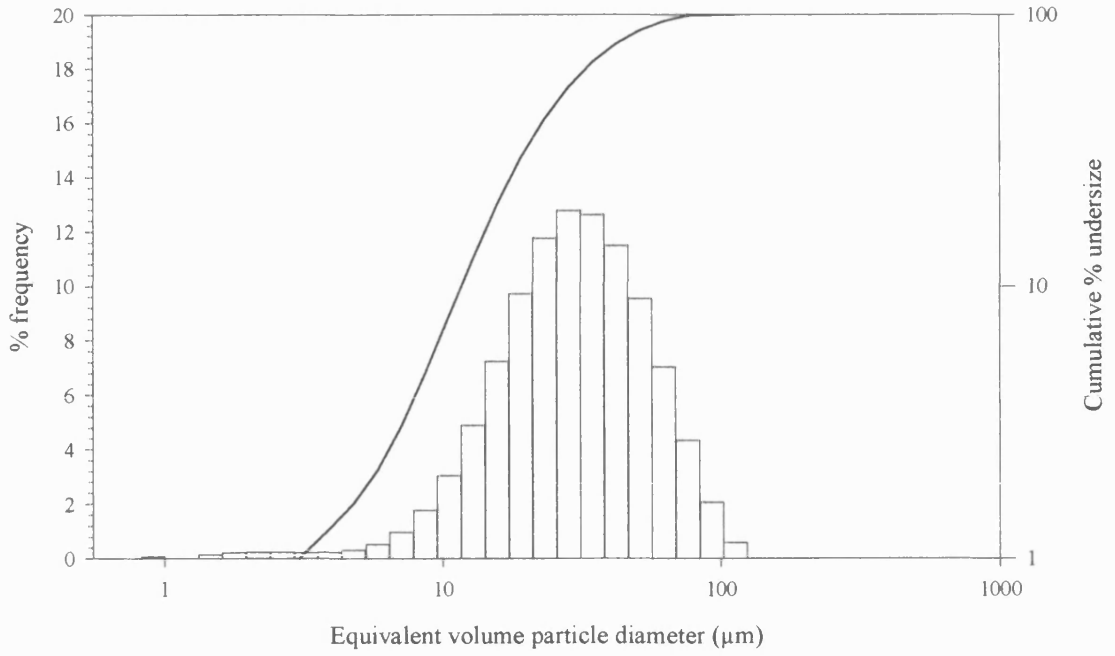

A 1.7. Particle size distribution of Emcocel XLM90 (sieve fraction below 45 µm).

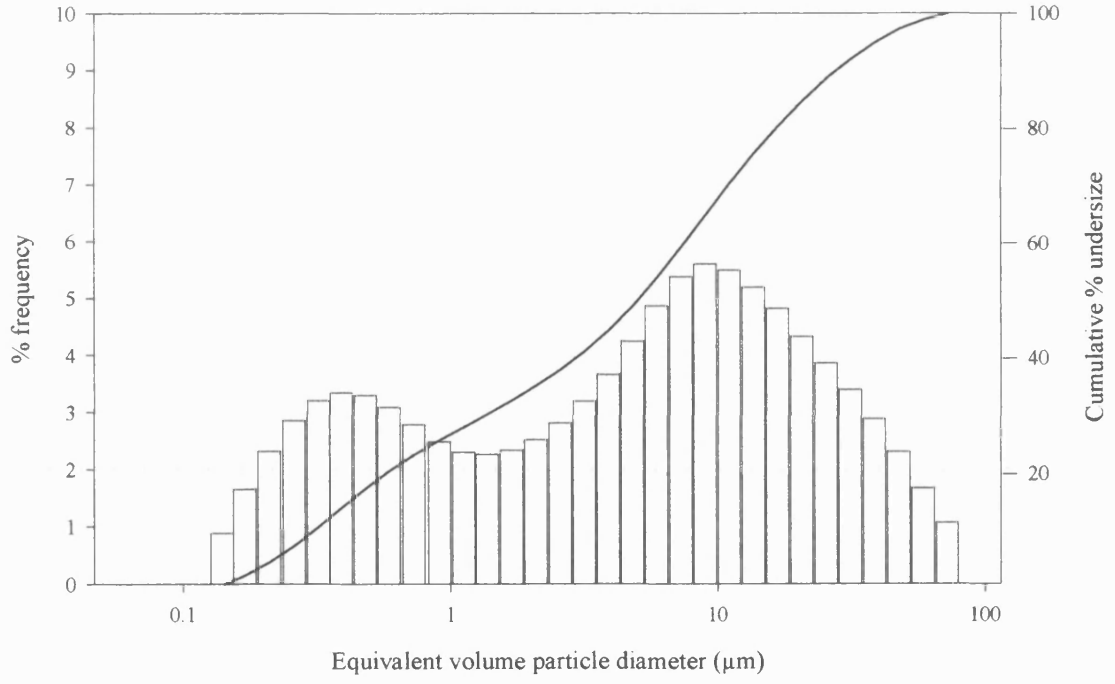

A 1.8. Particle size distribution of tacrine.

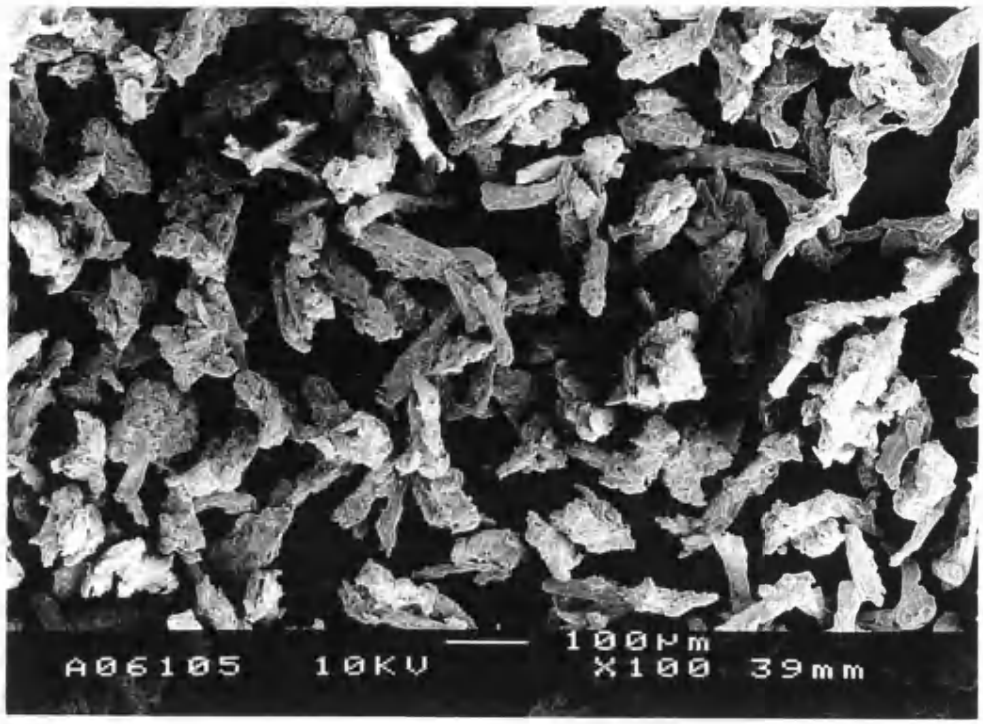

A 2.1. Scanning electron photomicrograph showing Emcocel 50M (sieve fraction 75 - 90 µm) at an accelerating voltage of 10 kV (x 100).

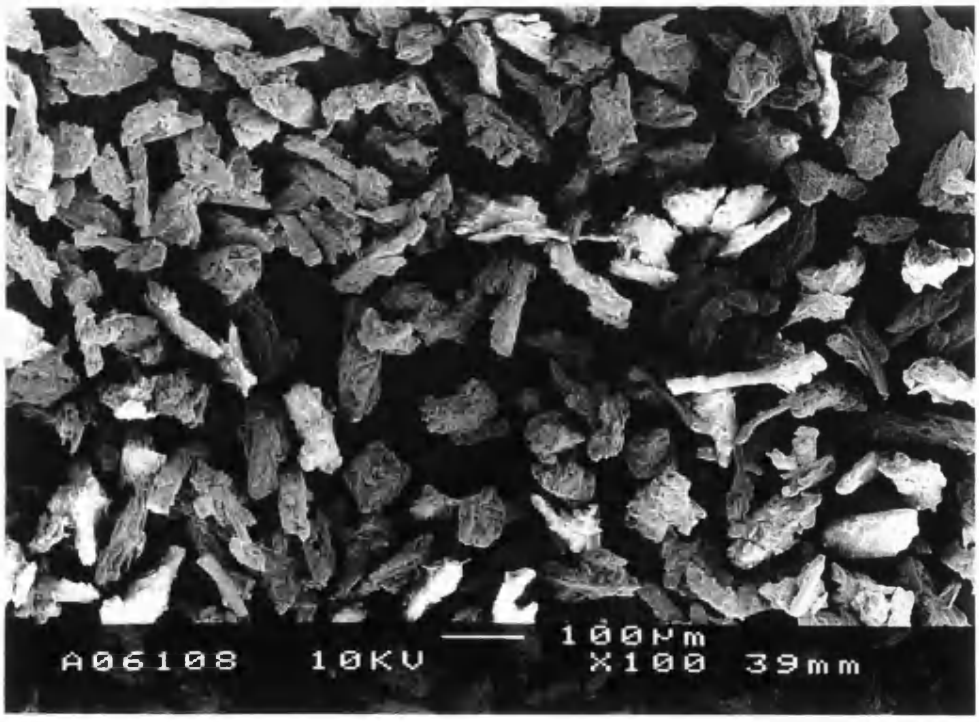

A 2.2. Scanning electron photomicrograph showing Emcocel 50M (sieve fraction 63 - 75 µm) at an accelerating voltage of 10 kV (x 100).

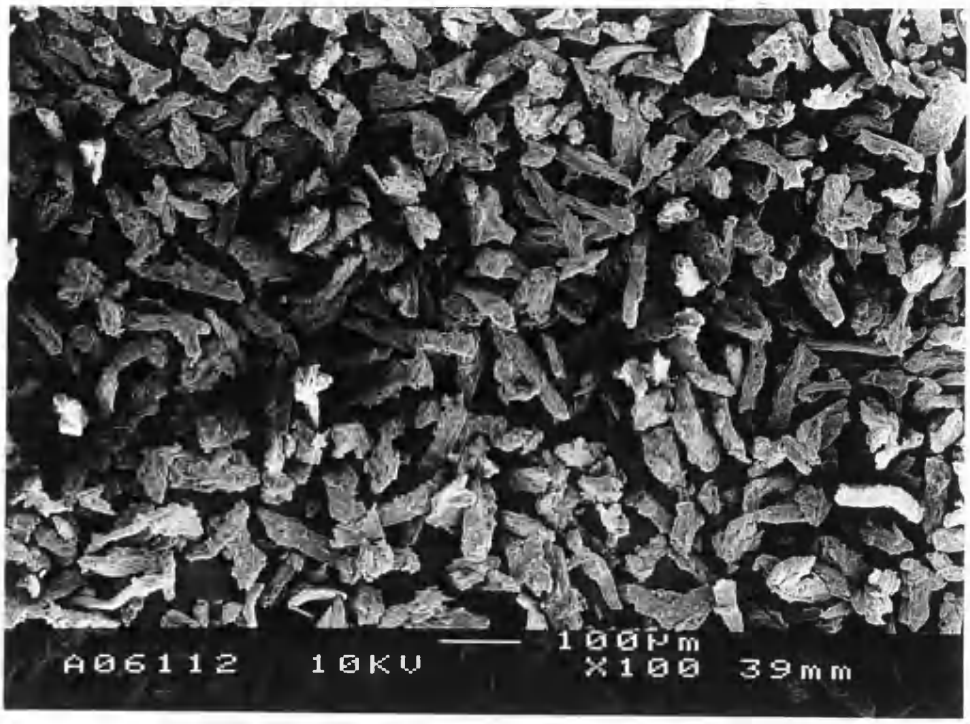

A 2.3. Scanning electron photomicrograph showing Emcocel 50M (sieve fraction 45 - 63 µm) at an accelerating voltage of 10 kV (x 100).

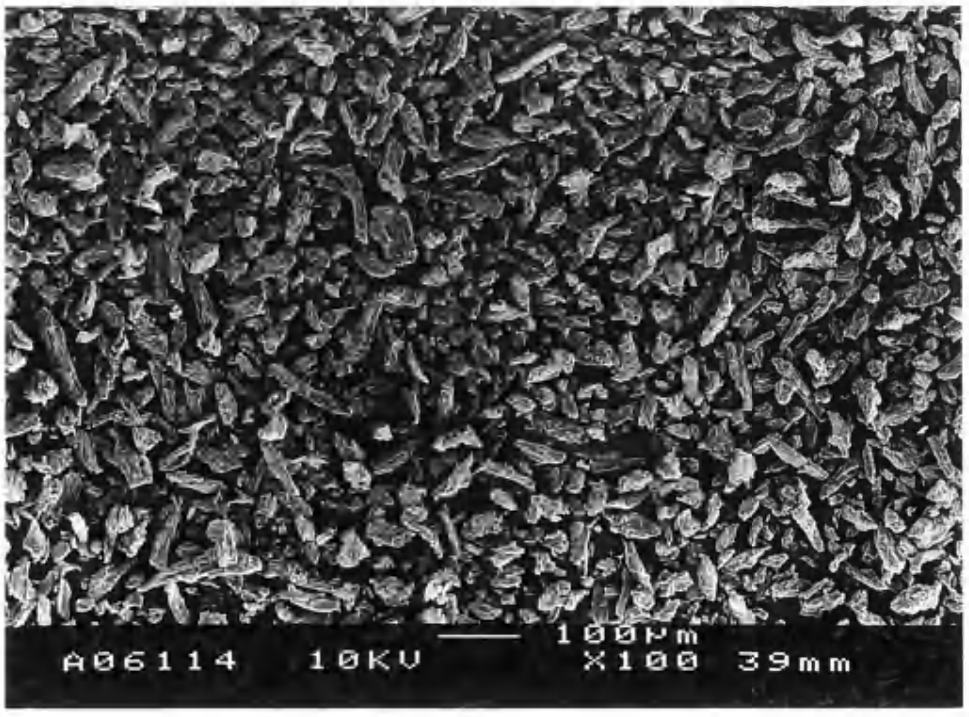

A 2.4. Scanning electron photomicrograph showing Emcocel 50M (sieve fraction below 45 µm) at an accelerating voltage of 10 kV (x 100).

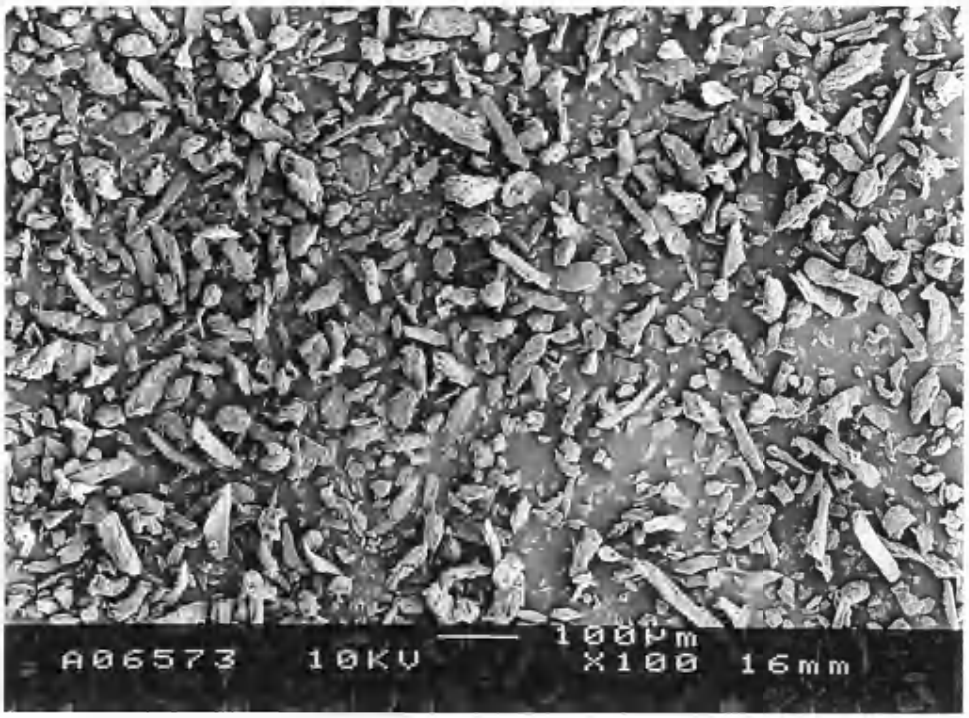

A 2.5. Scanning electron photomicrograph showing Emcocel LM50 (sieve fraction below 45 µm) at an accelerating voltage of 10 kV (x 100).

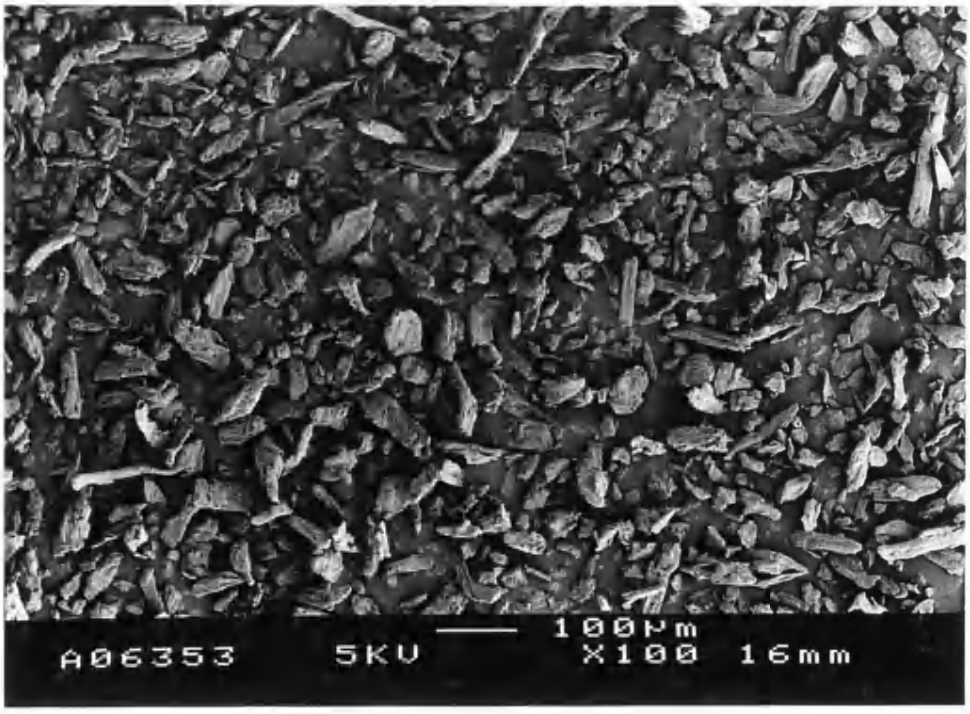

A 2.6. Scanning electron photomicrograph showing Emcocel XLM90 (sieve fraction below 45 µm) at an accelerating voltage of 10 kV (x 100).

References

References are in the style of the International Journal of Pharmaceutics.

Aboutaleb, A. E., Rahman, A. A., Saleh, S. I. and Ahmad, M. O., Factors affecting the release of diazepam from directly compressed tablets. I. Interaction of diazepam with certain directly compressible vehicles. *STP Pharma.*, 2 (1986) 23-27.

Abu-Jdayil, B. and Brunn, P. O., Effects of non-uniform electric field on slit flow of an electrorheological fluid. *J. Rheol.*, 39 (1995) 1327-1341.

Adriani, P.M. and Gast, A. P., A microscopic model of electrorheology. *Phys. Fluids,* 31 (1988) 2757-2768.

Albert, A. and Goldacre, R., The nature of the amino-group in aminoacridines. Part I. Evidence from electrometric studies. *J. Chem. Soc.*, (1943) 454-459.

Albert, A. and Goldacre, R., The ionisation of acridine bases. *J. Chem. Soc.*, (1946) 706-713.

Albert, A., Goldacre, R. and Phillips, J., The strength of heterocylic bases. *J. Chem. Soc.*, (1948) 2240-2249.

Albert, A. and Serjeant, E. P., The determination of ionization constants. Chapman and Hall, London (1962).

Aly, S. A. S. and Udeala, O. K., Dissolution of directly compressed thiamine hydrochloride tablets. *Drug Devel. and Ind. Pharm.*, 11 (1985) 1989-2007.

Asano, K., Suto, H. and Yatsuzuka, K., Influence of particle configuration on electrorheological effect. *J. Electrostatics,* 40 & 41 (1997) 573-578.

Bae, Y. H., Okano, T., Hsu, R. and Kim, S. W., Thermo-responsive polymers as on-off switches for drug release. *Makromol. Chem. Rapid. Commun.*, 8 (1987) 481-485.

Bagniefski, T. and Burnette, R. R., A comparison of pulsed and continuous current iontophoresis. *J. Control. Rel.*, 11 (1990) 113-122.

Banga, A. K. and Chien, Y. W., Iontophoretic delivery of drugs: fundamentals, developments and biomedical applications. *J. Control. Rel.*, 7 (1988) 1-24.

Barnes, H. A. and Walters, K., The yield stress myth. *Rheol. Acta,* 24 (1985) 323-326.

Barnes, H. A., Shear thickening ("Dilatancy") in suspensions of nonaggregating solid particles dispersed in Newtonian fluids. *J. Rheol.* 33 (1989) 329-366.

Barnes, H. A., Thixotropy - A Review. *J. Non-Newtonian Fluid Mech.*, 70 (1997) 1-33.

Barry, B. W., Rheology of Pharmaceutical and Cosmetic Semisolids. In Bean, H. S., Beckett, A. H. and Carless, J. E. (Eds.), *Advances in Pharmaceutical Sciences,* Academic Press, New York (1974) pp. 1-72

Barry, B. W., *Dermatological Formulations,* Swarbrick, J. (Ed.) Marcel Dekker, New York (1983).

Barry, B. W., Model action of penetration enhancers in human skin. *J. Control. Rel.*, 6 (1987) 85-97.

Blackshear, P. J., Implantable drug delivery systems. *Sci. Am.*, 241 (1979) 66-73.

Block, H. and Kelly, J. P., Electrorheology. *J. Phys. D: Appl. Phys.*, 21 (1988) 1661-1677.

Block, H., Kelly, J. P., Qin, A. and Watson, T., Materials and mechanisms in electrorheology. *Langmuir,* 6 (1990) 6-14.

Block, H., Electrorheological fluids. *Chemtech.*, 22 (1992) 368-373.

Bohon, K. and Krause, S., An electrorheological fluid and siloxane gel based electromechanical actuator: working towards an artificial muscle. *J. Polym. Sci. B: Polym. Phys.*, 36 (1998) 1091-1094.

Boissey, C., Atten, P. and Foulc, J.N., On a negative electrorheological effect. *J. Electrostatics,* 35 (1995) 13-20.

Bonnecaze, R. T. and Brady, J. F., Yield stresses in electrorheological fluids. *J. Rheol.*, 36 (1992a) 73-115.

Bonnecaze, R. T. and Brady, J. F., Dynamic stimulation of an electrorheological fluid. *J. Chem. Phys.*, 96 (1992b) 2183-2202.

Brannon-Peppas, L. and Peppas, N. A., Solute and penetrant diffusion in swellable polymers. IX. The mechanisms of drug release from pH sensitive swelling controlled systems. *J. Control. Rel.*, 8 (1989) 267-274.

British Pharmacopoeia, HMSO, London, 1993.

British Standard 5168 (1975) Glossary of Rheological Terms.

Brooks, D. Goodwin, J., Hjelm, C., Marshall, L. and Zukoski, C., Viscoelastic studies on an electrorheological fluid. *Colloids and Surfaces,* 18 (1986) 293-312.

Brooks, D. A., Devices using electrorheological fluids. *Electrorheological Fluids. Proceeding of the Second International Conference on ER Fluids.* Carlson, J. D., Sprecher, A. F. and Conrad, H. (Eds.) Technomic Publishing USA (1990).

Bronaugh, R. L. and Maibach, H. I., (Eds.) *Percutaneous Absorption: Mechanisms, Methodology, Drug Delivery.* Marcel Dekker, New York (1989) pp 1-12.

Brown, L., Wei, C. and Langer, R., *In vitro* and *in vivo* release of macromolecules from polymeric drug delivery systems. *J. Pharm. Sci.*, 72 (1983) 1181-1185.

Bullough, W. A., Solidifying fluids: the electrorheological clutch. *IEE Rev.*, 38 (1992) 348-349.

Burnette, R. R. and Ongpipattanakul, B., Characterisation of the pore transport properties and tissue alteration of excised human skin during iontophoresis. *J. Pharm. Sci.*, 77 (1988) 132-137.

Burnette, R. R., Pharmacokinetics and dynamics of temporal delivery. In Berner, B. and Dinh, S. M. (Eds.), *Electronically Controlled Drug Delivery*, CRC Press, New York, USA, 1998, pp 93-110.

Cardinal, J. R., Matrix systems. In *Medical Applications of Controlled Release. Volume I: Classes of Systems.* Langer, R and Wise, D. L. (Eds.) CRC Press, Florida (1984) pp 41-67.

Cerda, C. M., Foister, R. T. and Mason, S. G., Experimental observation of electrooptical phenomena in fibrated suspensions. *J. Coll. Int. Sci.*, 82 (1981) 577-579.

Chang, C. and Powell, R. L., Effect of particle size distributions on the rheology of concentrated bimodal suspensions. *J. Rheol.*, 38 (1994) 85 -98.

Chen, Y., Sprecher, A. F. and Conrad, H., Electrostatic particle-particle interactions in electrorheological fluids. *J. Appl. Phys.*, 70 (1991) 6796-6803.

Cheng, D. C., Yield stress: A time-dependent property and how to measure it. *Rheol. Acta,* 25 (1986) 542-554.

Conrad, H., Fisher, M. and Sprecher, A. F., Characterisation of the structure of a model electrorheoloigcal fluid employing stereology. *Electrorheological Fluids. Proceeding of the Second International Conference on ER Fluids.* Carlson, J. D., Sprecher, A. F. and Conrad, H. (Eds) Technomic Publishing USA (1990).

Conrad, H., Sprecher, A. F., Choi, Y. and Chen, Y., The temperature dependence of the electrical properties and strength of electrorheological fluids. *J. Rheol.*, 35 (1991) 1393-1409.

Conrad, H., Chen, Y. and Sprecher, A. F., The strength of electrorheological (ER) fluids. *Int. J. Mod. Phys.*, 6 (1992) 2575-2594.

Crank, J., *The Mathematics of Diffusion,* Oxford University Press, London (1975).

Davis, L. C., Polarisation forces and conductivity effects in electrorheological fluids. *J. Appl. Phys.*, 72 (1992) 1334-1340.

Deinega, Y.F. and Vinogradov, G.V., Electric fields in the rheology of disperse systems. *Rheol. Acta,* 23 (1984) 636-651.

D'Emanuele, A. and Staniforth, J. N., An electrically modulated drug delivery device: I. *Pharm Res.,* 8 (1991) 913-917.

D'Emanuele, A. and Staniforth, J. N., An electrically modulated drug delivery device: II. Effect of ionic strength, drug concentration and temperature. *Pharm Res.,* 9 (1992a) 215-219.

D'Emanuele, A. and Staniforth, J. N., An electrically modulated drug delivery device: III. Factors affecting drug stability during electrophoresis. *Pharm Res.,* 9 (1992b) 312-315.

D'Emanuele, A. and Staniforth, J. N., Feedback controlled drug delivery using an electro-diffusion pump. *J. Control. Rel.,* 23 (1993) 97-104.

Drozdov, A. D., A model of adaptive links in non-linear viscoelasticity. *J. Rheol.,* 41 (1997) 1223-1246.

Edelman, E. R., Kost, J., Bobeck, H. and Langer, R., Regulation of drug release from polymer matrices by oscillating magnetic fields. *J. Biomed. Mater. Res.,* 19 (1985) 67-83.

Edelman, E. R., Brown, L. and Langer, R., Quantification of insulin release from implantable polymer-based delivery systems and augmentation of therapeutic effect with simultaneous release of somatostatin. *J. Pharm. Sci.,* 85 (1996) 1271-1275.

Edwards, D. A. and Langer, R., A linear theory of transdermal transport phenomena. *J. Pharm. Sci.,* 83 (1994) 1315-1334.

Edwards, D. A., Prausnitz, M. R., Langer, R. and Weaver, J. C., Analysis of enhanced transdermal transport by skin electroporation. *J. Control. Rel.,* 34 (1995) 211-221.

Ekman, L., Lindstrom, B. and Roxin, P., Determination of tacrine and its 1-hydroxy metabolite in plasma using column liquid chromatography with ultraviolet detection. *J. Chromatogr.*, 494 (1989) 397-402.

Elias, P. M., Epidermal barrier function: intercellular lamellar lipid structures, origin, composition and metabolism. *J. Control. Rel.*, 15 (1991) 199-208.

Ferry, J. D., *Viscoelastic Properties of Polymers*, John Wiley, New York (1970).

Femenia, A., Rossello, C., Mulet, A and Canellas, J., Chemical-composition of bitter and sweet apricot kernels. *Journal of Agricultural and Food Chemistry*, 43 (1995) 356-361.

Filisko, F. E. and Radzilowski, L. H., An intrinsic mechanism for the activity of alumino-silicate based electrorheological materials. *J. Rheol.*, 34 (1990) 539-552.

Fischel-Ghodsian, F., Brown, L., Mathiowitz, E., Brandenburg, D. and Langer, R., Enzymatically controlled drug delivery. *Proc. Natl. Acad. Sci. USA*, 85 (1988) 2403-2406.

Floy, B. J., Visor, G. C. and Sanders, L. M., Design of biodegradable polymer systems for controlled-release of bioactive agents. *ACS Symposium Series*, 520 (1993) 154-167.

Forsyth, D. R., Wilcock, G. K., Morgan, R. A., Truman, C. A., Ford, J. M. and Roberts, C. J. C., Pharmacokinetics of tacrine hydrochloride in Alzheimer's disease. *Clin. Pharmacol. Therapeutics.*, 46 (1989) 634-641.

Freeman, S. A., Wang, M. A. and Weaver, J. C., Theory of electroporation of planar bilayer membranes: Predications of the aqueous area, change in capacitance and pore-pore separation. *J. Biophys.*, 67 (1994) 42-56.

Gallagher, T.J., *Simple dielectric liquids*, Claredon Press, Oxford (1975).

Gamota, D. R. and Filisko, F. E., Dynamic mechanical studies of electrorheological materials: Moderate frequencies. *J. Rheol.*, 35 (1991) 399-426.

Gandhi, M. V. and Thompson, B. S., Electro-rheological fluids. In Gandhi, M. V. and Thompson, B. S. (Eds.). *Smart Materials and Structures,* Chapman & Hall, London, 1992 pp. 137-174.

Gast, A. P. and Zukoski, C.F., Electrorheological fluids as colloidal suspensions. *Adv. Coll. Int. Sci.*, 30 (1989) 153-202.

Golomb, G., Dixon, M., Smith, M. S., Schoen, F. J. and Levy, R. J., Controlled release drug delivery of diphosphonate to inhibit bioprosthetic heart valve calcification: release rate modulation with silicone matrices via drug solubility and membrane coating. *J. Pharm. Sci.*, 76 (1987) 271-276.

Goodwin, J. W., Markham, G. M. and Vincent, B., Studies on model electrorheological fluids. *J. Phys. Chem. B,* 101 (1997) 1961-1967.

Goto, H. and Kuno, H., Flow of suspensions containing particles of two different sizes through a capillary tube II. Effect of the particle size ratio. *J. Rheol.*, 28 (1984) 197-205.

Gow, C. J. and Zukoski, C. F., The electrorheological properties of polyaniline suspensions. *J. Coll. Int. Sci.*, 136 (1990) 175-188.

Green, A. E., R. S. Rivlin, and A. I. M. Spencer, "The Mechanics of Non-linear Materials with Memory, Part II," Arch. Rat. Mech. Anal. 3, 62-90 (1959).

Green, A. E. and R. S. Rivlin, "The Mechanics of Non-linear Materials with Memory, Part III," *Arch. Rat. Mech. Anal.* 4, 3874 (1960).

Gummer, C. L., Hinz, R. S. and Maibach, H. I., The skin penetration cell: a design update. *Int. J. Pharm.*, 40 (1987) 101-104.

Halsey, T.C., Electrorheological fluids. *Science,* 258 (1992) 761-766.

Handbook of Chemistry and Physics: A Ready Reference Book of Chemical and Physical Data, Edited by R. C. Weast, The Chemical Rubber Co., 50th Edition,1969.

Handbook of Pharmaceutical Excipients, A joint publication of the American Pharmaceutical Press and the Royal Pharmaceutical Society of Great Britain Press, London, UK, 1994

Hao, T., The role of the dielectric loss of dispersed material in the electrorheological effect. *Appl. Phys. Lett.*, 70 (1997) 1956-1958.

Hao, T., Xu, Y., Chen, Y. and Xu, M., Dielectric polarisation of electrorheological suspensions. *Chin. Phys. Lett.*, 12 (1995) 573-576.

Harris, J., *Rheology and non-Newtonian Flow.* Longman, London and New York (1977)

Hartnett, J. P. and Hu, R. Y. Z., Technical note: The yield stress - an engineering reality. *J. Rheol.*, 33 (1989) 671-679.

Hartsock, D. L., Novak, R. F. and Chaundy, G. J., ER fluid requirements for automotive devices. *J. Rheol.*, 35 (1991) 1305-1326.

Hartvig, P., Askmark, H. and Aquilonius, S.M., Clinical pharmacokinetics of intravenous and oral 9-amino-1,2,3,4-tetrahydroacridine, tacrine. *Eur. J. Clin. Pharmacol.*, 38 (1990) 259-263.

Havelka, K. O. and Pialet, J. W., Electrorheological technology: The future is now. *Chemtech*, 26 (1996) 36-45.

Heller, J., Chemically self-regulated drug delivery systems. *J. Control. Rel.*, 8 (1988) 111-125.

Herschel, W. H. and Bulkley, R., Measurement of consistency as applied to rubber benzene solutions. *Proc. Am. Soc. Test. Matl.*, 26 (1926) 621-633.

Higuchi, T., Rate of release of medicaments from ointment bases containing drugs in suspension. *J. Pharm. Sci.*, 50 (1961) 874-875.

Higuchi, W. I., Analysis of data on the medicament release from ointments. *J. Pharm. Sci.*, 51 (1962) 802-804.

Hoffman, A. S., Afrassiabi, A. and Dong, L. C., Thermally reversible hydrogels: II. Delivery and selective removal of substances from aqueous solutions.. *J. Control. Rel.*, 4 (1986) 213-222.

Hrushesky, W. J. M., Circadian timing of cancer chemotherapy. *Science*, 228 (1985) 73-75.

Hsieh, D. S. T., Langer, R. and Folkman, J., Magnetic modulation of release of macromolecules from polymers. *Proc. Natl. Acad. Sci. USA*, 78 (1981) 1863-1867.

Imanidis, G., Waldner, C., Mettler, C and Leuenberger, H., An improved diffusion cell design for determining drug transport parameters across cultured cell monolayers. *J. Pharm. Sci.*, 85 (1996) 1196-1203.

Johnson, M. E., Mitragotri, S., Patel, A., Blankschtein, D. and Langer, R., Synergistic effects of chemical enhancers and therapeutic ultrasound on transdermal drug delivery. *J. Pharm. Sci.*, 85 (1996) 670-679.

Johnston, T. P., Bove, E. L., Bolling, S. F., Boyd, J. A., Ciesliga, B. L., Amidon, G. L., Schoen, F. J. and Levy, R. J., Controlled release of 1-hydroxyethylidene diphosphate: *in vitro* assessment and effects on bioprosthetic calcification in sheep tricuspid valve replacements. *Int. J. Pharm.*, 52 (1989) 139-148.

Jordan, T.C. and Shaw, M.T., Electrorheology. *IEEE Trans. Electr. Insulat.*, 24 (1989) 849-879.

Julian, T. N. and Zentner, G. M., Mechanism for ultrasonically enhanced transmembrane solute permeation. *J. Control. Rel.*, 12 (1990) 77-85.

Kalia, Y. N. and Guy, R. H., The electrical characteristics of human skin in vivo. *Pharm. Res.*, 12 (1995) 1605-1613.

Kawai, A., Uchida, K., Kamiya, K., Gotoh, A. and Ikazaki, F., Effect of adsorbed water contained in heat-treated silica particles on electrorheology. *Adv. Powd. Technol.*, 5 (1994) 129-141.

Kawai, A., Uchida, K., Kamiya, K., Gotoh, A., Hayashi, S. and Ikazaki, F., The effect of surface characteristics of silica particles on electrorheology. *Adv. Powd. Technol.*, 7 (1996) 153-160.

Keentok, M., The measurement of the yield stress of liquids. *Rheol. Acta*, 21 (1982) 325-332.

Kikkinides, E. S., Charalambopoulou, G. Ch., Stubos, A. K., Kanellopoulos, N. K., Varelas, C. G. and Steiner, C. A., A two-phase model for controlled drug release from biphasic polymer hydrogels. *J. Control. Rel.*, 51 (1998) 313-325.

Kitchell, J. P. and Wise, D. L., Poly(lactic glycolic acid) biodegradable drug polymer matrix systems. *Methods in Enzymology*, 112 (1985) 436-448.

Klass, D.L. and Martinek, T.W., Electroviscous fluids I. Rheoloigcal properties. *J. Appl. Phys.*, 38 (1967) 67-74.

Klingenberg, D. J., Vanswol, F. and Zukoski, C. F., Dynamic simulation of electrorheological suspensions. *J. Chem. Phys.*, 91 (1989) 7888-7895.

Klingenberg, D. J. and Zuksoki, C. F., Studies on the steady shear behaviour of electrorheological suspensions. *Langmuir*, 6 (1990) 15-24.

Klingenberg, D. J., Dirking, D. and Zukoski, C. F., Stress transfer mechanism in electrorheological suspensions. *J. Chem Soc. Faraday Trans.*, 87 (1991a) 425-430.

Klingenberg, D. J., van Swol, F. and Zukoski, C. F., The small shear rate response of electrorheological suspensions. 2. Extension beyond the point-dipole limit. *J. Chem. Phys.*, 94 (1991b) 6170-6178.

Klingenberg, D. J., Simulation of the dynamic oscillatory response of electrorheological suspensions: Demonstration of a relaxation mechanism. *J. Rheol.*, 37 (1993) 199-214.

Klingenberg, D. J., Zukoski, C. F. and Hill, J. C., Kinetics of structure formation in electrorheological suspensions. *J. Appl. Phys.*, 73 (1993) 4644-4648.

Klingenberg, D. J., Pakdel, P., Young, D. K., Belongia, B. M. and Kim, S., Protein enhanced electrorheological fluids. *Ind. Eng. Chem. Res.*, 34 (1995) 3303-3306.

Knutson, K., Harrison, D. J., Pershing, L. K. and Goates, C. Y., Transdermal absorption of steroids. *J. Control. Rel.*, 24 (1993) 95-108.

Kordonsky, V. I., Korobko, E. V. and Lazareva, T. G., Electrorheological polymer-based suspensions. *J. Rheol.*, 35 (1991) 1427-1439.

Korsmeyer, R. W. and Peppas, N. A., Effect of the morphology of hydrophilic polymeric matrices on the diffusion and release of water soluble drugs. *J. Membr. Sci.*, 9 (1981) 211-227.

Korsmeyer, R. W., Gurny, R., Doelker, E., Buri, P. and Peppas, N. A., Mechanisms of solute release from porous hydrophilic polymers. *Int. J. Pharm.*, 15 (1983) 25-35.

Kost, J., Noecker, R., Kunica, E. and Langer, R., Magnetically controlled release systems: Effects of polymer composition. *J. Biomed. Mater. Res.*, 19 (1985) 935-940.

Kost, J., Wolfrum, J. and Langer, R., Magnetically enhanced insulin release in diabetic rats. *J. Biomed. Mater. Res.*, 21 (1987) 1367-1373.

Kost, J., Leong, K. and Langer, R., Ultrasound-enhanced polymer degradation and release of incorporated substances. *Proc. Natl. Acad. Sci.*, 86 (1989) 7663-7666.

Kost, J., *Pulsed and Self Regulated Drug Delivery* . CRC Press (1990).

Kost, J. and Langer, R., Responsive polymer systems for controlled delivery of therapeutics. *TIBTECH.*, 10 (1992) 127-131.

Kost, J., Ultrasound induced protein delivery. *J. Control. Rel.*, 24 (1993) 247-255.

Kost, J., Pliquett, U., Mitragotri, S., Yamamoto, A., Langer, R. and Weaver, J., Synergistic effect of electric field and ultrasound on transdermal transport. *Pharm. Res.*, 13 (1996) 633-638.

Krieger, I. M. and Dougherty, T. J., A mechanism for non-Newtonian flow in suspensions of rigid spheres. *Trans. Soc. Rheol.*, 3 (1959) 137-152.

Kwon, J. C., Bae, Y. H. and Sim, S. W., Electrically erodible polymer gel for controlled release of drugs. *Nature*, 354 (1991) 291-293.

Kydonieus, A. F., Fundamental Concepts of Controlled Release. In Kydonieus, A. F. (Ed.), *Controlled Release Technologies: Methods, Theory, and Applications*, Vol. I, CRC Press, Boca Raton, Florida, USA, (1980) pp. 1-19.

Langer, R. and Folkman, J., Polymers for sustained release of proteins and other macromolecules. *Nature*, 263 (1976) 797-800.

Langer, R., Polymeric delivery systems for controlled drug release. *Chem. Eng. Commun.*, 6 (1980) 1-48.

Langer, R., Brem, H. and Tapper, D., Biocompatability of polymeric delivery systems for macromolecules. *J. Biomed. Mater. Res.*, 15 (1981) 267-277.

Langer, R. S. and Peppas, N. A., Present and future applications of biomaterials in controlled drug delivery systems. *Biomaterials*, 2 (1981) 201-214.

Langer, R., Drug delivery and targeting. *Nature*, 392S (1998) 5-10.

Ledger, P. W., Skin biological issues in electrically enhanced transdermal delivery. *Adv. Drug Del. Rev.*, 9 (1992) 289-307.

Lee, D. I., The viscosity of concentrated suspensions. *Trans. Soc. Rheol.*, 13 (1969) 273-288.

Lee, D. I., Packing of spheres and its effect on the viscosity of suspensions. *J. Paint Technol.*, 42 (1970) 579-587.

Lee, C-H., Bhatt, P. P. and Chien, Y. W., Effect of excipient on drug release and permeation from silicone-based barrier devices. *J. Control. Rel.*, 43 (1997) 283-290.

Lemaire, E. and Bossis, G., Yield stress and wall effects in magnetic colloidal suspensions. *J. Phys. D.*, 24 (1991) 1473-1477.

Levy, D., Kost, J., Meshulam, Y. and Langer, R., Effect of ultrasound on transdermal drug delivery to rats and guinea pigs. *J. Clin. Invest.*, 83 (1989) 2074-2078.

Levy, G., Chronotherapeutics pharmacokinetic constraints and opportunities. *Ann. N.Y. Acad. Sci.*, 618 (1991) 116-122.

Liu, J-C., Sun, Y., Siddiqui, O., Chien, Y. W., Shi, W-M. and Li, J., Blood glucose control in diabetic rats by transdermal Iontophoretic delivery of insulin. *Int. J. Pharm.*, 44 (1988) 197-204.

Lue, J-T. and Mao, C-C., Viscosity measurement of electrorheological fluids: corn starch and silicon microparticles mixed with silicone oil. *Meas. Sci. Technol.*, 8 (1997) 1323-1327.

Madden, S., Spaldin, V. and Park, B. K., Clinical pharmacokinetics of tacrine. *Clin. Pharmacokinet.*, 28 (1995) 449-457.

Mak, V. H. W., Potts, R. O. and Guy, R. H. J., Oleic acid concentration and effect in human stratum corneum: Non-invasive determination by attenuated total reflectance infrared spectroscopy *in vivo*. *J. Control. Rel.*, 12 (1990) 67-75.

Malins, C. and Lacey, D., Evaluation of electro-rheological fluids incorporating liquid-crystalline materials. *J. Mater. Chem.*, 4 (1994) 1029-1033.

Marshall, L., Zukoski, C.F. and Goodwin, J.W., Effects of electric fields on the rheology of non-aqueous concentrated suspensions. *J. Chem. Soc., Faraday Trans. 1*, 85 (1989) 2785-2795.

Mathiowitz, E and Cohen, M. D., Polyamide microcapsules for controlled release. 5. Photochemical release. *J. Membrane Sci.*, 40 (1989) 67-86.

McCarthy, M., Soong, D. and Edelman, E., Controlled drug release from porous matricies impregnated with magnetic beads: A proposed mechanism and model for enhanced release. *J. Control. Rel.*, 1 (1984) 143-147.

Medtronic Technical Manual on SynchroMed™ Programmable Pumps. Medtronic Inc., Minneapolis, USA.

Metzner, A. B., Rheology of suspensions in polymeric liquids. *J. Rheol.*, 29 (1985) 739-775.

Mitragotri, S., Blankschtein, D. and Langer, R., Ultrasound-mediated transdermal protein delivery. *Science,* 269 (1995a) 850-853.

Mitragotri, S., Edwards, D. A., Blankschtein, D. and Langer, R., A mechanistic study of ultrasounically-enhanced transdermal drug delivery. *J. Pharm. Sci.*, 84 (1995b) 697-706.

Mitragotri, S., Blankschtein, D. and Langer, R., Transdermal drug delivery using low-frequency sonophoresis. *Pharm. Res.*, 13 (1996) 411-420.

Miyazaki, S., Takeuchi, S., Sakamoto, M. and Takada, M., Controlled release of 5-fluorouracil from hydrophilic ethylene-vinyl alcohol copolymer matrices. *Chem. Pharm. Bull.*, 31 (1983) 3707-3713.

Miyazaki, S., Hou, W-M. and Takada, M., Controlled drug release by ultrasound irradiation. *Chem. Pharm. Bull.*, 33 (1985) 428-431.

Miyazaki, S., Yokouchi, C. and Takada, M., External control of drug release: controlled release of insulin from a hydrophilic polymer implant by ultrasound in diabetic rats. *J. Pharm. Pharmacol.*, 40 (1988) 716-717.

Monkman, G. J., Addition of solid structures to electrorheological fluids. *J. Rheol.*, 35 (1991) 1385-1392.

Monkman, G. J., Compliant robotic devices and electroadhesion. *Robotica,* 10 (1992) 183-195.

Monkman, G. J., Dielectrophoretic enhancement of electrorheological robotic actuators. *Mechatronics,* 3 (1993) 305-313.

Narasimhan, B and Langer, R., Zero-order release of micro- and maxromolecules from polymeric devices: The role of the burst effect. *J. Control. Rel.,* 47 (1997) 13-20.

Nguyen, Q.D. and Boger, D.V., Yield stress measurement for concentrated suspensions. *J. Rheol.,* 27 (1983) 321-349.

Nguyen, Q.D. and Boger, D.V., Measuring the flow properties of yield stress fluids. *Annu. Rev. Fluid Mech.,* 24 (1992) 47-88.

Oh, S. Y., Leung, L., Bommannan, D., Guy, R. H. and Potts, R. O., Effect of current, ionic strength and temperature on the electrical properties of skin. *J. Control. Rel.,* 27 (1993) 115-125.

Okabe, K., Yamaguchi, H. and Kawai, Y., New iontophoretic transdermal administration of the beta-blocker metropropol. *J. Control. Rel.,* 4 (1986) 79-85.

Okano, T., Bae, Y. H. and Kim, S. W., Temperature responsive controlled drug delivery. In *Pulsed and Self-regulated Drug Delivery* Kost, J. (Ed.), CRC Press, Boca Raton, FL pp. 129-140.

Ongpipattanakul, B., Burnette, R. R., Potts, R. O. and Francoeur, M. L., Evidence that oleic acid exists in a separate phase within the stratum-corneum lipids. *Pharm Res.,* 8 (1991) 350-354.

Ota, M. and Miyamoto, T., Many-body effect in the static yield stress of electrorheological fluid. *J. Appl. Phys.,* 74 (1993) 938-941.

Ota, M. and Miyamoto, T., Optimum particle size distribution of an electrorheological fluid. *J. Appl. Phys.*, 76 (1994) 5528-5532.

Otsubo, Y., Sekine, M. and Katayama, S., Effect of surface modification of colloidal silica on the electrorheology of suspensions. *J. Coll. Int. Sci.*, 146 (1991) 395-404.

Otsubo, Y. and Edamura, K., Creep behaviour of electrorheological fluids. *J. Rheol.*, 38 (1994) 1721-1733.

Otsubo, Y. and Edamura, K., Static yield stress of electrorheological fluids. *J. Colloid and Interface Sci.*, 172 (1995) 530-535.

Otsubo, Y. and Edamura, K., Relation between yield stress and column thickness in electrorheological fluids. *Colloids and Surfaces A.*, 109 (1996) 63-69.

Otsubo, Y., Effect of electrode pattern on the column structure and yield stress of electrorheological fluids. *J. Colloid and Inerface Sci.*, 190 (1997) 466-471.

Parera Morell, J. L., Contreras Claramonte, M. D. and Parera Vialard, A., Validation of a release diffusion cell for topical dosage forms. *Int. J. Pharm.*, 137 (1996) 49-55.

Parthasarathy, M. and Klingenberg, D.J., Electrorheology: mechanisms and models. *Mat. Sci. and Eng.*, 17 (1996) 57-103.

Peppas, N. A., Analysis of Fickian and non-Fickian drug release from polymers. *Pharm. Acta Helv.*, 60 (1985) 110-111.

Perrin, D. D., Dempsey, B. and Serjeant, E. P., *pK_a prediction for organic acids and bases*. Chapman and Hall, London and New York (1981).

Pliquett, U., Prausnitz, M., Chizmadzhev, Y. and Weaver, J., Measurement of rapid release kinetics for transdermal and other types of drug delivery. *Pharm. Res.*, 12 (1995) 549-555.

Pool, F., The fluids with a case of split personality. *Science*, 247 (1990) 1180-1181.

Prausnitz, M. R., Bose, V. G., Langer, R. and Weaver, J. C., Electroporation of mammalian skin - A mechanism to enhance transdermal drug delivery. *Proc. Natl. Acad. Sci.*, 90 (1993) 10504-10508.

Prausnitz, M. R., Gimm, J. A., Guy, R. H., Langer, R., Weaver, J. C. and Cullander, C., Imaging regions of transport across human stratum corneum during high voltage and low voltage exposures. *J. Pharm. Sci.*, 85 (1996a) 1363-1370.

Prausnitz, M. R., Lee, C. S., Liu, C. H., Pang, J. C., Singh, T-P., Langer, R. and Weaver, J. C., Transdermal transport efficiency during skin electroporation and iontophoresis. *J. Control. Rel.*, 38 (1996b) 205-217.

Probstein, R. F., Sengun, M. Z., Tseng, T-C., Bimodal model of concentrated suspension viscosity for distributed particle size. *J. Rheol.*, 38 (1994) 811-829.

Quemada, D. E. Advances in Rheology: Vol. 2. In *Fluids*. (Mena, B. et al. Eds) Universidad Nacional Autonama de Mexico, Mexico, (1984).

Reinberg, A., New concepts in chronopharmacology. *NIPS*, 3 (1988) 84-88.

Reinberg, A. E., Concepts in chronopharmacology. *Annu. Rev. Pharmacol. Toxicol.*, 32 (1992) 51-66.

Reiner, M., in Deformation, Strain and Flow. An Elementary Introduction to Rheology H. K. Lewis & Co. Ltd., London, 1960.

Rhine, W. D., Sukhatme, V., Hseih, D. S. T. and Langer, R. S., A new approach to achieve zero-order release kinetics from diffusion-controlled polymer matrix systems. In *Controlled Release of Bioactive Materials*, R. Baker (Ed.), Academic Press, New York, 1980 pp 177-187.

Rolland, A., Demichelis, G., Jamoulle, J-C. and Shroot, G., Influence of formulation, receptor fluid, and occlusion, on *in vitro* drug release from topical dosage forms, using an automated flow-through diffusion cell. *Pharm. Res.*, 9 (1992) 82-86.

Sakai, T., Kobayashi, K. and Sato, M., Static yield stress of ER fluids and the role of electric current. *J. Electrostatics.*, 40 & 41 (1997) 699-704.

Sathyan, G., Ritachel. W. A. and Hussain, A. S., Transdermal delivery of tacrine: I. Identification of a suitable delivery vehicle. *Int. J. Pharm.*, 114 (1995) 75-83.

See, H., Tamura, H. and Doi, M., The role of water capillary forces in electro-rheological fluids. *J. Phys. D: Appl. Phys.*, 26 (1993) 746-752.

Sefton, M. V., Implantable Pumps. In *Medical Applications of Controlled Release. Volume I: Classes of Systems.* Langer, R and Wise, D. L. (Eds.) CRC Press, Florida (1984) pp 41-67.

Sefton, M. V., Horvath, V. and Zingg, W., Insulin delivery by a diffusion-controlled micropump in pancreatectomized dogs: Phase 1. *J. Control. Rel.*, 12 (1990) 1-12.

Shih, Y-H. and Conrad, H., Influence of particle size on the dynamic strength of electrorheological fluids. *Int. J. Mod. Phys.*, 8 (1994) 2835-2853.

Shulman, Z.P., Gorodkin, R.G., Korobko, E.V. and Gleb, V.K., Electrorheological effect and its possible uses. *J. Non-Newt. Fluid Mech.*, 8 (1981) 29-41.

Shulman, Z.P., Korobko, E.V. and Yanovskii, Y. G., The mechanism of the viscoelastic behaviour of electrorheological suspensions. *J. Non-Newt. Fluid Mechan.*, 33 (1989) 181-196.

Siegel, R. A., Falamarzian, M., Firestone, B. A. and Moxley, B. C., pH controlled release from hydrophobic/polyelectrolyte copolymer hydrogels. *J. Control. Rel.*, 8 (1988) 179-182.

Siegel, R. A., Kost, J. and Langer, R., Mechanistic studies of macromolecular drug release from macroporous polymers. I. Experiments and preliminary theory concerning completeness of drug release. *J. Control. Rel.*, 8 (1989) 223-236.

Sinclair, G. W. and Peppas, N. A., Analysis of non-Fickian transport in polymers using simplified exponential expressions. *J. Membrane Sci.*, 17 (1984) 329-331.

Singh, J. and Bhatia, K. S., Topical iontophoretic drug delivery: pathway, principles, factors and skin irritation. *Med. Res. Rev.*, 16 (1996) 285-296.

Skaun, D. M. and Zentner, G. M., Phonophoresis. *Int. J. Pharm.*, 20 (1984) 235-245.

Small, G. W., Tacrine for treating Alzheimer's disease. *J. Am. Med. Assoc.*, 268 (1992) 1241-1245.

Sprecher, A. F., Carlson, J. D. and Conrad, H., Electrorheological at small strains and strain rates of suspensions of silica particles in silicone oil. *Mater. Sci. Eng.*, 95 (1987) 187-197.

Sprecher, A. F., Chen, Y. and Conrad, H., Measurement of forces between particles in a model ER fluid. *Electrorheological Fluids. Proceeding of the Seconmd International Conference on ER Fluids* (1990).

Sprecher, A. F., Chen, Y., Choi, Y. and Conrad, H., The effects of various dielectric oils and volume fraction of solids on the mechanical properties of hydrous based electrorheological fluids. *Int. J. Mod. Phys B.*, 15&16 (1992) 2625-2634.

Stangroom, J.E., Electrorheological fluids. *Phys. Technol.*, 14 (1983) 290-296.

Stangroom, J.E., U.S. Patent 4,483,788 (1984).

Stanway, R. and Sproston, J., Electro-rheological fluids - A systemic approach to classifying modes of operation. *Trans. ASME. J. Dynamic Systems, Measurement and Control*, 116 (1994) 498-504.

Stevens, N. G., Sproston, J. L. and Stanway, R. J., An experimental investigation of electro-rheological torque transmission. *ASME J. Mechanisms.*, 110 (1988) 182-188.

Takeo, K. and Omura, Y., U.S. Patent 3,984,339 (1976).

Tamura, H., See, H. and Doi, M., Model of porous particles containing water in electrorheological fluids. *J. Phys. D. Appl. Phys.*, 26 (1993) 1181-1187.

Tao, R. and Sun, J. M., 3-dimensional structure of induced electrorheological solid. *Phys. Rev. Lett.*, 67 (1991) 398-401.

Tervoort, T. A., Klompen, E. T. J. and Govaert, L. E., A multi-mode approach to finite, three-dimensional, non-linear viscoelastic behaviour of polymer glasses. *J. Rheol.*, 40 (1996) 779-799.

Trlica, J., Quadrat, O., Bradna, P., Pavlinek, V. and Saha, P., An anomalous electrorheological behaviour of magnesium hydroxide suspensions in silicone oil. *J. Rheol.*, 40 (1996) 943-946.

Tsai, S. C., Botts, D. and Plouff, J., Effects of particle properties on the rheology of concentrated non-colloidal suspensions. *J. Rheol.*, 36 (1992) 1291-1305.

Tyle, P. and Agrawala, P., Drug delivery by phonophoresis. *Pharm. Res.*, 6 (1989) 355-361.

Uejima, H., Dielectric mechanism and rheological properties of electro-fluids. *Jpn. J. Appl. Phys.*, 11 (1972) 319-326.

Weiss, K. D. and Carlson, J. D., Macroscopic behaviour of electrorheological fluids: techniques for measuring the response time. *Int. J. Mod. Phys. B,* 6 (1992) 2609-2623.

Weiss, K. D., Carlson, J. D. and Coulter, J. P., Material aspects of ER systems. *J. Int. Mater. Sys. Struct.,* 4 (1993) 13-34.

Weiss, K. D. and Duclos, T. G., Controllable fluids: The temperature dependence of post-yield properties. *Int. J. Mod. Phys.,* 8 (1994) 3015-3032.

Wen, W., Zheng, D. W. and Tu, K. N., Chain/column evolution and corresponding electrorheological effect. *J. Appl. Phys.,* 85 (1999) 530-533.

Winslow, W.M., U.S. Patent 2,417,850 (1947).

Winslow, W.M., Induced fibration of suspensions. *J. Appl. Phys.,* 20 (1949) 1137-1140.

Winslow, W.M., U.S. Patent 2,661,596 (1953).

Wu, C.W. and Conrad, H., Influence of a surface film on conducting particles on the electrorheological response with alternating current fields. *J. Appl. Phys.,* 81 (1997a) 8057-8063.

Wu, C.W., and Conrad, H., Negative electrorheological effect and electrical properties of Teflon/silicone oil suspension. *J. Rheol.,* 41 (1997b) 267-281.

Xu, Y-Z. and Liang, R-F., Electrorheological properties of semiconducting polymer-based suspensions. *J. Rheol.,* 35 (1991) 1355-1373.

Yatsuzuka, K., Miura, K., Kuramoto, N. and Asano, K., Observation of the electrorheological effect of silicone oil/polymer particles suspension. *IEEE Trans. Ind. Appl.,* 31 (1995) 457-463.

Zitter, R. N., Chen, T. J., Zhang, X. and Tao, R., Fluid flow and falling ball experiments in ER fluids. *Int. J. Mod. Phys. B,* 8 (1994a) 2823-2833.

Zitter, R. N., Zhang, X., Chen, T. J. and Tao, R., Falling ball experiments in a dilute electrorheological fluid. *J. Appl. Phys.,* 75 (1994b) 193-196.

Electrorheological behaviour at low applied electric fields of microcrystalline cellulose in BP oils

Jayne L. Davies, Ian S. Blagbrough*† and John N. Staniforth

Department of Pharmacy and Pharmacology, University of Bath, Bath, UK BA2 7AY

Electrorheological fluids have been prepared at low applied electric fields from BP oils containing microcrystalline cellulose (MCC); even at a low applied electric field of 500 V mm^{-1}, 10% MCC in oils rich in linoleic or oleic acids behave as electrorheological fluids with the latter displaying significantly higher yield stresses.

Electrorheology describes the rapid and reversible change in viscosity exhibited by certain suspensions of solid particles in electrically non-conducting liquids upon application of an electric field. Electrorheological (ER) fluids can run freely like water, ooze like honey or solidify like gelatine, depending upon the applied electric field. Winslow pioneered the use of ER fluids in the 1940s, with mechanical engineering applications ranging from a simple hydraulic valve[1] to a complex tracking device for copying machines.[2] The appeal of ER fluids is the rapid response, usually on the millisecond time scale, upon application of an electric field,[3–5] and this response is completely reversible upon removal of the electric field.[5,6] Although typically the electric fields necessary to provide an ER effect are in the region of 1–5 kV mm^{-1}, the power consumption is small (mW).[7]

Traditionally, ER fluids are composed of a dispersed particulate phase,[7,8] in the size range 0.5 to 100 μm, in an insulating base fluid.[9–11] In the absence of an electric field, most ER fluids behave, to a first approximation, as Newtonian fluids. When a continuous DC electric field E is applied to an ER fluid and the fluid is sheared in a direction perpendicular to the field, the relationship between the stress τ and the shear rate γ can be described by the Bingham model. According to this equation, flow only occurs once the applied stress exceeds the static yield stress $\tau_y(E)$. The flow equation is given in eqn. (1), where η_B is

$$\tau(E) = \tau_y(E) + \eta_B\gamma \qquad (1)$$

termed the Bingham viscosity. We are investigating the feasibility of using ER fluids as controllable drug delivery systems. In the absence of an electric field, a basal level of drug release will occur by diffusion across a mesh electrode. It is envisaged that upon application of an electric field, drug release will be controlled (hindered or halted).

We initially selected the pharmaceutically acceptable tablet excipient microcrystalline cellulose (MCC) in silicone oil as our ER fluid. This ER fluid has been recently reported, but only under high electric fields (in the range 1–3 kV mm^{-1}).[12,13] This project encompasses the search for pharmaceutically acceptable alternatives to traditional (engineering based) ER base fluid components. Thus, silicone oil (100 cS) or an alternative oil was used as the base fluid, together with sieved MCC (size fraction below 45 μm).‡ We have investigated the use of super refined BP oils as substitutes for silicone oil.‡ Oleic acid [(*Z*)-octadec-9-enoic acid] is the major constituent of apricot kernel (68%),[14] safflower (63%),‡ peanut (56%),[15] and sesame seed oils (45%).[15] Linoleic acid [(*Z*,*Z*)-octadeca-9,12-dienoic acid] is the primary constituent of sweet almond oil (75%)[16] and soyabean oil (50%).[15] In pharmaceutics, peanut and sesame seed oils find their uses as vehicles for sustained-release intramuscular injections.[16] Almond oil is also used as a vehicle for injections[17] and soyabean oil has replaced peanut oil in total parenteral nutrition regimens.[15]

A CSL^2 rheometer (TA Instruments, Leatherhead, UK) has been specially modified to allow the application of an electric field across the test fluid. A small electrolyte reservoir (approximately 0.5 ml) containing a 0.1% w/v solution of aq. KCl was used to form the electrical connection between the power supply (Model PS350 High Voltage Power Supply, Stanford Research Systems, Sunnyvale, CA, USA) and the rheometer geometry. The draw rod is insulated except for the threaded portion at the tip which makes contact with the geometry. In our experiments, we used a small volume (*ca.* 3.5 ml) concentric cylinder where the diameters of the cup and bob were 9.33 and 8.60 mm, respectively, resulting in a gap of 730 μm. All ER fluids were prepared using 10% w/w MCC (sieve fraction below 45 μm) in the appropriate oil, then sonicated (Decon FS300b) for two periods of 15 min prior to analysis. Temperature equilibration (37 ± 0.1 °C) of the sample was carried out for 15 min under the influence of an applied electric field (500 V mm^{-1}) prior to measurement. A continuous ramp of shear stresses from 0 to 50 Pa at a rate of 0.1 Pa s^{-1} was applied to each ER fluid with the resultant shear rate measured. A flow curve was plotted (Fig. 1) and the yield stress was determined by extrapolation of the experimental shear stress–shear rate data to zero shear rate using the Bingham model. Five measurements from each sample were taken and the associated mean and standard deviation were calculated (see Table 1).

In these studies, we have shown that, at a low applied electric field of 500 V mm^{-1}, suspensions of 10% w/w MCC in a range of BP oils behave as ER fluids. Furthermore, in general, BP oils afforded a higher Bingham yield stress than silicone oil (see Table 1), typically 12 Pa compared to 9 Pa. Using the ANOVA

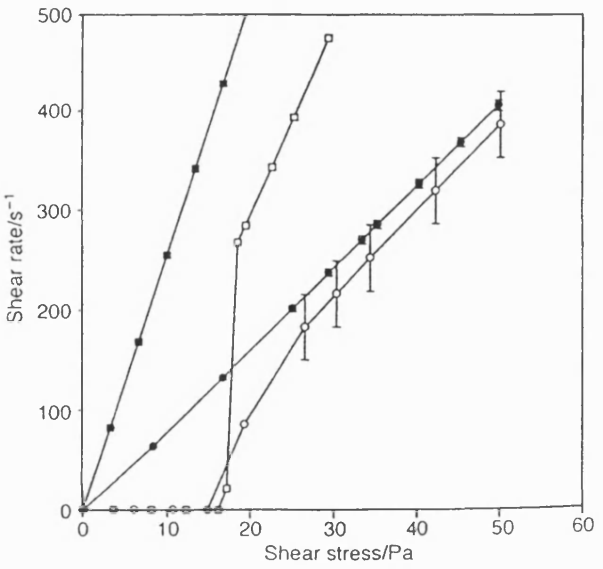

Fig. 1 Comparison of the flow behaviour at 0 V mm^{-1} [(●) silicone oil, (■) sesame seed oil] and 500 V mm^{-1} [(○) silicone oil, (□) sesame seed oil]

Table 1 The Bingham yield stress values for 10% w/w MCC in various oils at 500 V mm^{-1} (n = 5)

Oil	Bingham yield stress/Pa	Standard deviation
Almond	8.79	0.29
Apricot	12.54	0.39
Peanut	12.78	0.33
Safflower	12.17	0.47
Sesame seed	12.27	0.12
Silicone	8.94	0.26
Soyabean	10.53	0.37

test (one way), it was found that there were statistical differences ($p < 0.05$) between the oils. A Fisher analysis was carried out to highlight where differences were present. No significant difference ($p < 0.05$) was found between almond oil and silicone oil. Apricot oil, peanut oil, safflower oil, and sesame seed oils were also found not to be significantly different. In the light of these findings, we conclude that the BP oils which have oleic acid as the major constituent have significantly higher yield stress values compared with the BP oils having linoleic acid as their major constituent. Preliminary studies, using a parallel plate geometry, with 10% MCC in oleic and linoleic acids (*ca.* 95%)‡ also exhibited an ER response at 250 V mm^{-1}. This demonstration of ER responses below 1 kV mm^{-1}, using pharmaceutically acceptable oils, should find ready applications.[18–22]

We thank Hoechst Marion Roussel (Swindon, UK, and Kansas City, USA) for funding this studentship (to J. L. D.). We gratefully acknowledge the support and interest of Dr David Jordan (HMR, Swindon) in our studies.

Notes and References

† E-mail: prsisb@bath.ac.uk

‡ *Reagents*: Microcrystalline cellulose (MCC) (Lot No: E5D7C21, Emcocel 50M, Mendell, Patterson, NY, USA); 100 cS silicone oil, oleic and linoleic acids (Aldrich, Gillingham, UK); super refined BP oils (Croda Oleochemicals, Goole, UK).

1 W. M. Winslow, *U.S. Pat.* 2,417,850 (1947); W. M. Winslow, *J. Appl. Phys.*, 1949, **20**, 1137.
2 Z. P. Schulman, R. G. Gorodkin, E. V. Korobko and V. K. Gleb, *J. Non-Newtonian Fluid Mech.*, 1981, **8**, 29.
3 J. E. Stangroom, *Phys. Technol.*, 1983, **14**, 290.
4 T. C. Halsey, *Science*, 1992, **258**, 761.
5 K. D. Weiss and J. D. Carlson, *Int. J. Mod. Phys. B*, 1992, **6**, 2609.
6 N. Webb, *Chem. Br.*, 1990, **26**, 338.
7 H. Block and J. P. Kelly, *J. Phys. D., Appl. Phys.*, 1988, **21**, 1661.
8 T. C. Jordan and M. T. Shaw, *IEEE Trans. Electr. Insul.*, 1989, **24**, 849.
9 F. Pool, *Science*, 1990, **247**, 1180.
10 F. Filisko, *Chem. Ind.*, 1992, **10**, 370.
11 K. O. Havelka and J. W. Pialet, *Chemtech*, 1996, **26**, 36.
12 K. Yatsuzuka, K. Miura, N. Kuramoto and K. Asano, *IEEE Trans. Ind. Gen. Appl.*, 1995, **31**, 457.
13 A. Kawai, K. Uchida, K. Kamiya, A. Gotoh, K. Urabe and F. Ikazaki, *Int. J. Mod. Phys. B*, 1996, **10**, 2849.
14 A. Femenia, C. Rossello, A. Mulet and J. Canellas, *J. Agric. Food Chem.*, 1995, **43**, 356.
15 *Handbook of Pharmaceutical Excipients*, a joint publication of the American Pharmaceutical Association and the Royal Pharmaceutical Society of Great Britain, Pharmaceutical Press, London, UK, 1994.
16 *British Pharmacopoeia*, Her Majesty's Stationery Office, London, UK, 1993.
17 *Pharmaceutical Codex*, 11th edn, The Pharmaceutical Press, London, 1983.
18 L. Marshall, C. F. Zukoski and J. W. Goodwin, *J. Chem. Soc., Faraday Trans.*, 1989, **85**, 2785.
19 M. V. Gandhi and B. S. Thompson, *Electrorheological Fluids*, in *Smart Materials and Structures*, Chapman and Hall, London, UK, 1992.
20 M. Parathasarathy and D. J. Klingenberg, *Mater. Sci. Eng.*, 1996, **17**, 57.
21 T. Hao, *Appl. Phys. Lett.*, 1997, **70**, 1956.
22 K. Bohon and S. Krause, *J. Polym. Sci.*, 1998, **36**, 1091.

Received in Cambridge, UK, 19th August 1998; 8/06533K